N° of Dissertation	

A DISSERTATION

Submitted to the Doctoral Research Programme on Climate Change and Energy

University Abdou Moumouni of Niamey, Niger

in Fulfilment of the Requirements for PhD

DOCTORAL SCHOOL OF EXACTS AND TECHNICS SCIENCES

Domain: Sciences and Technologies

Mention: Physics

Specialty: Climate Change and Energy

by

ERIC MENSAH MORTEY

IMPACT OF CLIMATE CHANGE AND LAND USE LAND COVER CHANGE ON THE WATER-ENERGY-FOOD NEXUS IN WEST AFRICA

Thesis defence: On 11 January 2025 at 10:00 AM in Niamey, Niger

Members of jury

M. Makinta BOUKAR — **Président**
Professeur Titulaire, Université Abdou Moumouni, Niamey, Niger

M. Ibrahim HALIDOU — **Examinateur interne**
Maître de Conférences, Université Abdou Moumouni, Niamey, Niger

M. Bruno KORGO — **Examinateur externe**
Maître de Conférences, Université Joseph Ki-Zerbo, Burkina Faso

M. Ibrahim BOUBACAR — **Rapporteur interne**
Maître de Conférences, Université Abdou Moumouni, Niamey, Niger

M. Amos T. Kabo-bah — **Rapporteur externe**
Associate Professor, University of Energy and Natural Resources, Sunyani, Ghana

M. Saïdou Madougou — **Directeur de thèse**
Professeur Tutilaire, Université Abdou Moumouni, Niamey, Niger

Supervision team

Main supervisor: Saïdou Madougou, Prof., Université Abdou Moumouni, Niamey, Niger
Cosupervisor: Mamman Marouhi Innoussa, Ass Prof., Université Abdou Moumouni, Niamey, Niger
Cosupervisor: Thompson Annor, Ass Prof., Kwame Nkrumah University of Science and Technology, Kumasi, Ghana
Cosupervisor: Joël Arnault, PhD, Karlsruhe Institute of Technology, Campus Alpin, Garmisch-Partenkirchen, Germany

DEDICATION

This work is dedicated to God All Mighty and my family.

ACKNOWLEDGEMENT

I would first like to thank Prof. Saidou Madougou, Full Professor at Université Abdou Moumouni, my supervisor, for his scientific and human qualities. I thank him for his confidence in me and his ideas, advice, and support throughout my PhD journey.

I want to thank Prof. Mamman Marouhi Innoussa, Associate Professor at Université Abdou Moumouni, my co-supervisor, for his scientific contribution, comments and suggestions, moral support, and encouragement throughout my PhD journey.

Many thanks to Prof. Rabani Adamou, the former Vice Chancellor of Université Abdou Moumouni, and Director of the WASCAL Doctoral Programme in Climate Change and Energy. His advice at the beginning of my PhD was beneficial throughout my PhD journey.

I want to thank Prof. Thompson Annor, Associate Professor, Kwame Nkrumah University of Science and Technology, for his scientific contribution, encouragement, motivation, and guidance during the PhD period.

Professor Harald Kunstmann, Full Professor, University of Augsburg, Germany, my co-supervisor, made all the paper arrangements possible to travel to Germany. I am grateful for his support and comments, granting me access to the High-Performance Computing Infrastructure at the Karlsruhe Institute of Technology (KIT), Garmisch-Partenkirchen, Germany, and paying for the article processing charges for my second article.

Dr. Joël Arnault, Research Scientist at the KIT, my co-supervisor was my day-to-day instructor at KIT. I am grateful to him for following up with logistics and paperwork and making it possible for me to visit KIT. I am also thankful for training me to use the WRF-Hydro and for contributing immensely to various aspects of my thesis. I am grateful for his emails during the most difficult times.

Dr. Patrick Laux and Dr. Mame Diarra Bousso Dieng, research scientists at KIT have been of immense support during my stay at KIT. I am highly indebted to their encouragement, kindness, and company.

I want to thank Dr. Boubacar Ibrahim, Université Abdou Moumouni, for his intensive review of the PhD thesis, ensuring that form, structure, and constructions meet the standards required by Université Abdou Moumouni.

I thank Prof. Amos Kabo-bah, Associate Professor, University of Energy and Natural Resources, for offering significant contributions through review to improve the work.

To all jury members who agreed to attend the defense of this PhD thesis and to all who have contributed directly and indirectly, thank you. Special thanks to the chairman of the jury Prof. BOUKAR Makinta, full professor of UAM, and once again to Prof. MADOUGOU Saidou, my supervisor. I also want to thank the internal examiners, Dr. HALIDOU Ibrahim of UAM, Niger, and Dr. Korgo Bruno of Universite Joseph Ki-Zerbo de Ouagadougou, Ouagadougou, for their thorough examination of my thesis and for providing critical observations on the thesis. Finally, I thank my external reviewers, Dr. IBRAHIM FODI Boubacar and Prof. KABO-BAH Amos Tiereyangn, for their questions and contributions during the defense.

I am grateful to all the staff of WASCAL-DRP-CCE and all the lecturers who assisted us during the various courses in Climate Change and Energy and during my stay in Niamey. Special thanks to Mr. David Agbo and Alio Sanda M. Djibrilla for making the necessary arrangements for my thesis defense. I thank my colleague PhD candidates at WASCAL-DRP-CCE and UAM for their collaboration and team spirit. I am most grateful to Dr. Amega Kokou and Dr. Bagre Boubou for their encouragement during difficult times.

I thank my colleagues, Research Fellows, at the Earth Observation Research and Innovation Center (EORIC), University of Energy and Natural Resources, for their immense support and encouragement during my PhD. I am grateful to Dr. Martin Domfeh for offering his High-Performance Computer for some aspects of this work.

I thank the German Federal Ministry of Education and Research (BMBF) through the West Africa Science Service Center on Climate Change and Adapted Land Use (WASCAL) for providing the scholarship for the PhD.

I extend my gratitude to the Volta Basin Authority (VBA) in Ouagadougou, the Volta River Authority (VRA) at Akuse, Ghana, the Bui Power Authority at Bui, Ghana, and SONABEL in Ouagadougou, Burkina Faso for the provision of hydrological, and energy production data to make this work possible.

LIST OF ABBREVIATIONS

ACCESS-CM	Australian Community Climate and Earth-System Simulator - Coupled Model
ACCESS-ESM	Australian Community Climate and Earth-System Simulator - Earth System Model
AFOLU	Agriculture, Forest and other Land Use
AFRICOVER	Africa Cover
AGCM	Atmospheric Global Climate Models
AMJ	April-May-June
AMMA	African Monsoon Multidisciplinary Analysis
APSD	African Plantations for Sustainable Development
ARPEGE	Action de Recherche Petite Échelle Grande Échelle
ATEB	Australian Town Energy Budget
AWS	Advanced Water System
BCC-CSM2-MR	Beijing Climate Center Climate System Model version 2 Medium Resolution
BCSD	Bias Correction/Spatial Disaggregation
BMBF	German Federal Ministry of Education and Research
BPA	Bui Power Authority
C	Congolia
CanESM5	Canadian Earth System Model version 5
CC	Climate Change
CCAM	Conformal Cubic Atmospheric Model
CCI	Climate Change Initiative
CCI	Climate Change Initiative
CCLM	Consortium for Small-scale Modeling Climate Limited-area Modelling
CDO	Climate Data Operator
CESC	Climate and Environmental Services Center
CESM	Community Earth System Model
CHIRPS	Climate Hazards Group Infrared Precipitation with Stations
CHIRTS	Climate Hazards Group Infrared Temperature with Stations
CLIMWAT	Climatic Database for Irrigation Planning and Management
CMCC-CM2-SR5	Centro Euro-Mediterraneo sui Cambiamenti Climatici - Climate Model 2 - Standard Resolution 5
CMCC-ESM	Centro Euro-Mediterraneo sui Cambiamenti Climatici Earth System Model
CMIP6	Coupled Model Intercomparison Project (Phase 6)
CoC	Competence Center
CORDEX	Coordinated Regional Climate Downscaling Experiment
COSMO-CLM	COnsortium for Small-scale MOdelling-CLimate Model
CRCM5	Canadian Regional Climate Model fifth-generation
CRU-TS	Climatic Research Unit gridded Time Series
CWB	Climate Water Balance

DST	Decision Support Tool
ECMWF	European Centre for Medium-Range Weather Forecasts
ECOCLIMAPI	ECOlogical CLIMate MAPping I
ECOCLIMAPII	ECOlogical CLIMate MAPping II
EFW	Energy-Water-Food
ENVI	Environment for Visualizing Images
ERA5	ECMWF ReAnalysis fifth-generation
ERA5-Land	ECMWF ReAnalysis fifth-generation-Land
ERDAS	Earth Resources Data Analysis System
ESA	European Space Agency
ESM	Earth System Model
ESRI	Environmental Systems Research Institute
ET	Evapotranspiration
EWF	Energy-Water-Food
F	preferred flow direction
FAO	Food and Agriculture Organization
FEW	Food-Energy-Water
FGD	Focus Group Discussions
FLUXNET	Flux Network
FMAM	February-March-April-May
G	Guinea
GCM	Global Climate Model / Global Circulation Model
GEF	Global Environmental Fund
GEF	Global Environment Facility
GGW	Great Green Wall
GHG	Green House Gazes
GIEC	Gestion Intégrée des Ressources en Eau
GIA	Generic Investigation Areas
GIRE	Gestion intégrée des ressources en eau
GIS	Geographic Information System
GISS-E	Goddard Institute for Space Studies - Model E
GISS-E2-1-G	Goddard Institute for Space Studies - Model E2.1 - GISS Ocean Model
GJ	Gigajoule
GLACE	Global Land–Atmosphere Coupling Experiment
GLASS-GLC	Global Land Surface Satellite-Global Land Cover
GLC2000	Global Land Cover 2000
GLCC	Global Land Cover Characterization
GLCNMO	Global Land Cover by National Mapping

GLC-SHARE	Global Land Cover-SHARE
GLEAM	Global Land Evaporation Amsterdam Model
GMFD	Global Meteorological Forcing Dataset
GMRCA LULC	Global Mapping of Remote-sensing-derived Crop Area and Land Use Land Cover
GPWV4	Gridded Population of the World, Version 4
GRACE	Gravity Recovery and Climate Experiment
GWPV4	Gridded Population of the World (GPW) Version 4
HadGEM	Hadley Centre Global Environment Model
HydroSHEDS	Hydrological data and maps based on Shuttle Elevation Derivatives at multiple Scales
IBIS	Integrated Biosphere Simulator
IMERG	Integrated Multi-satellitE Retrievals for GPM
IMK-IFU	Institute of Meteorology and Climate Research Atmospheric Environmental Research
INDC	Intended Nationally Determined Contributions
IPCC	Intergovernmental Panel on Climate Change
ITCZ	Inter-Tropical Convergence Zone
IWRM	Integrated Water Resources Management
KB	Kulpawn Basin
Kc	crop coefficient
KGE	Kling–Gupta efficiency
KIT	Karlsruhe Institute of Technology
Ks	root zone Conductivity
LADA	Land Degradation Assessment
LAI	Leaf Area Index
LC	Land Cover
LC-CCI	Land Cover-Climate Change Initiative
LCCS	Land Cover Classification System
LEAP	Long-range Energy Alternatives Planning system
LMDZ	Laboratoire de Météorologie Dynamique Zoom
LSP	land surface processes
LST	land surface temperatures
LU	Land Use
LUC	Land Use Cover
LULC	Land Use/Land Cover
LVB	Lower Volta Basin
MCD12Q1	MODIS Collection 5.1 Land Cover Type Yearly L3 Global 500m
MCR	Modèles Climatiques Régionaux
MDG	Millennium Development Goals

MERIS	Medium Resolution Imaging Spectrometer
MIROC6	Model for Interdisciplinary Research On Climate version 6
MIROC-ES2L	Model for Interdisciplinary Research On Climate Earth System version 2-Low resolution
MJ	May-June
MODFLOW	MODular Finite-difference Ground-Water FLOW model
MODIS	Moderate Resolution Imaging Spectroradiometer
MPAS	Model for Prediction Across Scales
MPI-ESM1- 2-LR	Max Planck Institute Earth System Model version 1.2 - Low Resolution
MPI-ESM1-2-HR	Max Planck Institute Earth System Model version 1.2 - High Resolution
MRI-ESM2-0	Meteorological Research Institute Earth System Model version 2.0
NAMA	Nationally Appropriate Mitigation Actions
NAP	National Action Plans
NAPA	National Programs of Action
NCO	NetCDF Operator
NDC	Nationally Determined Contribution
NDVI	Normalized Difference Vegetation Index
NETW	North-East Trade Winds
NEX-GDDP	NASA Earth Exchange Global Daily Downscaled Projections
NEX-GDDP-CMIP6	NASA Earth Exchange (NEX) Global Daily Downscaled Projections (GDDP)
Noah-MP	Noah land surface model with multiparameterization options
NorESM2-LM	Norwegian Earth System Model version 2 - Low Resolution
Nor-ESM2-MM	Norwegian Earth System Model version 2 - Medium Resolution
NSE	Nash–Sutcliffe efficiency
OLAM	Ocean-Land Atmospheric Models
ON	October to November
OSM LULC	Open Street Map Landuse/Landcover
P	Precipitation
PBIAS	Percentage Bias
PEST	Parameter Estimation Tool
PET	Potential Evapotranspiration / Potential Evaporation
PG	Population Growth
PRT	Priority Research Themes
PRT	Priority Research Themes
QGIS	Quantum GIS
r2	coefficient of determination
RAMS	Regional Atmospheric Modeling System

RCM	Regional Climate Models
REMO	REgional Model
RMSE	Root-Mean-Square-Error
RRF	runoff resistance factor
S	Sudan
SADC	Southern African Development Community
SAFARI	Southern African Regional Science Initiative
SAH	Sahara
SB	Sissili Basin
SDG	Sustainable Development Goals
SDG	Sustainable Development Goals
SEDAC	Socioeconomic Data Center and Applications
SEI	Stockholm Environment Institute
SERVIR-ESA	SERVIR Eastern and Southern Africa
SH	Sahel
SKB	Sissili-Kulpawn Basin
SMAP	Soil Moisture Active Passive
SONABEL	Société Nationale d'Electricité du Burkina
SOND	September-October-November-December
SPEI	Standardized Precipitation Evapotranspiration Index
SPI	Standardized Precipitation Index
SRTM	Shuttle Radar Topographic Mission
SSPs	Shared Socioeconomic Pathways
SST	Sea Surface Temperature
STI	Standardized Temperature Index
SW	soil water capacity
SWAT	Soil Water Assessment Tool
TaiESM1	Taiwan Earth System Model version 1
TCM	TerraClimate
TGJ	Tokar Gap jet
TRMM	Tropical Rainfall Measuring Mission
TWS	Total Water Storage
UER	Upper East Region
UHI	Urban Heat Island
UMD LC	University of Maryland Land Cover
UN	United Nations
UN FAO	United Nations Food and Agricultural Organization
UNEP	United Nattions Environmetal Programme

VB	Volta Basin
VBA	Volta Basin Authority
VRA	Volta River Authority
WA	West Africa
WASCAL	West African Science Service Centre on Climate Change and Adapted Land Use
WEAP	Water Evaluation and Planning System
WEF	Water-Energy-food
WEFC	Water Energy Food Nexus Climate.
WEF-Volta	Water-Energy-Food NexusVolta model
WMO	World Meteorological Organization
WRAP 2.0	WASCAL Research Action Plan 2.0
WRF	Weather Research Forecasting Model
WRF-Hydro	Weather Research and Forecasting Hydrological modeling system

Abstract

The dynamic interaction between climate and land plays an important role in water, hydropower, and food production in West Africa (WA). However, the interaction between climate, land, and water is oversimplified in RCMs, leading to inaccurate predictions of the timing and availability of water resources. Moreover, most hydrological models' approach to resource management is water-centric based on IWRM frameworks but lacks a strong basis for WEF nexus studies. Furthermore, there is little research to understand the effects of deforestation and afforestation on the local water-food nexus. The first objective of this thesis aims to characterize the relationship between climate variability and land use/land cover change in WA using remote sensing and reanalysis products. The second objective aims to model the relationship between climate variability and land use/land cover change using the WRF-Hydro model. The third objective aims to assess the future impacts of climate change, land use and land cover change, and population growth on the WEF nexus components. Objective one (1) was achieved by analyzing climatic and land cover changes in West Africa. Objective two (2) was achieved by modeling the effects of afforestation and deforestation on the climatological water flow change in the SKB. Objective three (3) was achieved by building a Volta-WEF nexus to quantify future water and hydropower availability indices. The NSE and KGE of WRF-Hydro setup is 0.47 and 0.69, respectively, over the KB compared to the default setup values of -0.34 and 0.2. The Volta-WEF model in WEAP yielded an R^2 (NSE) of 0.74–0.85 (0.71–0.79) and 0.7–0.81 (0.66–0.81), respectively, over the calibration and validation periods. Over the 1992–2019 period, an interannual temperature change of 1.0 to 2.0 ℃, and a 50 mm change of precipitation and climatic water balance resulted in 20935–52133 km^2 land cover change intensities, while a temperature change of 0.5 ℃ and a precipitation change of 20 mm represented normal climatic conditions with land cover change intensities below 20000 km^2. The afforestation experiment yielded approximately 6% more precipitation, 3% more evapotranspiration, 27% more surface runoff, and 16% more underground runoff, while the deforestation experiment yielded 5% less precipitation, 3% less evapotranspiration, 3% less surface runoff, and 9% less underground runoff over the SKB. The future water demand index is estimated at 0.94 to 0.96 for SSP1-2.6 to SSP5-8.5 and the future hydropower generation index is between 1.001 and 1.002 for all SSPs, illustrating the water-energy nexus. Future works can consider implementing the climate-land relationship described in this work into RCMs. Moreover, staple crops could be included in the WEF-Volta model to account for food production.

Keywords

Land-atmosphere interactions, Climate-land interactions, Water-Energy-Food Nexus, Sustainable Development Goals, Climate change, WEAP, WRF-Hydro, Volta Basin, WEF-Volta, ESA CCI LC, Land use and land cover change, Population growth, climate services

Résumé

L'interaction dynamique entre le climat et la terre joue un rôle important dans la production d'eau, d'énergie hydroélectrique et de nourriture en Afrique de l'Ouest. Cependant, l'interaction entre le climat, la terre et l'eau est simplifiée à l'extrême par les Modèles Climatiques Régionaux, ce qui conduit à des prévisions inexactes quant au calendrier et à la disponibilité des ressources en eau. En outre, l'approche de la gestion des ressources de la plupart des modèles hydrologiques est centrée sur l'eau et basée sur les cadres de la GIRE, mais ne dispose pas d'une base solide pour étudier les interactions entre l'eau, l'énergie et l'alimentation. Le premier objectif vise à caractériser la relation entre la variabilité du climat et les changements d'utilisation et de couverture des sols en Afrique de l'Ouest à l'aide de produits de télédétection et de réanalyse. Le deuxième objectif vise à modéliser la relation entre la variabilité du climat et les changements d'utilisation et de couverture des sols à l'aide du modèle WRF-Hydro. Le troisième objectif vise à évaluer les impacts futurs du changement climatique, de l'utilisation des terres et de la modification de l'occupation des sols, ainsi que de la croissance démographique sur les composantes du nexus du WEF. Le premier objectif (1) a été atteint en analysant les changements du climat et de l'occupation des sols en Afrique de l'Ouest. L'objectif deux (2) a été atteint en modélisant les effets du boisement et du déboisement sur le changement climatologique du débit d'eau dans la SKB. Le troisième objectif (3) a été atteint en construisant un nexus Volta-WEF pour quantifier les futurs indices de disponibilité de l'eau et de l'énergie hydroélectrique. Le NSE et le KGE de la configuration WRF-Hydro sont respectivement de 0,47 et 0,69 sur le KB par rapport aux valeurs de la configuration par défaut de -0,34 et 0,2. Le modèle Volta-WEF dans WEAP a donné un R^2 (NSE) de 0,74-0,85 (0,71-0,79) et 0,7-0,81 (0,66-0,81), respectivement, sur les périodes de calibration et de validation. Au cours de la période 1992-2019, un changement de température interannuel de 1,0 à 2,0 °C et un changement de 50 mm des précipitations et du bilan hydrique climatique ont entraîné des intensités de changement de la couverture terrestre de 20935 à 52133 km^2, tandis qu'un changement de température de 0,5 °C et un changement de précipitations de 20 mm représentaient

des conditions climatiques normales avec des intensités de changement de la couverture terrestre inférieures à 20000 km^2. L'expérience de boisement a donné environ 6 % de précipitations en plus, 3 % d'évapotranspiration en plus, 27 % de ruissellement de surface en plus et 16 % de ruissellement souterrain en plus, tandis que l'expérience de déboisement a donné 5 % de précipitations en moins, 3 % d'évapotranspiration en moins, 3 % de ruissellement de surface en moins et 9 % de ruissellement souterrain en moins dans la SKB. L'indice de la demande future en eau est estimé entre 0,94 et 0,96 pour les SSP1-2,6 à SSP5-8,5 et l'indice de la production future d'hydroélectricité se situe entre 1,001 et 1,002 pour toutes les SSP, ce qui illustre le lien entre l'eau et l'énergie. Les travaux futurs peuvent envisager la mise en œuvre de la relation climat-terre décrite dans ce travail dans les MCR. En outre, les cultures de base pourraient être incluses dans le modèle WEF-Volta pour tenir compte de la production alimentaire.

Mots-clés

Interactions terre-atmosphère, Interactions climat-terre, Nexus eau-énergie-alimentation, Objectifs de développement durable, Changement climatique, WEAP, WRF-Hydro, Bassin de la Volta, WEF-Volta, ESA CCI LC, Changement de l'utilisation et de la couverture des sols, Croissance de la population, services climatiques.

TABLE OF CONTENTS

CHAPTER 1 – INTRODUCTION 1

1.1 Context 1
1.2 Problem statement 4
1.3 Aim and Objectives 9
1.4 Research questions 9
1.5 Motivation and Justification 9
1.6 Outline 10

CHAPTER 2 – LITERATURE REVIEW 12

2.1 Introduction to literature review 12
2.2 Literature selection 12
2.3 Land-atmosphere interaction research in Africa – Trends, models, and methods 21
2.4 The Weather Research and Forecasting Model (WRF) 25
2.5 The fully-coupled atmospheric hydrological WRF-Hydro model 27
2.6 Land use versus land cover 31
2.7 Available land use cover (LUC) datasets 32
2.8 Criteria for land use cover data selection 34
2.9 The ESA CCI LC 35
2.10 Land-atmosphere interactions in the water-energy-food nexus research 35
2.11 The Water-Energy-Food Nexus 36
2.12 Stressors of the Water-Energy-Food nexus system 39
2.13 The WEF nexus research trends in Africa 54
2.14 West Africa and Water-Energy-Food Nexus 56
2.14.1 The Climate system of West Africa 56
2.14.2 The Volta Basin 57
2.14.3 Climate of the Volta Basin 59
2.14.4 Socioeconomic activities in the Volta Basin 62
2.14.5 WEF nexus in the Volta Basin 70
2.15 The Shared Socioeconomic Pathways 71

2.15.1 SSP1-2.6 72
2.15.2 SSP2-4.5 72
2.15.3 SSP3-7.0 73
2.15.4 SSP4-6.0 74
2.15.5 SSP5-8.5 74
2.16 Partial conclusion on literature review 75
CHAPTER 3 – MATERIALS AND METHOD 76

3.1 Introduction to material and methods 76
3.2 Study area 76
3.3 Data collection 80
3.3.1 Climate Data 80
3.3.2 Land cover data 83
3.3.3 Socioeconomic data 84
3.3.4 Hydrological Data 84
3.3.5 Hydroelectric dam Data 84
3.3.6 Water demand data 84
3.3.7 Irrigation Water Requirement 85
3.4 Data analysis 85
3.4.1 Climate-land interactions using satellite and reanalysis products 85
3.4.2 Extreme climate indices computation 87
3.4.3 Analysis of land cover trajectory, changed pixels and the total changes per pixel. 88
3.4.4 Changes in land cover area (intensity) 89
3.4.5 Linking land–climatic changes 89
3.4.6 Average rate of climatic change 89
3.4.7 Climatic indices frequency and occurrence probability 90
3.5 Modeling 90
3.5.1 Overview of methods 90
3.5.2 Climate-land interactions using fully coupled land-atmosphere model (WRF-Hydro) 92
3.5.3 Climate-land interactions using the WEAP hydrological model 101
3.6 Partial conclusion on material and methods 105
CHAPTER 4 – RESULTS AND DISCUSSION 106

4.1 Introduction to results and discussion 106
4.2 Climate-land cover interactions using Satellite Remote Sensing and Reanalysis products 106
4.2.1 Extreme climatic indices over West Africa (1980-2020) 107
4.2.2 Spatiotemporal land use/cover change analysis 109
4.2.3 Annual land cover change intensities over West Africa 110
4.2.4 Linking climatic indices and land use/cover changes 111
4.2.5 Mathematical formulation of the climate-land use/cover change impact (1980-2020) 116
4.2.6 Quantifying climate conditions with abrupt land cover change effects 116
4.2.7 Quantifying climate conditions with non-abrupt land cover change effects 119
4.2.8 Latitudinal change occurrence frequency 121
4.2.9 Land cover transition 122
4.3 Climate-land cover interactions from the modeling perspective – WRF-Hydro 125
4.3.1 Effects of numerical land cover changes experiment on in biophysical parameters .. 125
4.3.2 Spatial validation of simulated Energy fluxes 128
4.3.3 Validation of WRF-Hydro simulated rainfall and temperature 130
4.3.4 Temporal validation of WRF-Hydro simulated rainfall and streamflow 132
4.3.5 Climatological evaluation of simulated rainfall, discharge, temperature and energy fluxes over the Sissili Basin 134
4.3.6 Climatological evaluation of simulated rainfall, discharge, temperature and energy fluxes over the Kulpawn Basin 137
4.3.7 Impact of land use/land cover change on energy fluxes 139
4.3.8 Impact of land use land cover change on water fluxes 141
4.3.9 Impacts of land use/land cover change on temperature and precipitation 143
4.3.10 Climatology of water and energy budget under land cover change numerical experiment: Sissili Basin 146
4.3.11 Climatology of water and energy budget under land cover change numerical experiment: Kulpawn Basin 150
4.4 Climate- land use/land cover interactions under future scenario 153
4.4.1 The Volta-WEF nexus model 153
4.4.2 The Volta-WEF nexus model calibration and validation 155
4.4.3 Impact of historical and future population growth on water demand 158

4.4.4 Changes in annual mean temperature over the Volta Basin 163
4.4.5 Changes in annual total precipitation over the Volta Basin 165
4.4.6 Changes in water demand under climate change and population change scenarios... 166
4.4.7 Projected changes in system hydropower generation 173
4.5 Partial conclusion on results and discussion 179
CHAPTER 5 – CONCLUSION, RECOMMENDATION, AND FUTURE WORKS 180

APPENDIX 220

LIST OF TABLES

Table 2.1 Land atmospheric interactions research over Africa 22
Table 2.2 WRF-Hydro researches conducted in Africa 29
Table 2.3 Globally available LUC datasets with a single date 32
Table 2.4 Globally available LUC timeseries datasets 33
Table 2.5 Available LUC datasets for Africa 33
Table 2.6 WEF nexus publications in Africa 55
Table 2.7 Respective countries and their land cover area in the Volta Basin of West Africa 59
Table 2.8 Basic data on elevation across the basin 59
Table 2.9 Population trends in the Volta Basin 62
Table 2.10 Projected water use rate of towns/cities per country in the Volta basin 65
Table 2.11 Projected irrigable land for rice production per country in the Volta Basin 66
Table 2.12 Existing hydroelectric plants and their installed capacity 70
Table 2.13 Details of hydro sites on the main tributaries of the Volta Basin in Ghana 70
Table 3.1 Climate data used to compute standardized climatic indices 81
Table 3.2 Observational products used to validate the simulated outputs of the WRF-Hydro 81
Table 3.3 Historical and future climate datasets used in the CMIP6 model 82
Table 3.4 SPI and SPEI-based classification for the various drought categories. 87
Table 3.5 Heat categorization based on STI values. 88
Table 3.6 WRF and WRF-Hydro physical parameterization 95
Table 3.7 Total land cover in km^2 and % of land cover types categorized 99
Table 3.8 Total land cover in km^2 and % of each land cover category 99
Table 3.9 Share of land cover in km^2 and % of the land cover categories 100
Table 3.10 Share of land cover in km^2 and % of the land cover categories 100
Table 4.1 Climatic conditions leading to abrupt land cover area changes 119
Table 4.2 Differential changes in water flow terms over the Sissili river basin 149
Table 4.3 Differential changes in water flow terms over the Kulpawn river basin 153
Table 4.4 Water-Energy-Food Nexus sites delineated for this work 154
Table 4.5 Projected water demand over the Volta Basin in Mm^3 161
Table 4.6 Projected change in annual average water demand (in Mm^3) in the Volta Basin 171

Table 4.7 Projected change in monthly average water demand (in Mm^3) in the Volta Basin.... 172
Table 4.8 Projected change in annual average of total generation for hydropower systems..... 177
Table 4.9 Projected change in monthly average generation for hydropower systems..... 178

LIST OF FIGURES

Figure 2.1 Approach to literature review and model selection process 14
Figure 2.2 Number of articles published between 1990 and 2024. 15
Figure 2.3 Number of articles classified by the type of document 16
Figure 2.4 Total number of articles classified according to the subject area 17
Figure 2.5 Total number of articles classified according to source 18
Figure 2.6 Total number of articles classified by continents 19
Figure 2.7 A word cloud analysis of (a) title, (b) abstract, and (c) keywords 19
Figure 2.8 A word cloud analysis of (a) Title, (b) Abstract, and (c) Keywords 20
Figure 2.9 Basic water-energy-food nexus showing each nexus node (water, energy, food) 38
Figure 2.10 Historical evolution of the WEF nexus timeline and the various actors involved 39
Figure 2.11 Water-Energy-Food Nexus from Hoff 2011 (Albrecht et al., 2018). 41
Figure 2.12 Number of articles published between 2012 and 2024. 44
Figure 2.13 Number of Documents retrieved classified by the documents type 44
Figure 2.14 Number of Documents classified by the continent 45
Figure 2.15 Documents on the WEF nexus reviewed classified by the subject area 45
Figure 2.16 First 21 Journals with the highest list of publications on the WEF nexus 46
Figure 2.17 Articles reviewed classified according to the nexus type 47
Figure 2.18 Keyword analysis of global research on the WEF nexus (2012 - 2015) 48
Figure 2.19 Keyword analysis of global research on the WEF nexus (2016 - 2019) 49
Figure 2.20 Keyword analysis of global research on the WEF nexus (2020 - 2024) 50
Figure 2.21 Keyword analysis of WEF Nexus research in Africa (2012- 2015) 51
Figure 2.22 Keyword analysis of WEF Nexus research in Africa (2016- 2019) 52
Figure 2.23 Keyword analysis of WEF Nexus research in Africa (2020- 2024) 53
Figure 2.24 The five bioclimatic zones of West Africa 57
Figure 2.25 The Volta Basin and its four sub-basins 58
Figure 2.26 Average annual rainfall evolution - Decennal period (1960-2000) 61
Figure 2.27 Drinking water supply in the Volta Basin 64
Figure 2.28 Irrigation water demand for 2010 at specific sites in the Volta Basin 67
Figure 2.29 Existing dams and their capacity in the Volta Basin 69

Figure 3.1 Map of West Africa showing five bioclimatic zones 79
Figure 3.2 Overall procedure for assessing land- and climatic change interactions..... 86
Figure 3.3 Overall method for investigating the links between climate-land cover change..... 92
Figure 3.4 Study area 94
Figure 3.5 Maps of European Space Agency (ESA) land cover..... 98
Figure 3.6 WEAP model setup for Water-Energy-Food Nexus in the Volta Basin 102
Figure 4.1 Standard climatic indices for the five bioclimatic zones in West Africa 108
Figure 4.2 ESA CCI LC showing land cover changed pixels from 1992 and 2019..... 110
Figure 4.3 Annual variation of land cover change area 111
Figure 4.4 Standard climatic indices for the five bioclimatic zones in West Africa 114
Figure 4.5 Hovmöller plots for standardized climatic indices over West Africa 115
Figure 4.6 Changes in temperature, precipitation, and climatic water balance 118
Figure 4.7 Maps of temperature, precipitation, and climatic water balance changes..... 120
Figure 4.8 Area variation of land cover change over West Africa 122
Figure 4.9 Land cover transitions from 1992–2019 over West Africa..... 124
Figure 4.10 Maps of biogeophysical parameters 127
Figure 4.11 Validation of net radiation, sensible and latent heat fluxes..... 129
Figure 4.12 Validation of daily mean precipitation and temperature 131
Figure 4.13 Validation of rainfall and discharge over the Sissili-Kulpawn Basin (2010-2016). 133
Figure 4.14 Climatology evaluation of water and energy fluxes over the Sissili river basin..... 136
Figure 4.15 Climatology evaluation of water and energy fluxes..... 138
Figure 4.16 Difference in radiation and heat fluxes 140
Figure 4.17 Difference in water fluxes 142
Figure 4.18 Difference between reference and land cover change experiments 145
Figure 4.19 Monthly climatology of water flow change over the Sissili river basin..... 149
Figure 4.20 Monthly climatology of water flow change over the Kulpawn river basin..... 152
Figure 4.21 Calibration and validation of WEAP setup simulated discharge 157
Figure 4.22 Validation of simulated discharge and dam storage in the Volta Basin..... 158
Figure 4.23 Water demand estimate based on population growth..... 160
Figure 4.24 Water demand estimate based on Share Socio-economic Pathways..... 161

Figure 4.25 Changes in water demand at WEF nexus sites 162
Figure 4.26 Change in annual mean temperature over the Volta Basin 164
Figure 4.27 Change in annual total precipitation over the Volta Basin 166
Figure 4.28 Change in water demand under climate, population growth and land use change.. 169
Figure 4.29 Mean monthly change in water demand 170
Figure 4.30 System hydropower generation in the Volta Basin of West Africa 175
Figure 4.31 Climatology of change in system hydropower generation for various scenario 176

CHAPTER 1 – INTRODUCTION

1.1 Context

Climate and land interact with each other in a two-way loop. Climate variability and change impact land through changes in global air surface temperature, changes in aridity, climate change influence on food security, climate-driven changes in terrestrial ecosystems, climate extremes and their effects on land functioning, impacts of heat extremes and drought on land, changes in heavy precipitation, and impacts of precipitation extremes on different land cover types (Jia et al., 2019). On the other hand, land impacts climate and weather through changes in biophysical and greenhouse gas effects (Jia et al., 2019). Through the combined effects of land use and land cover change (LULCC), global and regional climate are strongly influenced by both geophysical and biogeochemical processes (Liu et al., 2016). Land use changes alter the energy balance and the surface radiative budget by altering the surface albedo, which generates radiative forcing, impacting the regional and global climate (Zhao et al., 2021). Research has shown that a negative radiative budget caused by albedo could cool the Earth's surface while a positive radiative forcing could warm it (Zhao et al., 2021). In tropical areas, deforestation is suggested to exacerbate climate warming by reducing evapotranspiration (Bonan, 2008; Bounoua et al., 2002; Zeppetello et al., 2020; Zhao et al., 2021). In West Africa (WA), climate change and variability have impacted and continue to impact land cover by changing the timing and amount of water available for vegetation cover (Cotillon & Tappan, 2016). Land use decision-making responds to these changes in ways that further alter land cover, from slight modifications to land cover quality to drastic transformations of the land cover type (Cotillon & Tappan, 2016). Global climate and regional climate modeling have the longest-standing history of helping humans understand the interactions between the atmosphere and the land surface (e.g. Polcher and Laval, 1994; Robert Dickinson and Henderson-sellers, 1988). The preference between Regional Climate Models (RCMs) and Global Climate Models (GCMs) depends on the specific application and the spatial and temporal scales of interest. Regional Climate Models (RCMs) have a comparative advantage over Global Climate Models (GCMs) in regional studies because of their relatively high resolution, including a land surface model that helps to better simulate atmosphere-land surface interactions (Deng et al., 2014; Rummukainen, 2016). RCMs are often equipped with economic models that calculate land use

change demand based on economic activities, and a land surface model that calculates vegetation change resulting from climate change (Deng et al., 2014). With this inclusion, RCMs can simulate the impact of land cover change on various climatic factors such as precipitation, temperature, dew point, and radiation in West Africa (Achugbu et al., 2022a; Achugbu et al., 2022b; Diba et al., 2018; Sylla et al., 2016), considering critical drivers such as population growth, climate change and socioeconomic growth of the region (Cotillon & Tappan, 2016; Herrmann et al., 2020). However, the dynamic interactions between the climate and land cover change in WA are not fully understood using the RCMs for some reasons. Firstly, because of the unavailability of annual land cover timeseries data, RCMs makes use of one year of land cover data and keeps it constant throughout the simulations and thus neglects the dynamic interactions between the climate and the land surface conditions. While this may be justified because land cover does not change drastically from one year to the other, it is an oversimplification of the complex interactions between climatic changes and land cover changes (Dale, 1997; Gao & Liu, 2011). This oversimplification is embedded in most RCMs and hydrological models in WA often leads to inaccurate representation of the climatic effects of land cover change and its impact on the timing and availability of water resources from local to regional scale. Thus, a process in RCMs that can account for the dynamic interactions between the climate and land is required to improve it to simulate the timing and occurrence of wet and dry conditions. This is crucial for critical decision-making such as irrigation and predicting and adapting to extreme climatic conditions.

In the Volta Basin (VB) of West Africa, rainfall is stored as surface and groundwater, for domestic, industrial, agricultural, and energy production (hydropower) purposes. Effective RCMs and hydrological models used for decision-making in the VB must therefore simulate accurately the occurrence of water in space and time considering the economic and population growth and the ever-increasing demand for water. Previously, the water, energy, and food resources in the VB have been addressed based on the integrated water resource management principle which is water-centric (Amisigo et al., 2015; McCartney et al., 2012). In recent times, however, the water, food, and energy resources have been recognized to be intricately linked to each other, and therefore the need for a holistic approach to resource utilization and management with multiple stakeholders across various scales (global, continental, transnational, national, basin scale, local, and urban). This concept of interrelatedness and interaction of things and viewing natural resources as a system

of interconnected things rather than silo systems defines the nexus concept. Water-Energy-Food (WEF) nexus is therefore used in recent scientific literature to refer to the tight interconnection of water, energy, and food resources at a certain scale (McCarl et al., 2017; Molajou et al., 2021; Rasul & Neupane, 2021). Since the WEF nexus came to the limelight in 2011, the scientific research and publication in WA and the VB is scanty. Amuji, (2021) investigated the WEF nexus components interactions using spatial analysis in Ghana and Malawi, showing that the flooding mediated by hydropower increased in the White Volta Basin inundating groundwater points whereas there is an overlap between cropping areas and water points from 2000 to 2020 for both countries. Bruns et al. (2022) reviewed heterogeneous case studies in sub-Saharan Africa and noted that a more just nexus could be achieved by focusing on people and practices as it draws attention towards agency and change. Some studies also envisaged WEF nexus as the means to achieving sustainable Development Goals 2, 6, and 7 through increasing the reliability of water supply in line with SDG6, improving access to and use of renewable energy consistent with SDG7 and enabling digital technologies and irrigation in agriculture and operation for food preservation in line with SDG2 (Sanchez Santillano et al., 2022). Despite the progress made in WEF nexus research globally and across Africa, there is still a paucity of WEF nexus research in West Africa, particularly for important Basin like the Volta River Basin, where future climate change, socioeconomic development, and land use land cover change plays a crucial role in resource availability. Previous researches have used the Water Evaluation and Planning (WEAP) model to study the climate change effects on water availability for agriculture, hydropower, and domestic demand, however, they are based on (IWRM) which is water-centric (Amisigo et al., 2015; McCartney et al., 2012). Recent development in the WEF requires a multi-centic approach for resource management focusing concurrently on water, energy and food resources. In this respect, the WEF nexus implementation is crucial to achieving the multi-centric and cross-sectoral WEF resource management for sustainable development.

In the Sissili-Kulpawn Basin (SKB), there is a growing need for irrigation to increase food production in rural communities in line with Sustainable Development Goal 6 (SDG6), while increasing farmers' gains. This however comes with the conversion of land cover for food production. Akomeah et al. (2018) estimated the potential irrigable areas of about 28% of the entire Upper East Region (UER) which includes parts of the SKB. This could result in deforestation

which could have consequences on the local climate and water availability. RCMs prove potent in simulating the climatic effects of land cover change and the climatic-land-water-food interactions (nexus) such as the Sissili-Kulpawn project. This nexus can, however, improve greatly with an accurate representation of dynamic land-atmosphere or land-climate interactions in RCMs.

From the foregoing, RCMs and hydrological models play a crucial role in understanding the climate-land interactions in West Africa, as well as water resource generation for domestic, agricultural, industrial, and energy (hydropower). However, climate variability-land cover interactions which determine the water availability at a certain instance in space and time is not fully represented in RCM and hydrological models, and therefore require some modifications to mimic reality. In addition, there is scanty information on the current WEF nexus status of the Volta Basin and the potential impacts of population growth, climate change, and land use/land cover change. In context, investigating the interactions between climatic changes and land cover changes at annual timescales helps to understand the land use/land cover dynamics nexus to climate variability/climate change in West Africa. Similarly, the WEF nexus gap and the implications of future climate change, population growth, and socioeconomic conditions in the Volta Basin are required to understand the vulnerability of hydropower to climate change, and the impact of climate change on hydropower systems. Finally, the climate-land interactions implications for food production in the SKB provide an assessment of the impact of land use/land cover change on hydrology and hydrological cycle.

1.2 Problem statement

Past and ongoing research to understand the interactions between climate change/variability and land cover change in West Africa can be categorized based on the scale (regional, basin-wide, local) of the research and the approaches used (methods and models). RCMs, including the Regional Climate Model (RegCM), the Weather Research and Forecasting Model (WRF), and the hydrologically advanced version of the WRF model (WRF-Hydro), are mostly employed in the study of climate-land cover interactions in the West African region (Achugbu et al., 2022a; Achugbu et al., 2022b; Diba et al., 2018, 2019). Diba et al. (2018) investigated the potential impacts of land use/land cover change on Sahelian rainfall and showed that afforestation increases rainfall substantially over the Sahel with strong interannual variability. Odoulami et al. (2019)

investigated the effects of afforestation using WRF and RegCM and found that afforestation increases the total annual wet day precipitation but decreases consecutive dry days over the afforestation area which affects all the ecological zones in West Africa. Achugbu et al. (2022a) modeled the spatiotemporal response of rainfall, dewpoint, and temperature to three deforestation scenarios and found 41.5-44.7%, 0.8-1.1%, and -0.2-0.3% increases respectively. Similarly, Achugbu et al. (2022b) investigated the spatiotemporal effects of six land use types on rainfall, dew point, and air temperature over West Africa showing that while afforestation of the Sahel region increases rainfall due to enhanced ET, only the total afforestation scenario increased rainfall in the Sahel-Sahara interface, while deforestation of the Guinea zone reduced rainfall in the Sahel-Sahara interface and the entire West Africa. Achugbu et al. (2022a) and Achugbu et al. (2022b) highlighted the need for sustainable land management practices due to the strong influence of LULC on WA, also acknowledging that the effects of LULC change on precipitation are complex and in-depth analysis of the effects on major features of the general circulation of WA is needed. While the research above gives important information on how changes in land use/land cover could affect the climate of West Africa, none of the research provides how modeling of interannual variability of the West African climate is affected by dynamic land cover conditions or vice versa. At least there is no quantitative description of how a change in climatic conditions affects land cover conditions even though it is widely accepted that climate change has effects on land cover change at decadal and annual timescales (Cotillon & Tappan, 2016). Thus, most of the RCMs used changing climatic data but static land cover data, neglecting the dynamic effects of the climate on land cover changes in the simulation. This gap highlights the land use/land cover dynamics nexus to climate variability in West Africa. Understanding and quantifying this nexus will help modify existing RCMs and other models to incorporate peculiarities of the West Africa system. This will improve land-atmosphere parameterization in existing RCMs in WA in order to improve their accuracy in providing climate services for the region.

At the basin-wide scale, most of the research focuses on the water resource implications due to climate change/variability and land use/land cover changes. Within the Volta Basin in West Africa, the research areas encompass climate change impacts on hydrology and streamflow, land use land and cover dynamics, the impacts of land use and land cover dynamics on streamflow generation, water quality, and groundwater (Akpoti et al., 2016; Kabo-Bah et al., 2016; Koranteng et al., 2019;

Mensah et al., 2022; Obahoundje et al., 2017; Yangouliba et al., 2023). Yangouliba et al. (2023) employed machine learning algorithms and Markov Chain and the Multi-Layer-Perceptron neural network to assess the dynamics of current (1990, 2005, 2020) and future (2050) land cover in the Nakambe Basin. Koranteng et al. (2019) investigated the land use land cover dynamics under the African Plantations for Sustainable Development (APSD) which aims to slow down the advancement of desert into the transitional zone, and showed that over 20 years substantial increase in urban areas, agriculture lands, wood fuel harvesting and charcoal production, riverine forest and a decline in open woodland agriculture/grassland and settlement areas. Awotwi et al. (2016) and Tahiru et al. (2020) both investigated the implication of land cover dynamics on water quality and showed that land cover dynamics cause changes to water quality. Just like the regional scale, most of the research conducted on land use land cover dynamics in the Volta Basin does not provide insight or linkage with the interannual climate variability which is crucial for decision-making. Other studies like Akpoti et al., (2016) used the Soil Water Assessment Tool (SWAT) model to investigate the impacts of rainfall variability and land use land cover change on the Black from 2000 to 2013 and remarked that grassland decreased by 44.54% whilst the remaining land cover classes increased (7.62% for water bodies, 67.06% for bare land, 38.38% for evergreen forests, 29.66% for agricultural lands, 60.18% deciduous forests, 33.22% for urban areas). In terms of discharge, Akpoti et al., (2016) found that the seasonal discharge for wet and dry seasons increased by 1% and 6% respectively. Other studies used the SWAT model to investigate the hydrological impacts of climate change (Sood et al., 2013), streamflow response to different climate change scenarios (Abubakari et al., 2017, 2018; Kankam-Yeboah et al., 2013), impacts of land cover changes on water balance components (Awotwi et al., 2015), and groundwater estimation (Dekongmen et al., 2022). Again, while research conducted using the SWAT model provides useful insights into hydrology and streamflow response to climate change and land use/land cover changes, it provides very little insight into how climate variability is linked to the land cover changes observed. Moreover, these studies reveal that the SWAT model may have limited applicability for modeling agriculture production and hydropower and hence the link between water, energy, and food resources in the Volta Basin. The WEAP model provides the capability of investigating the links between agricultural, water demands and hydropower production and this has been used quite extensively in West African Basins (Amisigo et al., 2015; de Condappa et al.,

2009; McCartney et al., 2012; Mensah et al., 2022; Obahoundje & Diedhiou, 2022). McCartney et al. (2012) combined SWAT, WEAP, and the COSMO-CLM (COnsortium for Small-scale MOdelling-CLimate Model) to investigate the joint impact of climate change and greater water demand and show that annual hydropower generation will reduce by approximately 30% and annual irrigation demand will quadruple by the mid-century, while the technical performance of reservoirs at the end of the century will even greatly reduced. Amisigo et al. (2015) investigated the impact of climate change on water resources and agricultural development in the Volta basin and concluded that the demand for agriculture, hydropower, and municipal water demand cannot be met simultaneously under any of the scenarios used, including future scenarios, and therefore called for an evaluation of groundwater resource as an alternative to help achieve socioeconomic development. Mensah et al. (2022) assessed the present and future groundwater demands under changing climate and socioeconomic conditions for nine catchments in the Ghana section of the White Volta Basin, concluding that socioeconomic and climatic conditions will lead to a disparity between groundwater demand and supply with four out of the nine catchments will experience water scarcity under all future scenarios (RCP 4.5, RCP 8.5, SSP2, SSP3, and SSP5). Obahoundje et al. (2022) investigated the uncertainties regarding hydropower production in the Mono Basin under the combined effect of land use land cover change, climate change and socio-economic scenarios, and showed that changes in climate variables affected simulated water demand available for hydropower generation in the near-future and far future. The modeling and machine learning approaches in McCartney et al. (2012), Amisigo et al. (2015), and Obahoundje et al. (2017), and Obahoundje et al. (2022) were done without careful consideration of historical reservoir operations. As there are no calibration and validations of historical reservoir operations, the results are based on wet and dry scenarios which is purely an integrated water resource management approach and so do not have a strong basis for future hydropower prediction. Thus, for hydropower projections calibration and validation of the reservoir operations over a historical operation is critical to ensure the model mimics the historical operations before using it for future projections. Therefore, whilst these studies are sufficient from the IWRM point of view and help to envisage the future, they could be limited to application in practical application. Moreover, its application in the recent Water-Energy-Food nexus which intends to incorporate all three resources (water, food, and hydropower) at the same time is limited. The need for a WEF nexus model for the Volta-

Basin and other basins is thus eminent. So far, a study in the Volta Bain that comes close to developing a WEF nexus for the Volta Basin is de Condappa et al. (2009) who calibrated and validated the hydropower reservoir at the Akosombo dam and Bagre dams. de Condappa et al. (2009) combined a hydrological spreadsheet module and WEAP to create a Decision Support System for the Volta Basin which considers the impacts of hydropower development, irrigation from huge reservoirs, riverside irrigation, and livestock consumption, domestic for urban zones, and development of upstream reservoirs in Burkina Faso. Even though the tool showed a good performance in calibrating streamflow and hydropower reservoir, de Condappa et al. (2009) noted that the tool was parameterized and calibrated for the Basin with limited data on river flows and water uses, hence its utilization for a particular scenario may require further tuning with specific data. Furthermore, de Condappa et al. (2009) showed that the hydropower generation at Akosombo which remains sustainable up to the level observed in the late 1990s would only be sustainable in the wetter scenario. Socioeconomic development nearly 20 years after de Condappa et al. (2009) necessitates a reconsideration of the Volta Basin from a WEF nexus point of view where all demand sites are represented to build a WEF nexus model for the Volta Basin. The WRAP 2.0 RPT5 on renewable energy and GIA 1 and 2, which stresses the need to assess both the vulnerability of renewable energy systems to climate change and the impact of climate change on renewable energy systems expresses the WEF nexus gap that needs to fill this gap (see appendix).

Within the VB, the SKB is proposed for irrigation expansion to improve the livelihood of farmers in the region. Medium- to large-scale irrigation means converting large areas of land for irrigation, which implies more land use and more water requirements. However, the effects of land conversion on regional climate and whether enough water will be available for the project need to be investigated. This research gap is in line with RTP2 which is related to risk and vulnerability to extremes and GIA 12 which focuses on the impact of national adaptation strategies on local communities.

From the foregoing, there is no quantitative measure of how climate variability affects land cover change in existing regional climate models in West Africa, and hence a need to quantify these effects for parametrizing climate-land interaction effects in existing RCMs. Moreover, there is no existing WEF nexus model for the Volta, as previous models are often based on the IWRM

principles and do not accurately represent hydropower operations. Finally, the Sissili-Kulpawn Basin project is an irrigation project being pursued by the government of Ghana to improve conditions for the farmers of the SKB but there is no study on regional climate response to land cover changes associated with the project to evaluate if the project is worth pursuing. This thesis is thus designed in line with the above problems and specific WRAP 2.0 RPTs and GIAs to fill research gaps from the regional scale (WA), basin-wide scale (VB), and local scale (SKB).

1.3 Aim and Objectives

This thesis aims to assess the climate-land-water-energy-food interactions over West Africa with a specific focus on the VB and the SKB. The specific objectives are:

(i) to characterize the relationship between climate variability/extremes and land use/land cover change in West Africa using Remote sensing observations and reanalysis products.

(ii) to model the relationship between climate variability/extremes and land use/land cover change using a fully coupled land-atmosphere model.

(iii) to evaluate the future impacts of climate change, land use/land cover change and population growth on the WEF nexus components.

1.4 Research questions

The research questions that guide this study are:

(i) What is the relationship between climate variability and land cover change over West Africa from an analysis point of view?

(ii) What is the relationship between climate variability and land use/land cover change from a fully coupled land-atmosphere modeling point of view?

(iii) What is the future impact of climate change, land use/land cover change, and population growth on the WEF nexus components in the Volta Basin?

1.5 Motivation and Justification

It is well established that climate variability and change impact the land cover conditions in West Africa at annual and decadal timescales. However, the magnitude of the impact is hardly quantified resulting in an incomplete understanding of the linkage between climate variability and land use

land cover change in the region. RCMs in the region have this inherent limitation as they often treat land cover as a static component of the climate systems while the atmospheric component is treated as a dynamic system. While this practice might be arguably correct and the usual practice in climate modeling and hydrological modeling, a more realistic approach that takes into account dynamic land cover change needs to be considered. That said, dynamic land cover change modeling also means higher computational cost and simulation period which may attract rejection from the regional climate modeling community. In place of dynamic land cover data in RCMs, a dimensionless climate-land variability index might be necessary to account for the dynamic interactions between the land surface and the atmosphere when static land cover datasets are being used. The motivation of this thesis is thus to investigate and understand the relationship between climate variability/extremes and land use land cover change from satellite and reanalysis datasets, and subsequently use it to develop a climate-land cover change variability index to account for the dynamic interactions between the climate and land cover change in the region. Optimally, it could be more useful to improve the parameterization of the atmosphere-land cover change interactions in the region and also evaluate future impacts of climate change on the WEF components to guide policymakers.

1.6 Outline

This thesis is organized into six (6) chapters. Chapter 1, presents the context, the problems, the aim and objectives, the motivation and justification, and the outline of the thesis. Chapter 2 presents a systematic literature review of land-atmosphere or climate-land interactions and water-energy-food nexus from the global scale, through Africa, West Africa to the Volta basin. Chapter 2 also presents the factors influencing water-energy-food nexus including climate, socioeconomic conditions, population, water use, water abstraction for irrigation, and hydropower generation in the Volta Basin. Chapter 3 presents the study area, data, and analysis method of investigating the relationship between climate variability and land cover change, and then the modeling approach to investigating the relationship between climate variability and land cover change. Chapter 3 also presents the modeling of the WEF nexus in the Volta Basin. Chapter four (4) presents and discusses the results on climate variability and land use and land cover change relationship, and the status of the WEF nexus under land cover change, climate change, and population growth scenarios.

Chapter 5 summarizes and concludes the findings of the thesis. Chapter six outlines the recommendations and directions for future research.

CHAPTER 2 – LITERATURE REVIEW

2.1 Introduction to literature review

The literature review includes a systematic review of land-atmosphere interactions and the WEF nexus, which included identifying the methods and models in land-atmosphere and WEF nexus research, the land cover datasets used, the research trends and the WEF nexus system in West Africa and the Volta Basin. To fully comprehend the impact of climate variability and change on the WEF nexus, it was necessary to decompose the topic into bits and understand the trend in research globally. A systematic literature review was used to investigate the land-atmosphere/climate-land interactions from 1990 to 2024 and the WEF nexus from 2011 to 2024. The literature review analyzes topics, abstracts, and keywords to identify methods and models for investigating land-atmosphere/climate-land interactions and the WEF nexus. Land-atmosphere/climate-land interaction models with hydrological modeling capabilities and WEF nexus capabilities were identified. Specific model selection and approaches for the thesis are also outlined based on the literature review. The trend of WEF nexus from global, Africa, West Africa, and the VB was investigated with specific case studies. Finally, a specific focus on the WEF nexus in West Africa and the Volta Basin was reviewed, including the current water, energy, and food systems and the socioeconomic activities in the Volta Basin. The literature review also included an analysis and selection of land cover dataset suitability for the thesis. Sections 2.2 to 2.14 give details on the literature review. Section 2.15 concludes briefly on important information derived from the literature review.

2.2 Literature selection

A systematic review approach of articles obtained from the Scopus database served the purpose of literature review. For initial investigations, a Boolean search with keywords including “land”, “atmosphere”, “climate”, and “interactions” in their various combination was used to extract articles from the Scopus database. Figure 2.1 shows the literature review approach and model selection process for investigating land-atmosphere interactions and water-energy-food nexus modeling. A total of 1301 articles were retrieved spanning from 1990 to 2024 (Figure 2.2). Of these articles, 1156 (88.9%) are journal articles, 59 (4.5%) are conference papers, 45 (3.5%) are

reviews, 22 (1.7%) are book chapters, 6 (0.5%) are data papers, 4 (0.3%) are editorial, 4 (0.3%) are letters, 2 (0.2%), 2 (0.2%) are notes and 1 (0.1%) is a conference review (Figure 2.3). In terms of subject areas, the articles cover from Earth and Planetary Sciences to Neuroscience as shown in Figure 2.4. The Journal of Climate has the most published articles 189 (16.1%), followed by the Journal of Geophysical Research with 75 (6.4%), the Journal of Applied Meteorology with 64 (5.5%), and Geophysical Research Letters with 55 (4.7%) (Figure 2.5). In terms of continents, Africa the has least publication of 29 (1.3%) on land-atmosphere interactions, while North America has the highest publication of 796 (36.7%) (Figure 2.6). United States has the most published articles 731 (33.7%), followed by China, Germany, and the UK with 352 (16.2%), 132 (6.1%), and 91 (4.2%) respectively. The remaining journals have less than 38 (3.2%) published articles on the subject. To determine the historical evolution of methods used in the land-atmosphere interaction research, the title, abstract, and keywords of the selected articles were analyzed according to three different timelines 1990–2000, 2001–2015, and 2016–2024. A word cloud was used to determine the method and central theme in the land-atmosphere interaction discourse, after excluding the keywords used in the search. The word cloud analysis revealed that "model (modeling)" is the most used approach in investigating the land-atmosphere interactions between 1990-2024 (see Figure 2.7). The word cloud analysis for the 1990–2000, 2001–2015, and 2016–2024 also reveals that modeling is the most used approach for investigating the interactions between the atmosphere and the land surface (Figure 2.8). The Global Circulation models (GCMs) (Arjdal et al., 2024; Dee et al., 2015; Koster et al., 2016; Matsumura et al., 2010; Mohino et al., 2011; Yamada et al., 2013; Yoshida et al., 2015), coupled Atmospheric Ocean General Circulation Model (AOGCM), Ocean-Land Atmospheric Models (OLAM) (S. Liu et al., 2023; Medvigy et al., 2013), Regional Climate Models such as RegCM, Regional Model (REMO), fifth-generation Canadian Regional Climate Model (CRCM5), Regional Models participating in the Coordinated Regional Climate Downscaling Experiment (CORDEX) project, and Weather Research and Forecasting Model (Daloz et al., 2022; Diro & Sushama, 2017; García-García et al., 2020, 2022; Lodh, 2020; Mooney et al., 2020, 2022; Tamoffo et al., 2022) have played crucial roles in the land-atmosphere interaction research. The majority of the articles reviewed focused on the interaction of the land-atmosphere, ocean-land-atmosphere, or land-ocean interactions using individual models or coupling various models. For this work, hydrological modeling is a crucial part, so the

literature search above was further screened to land-atmospheric interaction models with hydrological modeling capabilities. The results show only two models: Rainfall-Runoff Inundation for estimating river discharge and flood inundation risks (Bhagabati & Kawasaki, 2017), and the hydrological enhanced version of the Weather Research and Forecasting Models which has been used in some studies for West Africa and the Volta Basin (Bliefernicht et al., 2013; G. Li et al., 2021; J. Yang & Wang, 2014; Z. Zhang et al., 2019).

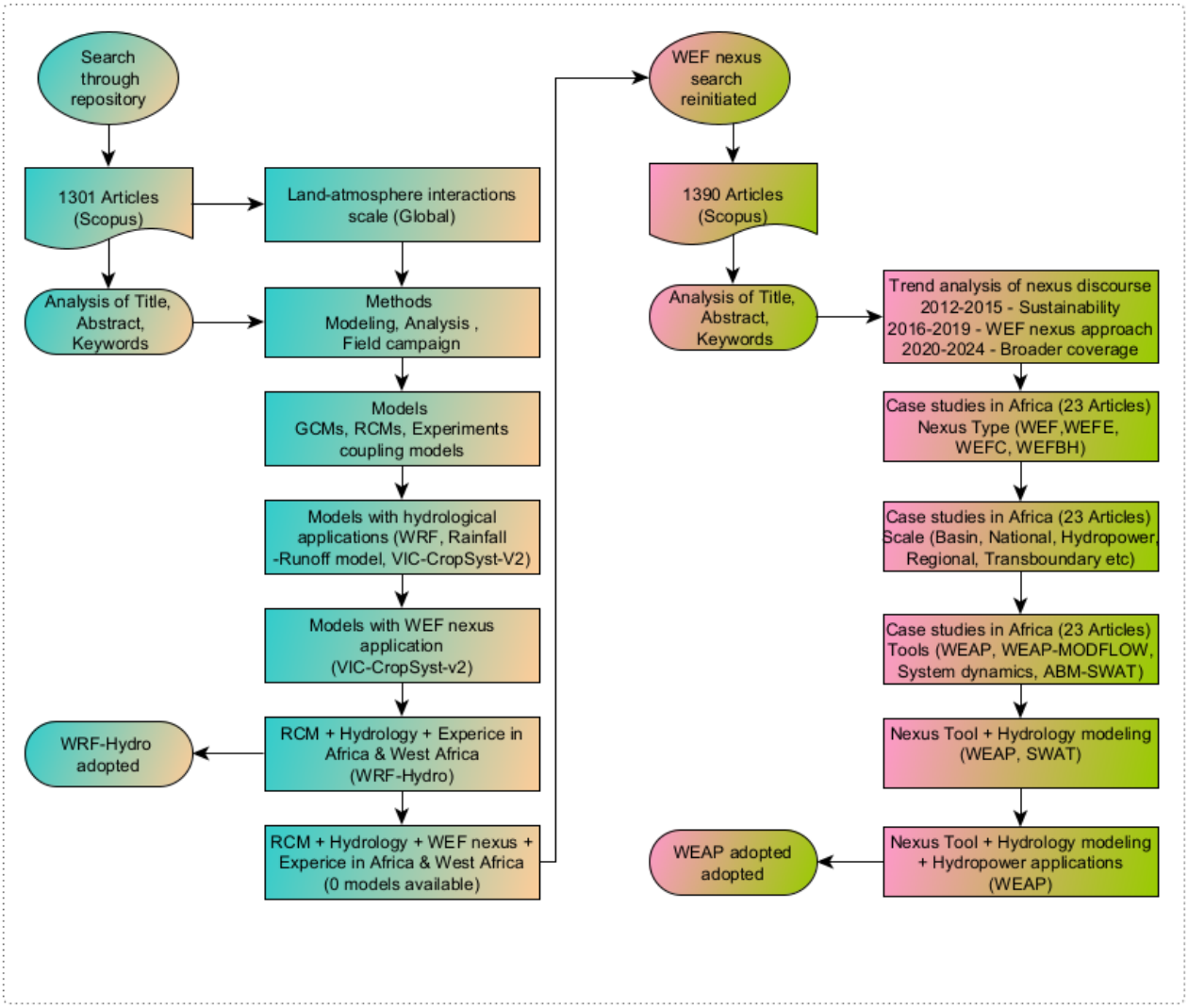

Figure 2.1 Approach to literature review and model selection process for land-atmosphere interactions and water-energy-food nexus modeling

Based on this literature review, the WRF-Hydro model was adopted for aspects of this thesis which aims to assess the interactions between the atmosphere-land surface changes and evaluate its implication for regional and local climate. The next sections review trends of land-atmosphere interaction research in Africa and then focus on WRF and WRF-Hydro publications in land-atmosphere interaction research, especially with land use and land cover changes which is a crucial part of this work.

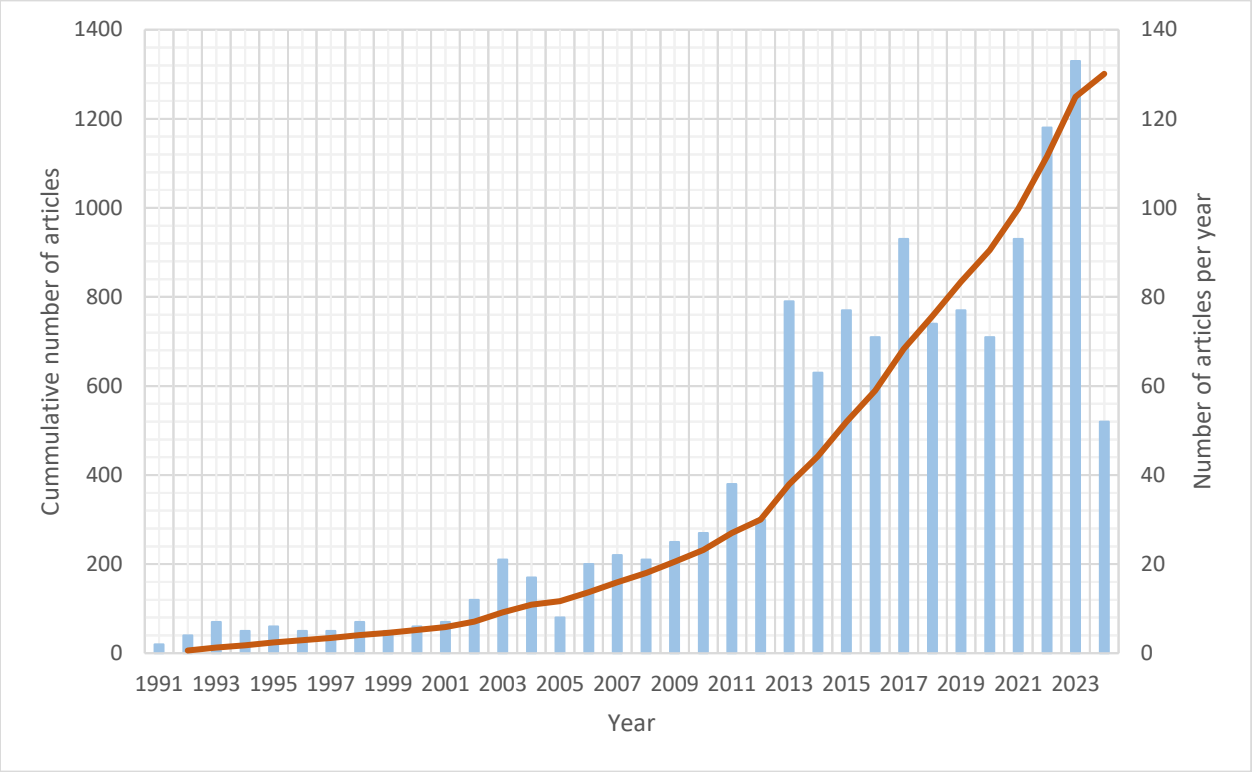

Figure 2.2 Number of articles published between 1990 and 2024. The bar graph shows the number of articles published per year while the line graph shows the total number of articles published over time.

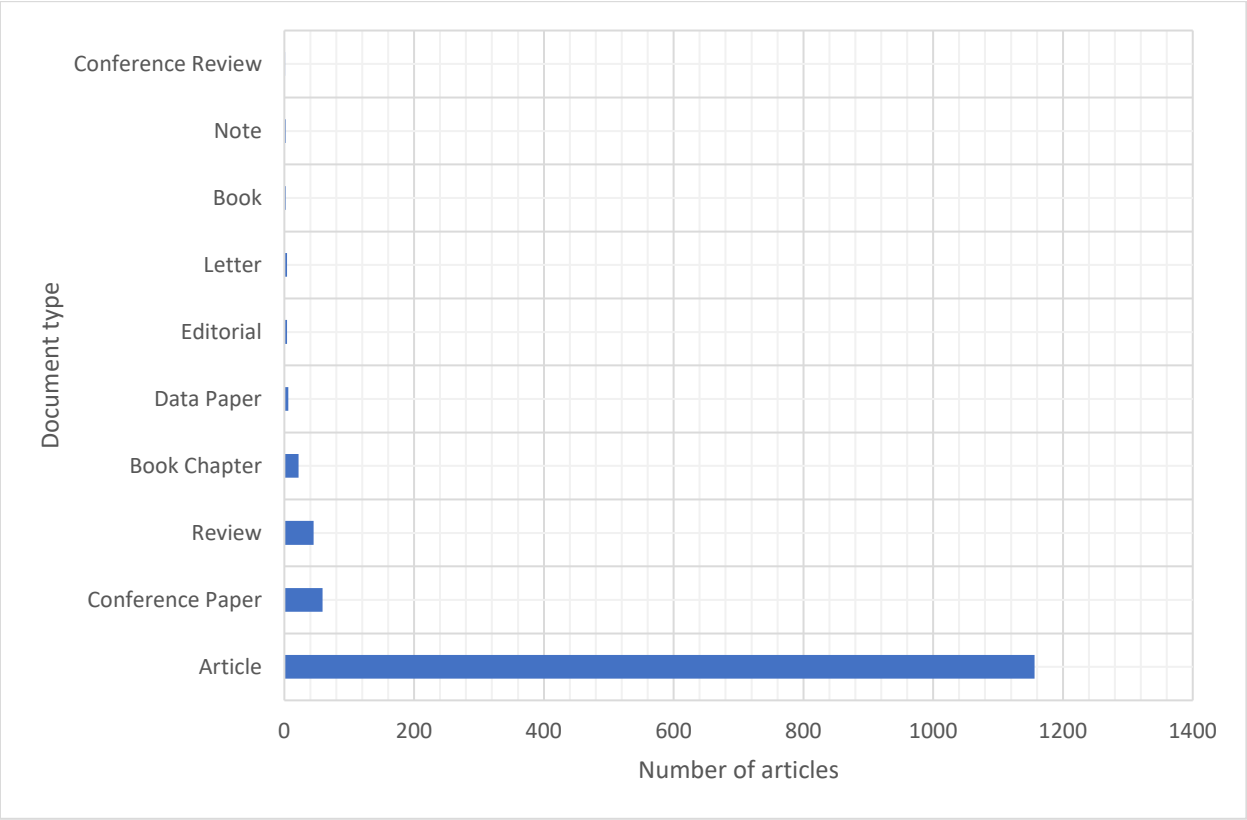

Figure 2.3 Number of articles classified by the type of document

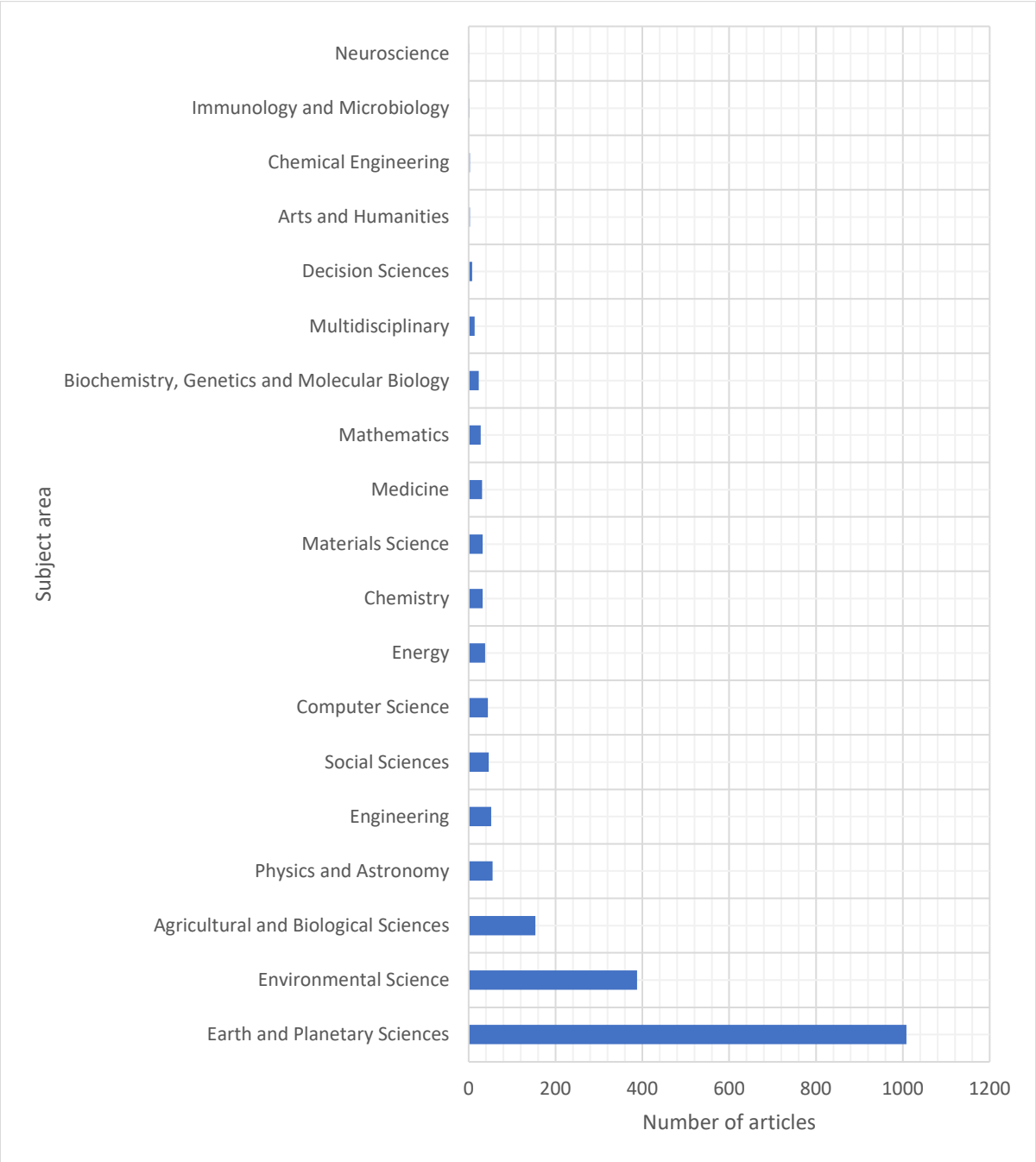

Figure 2.4 Total number of articles classified according to the subject area

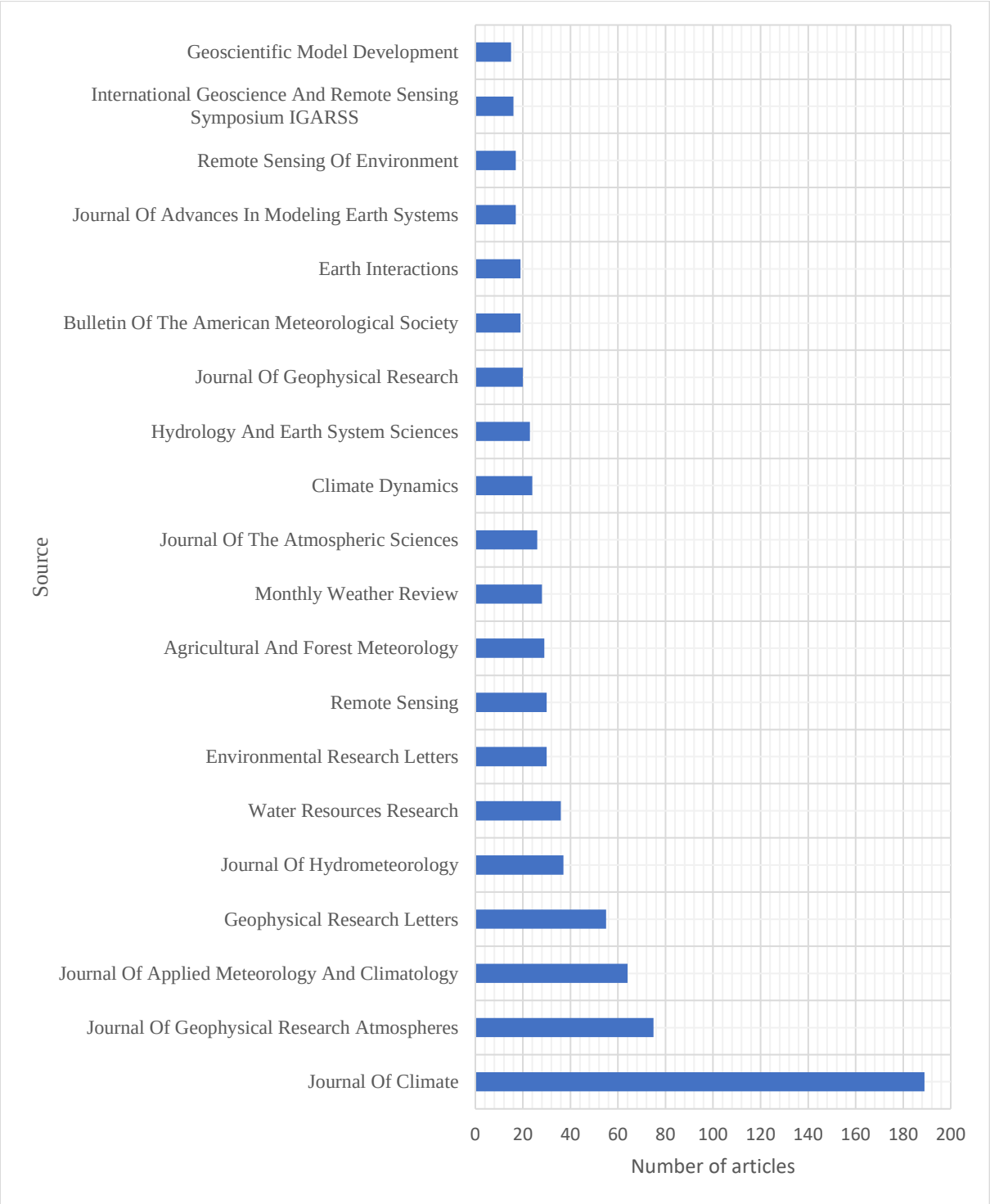

Figure 2.5 Total number of articles classified according to source (Limited to the first 20 sources).

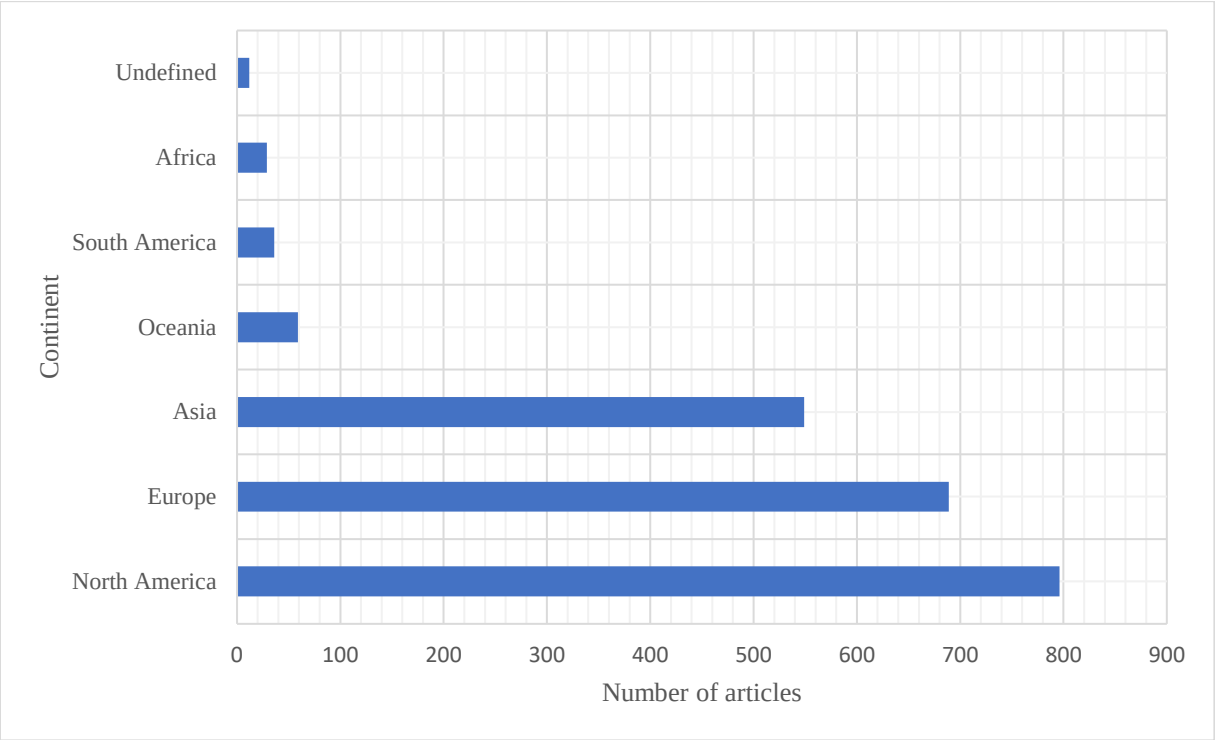

Figure 2.6 Total number of articles classified by continents

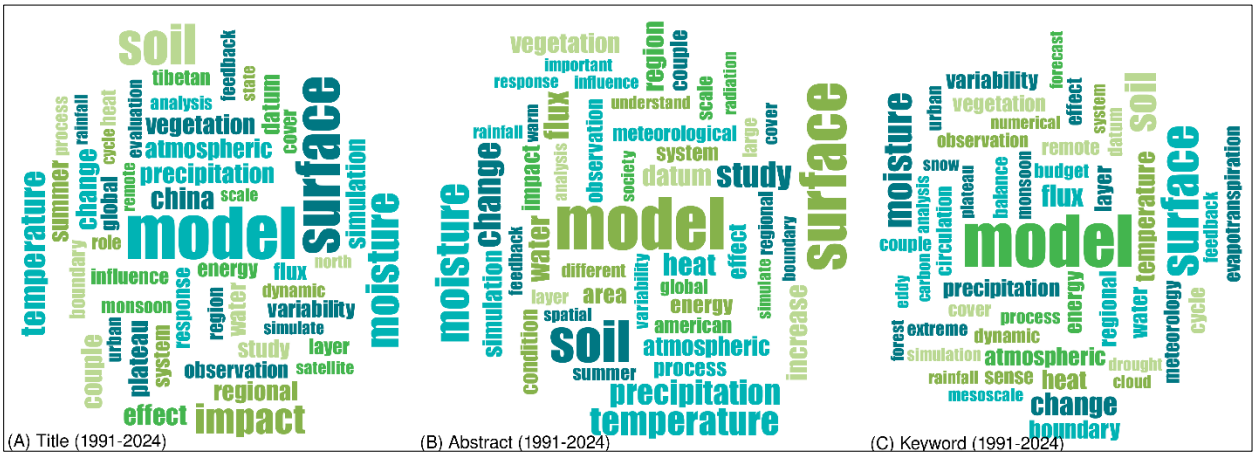

Figure 2.7 A word cloud analysis of (a) title, (b) abstract, and (c) keywords of 1301 documents retrieved from 1990 – 2024

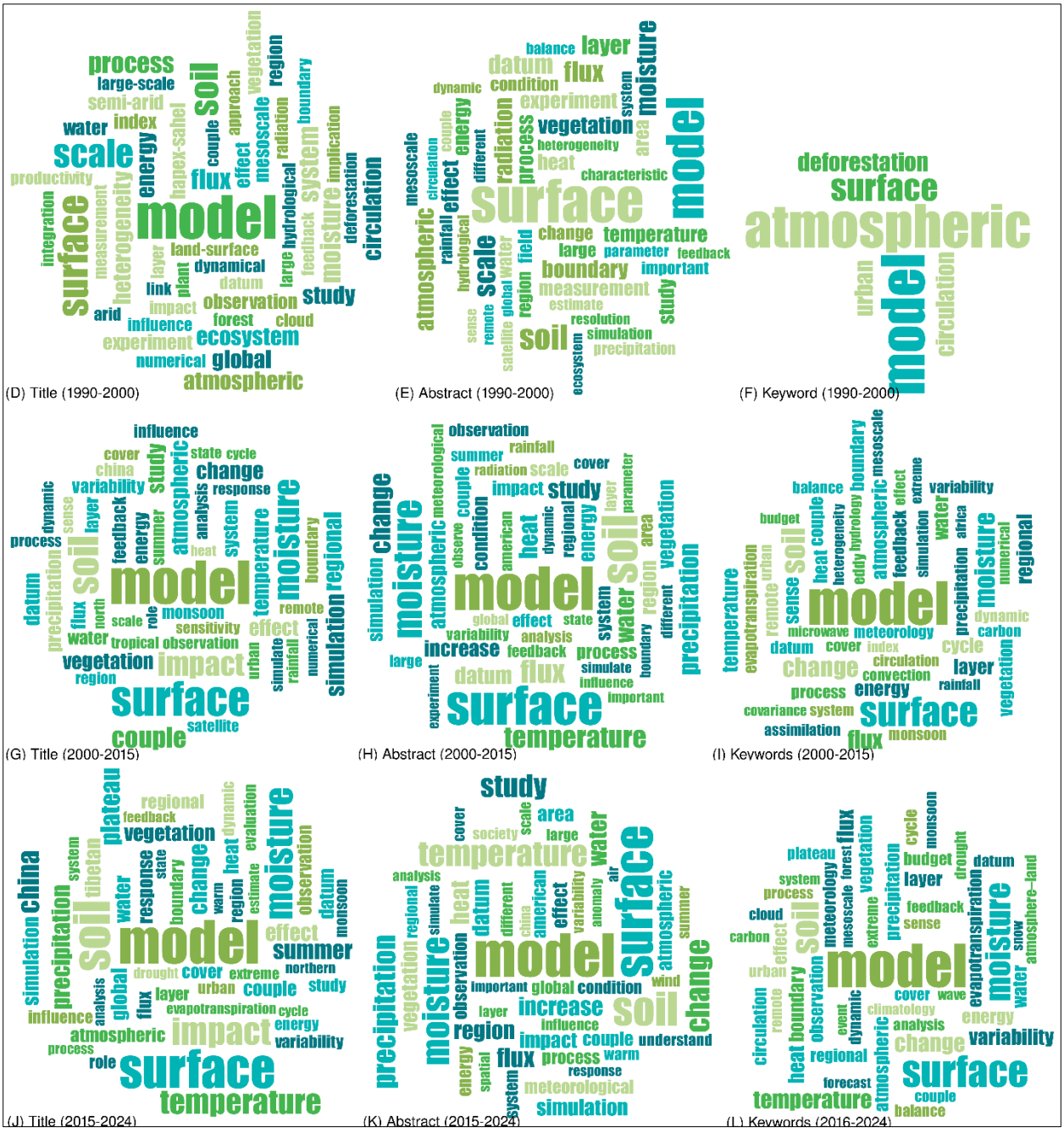

Figure 2.8 A word cloud analysis of (a) Title, (b) Abstract, and (c) Keywords of 52 articles published between 1990 – 2000; (d) Title, (e) Abstract, (f) Keywords of 782 articles published between 2001 – 2015; (g) Title, (h) Abstract, (i) Keywords of article 467 articles between 2016 – 2024.

2.3 Land-atmosphere interaction research in Africa – Trends, models, and methods

Early research in climate-land/land-atmosphere interactions in Africa focuses on understanding the interactions between the land surface and the atmosphere by performing a sensitivity analysis of rainfall to the land surface using global circulation models (GCM) (Goutorbe, 1993). Other works attempted to improve land surface schemes and compare the results of such improvements with existing parameters (Taylor & Clark, 2001), including assessing the effects of tropical forest removal on rainfall using a coupled atmosphere-biosphere model (Snyder et al., 2004). Regional campaigns such as the Southern African Regional Science Initiative (SAFARI 2000), ECOlogical CLIMate MAPping I (ECOCLIMAPI) and ECOlogical CLIMate MAPping II (ECOCLIMAPII) were to support the modeling of land-atmosphere interactions (Kaptue Tchuente et al., 2010; Swap et al., 2003). While the SAFARI 2000 campaign was a land surface, space-borne, and air-borne campaign to address land-atmosphere interactions and the biogeochemical functioning of the southern African system, the ECOCLIMAPI and ECOCLIMAPII were field campaigns developed within the framework of the African Monsoon Multidisciplinary Analysis (AMMA) program to support the modeling of the land-atmosphere interactions over West Africa through the provision of physiological parameters such as albedo, land cover classification, leaf area index, and fractional vegetation cover (Kaptue Tchuente et al., 2010; Swap et al., 2003). Other researches on land-atmosphere interactions in Africa focus on the analysis or the evaluation of regional climate model (RCM) outputs with observational data products (Krähenmann et al., 2013; Mohino et al., 2011; Tamoffo et al., 2022). The GCMs, coupled earth system models with statistical validation, RCMs, and Atmospheric Regional Climate Models (AGCM) have all contributed to understanding the land-atmospheric research in Africa (Berg et al., 2017; Goutorbe, 1993; Yu et al., 2018). The coupling of atmosphere and biosphere models (Snyder et al., 2004), RCM with Australian Town Energy Budget (ATEC) (Maisha et al., 2023), RCM with irrigation model (Marcella & Eltahir, 2014), have been used to study the effects of deforestation, urban heat island, and irrigation simulations respectively. Mohino et al. (2011) assessed the impacts of oceanic anomalies on West African climate by identifying when the SST anomalies in the Pacific/Indian Oceans during spring and summer seasons, were significant. Olson et al. (2008) proposed the methodological framework to quantify the two-way interactions between land use and regional climate systems in East Africa, using ongoing work by a team of multi-disciplinary scientists examining climate–land

dynamics at multiple scales. Davis et al. (2015) used the Weather Research and Forecasting Model (WRF) to describe the structure, variability, and regional connectivity of the Tokar Gap jet (TGJ). The WRF model has also been employed to the urban effects on precipitation by investigating the city-EP interactions (Doan et al., 2023). Table 2.1 summarizes GCMs, RCMs, AGCMs, and coupled RCMs that have participated in the land-atmosphere interaction research in Africa. Amongst the models in Table 2.1, WRF provides numeric modeling capabilities with an immense description of various interactions of the Earth system's physical, chemical, and biological characteristics and is thus adapted for some aspects of this study. Aside from using GCMs and RCMs to investigate the land-atmosphere or climate-land interactions, some studies have tried to establish a link between a land surface parameter and atmospheric components using land surface and atmospheric data products. For instance, Saha et al. (2016) analyzed satellite-observed MODIS fire data and satellite TRMM precipitation data to understand the impact of wildfire on local precipitation. Saha et al. (2019) analyzed MODIS burnt areas and MODIS black sky albedo products to account for albedo anomalies induces by wildfires greater than 1 km^2 in sub-Saharan Africa. Feldman et al. (2022) analyzed land surface temperatures (LST), CHIRPS precipitation product, and SMAP soil moisture product to determine why land surfaces show varying responsiveness to environmental forcing, and to establish if regions with the largest land surface variability necessarily have the most variable environmental forcing. Keys et al. (2022) also examined the annual and seasonal changes in moisture sources and sinks using MERRA 2 reanalysis data and the Water Accounting Model 2. Thus, it is common to see a direct analysis of land surface parameters such as LST, soil moisture, albedo, and burnt areas, and atmospheric parameters such as precipitation from reanalysis, satellite-based products, and satellite merged with observations, in the attempt to establish links between the surface component and atmospheric component in land-atmospheric interaction studies. In this work, the analysis will be used to complement the modeling approach with WRF.

Table 2.1 Land atmospheric interactions research over Africa

Study	Aim	Model	Method
Yu et al. (2018)	To present the capabilities of GEFA as a multivariate statistical tool for extracting vegetation feedback to the atmosphere in either observations or coupled Earth system models	Community Earth System Model (CESM)	Modelling + Statistical analysis
Doan et al. (2023)	Investigate the urban effects on extreme precipitation through city-EP interaction	WRF	Modeling
Davis et al. (2015)	To describe the structure variability, and regional connectivity of the Tokar Gap jet (TGJ) in summer 2008	WRF	Modeling + supporting atmospheric datasets from the East African–Red Sea–Arabian Peninsula (EARSAP)
Hilland et al. (2022)	To investigate three-dimensional surface layer turbulence and the spatiotemporal patterns of heat transfer between the subsurface, surface, and atmosphere	Field campaign	A novel combination of instruments was used to simultaneously measure variables and processes relevant to heat transfer.
Goutorbe, (1993)	To introduce a land surface scheme with an improved description of sparse vegetation cover which characterizes the Sahel and compare the results with simulations using existing parameters.	General Circulation Model (GCM)	Sensitivity analysis of the land surface to rainfall at short time-scales in a general circulation model (GCM)
Keys et al. (2022)	To examine the annual and seasonal changes in moisture sources and sinks	MERRA-2 Water Accounting Model 2	Climate reanalysis and the Water Accounting Model 2 layers
Snyder et al. (2004)	To present a new moist static energy budget method for examining the regional atmospheric response to removal of tropical forests and how land surface forcing is propagated into the atmosphere	Coupled atmosphere-biosphere model (Community Climate Model, Version 3–Integrated Biosphere Simulator (CCM3-IBIS))	Coupled regional climate modeling
Kaptue Tchuente et al. (2010)	To present the ECOCLIMAP-II database for Western Africa, which is an upgrade for this region of the former initiative, ECOCLIMAP-I, implemented at global scale.	land-atmosphere interactions	Updating of the ECOCLIMAP-I database
Krähenmann et al. (2013)	To evaluate daily maximum and minimum 2-m temperatures as simulated with the Regional Climate Model COSMO-CLM over Africa.	Regional Climate Model (COSMO-CLM)	Regional climate modeling
A. Chen et al. (2019)	To examine global moisture-air temperature coupling based on monthly air temperature anomalies and the Gravity Recovery and Climate	Model dataset including ERA-Interim	Coupling GRACE TWS and precipitation to explain temperature variability and then applying discrete wavelet decomposition

	Experiment (GRACE) terrestrial water storage (TWS).		
Z. Zhang et al. (2023)	To investigate the simulated land-atmosphere interactions in southern Africa in the context of the uncertainties from applying different global soil datasets.	Coupled Weather Research and Forecasting Hydrological Modeling system (WRF-Hydro)	Model simulations (quantifying model's internal variability + comparing the modeling results)
Tamoffo et al. (2022)	To identify those from SST anomalies in the Pacific/Indian Oceans during spring and summer seasons, when they were significant	4 AGCM ("ARPEGE, version 3", "ECHAM4" ,"LMDZ4" , "UCLA 7.3")	Idealized sensitivity experiments
Olson et al. (2008)	To quantify the two-way interactions between land use and regional climate systems, using ongoing work by a team of multi-disciplinary scientists examining climate–land dynamics at multiple scales in East Africa	Regional Atmospheric Modeling System (RAMS) version 4.4	Regional climate modeling
Marcella & Eltahir, (2014)	To introduce an irrigation scheme to a regional climate model in West Africa	Integrated Biosphere Simulator (IBIS), coupled to version 3 of the Regional Climate Model (RegCM3-IBIS)	Couple modeling
Saha et al. (2019)	To present the first object-based accounting of albedo anomalies induced by larger (>1 km^2) individual wildfires in sub-Saharan Africa	MODIS burnt areas, and MODIS black sky albedo products	Analysis of modeled products
Kumar et al. (2013)	To assess LU change impacts that can be applied to common "all-forcings" experiments and does not require single-forcing LU change experiment	Analysis of 16 CMIP6 model datasets	Proposed methodology
Mohino et al., 2011)	To highlight misleading mechanisms in models that lead to errors in rainfall climatology	REMO 2015, REGCM4v7	process-based evaluation
Feldman et al. (2022)	To determine why land surfaces, show varying responsiveness to environmental forcing by asking if regions with the most variable environmental forcing are necessarily the regions with the largest land surface variability	Analysis of LST, CHIRPS, SMAP datasets	Analysis of LST, CHIRPS, SMAP soil moisture, and solar radiation
H.-Y. Ma et al. (2013)	To evaluate the impact on tropical climate of continental-scale perturbations given by different representations of land surface processes (LSPs) in a general circulation model that includes atmosphere– ocean interactions.	GCMs	Comparative analysis of different vegetation model ("simple land scheme" vrs "Simplified Simple Biosphere Model")

(Smiatek & Kunstmann, 2023)	To investigate characteristics of mean precipitation due to proposed land-use changes to woody savannah with three hypothetical courses of the GGW, with an area between 0.8 and 1.25 million km^2, and between the 100- and 400-mm isohyets	MPAS	Regional Climate Modeling
Pietschnig et al. (2021)	To understand the projected amplification of precipitation decreases over the Amazon basin and increases with warming over the Maritime Continent seen in Earth system models in response to plant physiological changes	Atmospheric GCM	Modeling
F. Li & Lawrence, (2017)	To provide the first quantitative assessment and understanding about the influence of fire on the global land water budget due to changing terrestrial ecosystems during the twentieth century.	Community Earth System Model (CESM)	Modeling
Maisha et al. (2023)	To evaluates the performance of the Conformal Cubic Atmospheric Model (CCAM) when simulating an urban heat island (UHI) over the city of eThekwini, located along the southeast coast of South Africa	CCAM-ATEB	coupled modeling CCAM-ATEB
Berg et al. (2017)	This study focuses on the large-scale influence of soil moisture variability on the mean circulation and precipitation in the West African monsoon.	Global Land–Atmosphere Coupling Experiment (GLACE)-CMIP5	Coupled Modeling
Saha et al. (2016)	To understand the impact of fire on local precipitation	MODIS fire data and TRMM climate data	Analysis of satellite observations (MODIS) and TRMM
Taylor & Clark, (2001)	The strong variability exhibited by fluxes from the land surface into the atmosphere over the Sahel using a GCM.	GCM	Comparism of an improved land surface scheme + simulations using existing parameters
Mitchard & Flintrop, (2013)	To analyze deforestation by reviewing 16 articles where woodland dominates and supplementary the literature review by NDVI analysis	NDVI analysis	Literature review and analysis of NDVI

2.4 The Weather Research and Forecasting Model (WRF)

The Weather and Research Forecasting model (WRF) developed in the early 1990s is one such numerical weather prediction system designed to serve both operational forecasting needs and atmospheric research. The WRF model is a highly flexible and versatile model that can be configured for a wide range of applications, from simulating weather from local to regional and

global scales. WRF is often used by meteorologists, researchers, and forecasters for a wide range of applications including weather forecasting, climate research, air quality research, hydrological applications, renewable energy assessment, aviation weather, extreme weather events, agricultural applications, ocean-atmosphere interactions, etc. The capabilities of WRF are further enhanced by coupling with various models to simulate complex interactions within the Earth System. WRF can be coupled with chemistry modules (WRF-Chem) to simulate the transport, transformation, and deposition of pollutants and atmospheric constituents including aerosols, gases, and chemical species (Fang et al., 2023; Lu et al., 2019, 2021; J. Wang et al., 2022; Xu et al., 2018; H. Zhang et al., 2014; J. Zhang et al., 2020). WRF-Land surface model couples the WRF and land surface models to simulate biogeochemical and biogeochemical processes at the land-atmosphere interface, improving the representation of surface energy and water fluxes for better climate and weather simulations. The WRF-Fire models couple WRF with fire models to simulate wildfire behavior and smoke dispersion which are critical for wildfire forecasting, air quality monitoring, and management. WRF-Ocean model couples WRF and ocean models to simulate interactions between air and sea, including the exchange of heat and moisture, between the atmosphere and the ocean. The WRF-Wave model couples WRF to wave models to simulate the generation, propagation, and dissipation of ocean waves driven by atmospheric forcing, useful for understanding climate variability, marine forecasting, and coastal engineering. WRF can also be coupled with hydrological modules to simulate the interaction between the land surface, and the atmosphere, including streamflow, runoff, soil moisture, and moisture dynamics. This ability of WRF to simulate regional-scale processes, responses, and feedback across different parts of the Earth's System is its main advantage over most RCMs and is also the reason for its selection in this work. The WRF-Hydro modules also include critical extensions for hydrological forecasting, the study of climate impacts on water resources, and water resource management. Based on the literature the review discussed above, the WRF-Hydro model which is a coupling of WRF with a hydrological module is most suitable and therefore adapted for some aspects of the land-atmosphere interaction studies in this work. A review of the WRF-Hydro for atmospheric-hydrological research and regional effects of land use land cover is presented below.

2.5 The fully-coupled atmospheric hydrological WRF-Hydro model

Recent advancements in hydrometeorological modeling aimed towards a more sophisticated treatment of terrestrial processes by including a lateral flow in the default WRF model led to a hydrological enhanced version of the WRF regional climate model; the WRF-Hydro modeling system. The WRF-Hydro has been shown in most cases to have similar or even improvements in atmosphere-terrestrial water balance studies (Arnault et al., 2016; Arnault, Fersch, et al., 2021a; Rummler et al., 2019) compared to the default WRF regional climate model. Specific applications include streamflow simulation (Achugbu et al., 2022b), different flood event simulation (Cerbelaud et al., 2022; Dixit et al., 2019), urbanization impacts on underground water (Pasquier et al., 2022), water budget estimations (Somos-Valenzuela & Palmer, 2018), projecting future drought events based on land cover change and climate regimes (Lee et al., 2020), quantifying surface energy fluxes and their cycles (Mercer & Dyer, 2021; Xiang et al., 2017), and regional climate response to afforestation in (Arnault et al., 2023). For instance, Fersch & Kunstmann (2014) showed that including the influence of saturated zone in the WRF with default LSM could result in an increase in 20% of volumetric soil content of the soil, by 6 to 67mm for the surface runoff, and by -10 to 75% for transpiration. Arnault et al. (2016) and Kerandi et al. (2017) also found WRF-Hydro suitable for the potential joint atmosphere-terrestrial water balance for the Sissili and Tana basins in western and eastern Africa respectively. In other studies, the WRF-Hydro is found to increase the water recycling rate indicating its lateral terrestrial flow influences regional climate (Z. Zhang et al., 2019). In some other studies, WRF-Hydro shows potential to predict potential changes in the atmospheric hydrological cycle of gauged and ungauged, and poorly gauged basins, as well as reproducing observed streamflow (L. Li et al., 2017; Rummler et al., 2019). In terms of land use land cover change research, Z. Zhang et al. (2021) showed that incorporating lateral processes, diurnal cycles follow the local terrain and vegetation features. Cerbelaud et al. (2022) and Dixit et al. (2019) find the WRF-Hydro modeling system suitable to understand the hydrological processes and prospective modification of Caledonia's land cover and regional climate regimes. Dixit et al. (2019) on the other hand showed that the contribution of August flooding in Kerala was due to the deforestation activities of the 1995 to 2005 period. Achugbu et al. (2022b) in similar research showed that afforestation increases streamflow during the dry period and deforestation decreases streamflow during the same period. WRF/WRF-Hydro

has contributed to the growth in modeling the effects of land-atmospheric interaction research, especially the impacts of afforestation and deforestation. That notwithstanding, there are varying conclusions on the impacts of afforestation and deforestation across publications owning to the different physical, biological, and chemical characteristics of different land surfaces in different parts of the earth (Deng et al., 2014). For instance, whilst Wulfmeyer et al. (2014), and Y. Liu et al., 2023) indicate that afforestation in an arid region can trigger more precipitation, also noted that enhanced precipitation can be associated with deforestation as well. Thus, region-specific research is still necessary to fully comprehend the interactions between land cover changes and climatic factors in land-atmosphere interaction research. Table 2.2 shows the research publications in Africa that have used the WRF-Hydro model.

Just like the WRF/WRF-Hydro model, most RCMs often have Land Surface Models which simulate the interactions between the vegetation cover and atmospheric conditions. However, land-atmosphere interaction in most RCMs is an oversimplification of reality for some reasons. To begin with, the vegetation cover in RCMs uses one year of historical data and remains static neglecting the interactions between land use changes and climate variability throughout the simulation period (Deng et al., 2014). While this may be attributed to the need for extra computational resources for such simulations, it is also due to the lack of global consistent land cover data with high spatial and temporal resolution. In addition, as the focus of model-based land-atmosphere interactions/climate-land simulation is often the impact of a third environmental variable, the direct impact of land cover/use on climate and vice versa is often rarely simulated or unreported in most cases. Alternative to the model-based climate-land simulations is the use of analysis to assess the direct impact of climate on land changes and vice versa (Gao & Liu, 2011; Hou et al., 2021; Wajid et al., 2020). While the analysis-based approach may be significantly more limited than the model-based approaches in general and in terms of future prediction capabilities, it allows for the analysis of climate variations with historical land use and land cover changes. It can be the basis for validating model-based simulations over the historical period and the development of climate-land use change scenarios based on historical land-climate information. In this work both the analysis approach and model-based approaches are employed to investigate the relationship between land cover changes and climatic changes, outlining the advantages and

limitations of each. In the next section, the land use land cover products available from global scales to national levels are reviewed to select the most appropriate for this work.

Table 2.2 WRF-Hydro researches conducted in Africa

Study	Aim	Model	Method
Arnault et al. (2016)	To analyze the impact of runoff-infiltration partitioning and resolved overland flow on land-atmosphere feedbacks in WRF model and WRF-hydro.	Coupled WRF, WRF-Hydro	Sensitivity analysis of WRF results to the runoff-infiltration partitioning parameter and a comparison between WRF and WRF-Hydro results, respectively.
Arnault et al. (2021)	To assess the ability of climate models in the representation of realistic atmospheric- terrestrial water pathways using water isotopologues as natural tracers	Coupled Community Earth System Model Version 1. WRF-Hydro-iso	Modeling, validation and sensitivity analysis
Arnault et al. (2021)	To assess the contribution of lateral terrestrial water flow to summer precipitation in two different climatic regions, Europe and West Africa, for the period and its impact on soil moisture-precipitation feedback	Coupled WRF-Hydro, WRF-Hydro-tag	Simulations
Arnault et al. (2022)	To enhance the understanding of the processes affecting precipitation isotopic compositions and to improve the interpretation of paleoclimate isotopes records by using the newly developed WRF-Hydro-iso-tag	Community Earth System Model, WRF-Hydro-iso-tag	Simulations, comparison, and validation of results
Arnault et al. (2023)	To assess the potential climate impacts of afforestation strategies on the surface energy budget, temperature and precipitation in Nzoia Basin in Tropical Africa	WRF-Hydro	Simulation + Synthetic numeric sensitivity experiment
Graf et al. (2021)	To investigate the strength sign and variables involved in the soil moisture-precipitation feedback in Ammer catchment in Germany and Sissili catchment in West Africa	Coupled WRF, WRF-Hydro	Simulation of atmospheric processes
Kerandi et al. (2017)	To improve the understanding of the hydrometeorological conditions of the Tana River Basin in Kenya, East Africa,	Coupled WRF, WRF-Hydro	Simulation of atmospheric processes
Naabil et al. (2017)	To explore the potential of using the WRF-Hydro model in a fully coupled mode to	Coupled WRF-Hydro	Simulation + Calibrations + Validation

	assess water resources in the Tano Basin in Ghana		
Naabil et al. (2022)	To determine the added value of a hydrological-atmospheric coupled model in improving river basin climate modelling, and to investigate its usefulness in simulating sub-grid hydrological features	Coupled WRF, WRF-Hydro	Simulations, Statistical analysis, Spatial Bias Analysis
Quenum et al. (2022)	To investigate flood events in the Oueme River Basin in Benin using the coupled atmosphere-hydrology model system to assess its potential for accurate streamflow simulation and early warnings	Coupled WRF-Hydro	Simulate + Calibrations + Validation
Z. Zhang et al. (2023)	To investigate the impact of different global soil database on simulated land-atmosphere interactions in southern Africa, using the fully coupled WRF-Hydro	Coupled WRF-Hydro	Simulation Analysis

2.6 Land use versus land cover

Land use and land cover are mostly combined as land use /land cover even though their meanings are quite different. Land cover refers to the physical and biological cover of the Earth's surface, including natural features such as forests, grasslands, water bodies, and human-made features such as urban areas, agricultural fields, and bare soil. Land use refers to territory characterized according to current or future planned functional dimensions or socioeconomic purpose (e.g. agricultural, industrial, commercial, forestry, residential, recreation). Thus, while land cover refers to the earth’s biophysical cover including places such as bare rock or bare soil, land use refers to activities that humans carry out on the Earth’s surface on a specific land cover. Whereas land cover is usually visible from satellite imagery, land uses are often difficult to distinguish from a typical satellite image. Land uses are therefore derived from contextual images with additional information requirements. This also makes map production difficult and expensive such that most maps only provide information on land cover or specific land cover such as agricultural or artificial areas, thereby providing both land use and land cover data. This also accounts for why land use cover (LUC) science generally refers to Land Use and Land Cover information, as the two aspects tend to be combined within the same dataset (García-Álvarez et al., 2022).

2.7 Available land use cover (LUC) datasets

Prior to the advent of Remote Sensing, some information on land cover and land use were available. Land use and land cover information has however increased the production of systematic LUC maps at regional, continental and global scales (Loveland & Giri, 2012). Tables 2.3 shows existing single-date LUC maps at global coverage, their spatial and temporal resolutions. The full name of each dataset is also presented below in Table 2.3. Table 2.4 shows existing timeseries LC maps, their spatial and temporal resolution, number of classes and the links to the datasets. Finally, Table 2.5 shows available land cover data focus on Africa, their spatial and temporal resolutions, number of classes and whether the support change detection or not. It is important to note that most of the LUC datasets are sponsored by international project, mostly by the European Space Agency (ESA), and once the project is over their updates also comes to an end (García-Álvarez et al., 2022).

Table 2.3 Globally available LUC datasets with a single date

LULC Map	Spatial Resolution	Temporal timescale
Mathews Global Vegetation/Land Use	1.0°	1983
UMD LC Classification	0.01°	1992/1993
GLCC 2.0 Global	0.01°	1992/1993
GLC2000	0.01°	1999/2000
GMRCA LULC	0.1°	2000
Geo-Wiki Hybrid	0.0027°	2000/2005
LADA LULC map	0.075°	2007
GLC-SHARE	0.01°	≤ 2014
OSM LULC	0.00009°	≤ 2017

LUC—Land Use Cover, UMD LC Classification—University of Maryland Land Cover Classification, GLCC 2.0 Global—Global Land Cover Characterization 2.0, GLC2000—Global Land Cover 2000, OSM LULC—Open Street Map Landuse/Landcover, LADA LUC Map—Land Degradation Assessment in Drylands, GLC-SHARE—Global Land Cover-SHARE

Table 2.4 Globally available LUC timeseries datasets

LULC Map	Spatial Resolution	Temporal timescale	Change detection Support
GLASS-GLC	0.045°	1982-2015	Yes
LC-CCI	0.0027°	1992-2018	yes
GLC30	0.00027°	2000, 2010,2020	yes
GLC250	0.0023°	2001, 2010	NR
MCD12Q1	0.0045°	2001–2010	NR
GLCNMO	0.009°	2003	No
	0.0045°	2008	
		2013	
GlobCover	0.0027°	2005	No
FROM-GLC	0.00027°	2010	No
	0.00009°	2015	
		2017	
CGLS-LC100	0.0009°	2015–2019	No

GLASS-GLC—Global Land Surface Satellite-Global Land Cover; LC-CCI—Land Cover-Climate Change Initiative; GLC30—GlobeLand30; GLC250—Global Land Cover 250 m; MCD12Q1—MODIS Land Cover Type Product; GLCNMO—Global Land Cover by National Mapping. NR – Not Recommended.

Table 2.5 Available LUC datasets for Africa

LULC Map	Extent	Spatial Resolution	Temporal timescale	Change detection Support?
WA LULC	WA	0.018°	1975, 2000, 2013	Yes
SERVIR-ESA	SA and EA	0.00027°	Country specific dates (1990–2015)	Yes
SADC Land Cover Database	SA Development Community	0.00027°	Country specific dates (1990/1999)	No
AFRICOVER	Malawi, Libya, Tanzania, Sudan, Rwanda, Kenya, Egypt, Uganda,DR Congo, Burundi	1:200,000	Country specific dates (1994/2001)	No
CCI LAND COVER—S2 PROTOTYPE	Africa	0.00018	2016	No
Congo Basin Vegetation Types	Congo Basin	0.0027	2000/2007	No

WA – Western Africa; EA – Eastern Africa; SA – Southern Africa; SERVIR-ESA—SERVIR Eastern and Southern Africa, SADC—Southern African Development Community, CCI—Climate Change Initiative Land cover; ESA – European Space Agency.

2.8 Criteria for land use cover data selection

The criteria for land use data selection depend on availability and cost, spatial and temporal resolution, accuracy and validation, classification scheme and legend, coverage and extent, method and data sources, and whether the datasets are suitable for change detection. For studies whose interest is in change detection over time, the single-year land use cover datasets are unusable, such as Mathews Global Vegetation/Land Use, UMD LC Classification, GLCC 2.0 Global, GLC2000, GMRCA LULC, Geo-Wiki Hybrid, and LADA LULC map in Table 1. Moreover, only GLASS-GLC, LC-CCI, and GLC30 support change detection. Thus, an analysis of the LUC datasets with global coverage shows only GLASS-GLC, LC-CCI, and GLC30 are recommended for change detection. The GLASS-GLC is relatively coarser and not suitable for studies where high-resolution LUC are needed. GLC30 has the highest resolution of 30 m but only three (3) LUC data over 20-years (poor temporal resolution). The LC-CCI, otherwise known as the ESA CCI LC is ten times (10×) coarser than the GLC30 but has 27 annual LUC maps over 27 years. While the GLC wins over LC-CCI in terms of spatial resolution and change detection over a 10-year interval period, it is impossible to tell what happens between 2001–2009, and 2011–2019 limiting its usage in studying the interactions between climate and land use cover changes at an annual timescale. In terms of regional LUC datasets, WA LULC is coarser (2 km) and not useful for climate-land interaction studies for the same reasons as mentioned for GLC30. SERVIR-ESA, SADC Land Cover Database, AFRICOVER are available at varying dates (country-specific dates) and so lack consistency and continuity and are therefore unusable for studies over Africa and West Africa. The CCI-LAND COVER-S2 PROTOTYPE has a relatively high resolution of 20 m but is also available for only 2016 and therefore not usable for change detection or climate-land interaction studies. The extent and coverage of the Congo Basin vegetation types are its limitations. From the foregoing, the LC-CCI, otherwise known as the ESA CCI LC is the most suitable for both change detection and climate-land interaction studies and therefore has been adopted to study this thesis. Hereafter, the LC-CCI will be referred to as the ESA CCI LC dataset.

2.9 The ESA CCI LC

The ESA CCI LC is a global annual land cover map generated at 300m spatial resolution from 1992 to 2015 (Jiang & Yu, 2019; S. Liu et al., 2021; X. Liu et al., 2018; W. Li et al., 2018). The maps were produced initially as a 10-year baseline map (2003 to 2012) based on a classification of the Medium Resolution Imaging Spectrometer (MERIS) Full and Reduced resolution data archive, and subsequently backdating and updating the baseline maps into 24 annual LC maps. The overall thematic accuracy of the 2010 LC map based on the same sample from Globalcover-2009 was found to be 74.4% (Guidigan et al., 2019; Tsendbazar et al., 2015), weighted-area accuracy is about 71.1% respectively (Defourny et al., 2017; X. Liu et al., 2018). The ESA CCI LC maps are based on the United Nations Food and Agricultural Organization (UN FAO) land cover classification scheme (LCCS). The ESA CCI LC datasets are designed to meet the desires of the climate modeling community to avoid false change detection between semantically closed LC classes (Defourny et al., 2017), and are therefore recommended for use by the climate modeling community (Reinhart et al., 2021). It is also the default land cover data for automatic catchment delineation in the Water Evaluation and Planning (WEAP) Model, of the Stockholm Environment Institute (SEI). Moreover, the ESA CCI LC has a higher resolution of 300 m compared to the MODIS LC data of 500 m resolution which is used in the WRF-Hydro. For the above-mentioned reasons, the ESA CCI LC is adopted as the main LC data for the regional climate modeling in WRF-Hydro, the Water-Energy-Food Nexus modeling in WEAP, and for establishing the relationship between climate variability and land use land cover change over West Africa. In the next section, land-atmosphere interaction is discussed within the water, energy, and food nexus concepts.

2.10 Land-atmosphere interactions in the water-energy-food nexus research

The nexus is the link or interconnection between water, energy, and food systems. Fundamentally, the land-atmosphere interactions determine water exchange between the land surface and the atmosphere. The atmosphere gives water to the land surface through precipitation and the land surface characteristics such as soil moisture and vegetation cover determine the rate of evapotranspiration. This cycle determines the regional water availability and impacts the hydrological cycle. Runoff rates, soil moisture, and groundwater, are affected by human activities

such as agricultural practices, urbanization, afforestation, and deforestation. In terms of energy, the land-atmosphere interaction regulates the exchange between the earth's surface and the atmosphere, ultimately determining energy balance. Surface properties such as vegetation cover, albedo, LAI, and surface roughness determine how the surface absorbs, reflects, and distributes solar radiation. Changes in land cover affect the surface energy fluxes such as sensible and latent heat fluxes and consequently the regional climate patterns and temperature regimes. Land cover changes and land use decisions also determine the suitability of land for renewable energy generation such as wind and solar. Land-atmosphere interactions also determine water availability for hydropower systems. In terms of food, the land-atmosphere interactions directly affect agricultural productivity through climate variability and water availability. Extreme climatic conditions affect soil moisture, crop growth, and yield. Land use decisions such as urbanization, and deforestation can impact agricultural expansion. Thus, the land-atmosphere interactions serve as the nexus between water, energy, and food systems. In the current water-energy-food nexus concept, however, the land-atmosphere interactions are often regarded as external factors influencing the links between water, energy, and food systems. Such external factors are broadly classified into two categories: climate change and land use land cover change, which are often influenced by human population growth. Thus, in the current water-energy-food nexus research, climate change, land use land cover change, and population growth are regarded as the external influences on water, energy, and food systems. Sometimes the WEF nexus is simply extended to cover other aspects deemed important for researchers or proposed frameworks for achieving sustainable development or integration into life cycle assessment frameworks (Fleischmann et al., 2024; Malagó et al., 2021; Schlemm et al., 2024). Of all articles reviewed on land-atmosphere interaction, only one research directly used the WEF nexus terminology, which is also the only article that focuses on the current WEF nexus research (Malek et al., 2017). For this reason, a new search on the WEF nexus in the current research is conducted, considering articles published from 2012 to 2024.

2.11 The Water-Energy-Food Nexus

The WEF nexus first came to the limelight after the Bonn conference in 2011 as a conceptual framework for increasing resource security, reducing tradeoffs, increasing efficiency, building

synergies, and improving governance across the water, energy, and food sectors (Hoff, 2011). The term ‘nexus’ means a link or connection, and the water-energy-food nexus is used to express the interrelatedness and interconnection between the water, energy, and food systems. Thus, the WEF nexus approach proposes the integration and interdependence across sectors as the basis for ensuring resource security in competing demands for water, energy, and food, resource scarcity, and climate crisis (Fao, 2014; Hoff, 2011; Lazaro et al., 2022). Global challenges such as climate change, population growth, land degradation, rapid urbanization, and migration, amongst others, have contributed to an increase in pressure on global water, energy, and food resource systems (Namany et al., 2019; Nhamo et al., 2020). In the past century, water, energy, and food resource-related challenges have been addressed separately to attain water security, food security, and energy security. Concepts like the IWRM played a crucial role in interdisciplinary collaborations by focusing on the role of water as having important connections to other sectors (Grigg et al., 2018; Lazaro et al., 2022), engaging sectors at a river basin scale. However, the interrelatedness and interdependence nature of the water, energy, and food resources means water security, food security, and energy security cannot be achieved separately and so the necessity for integrated and sustainable resource planning and management of these resources across multiple scales, also highlighting the multi-centric aspects and the need for equal importance on all sectors (Grigg et al., 2018; Lazaro et al., 2022). The water, energy, and food (WEF) nexus approach represents a global shift in identifying the risk to these primary resources, the security of which is expected to be severely impacted by dynamic climate, demographic, societal, and infrastructural changes in the twenty-first century (Elagib & Al-Saidi, 2020; Mohtar & Daher, 2016). The nexus approach aims to identify tradeoffs and synergies of water, energy, and food systems, internalize social and environmental impacts, and guide the development of cross-sectoral policies (Albrecht et al., 2018b). While the WEF nexus originally focused on resource security in its early years (Pahl-wostl, 2017; Simpson et al., 2019), further refinements of the nexus concept recognize the need to incorporate environmental, economic, political, and social dimensions (Albrecht et al., 2018b; Lawford et al., 2013). Most nexus studies aim to improve the coordination and integration of sector-based resource policies. Figure 2.8 show the WEF nodes (water, energy, and food), the links or connection (nexus) between each node showing the way the nodes interact with each other. Aside from the WEF nodes and links, the nexus boundary defines the scale at which the research

was carried out and could be global, national, transboundary, regional, local, city scale, etc., as shown by Albrecht et al. (2018b). Figure 2.9 shows the basic concept of the WEF nexus, while Figure 2.10 shows the historical evolution of the WEF nexus timeline and the various actors involved in the development of the WEF nexus concept. The external factors or additional components considered in the WEF Nexus research are discussed in the next section.

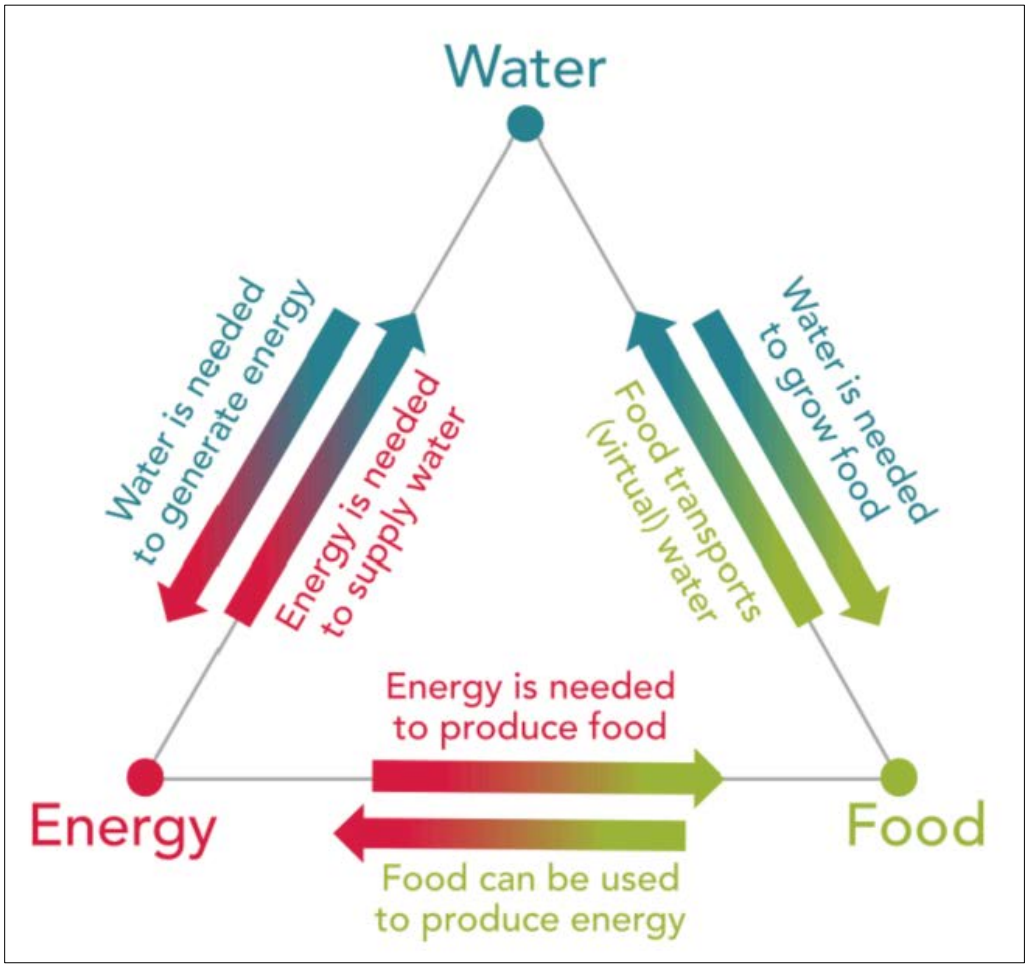

Figure 2.9 Basic water-energy-food nexus showing each nexus node (water, energy, food) and the interactions between the nexus nodes (Source Roidt & Avellán, 2019)

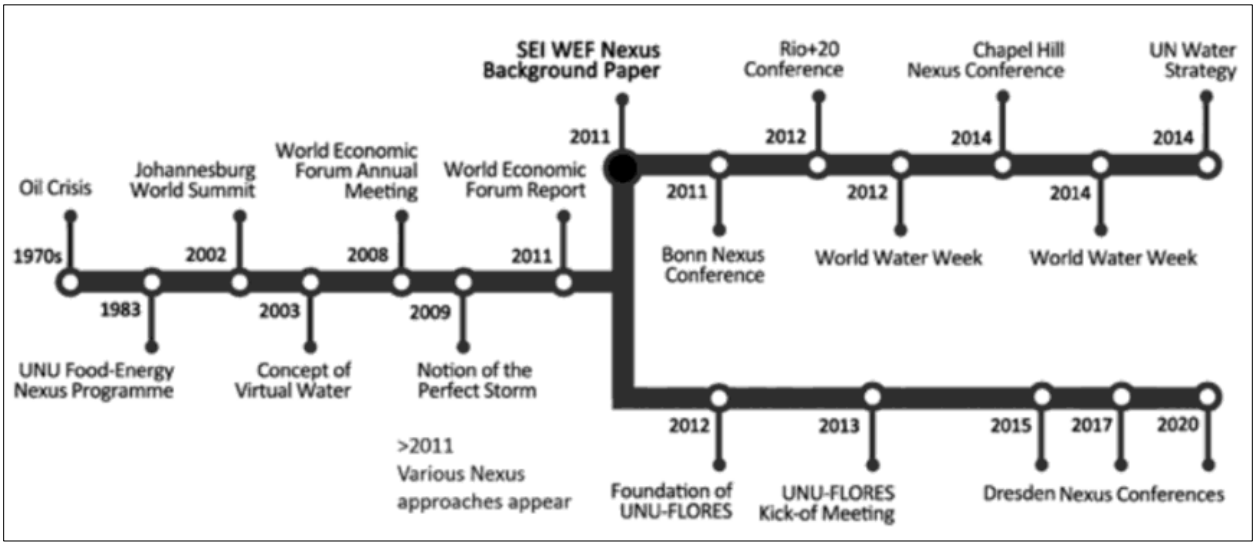

Figure 2.10 Historical evolution of the WEF nexus timeline and the various actors involved in the development of the WEF nexus concept (Source Avellán & Roidt, 2019)

2.12 Stressors of the Water-Energy-Food nexus system

Since the nexus approach is founded on the recognition that natural processes are interconnected within a system, each new difficulty that arises in one component of the system inevitably disrupts the entire system (Nhamo et al., 2020). This is the major internal complexity of the nexus approach which is often resolved by defining the nexus problem to include a detailed interaction of all the subsystems. On the other hand, **c**limate change, socio-economic conditions, and population growth are the most external factors noted in scientific literature to increase the complexity of the WEF nexus (Collins & Gaetani, 2023). The prevailing uncertainties surrounding future alterations in population growth, socioeconomic, and climatic conditions have amplified curiosity in water-energy-food-ecology nexus-oriented frameworks concerning water resources analysis (Shi et al., 2020). The water-energy-food nexus is receiving increased attention worldwide because of climate change and the rising population (Hanjra, 2013). Population growth is projected to increase demand for food, water, and energy exerting pressures on soil, water, and ecosystems (Del Borghi et al., 2022; Dembélé et al., 2022). Projected climate change will lead to warmer, with more frequent and intense rainfall, a decrease in rainfall reliability for agriculture and water availability (Dembélé et al., 2022; Hanjra, 2013). Population growth coupled with climate change and socioeconomic development will result in a steady rise in global demand for water, energy,

and food resources (Falchetta et al., 2022; Lahmouri et al., 2019; J. Li et al., 2021), water stress (Peña-Torres et al., 2022), resource scarcity (Peña-Torres et al., 2022), increased competition for water resources (De Vos et al., 2021). Another important external component which impacts the WEF nexus system, recommended by some researchers as a fourth component that needs to be added to the WEF Nexus system is land and its related activities such as land use and land cover change (Blanchon & Le Tourneau, 2022). The importance of land as a component of WEF Nexus system worth considering is heightened by the competing need for it either for food production, energy generation or others (Midgley et al., 2018; Simpson et al., 2019). This is often seen in researches trying to evaluate and choose between the use of land for either agriculture or energy (Sargentis et al., 2021; Viccaro et al., 2022), while some try to balance the benefits of water-energy-food-land nexus through agroforestry (Elagib & Al-Saidi, 2020). A recent study of the impact of the Russian-Ukraine war suggests that the decision of the Western elites to sanction Russia has dramatically transformed the global WEF equilibrium, as Russian and Ukraine are major supplies of energy sources, food, and fertilizer (Sargentis et al., 2022). The authors suggest the situation has also led to a collapse of social cohesion. The nexus approach to resource management is thus complex and becomes increasingly complex as these external factors (stressors) that highlight the fragility of the WEF systems come into play. To accurately evaluate a nexus problem, these external influences need to be considered to unravel the uncertainties of a nexus problem. Accounting for these stressors is the surest way to prepare for a future full of uncertainties. A pictorial representation of WEF Nexus concept and external influencing factors is shown in Figure 2.11. In the next section, as systematic review of articles on the water-energy-food nexus from 2012 to 2024 is discussed examining the trends in the WEF nexus from global perspectives to West Africa.

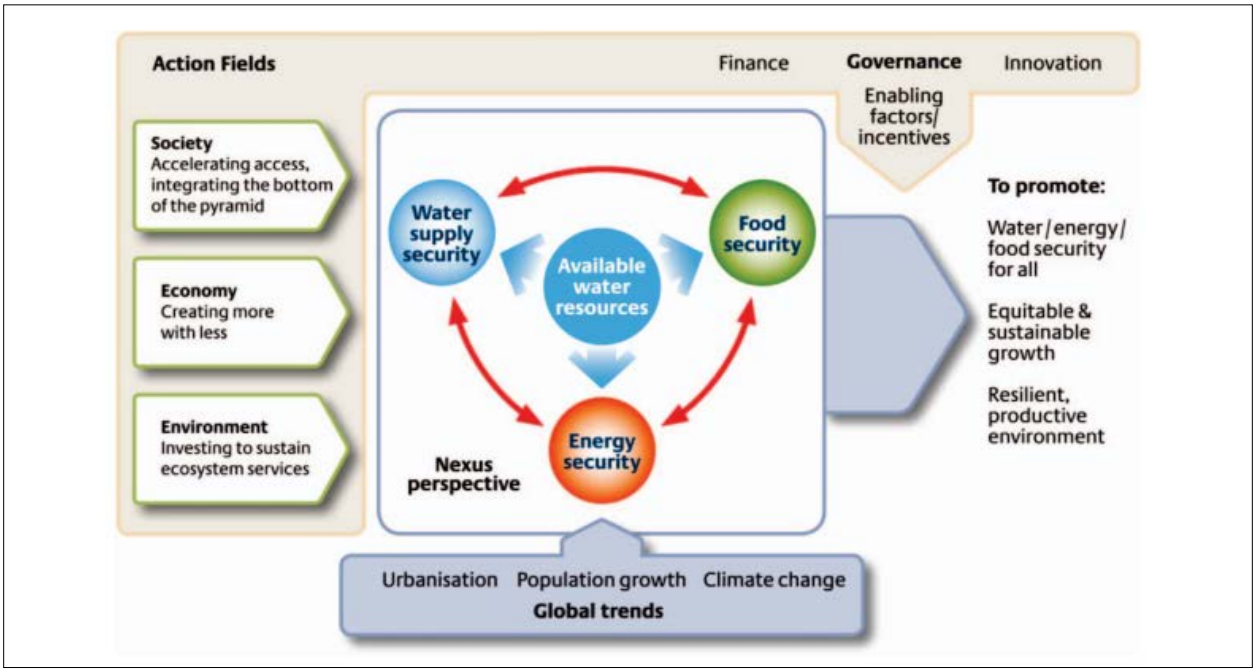

Figure 2.11 Water-Energy-Food Nexus from Hoff 2011 (Albrecht et al., 2018).

Trends in WEF-Nexus research 2012 - 2024

The systematic review of land-atmosphere interactions yielded one search item which attempt to model the water-energy-food nexus. The study proposes a regional scale modeling platform to simulate the nexus of hydrology (water), climate, cropping systems (food), and human decisions (Malek et al., 2017). Recognizing the limitations of the search to the current discourse on water-energy-food nexus research, a separate search for water-energy-food nexus was conducted using the Scopus database to retrieve relevant peer-reviewed for the analysis of the trends in water-energy-food research from 2012 to 2024. A Boolean search of “water”, “energy” and “food” hyphenated in all six arrangements (EFW, EWF, FEW, FEW, WEF, WFE) was combined with “nexus” to retrieve possible publications on WEF nexus. In all 1390 articles from 2012 to 2024 were retrieved for a systematic literature review (Figure 2.12). Of these 1 (0.01%) was a letter, 1 (0.01%) was a Data paper, 6 (0.4%) were Short Surveys, 8 (0.6%) were Errata, 9 (0.6%) were Notes, 10 (0.7%) were conference reviews, 21(1.5%) were books, 24 (1.7%) were Editorial, 98 (7.1%) were Conference Papers, 151 (10.9%) were reviews, 158 (11.4%) were Book Chapters, and 903 (65%) were Articles (Figure 2.13). Europe has the number of publications with 729

(31.1%) items, followed by 705 (30.1%) from Asia, 561 (24%) from North America, 171 from Africa (7.3%), 76 (3.2%) from Oceania, 71 (3%) from South America and 29 (1.2%) items from unidentified sources (Figure 2.14). The United States has the most publications with 465 (19.9%), followed by China with 248 (10.6%) publications, the United Kingdom with 176 (7.5%) publications, Germany with 113 (4.8%) publications, the Netherlands with 79 (3.37%) publications, Italy with 76 (3.25%) publications, India with 71 (3.03%). All other countries contributed less than 68 (~3%) of publications. In terms of discipline, the publications ranged from Environmental Sciences with the largest publications of 1015 (32.6%) to Health Professionals with 1 (0.03%) publication (Figure 2.15). In the list of 138 Journals, the Journal of Cleaner Production has the largest published article with 86 (8.7%) publications, and Environmental Science and Air Pollution Research has the 21st largest publication with 13 (1.3%) publications (see Figure 2.16) whilst Journals with 2 publications are the least contributors in the WEF nexus subject. In terms of the type of nexus considerations 18 (1.3%) articles were focused on the EFW nexus between 2013 and 2023, 83 (5.8%) articles on the EWF nexus between 2013 and 2024, 326 (22.9%) on the FEW nexus between 2015 to 2024, 86 (6%) on the FEW nexus 2014 and 2024, 744 (52.2%) on the WEF nexus from 2012 to 2024, and 169 (11.9%) on the WFE nexus 2013 and 2024 (Figure 2.17). This shows that the "WEF" is the mother of all the nexus began with a focus on "water" and then keeps expanding to be more multi-centric to include all other WEF nexus nodes. Thus, while the energy sector speaks of the energy-water-food (EWF) nexus, hydrologists and water engineers call it the water-energy-food (WEF) nexus, while those in the agricultural fraternity use the term, the food-energy-water (FEW) nexus (Simpson et al., 2019). It is worth mentioning that the WEF nexus does not always have three components. An interaction between any two WEF nexus nodes is a nexus in itself. For such there is WE nexus, WF nexus, EF nexus. It is also important to note that the articles have some overlaps and a particular article, especially review articles could mention many of the nexus at the same time. For preliminary analysis, all articles have been used. Based on co-occurrence analysis of Keyword analysis the "water-energy-food nexus", "food-energy-water nexus", "sustainable development", "sustainability", "nexus", and "nexus approach" were the most occurrent and the major discourse between 2012 and 2015 (Figure 2.18). This is to be expected as the Sustainability Development Goals (SDGs) were introduced in 2015, after the end of the Millennium Development Goals (MDGs). The analysis shows that globally, "water-

energy-food nexus" and all other related keywords were all in use with no distinct focus on any singular Keyword at the end of 2015 (Figure 2.18). Between 2016 to 2019, the discourse in the scientific community has drifted from Keywords such as "integrated water resources management", and related keywords such as "water resources management", "integrated assessment", "global change", "water-use efficiency", "energy efficiency" had declined as the water-energy-food nexus" continues to take the center stage of discourse in the scientific community (see Figure 2.19). This is easily noticeable in the difference between Figures 16 and 17 and shows that the water-energy-food nexus concept started gaining ground at the end of 2019. Between 2020 and 2024 the "water-energy-food" nexus has increased significantly, with previously existing keywords been discussed within the framework of the "water-energy-food nexus" concept (Figure 2.20). After 2021, the WEF nexus is being discussed in relation to other concepts leading to the expansion of the WEF nexus even further. The case of Africa is the same as the global, however, because there are few publications in the region, the threshold for co-occurrence of keywords was reduced to two (2), compared to 5 at the global level. The WEF nexus research has increased over the region over time and its discussions in light of approaches for assessing the WEF nexus such as systems dynamics modeling is increasing. WEF nexus discussions in light of sustainability and sustainable development, resource security, governance, energy security, and food security has also increased by the end of 2023 (compare Figure 2.12, Figure 2.22, and Figure 2.23). The WEF nexus discourse in terms of hydropower, water management, and agriculture is still lagging behind time, which could be attributed to the multi-centric nature of the WEF nexus (Figure 2.21). This however shows that the WEF nexus research which integrated a hydropower system, an agricultural system, and a water system in Africa is still lacking. Climate change and variability are also missing or very limited in the WEF nexus discourse in Africa such that it did not make the 2-occurrence threshold. In light of the above, the WEF nexus of the Volta Basin in West Africa is investigated considering the hydropower systems as the energy node, the rivers and lakes as the water node, and the agricultural systems as the food node. In the next sections, WEF nexus research in Africa are reviewed focusing specifically on hydrology-related studies.

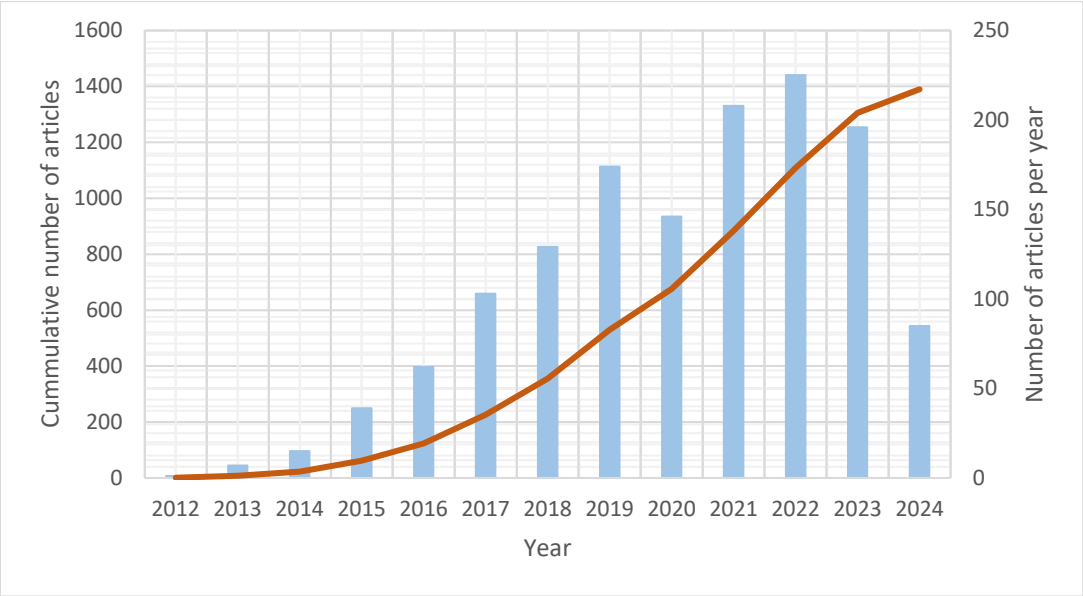

Figure 2.12 Number of articles published between 2012 and 2024. The bar graph shows the number of articles published per year while the line graph shows the total number of articles published over time.

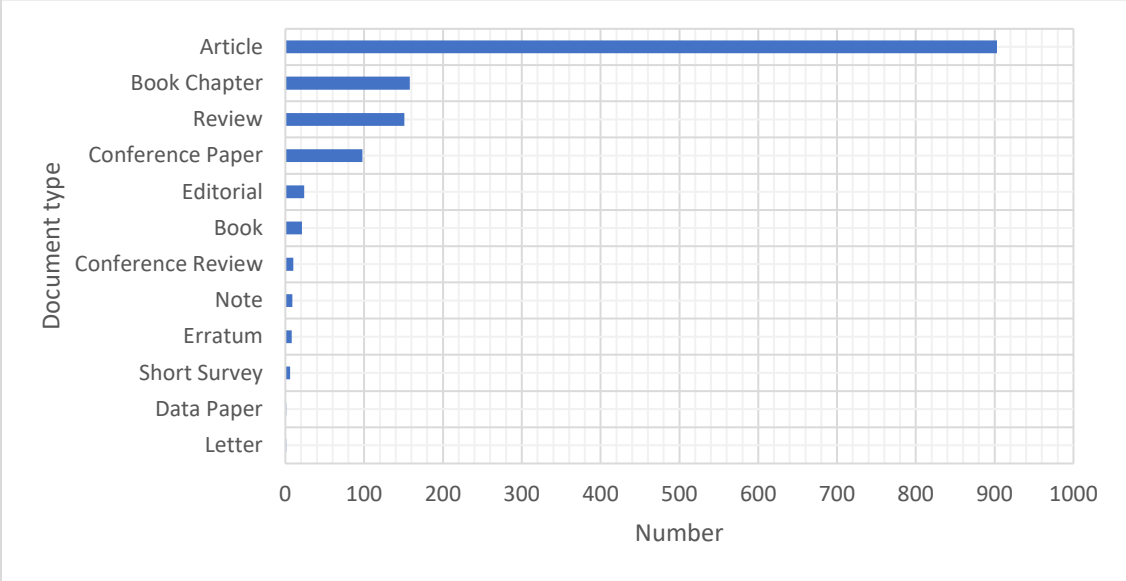

Figure 2.13 Number of Documents retrieved classified by the documents type

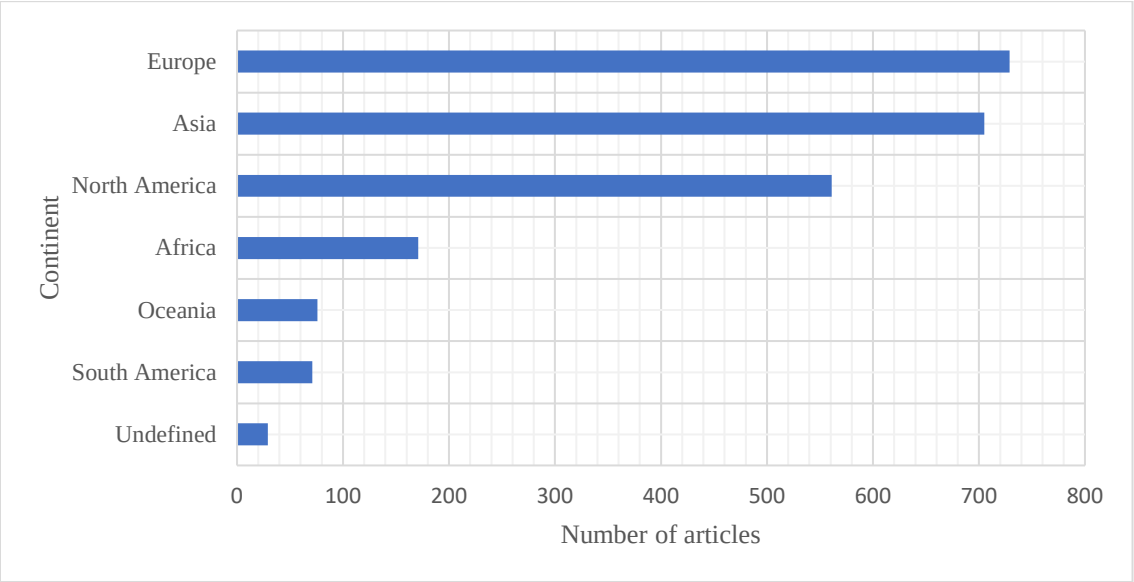

Figure 2.14 Number of Documents classified by the continent

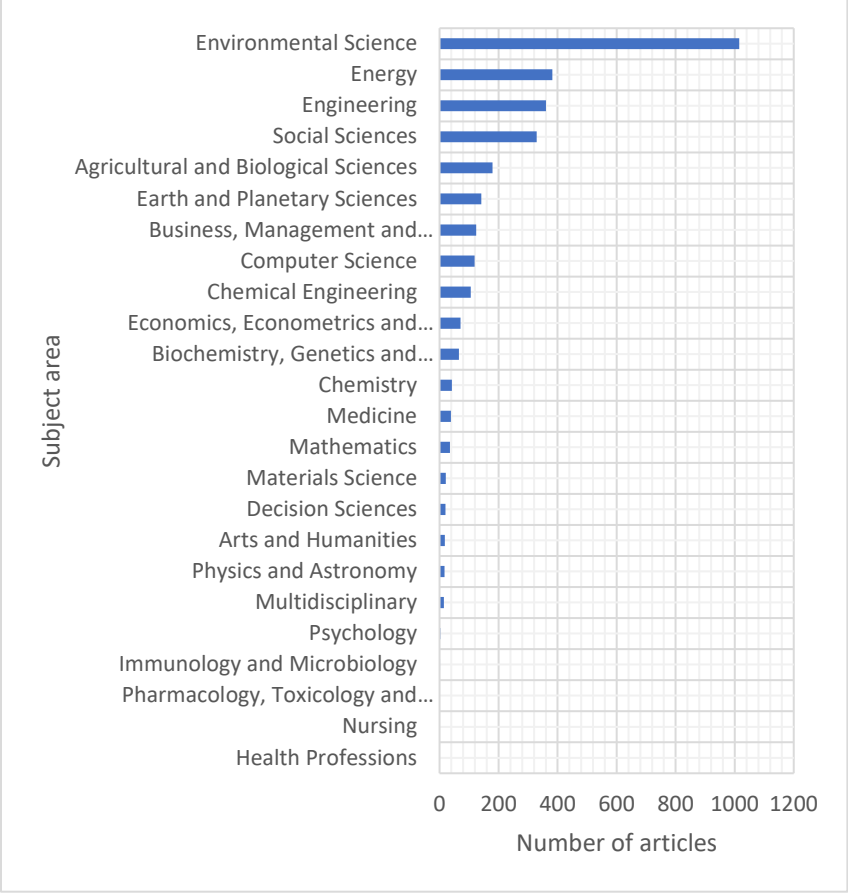

Figure 2.15 Documents on the WEF nexus reviewed classified by the subject area

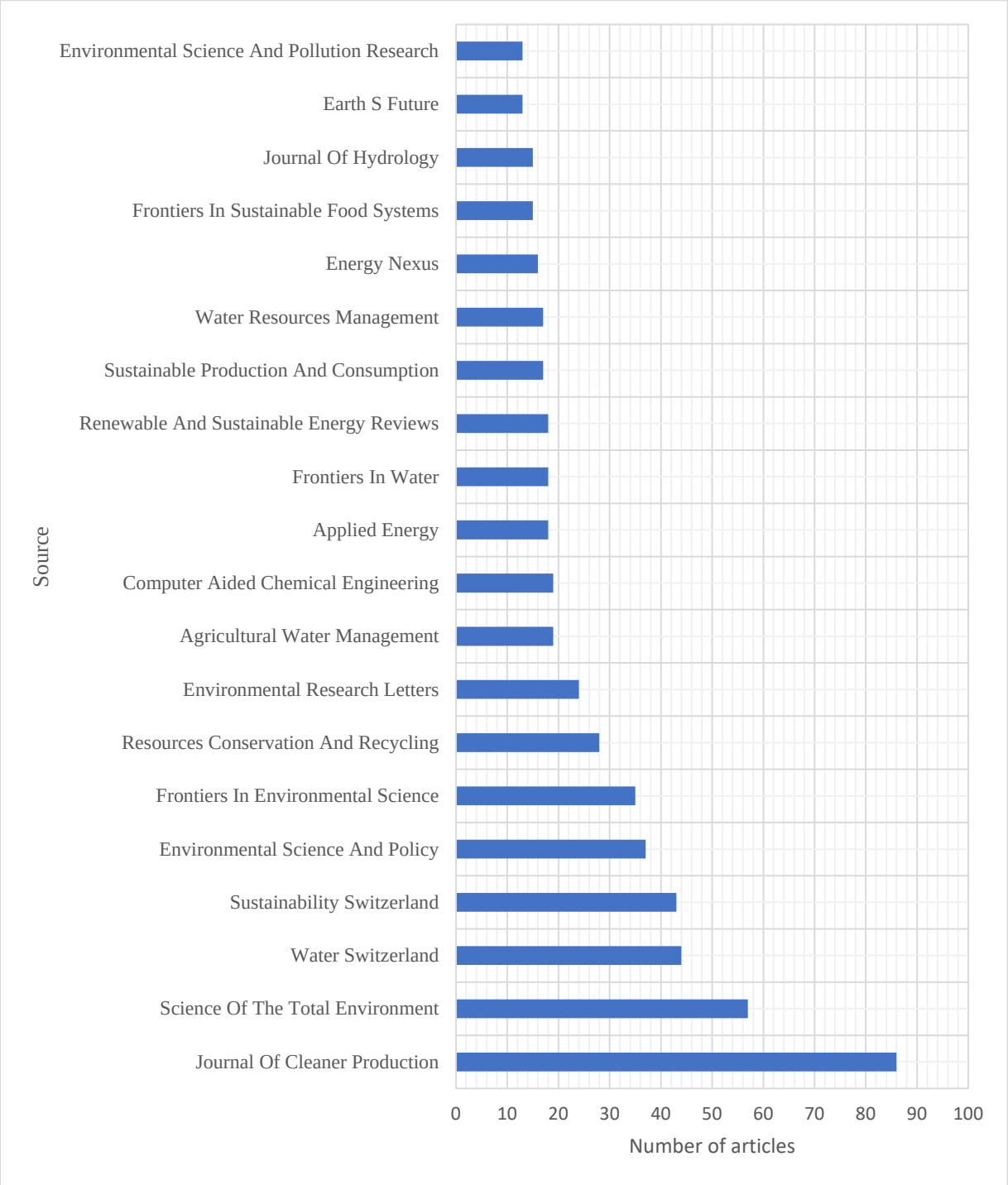

Figure 2.16 First 21 Journals with the highest list of publications on the WEF nexus

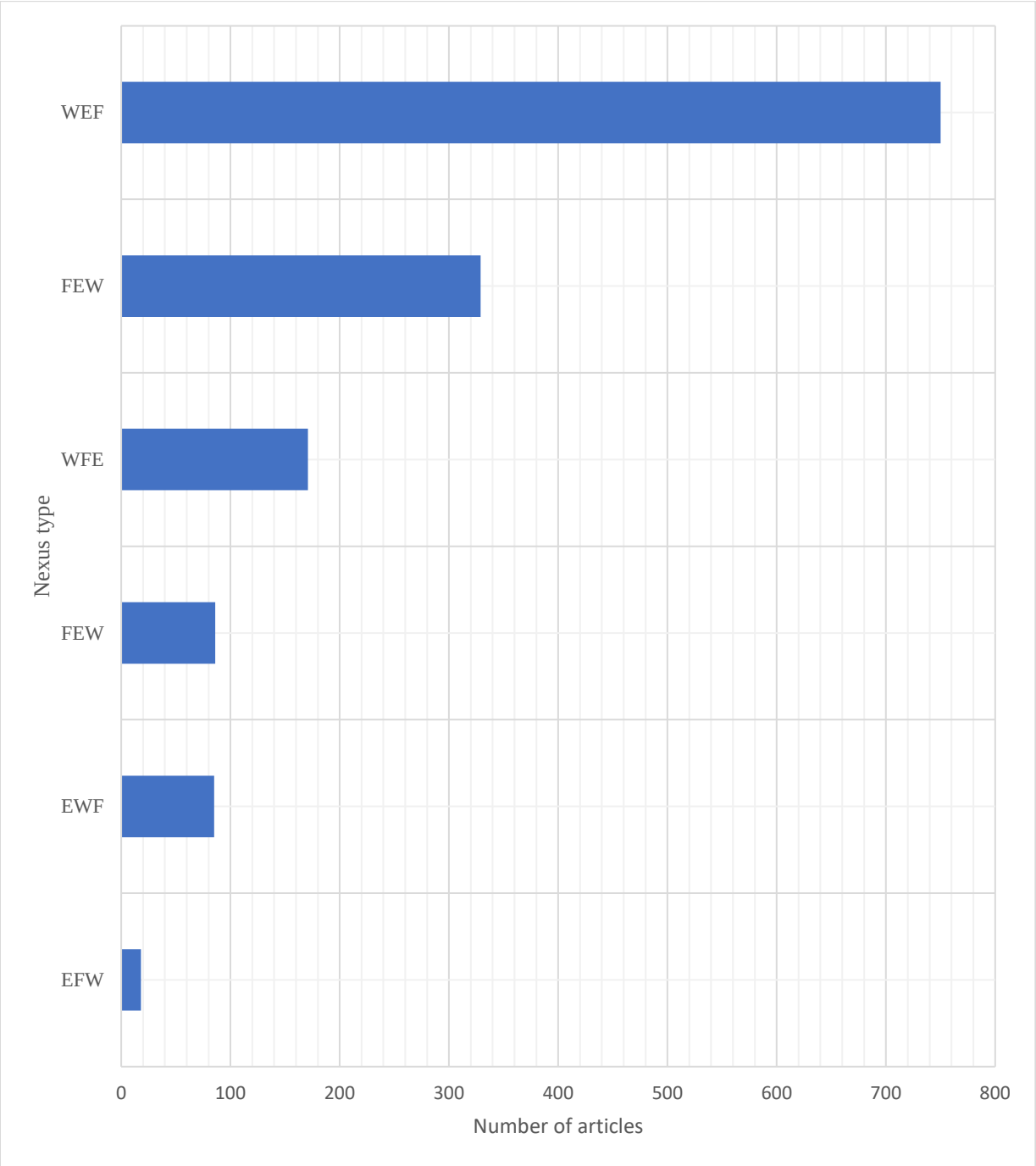

Figure 2.17 Articles reviewed classified according to the nexus type

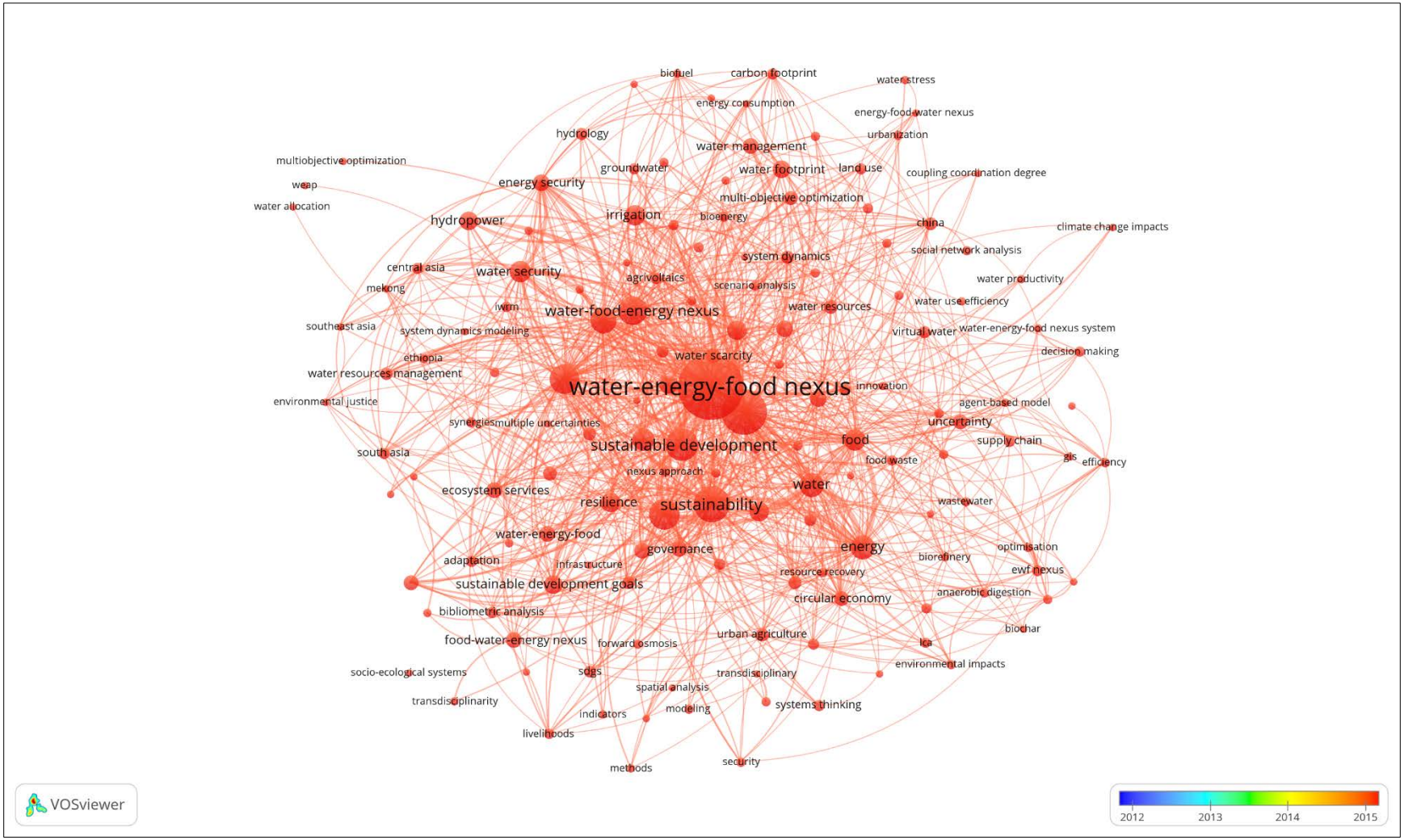

Figure 2.18 Keyword analysis of global research on the WEF nexus (2012 - 2015)

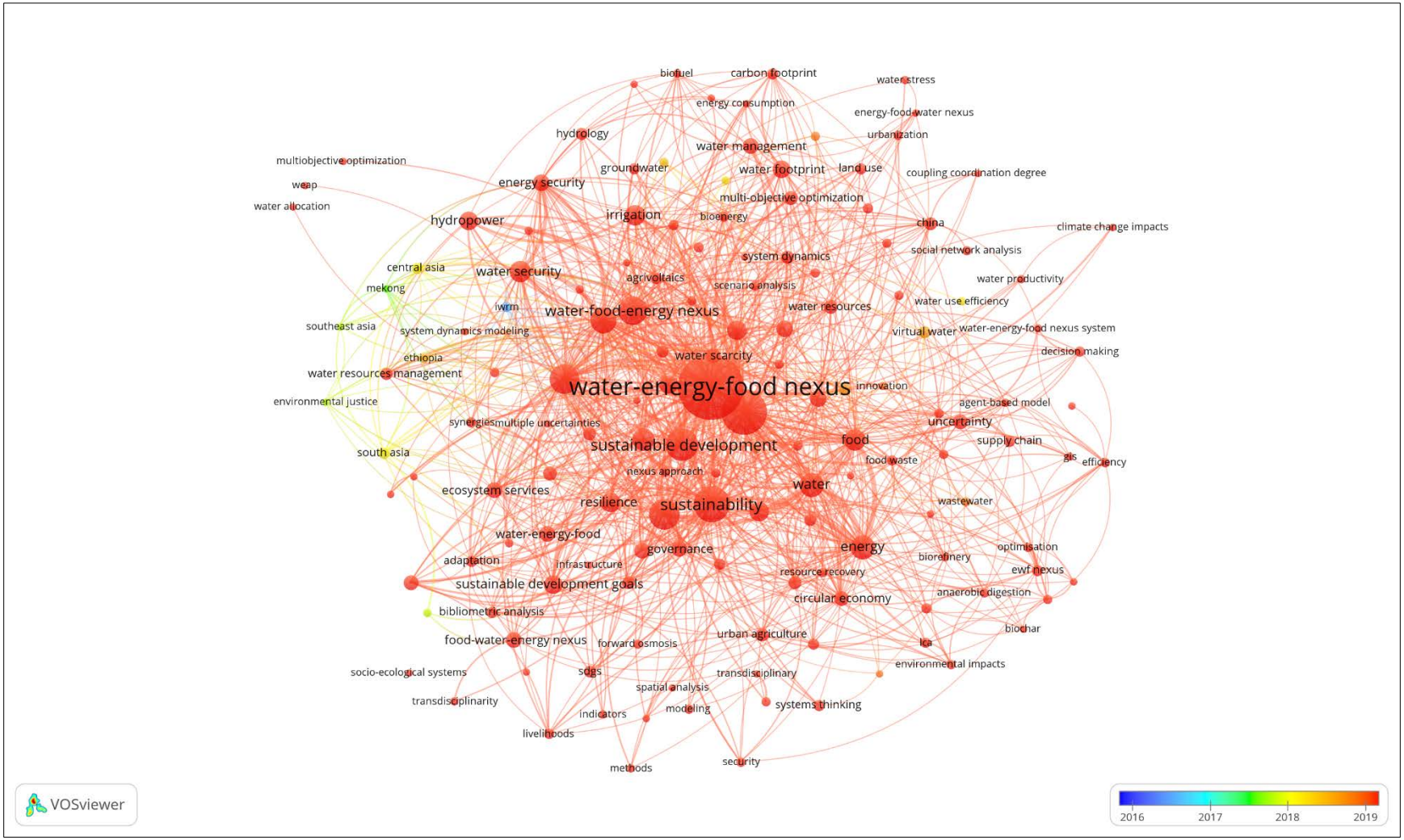

Figure 2.19 Keyword analysis of global research on the WEF nexus (2016 - 2019)

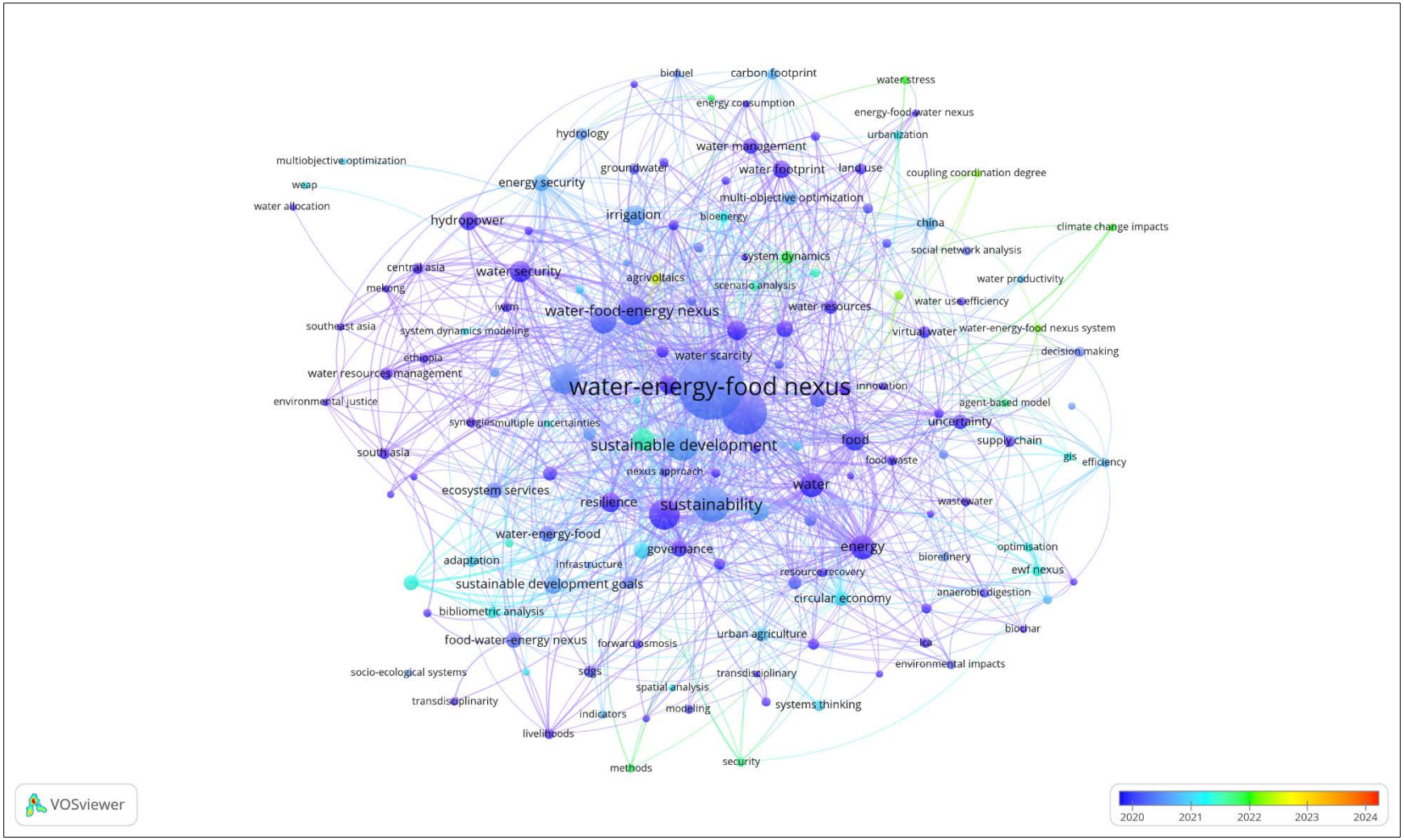

Figure 2.20 Keyword analysis of global research on the WEF nexus (2020 - 2024)

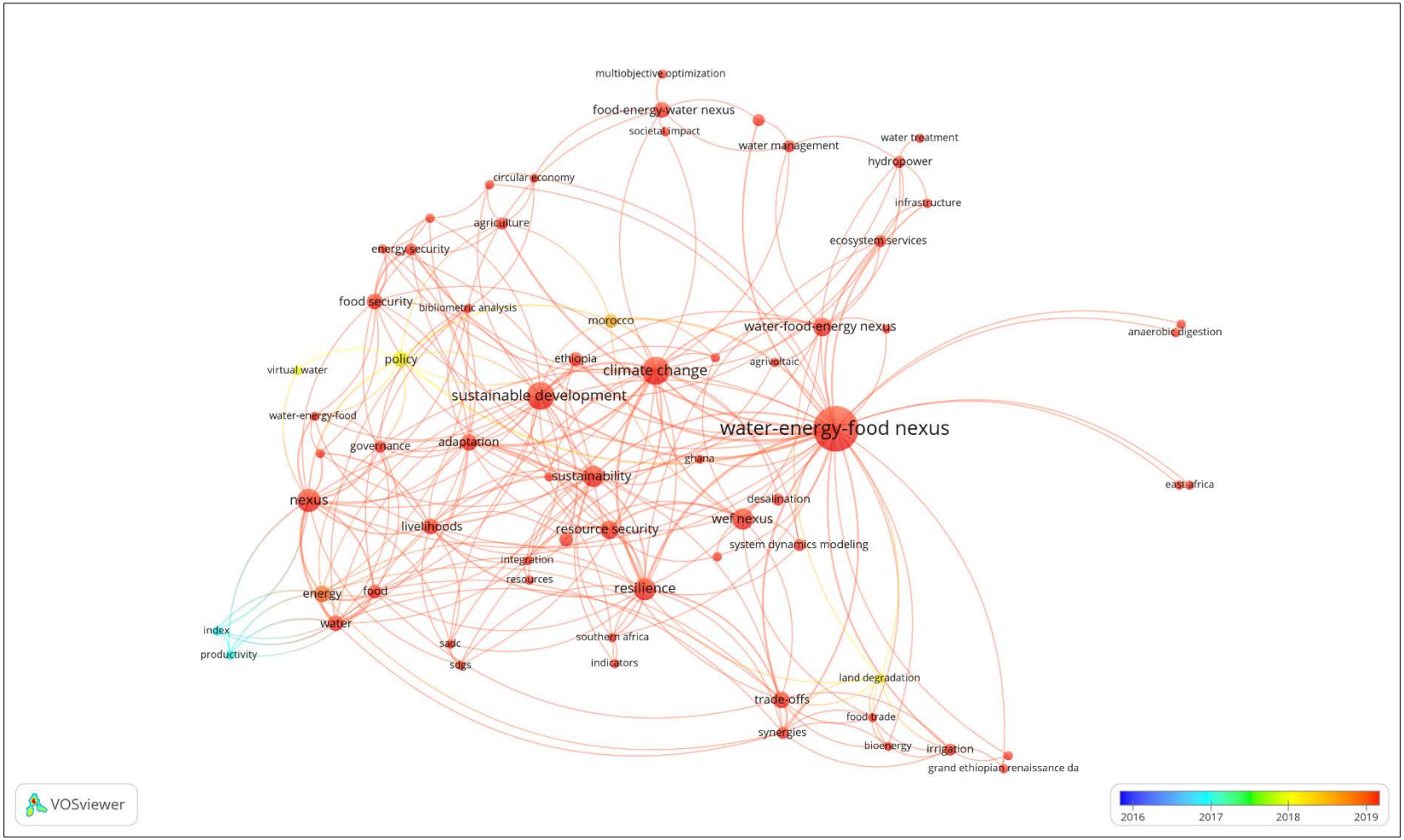

Figure 2.21 Keyword analysis of WEF Nexus research in Africa (2012- 2015)

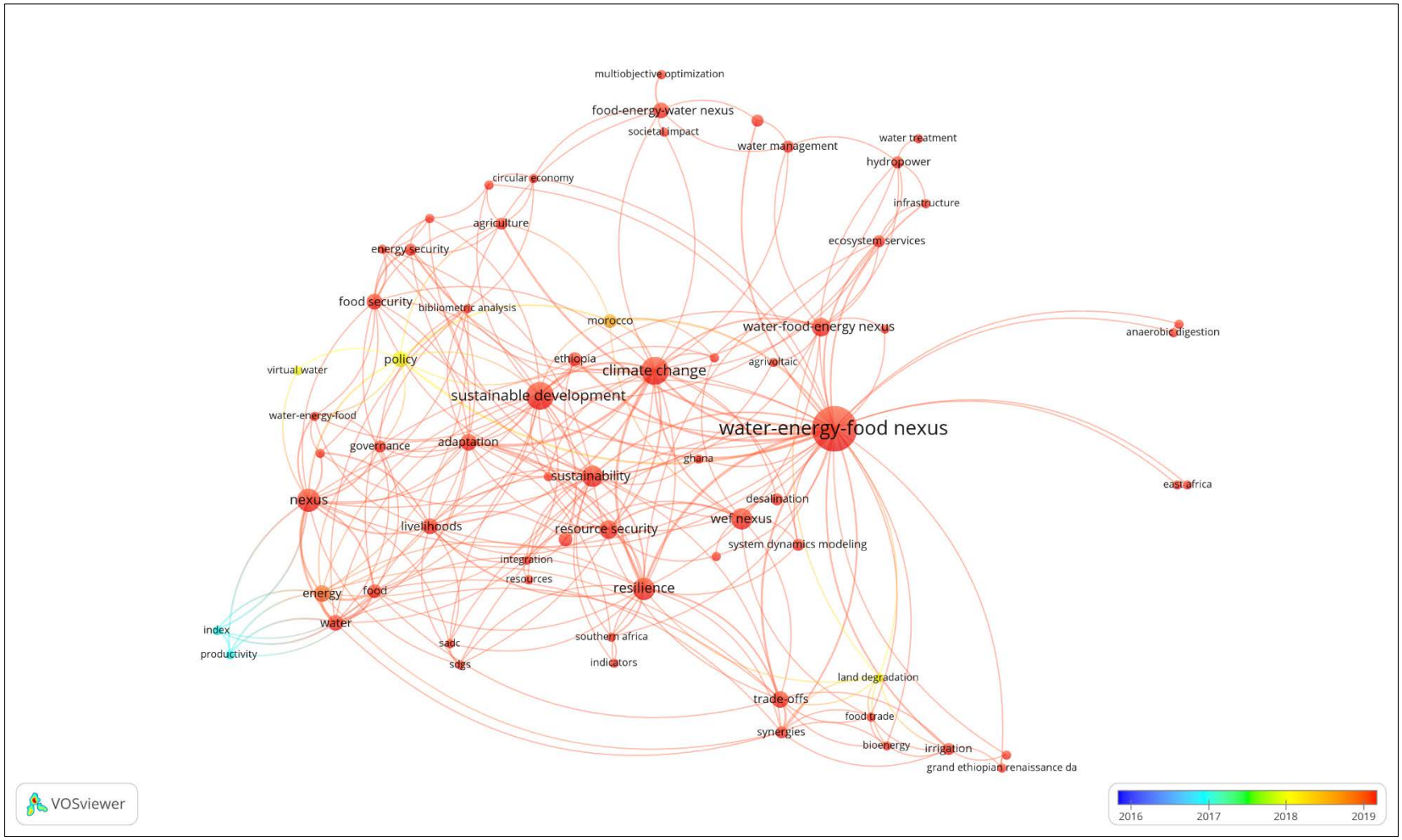

Figure 2.22 Keyword analysis of WEF Nexus research in Africa (2016- 2019)

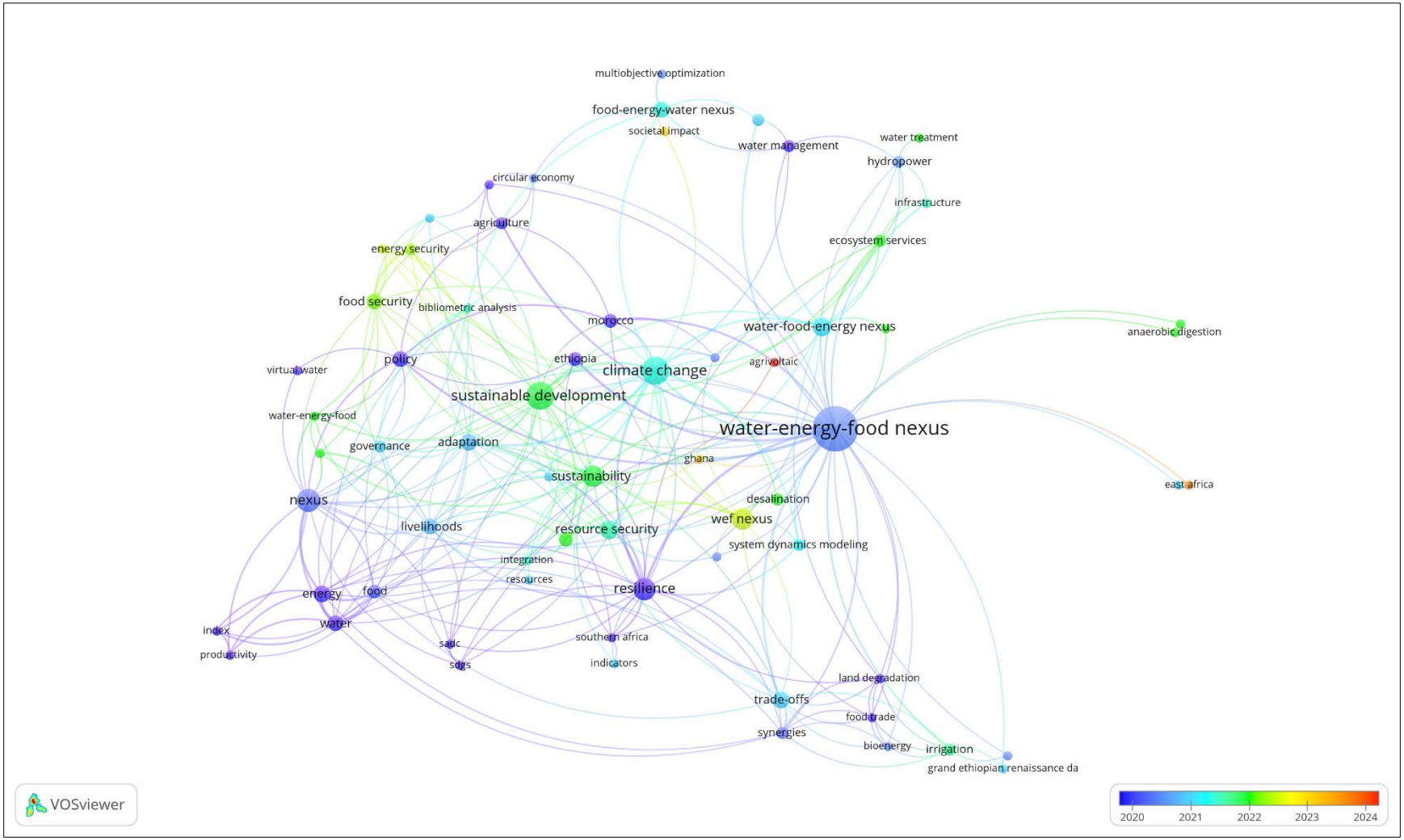

Figure 2.23 Keyword analysis of WEF Nexus research in Africa (2020- 2024)

2.13 The WEF nexus research trends in Africa

The WEF nexus research in Africa have increased since it came to lime light in 2011. The publications reveal that there is no single tool, approach or method for assessing the WEF nexus at any scale. Instead, the WEF nexus research tool vary widely in their use and application. As a relatively younger concept, all the WEF nexus is continually immerging with different tools, frameworks been proposed and applied to specific context. To begin with, some WEF nexus studies have used hydrological models such as the WEAP and WEAP-MODFLOW to quantitatively analyze and water-energy-food nexus in an agricultural watershed and assessed the water-energy-food nexus in the context of climate change respectively (Ouedraogo et al., 2024; Y. Liu et al., 2022). In addition, some studies have used literature reviews and interviews to highlight how climate change is being addressed in policy documents, examining closely how these policies are being mainstreamed to the water, energy and food sectors to enable cross-sectoral coordination (Pardoe et al., 2018). Other studies within the same category have used literature to analyze the complexity of the water-energy-food nexus from the political point of view (Siakwah & Torto, 2022), while others combined literature review, key informant interview and focused group discussions to try to understand the security of water, energy, and food resources associated with hydroelectric dam construction and suitability and shortcomings of applying the nexus approach to them (Mujere & Chanza, 2022; Müller-Mahn & Gebreyes, 2019). In additions some studies have proposed conceptual and methodological frameworks, new approaches, analysis and Decision Support Tool for optimal allocation of land and water resources, exploring transboundary cooperation opportunities, and implementing WEF nexus at River Basin. Regional and transboundary scales (Allam & Eltahir, 2019; Elsayed et al., 2020; John et al., 2023; Nhamo et al., 2018). Furthermore, some studies have used mixed method approach by combining river flow analysis, field observations, water turbidity data, questionnaire administration, field observations and interviews with farmers to assess to understand urban WEF nexus (Elagib et al., 2021). A summary of WEF nexus publications in Africa are shown in Table 2.6, identifying the nexus type, scale of research, method and models used are presented. In this work, the WEAP model is adopted for a transboundary analysis of WEF nexus under climate change, land use and land cover change, and socioeconomic development scenarios. This is the first attempt to build a WEF nexus model for the Volta Basin in West Africa, which can be a Decision Support Tool (DST) for the VBA.

Table 2.6 WEF nexus publications in Africa

Article	Country	Nexus Type	Scale	Method	Tool
(Y. Liu et al., 2022)	Eastern Africa	WFE	Watershed	Modeling	WEAP-MODFLOW
(Ouedraogo et al., 2024)	Burkina Faso	WEF	Hydropower	Modeling	WEAP
(Siakwah & Torto, 2022)	Ghana	WEF	Hydropower	Analysis	Literature review
(Mpandeli et al., 2018)	Southern Africa	WEF	Regional	Review	Literature review
(Pardoe et al., 2018)	Tanzania	WEF	National	Document Analysis + Interviews	Literature review + Interview
(Siderius et al., 2021)	Tanzania/Malawi	WEF	Regional	Past/ Future Climate Analysis	Climate variability analysis
(Müller-Mahn & Gebreyes, 2019)	Ethiopia	WEF	National	Interviews + Discussions	KII + FGD
(Mujere & Chanza, 2022)	Zimbabwe	WEF	Hydropower	Review	Dam reports/WEF literature
(Elagib et al., 2021)	Sudan	WEF	Urban	Mixed research methods	RF+WT+FO+PQ+IF
(Y. C. E. Yang & Wi, 2018)	Tanzania	WEF	River Basin	AWS Modeling	HBV + Water System Model
(Hirwa et al., 2021)	Africa	WEFBH	Multi-national	WEFBH nexus index	MCDM +AHP
(Gebreyes et al., 2020)	Ethiopia	WEF	Hydropower	Semi-structured interviews	Questionnaires
(Matthews & McCartney, 2018)	Africa-Asia	WEF	Hydropower	Case studies of dams	Analysis
(Basheer et al., 2018)	Ethiopia + Sudan	WEF	Transboundary	Modeling	HEC-HMS and CropWat
(J. Yang et al., 2018)	West Africa	WFEE	River Basin	Couple modeling	ABM-SWAT
(Elsayed et al., 2020)	Ethiopia	WEF	Hydropower	Proposed nexus approach in SD	System Dynamics
(Nhamo et al., 2018)	Southern Africa	WEF	Regional	Proposed Framework	C+M Framework
(Siderius et al., 2022)	Tanzania	WEFE	River Basin	Modeling + Analysis	Crop-hydrology model
(Allam & Eltahir, 2019)	Egypt + Sudan	WEF	River Basin	Proposed Framework	DPAL+OM+LWAIRA
(Basheer et al., 2024)	Ethiopia + Sudan	WEF	River Basin	Proposed analytic Framework	Model + Optimization
(Elsayed et al., 2022)	Eastern Africa	WEF	Regional	Modeling	System Dynamics
(Payet-Burin et al., 2019)	Africa	WEFC	Transboundary	Decision Support Tool	WHAT IF
(John et al., 2023)	Tanzania+ Malawi	WEF	River Basin	Analysis	CF + SI + DA

KII – Key Informant Interview; FGD – Focus Group Discussions; WEFBH – WEF-Biodiversity-Health; AWS – Advanced Water System; WEFE – WFE-Ecosystem; CF+SI+DA - Conceptual Framework + Structured Interviews + Document Analysis; RF+WT+FO+PQ+IF – Analysis of River Flow and Water Turbidity data, Field Observations, a Printed Questionnaire and an Interview of Farmers; ABM-SWAT – Agent Based Model-Soil Water Assessment Tool; SD – System Dynamics; C+M – Conceptual and Methodological Framework; DPAL+OM+LWA1RA – Delineation of Potential Arable Land+Optimization Model+Land-Water Allocation to Rain-Fed and Irrigated Agriculture; Appl – Application ; DSS – Decision Support Tool; WEFC – Water Energy Food Nexus Climate.

2.14 West Africa and Water-Energy-Food Nexus

2.14.1 The Climate system of West Africa

West Africa lies between 18°W−18°E and 4°N− 20°N with five bioclimatic zones, namely, the Guineo-Congolia, Guinea, Sudan, Sahel, and Sahara zones (Cotillon & Tappan, 2016). Per climate classifications, West Africa can be divided into four climatic zones from South to North: Guinean zone ($18°W - 18°E, 4°N - 8°N$), Sudano-Sahel zone ($18°W - 18°E, 8°N - 12°N$), Sahelian zone ($18°W - 18°E, 12°N - 16°N$), and Saharan zone ($18°W - 18°E, 16°N - 20°N$) (Annor et al., 2022; Sawadogo et al., 2019). Guinea–Congolia is the wettest region with average annual rainfall ranging from 2200 mm to 5000 mm (Cotillon & Tappan, 2016). It has two major rainy seasons and a short dry season. The land cover types are mostly forest, which keeps degrading with time. The Guinea region is a seasonally wet-and-dry deciduous or semi-deciduous forest, characterized by annual rainfall between 1200-2200 mm with a 7 to 8 months distinct dry season. The Sudanian region is mostly open woodland, open tree savannas, and wooded savannas with annual rainfall between 600 and 1200 mm and a 5 to 7-month dry season. The Sahelian region is characterized by a mixture of steppe, short grass savanna (open herbaceous types), and woody plants, with an average rainfall of 150 and 600 mm, and 8 to 9 months of dry season. The annual average rainfall of the Saharan region ranges from 0 to 150 mm with vegetation varying from sparse to absent except in wadis, oases, and depressions, where water is present at or just below the surface. The West African climate is related to the advanced north-to-south retreat of the intertropical front which is associated with rainfall migration between the south and north latitudes. Maximum temperatures and temperature ranges vary slightly in the South, and to over 45˚C in the arid north (Cotillon & Tappan, 2016). The West African land surface is complexly influenced by topography, climate, vegetation, geology, hydrography, and human activities, which determine land cover and land use changes in the region. Rapid population growth has led to the transformation of forests, woodlands, steppes, and savanna into agricultural lands to feed the growing population. In this paper, five bioclimatic regions defined by the intersection of the climatic zones (Cotillon & Tappan, 2016), and the bioclimatic zones (Annor et al., 2022; Sawadogo et al., 2019) described above is adopted. The fiver bioclimatic zones are shown in Figure 2.24.

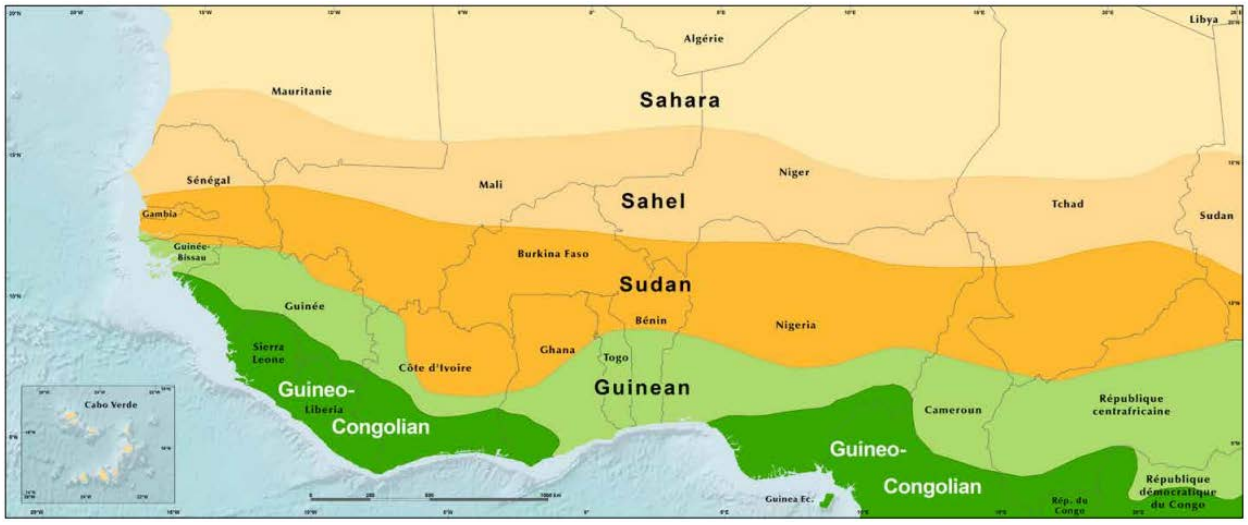

Figure 2.24 The five bioclimatic zones of West Africa

2.14.2 The Volta Basin

The Volta Basin of West Africa is located between longitudes 2° E and 5.5° W and latitudes 5.5° N and 14.5° N. It covers approximately 400,000 km^2 and is the ninth (9th) largest river basin in sub-Saharan Africa with its resources shared by six countries: Benin, Burkina Faso, Côte d'Ivoire, Ghana, Mali, and Togo (UNEP-GEF Volta Project, 2012). The Black Volta, White Volta, Oti, and the Lower Volta are the four principal sub-basins of the Volta Basin. The White Volta originates as the Nakambe in Burkina Faso whilst the Black Volta originates as the Mouhoun also in Burkina Faso and drains parts of Mali and Cote d'Ivoire. The Oti originates as Penjari in Benin flowing through Togo. The Lower Volta consists of a series of small rivers flowing into the Akosombo lake and portions of the river downstream of the Kpong dam which flows to the sea. The Oti, White Volta, Black Volta, and most rivers in the lower Volta flow into the Akosombo lake. Downstream of the lake, the Volta River empties into the Gulf of Guinea in the Atlantic Ocean through the Volta estuary at Ada, about 100 km from Accra (Ghana). Figure 2.25 shows the Volta basin and its four sub-basins. Table 2.7 shows the Volta Basin area shared by the six respective countries. The Volta basin is low-lying with altitudes varying between 0 and 920 masl. The mean altitude of the basin is approximately 257m, with more than half the basin between 200m – 300m. According to (UNEP-GEF Volta Project, 2012), the global slope index is 25-50 cm/km. Table 2.8 illustrates and characterizes the relief in the main sub-basins of the Volta basin.

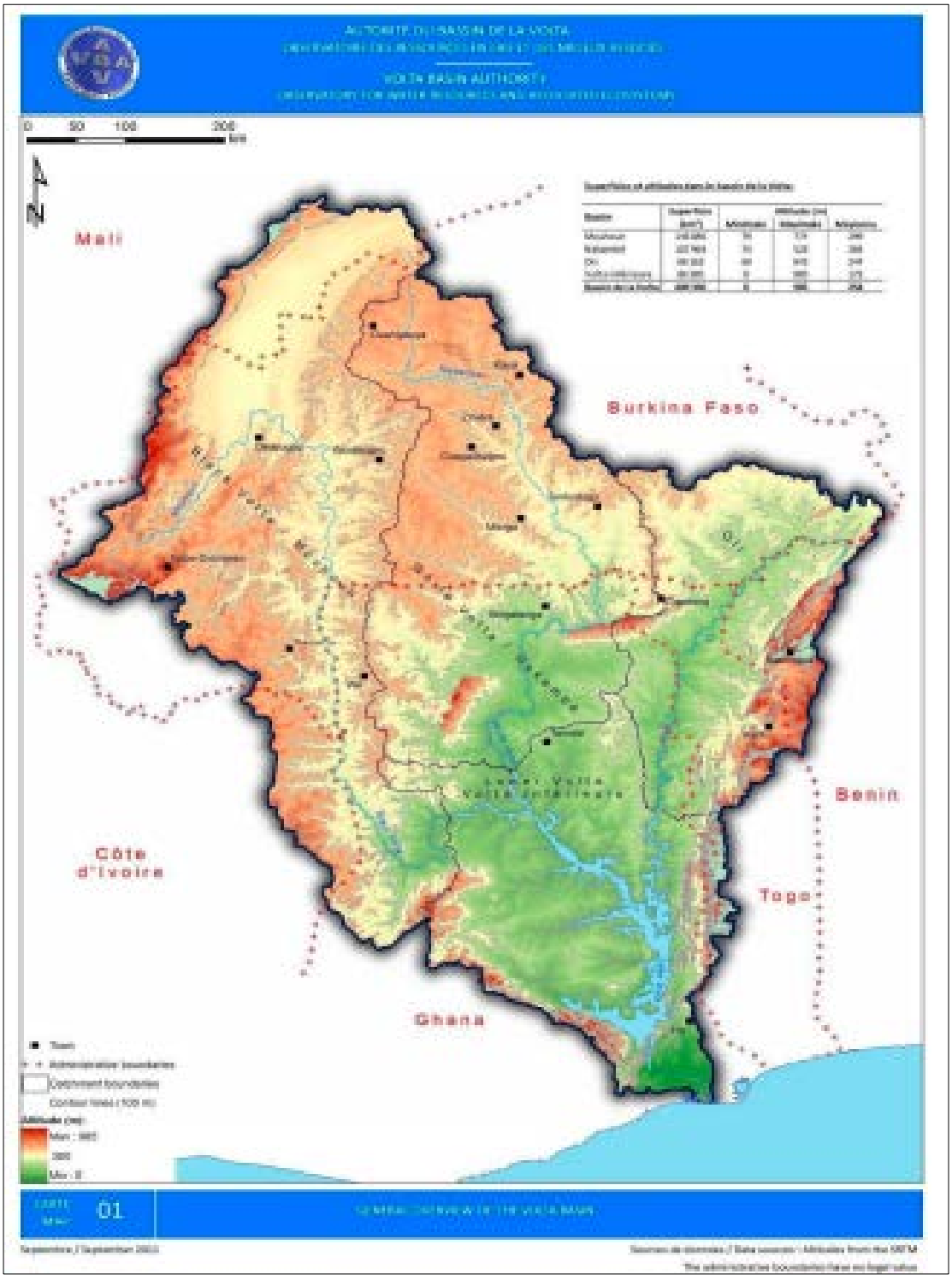

Figure 2.25 The Volta Basin and its four sub-basins

Table 2.7 Respective countries and their land cover area in the Volta Basin of West Africa

Country	Area of Volta River Basin (km^2)	% of the Basin in the country	% of the country in the Basin
Benin	13,590	3.41	12.10
Burkina Faso	171,105	42.95	62.40
Cote d'Ivore	9,890	2.48	3.07
Ghana	165,830	41.62	70.10
Mali	12,430	3.12	1.00
Togo	25,545	6.41	45.00
Total	398,390	100.00	

Source: (UNEP-GEF Volta Project, 2012)

Table 2.8 Basic data on elevation across the basin

Elevation (m)	Black Volta Basin (including Mouhoun and Sorou)	White Volta Basin (including Nakambe and Red Volta)	Oti/ Penjari
Minimum altitude	60	60	40
Maximum altitude	762	530	920
Average altitude	287	270	245

Source: (UNEP-GEF Volta Project, 2012)

2.14.3 Climate of the Volta Basin

The Volta Basin is divided into three (3) primary climatic zones: the tropical south which makes up the majority of the basin, the tropical transition zone, and the wet south which are both distinguished by two distinct rainy seasons. The wet south has a single dry season lasting from November to March and a wet season from April to October. The average annual rainfall of the three climatic zones south to north is between 1100-1400mm, 900-1100mm, and 500-900mm respectively (UNEP-GEF Volta Project, 2012). Rainfall distribution in the basin exhibits extreme variability both spatially and temporally. The climate of the Volta Basin is also regulated by two air masses, the Harmattan often referred to as the North-East Trade Winds (NETW) which are dry and dusty and originates from the heart of the continent, and the South-West Monsoon, which are in contrast moist winds that blow from across the sea (Cotillon & Tappan, 2016; UNEP-GEF Volta

Project, 2012). The Inter-Tropical Convergence Zone (ITCZ) defines where the two air masses meet and is often characterized by high-level convective activities with lots of rainfall. From March to October, the ITCZ travels north and south across the basin. The mean annual temperature varies from 36°C in the north and 27°C in the south. During march (the warmest month of the year), the Volta basin has daily mean temperatures between 24°C and 30°C, and daily temperatures changes range between 3-5°C. Potential evapotranspiration (PET) for the Basin ranges from 1176 mm to 2400 mm annually. Like rainfall, the PET in the Volta basin exhibits high space-time variability. During the wet season, humidity is very high, while during the dry season, it is particularly low. The winds are characterized by a constant south-westerly monsoon which is modulated by the land and sea breeze in the coastal region. Figure 2.26 shows the mean annual rainfall over the 1960 – 2000 over the Volta basin.

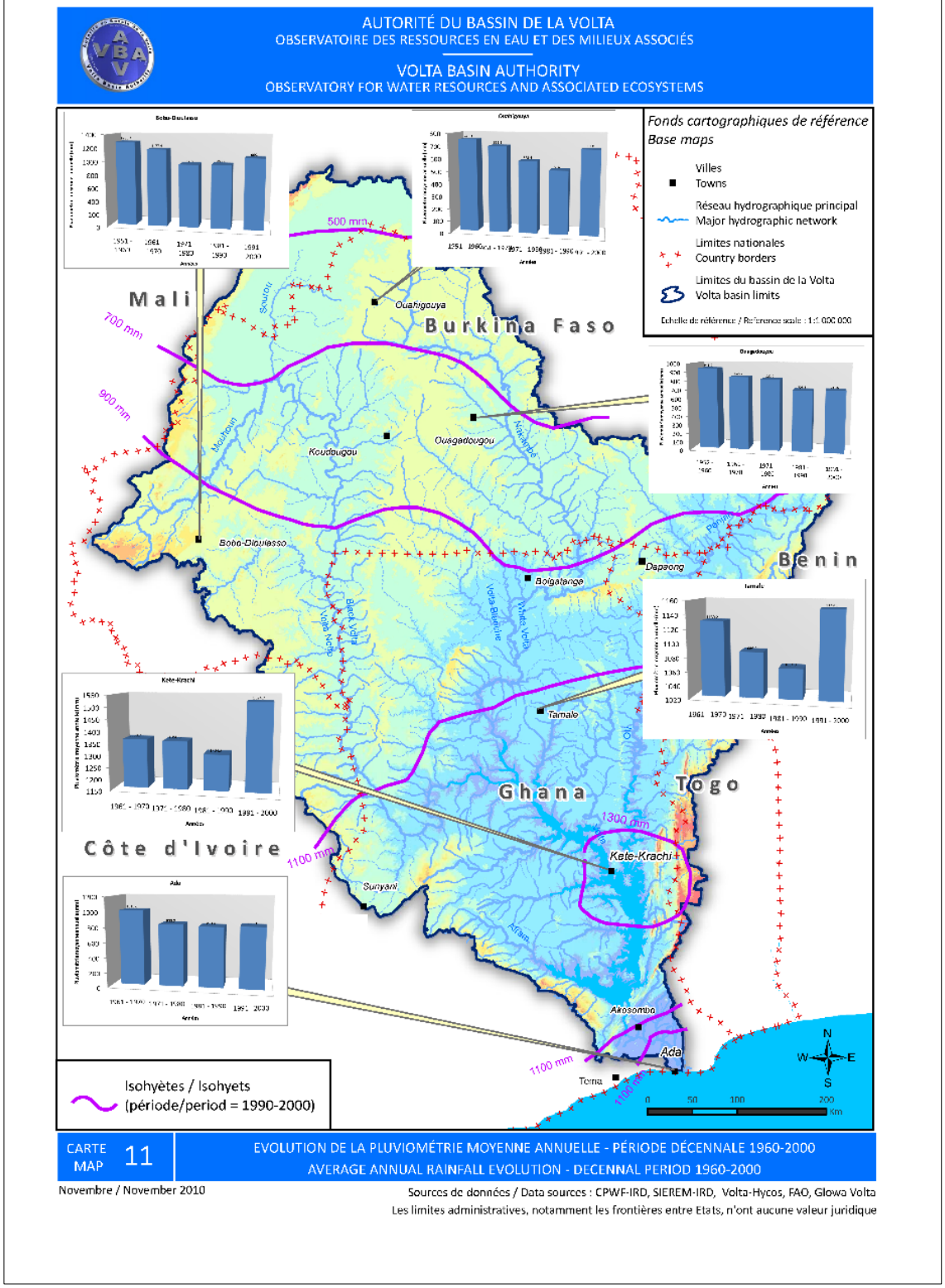

Figure 2.26 Average annual rainfall evolution - Decennal period (1960-2000)

2.14.4 Socioeconomic activities in the Volta Basin

The predominant economic sectors are agriculture (mostly rainfed), livestock raising, fisheries, forestry and biodiversity harvesting. The basin resources serve primarily its population and development of the aforementioned sectors and other sectors such as industry, energy, trade, mining, recreation and tourism, amongst others. Thus, the critical factors that determine resource utilization in the Volta basin are population (rural and urban), agricultural activities (primarily irrigation), livestock raring, and energy production (hydropower). Details of the critical factors are presented below.

2.2.4.1 Population

As of 2000, the population of the Volta Basin is estimated at 18.6 million and is projected to reach 33.9 million by 2025. According to (UNEP-GEF Volta Project, 2012), the population of the Volta Basin is predominantly rural and it will continue in the foreseeable future despite the trend towards urbanization which also increases pressure on resources. The rural population has direct dependence on natural resources base. The growing urban and rural population suggests increase pressure on natural resources, notable water. The population and trend across the Volta Basin are summarized below. Table 2.9 shows the 2008 population of the Volta basin per country, and the projected population at the end of 2025.

Table 2.9 Population trends in the Volta Basin

Country	Country population	Basin population				
	2008 (thousands)	2008 (thousands)	% of country population	Rural population (thousands)	% rural	Population projections for 2025 (thousands)
Benin	8290	590	7.12	378	64	820
Burkina Faso	15850	11227	70.83	7186	77	15997
Côte d'Ivoire	18400	497	2.70	318	77	718
Ghana	23383	8570	36.65	5484	84	11696
Mali	14517	880	6.06	563	88	1260
Togo	5870	2154	36.70	1378	70	3385
TOTALS	86310	23918	27.71	15307		33876

Source UNEP-GEF Volta Project, 2012

2.2.4.2 Water use

There are primarily two water sources in the Volta Basin: groundwater system, and surface water system which consist of the river systems and lakes such as the Volta Lake which formed from the construction of the Akosombo dam. Water resources play a vital role in economic growth and are critical for poverty reduction in the Basin. The water resources serve the purpose of domestic, agriculture (irrigation), hydropower generation, recreation, mining, industrial consumption, and environmental enhancement. Figure 2.27 shows water extraction for urban areas in the Volta Basin and the rate of access to drinking water in the rural areas. Population growth could increase pressure on water resources demand to meet the needs of the aforementioned sectors. Moreover, low rainfall due to long continuous dry years will pose significant challenge main rivers as well as tributaries leading to lesser amounts of surface and ground waters available for the increasing population. Table 2.10 shows the projected water use rate of towns/cities per country in the Volta basin of West Africa.

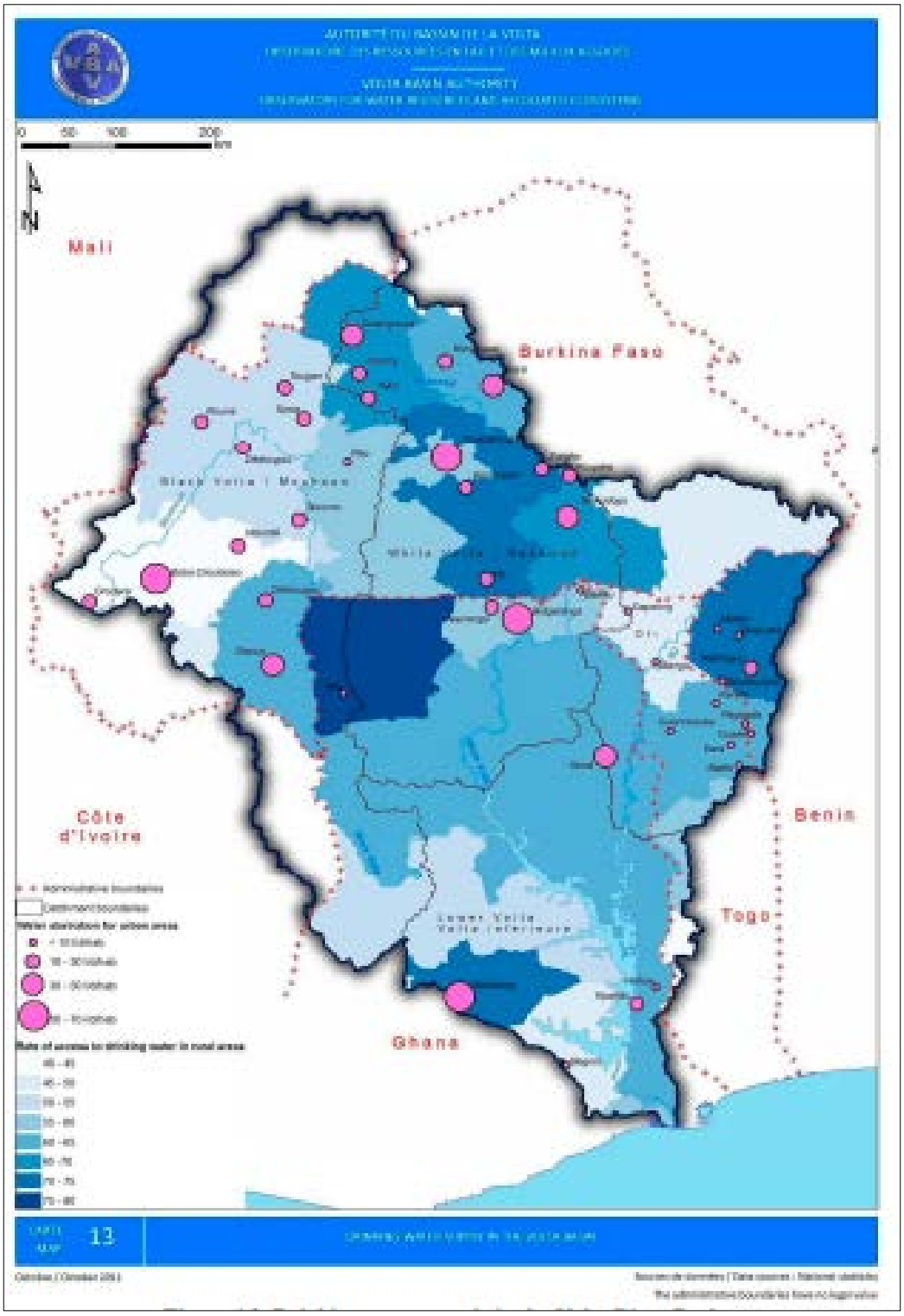

Figure 2.27 Drinking water supply in the Volta Basin

Table 2.10 Projected water use rate of towns/cities per country in the Volta basin

Country	Cities	Population	Water use rate per inhabitant (liters per day)				
			Year				
		2010	2010	2015	2020	2025	2030
Benin	Natittingou	75629	40	50	55	60	60
	Materi	83721	50	50	55	60	65
	Tanguieta	54719	50	50	55	60	65
Burkina Faso	Ouagadougou	1603641	65	70	80	90	100
	Koudougou	125626	50	50	55	60	65
	Pouytenga	66922	40	40	45	45	50
	Tenkodogo	49110	40	50	55	60	60
	Bobo Dioulasso	772006	65	70	75	80	90
	Ouahigouya	112829	50	50	55	60	60
	Yako	26234	40	40	45	45	50
	Koupela	25937	40	40	45	45	50
	Manga	24856	40	40	45	45	50
	Gaoua	29581	40	40	45	45	50
	Fada N'Gourma	57542	40	50	55	60	60
	Kaya	60000	40	40	45	50	50
	Dedougou	50501	40	45	45	50	50
Cote d'Ivoire	Bouna	90000	40	40	45	45	50
	Bondoukou	125138	40	40	45	45	50
Ghana	Bolgatanga	68019	65	70	70	75	80
	Damongo	19409	50	50	55	55	60
	Chireponi	8387	40	40	45	50	50
	Wulensi	10235	50	50	55	55	60
	Bimbila	28244	50	50	55	55	60
	Zabzugu	15145	40	40	45	50	50
	Saboba	5101	40	40	45	50	50
	Tamale	384528	65	75	80	90	100
Mali	Bankass	270796	25	30	35	35	40
	Koro Cercle	372206	25	30	35	35	40
Togo	Kara	215371	65	75	80	90	100
	Dapaong	500000	50	55	60	65	70

Source: UNEP-GEF Volta Project, (2013)

2.2.4.3 Water abstraction for irrigation

Water used for irrigation is the highest followed by domestic/industrial and then livestock. Irrigation water requirement in the Volta Basin was expected to increase from 69% in 2000 to 82% in 2020. Projected irrigable land areas by 2030 in ha are 10,503, 27,070 18,361, 4,300, 11,300, and 12,400 respectively for Benin, Burkina Faso, Cote d'Ivoire, Ghana, Mali, and Togo (Allwaters Consult Limited, 2012). Their annual water use rates are respectively 15,000 m^3/ha/year, 55,850 m^3/ha/year, 15,000 m^3/ha/year, 60,000 m^3/ha/year, 18,000 m^3/ha/year, and 18,000 m^3/ha/year. The major irrigation schemes are located at Porga in Benin, Samendeni, Sourou and Bagre in Burkina Faso, Nord-Zanzan in Cote D'Ivoire, Tono, Vea in Ghana and Bui in Ghana, Sourou in Mali and Dapaong in Togo. Figure 2.28 also shows the irrigation water demand for specific sites in the Volta Basin as of 2010. Table 2.11 Summarizes projected irrigable lands for rice cultivation per country in the Volta Basin of West Africa.

Table 2.11 Projected irrigable land for rice production per country in the Volta Basin

Country	Sub-basin	Irrigation site	Irrigable land areas and projections (ha)					Water use rate m^3/ha/year
			2010	2015	2020	2025	2030	
Benin	Oti-Pendjari	Porga	10,530	10,530	10,530	10,530	10,530	15,000
Burkina	Black Volta	Samendeni	2,500	5,000	7,500	8,900	10,500	15,850
Faso	Black Volta	Sorou	3,360	3,710	4,090	4,520	4,990	20,000
	White Volta	Bagre	3,380	7,680	8,980	10,280	11,580	20,000
Cote d'Ivoire	Black Volta	Nord-Zanzan	138	16,781	17,292	17,818	18,361	15,000
Ghana	White Volta	Tono	1,432	1,699	1,966	2,233	2,500	20,000
	White Volta	Vea	850	887	925	962	1,000	20,000
	Black Volta	Bui	50	600	700	750	800	20,000
Mali	Black Volta	Sourou	9,000	10,750	11,050	11,175	11,360	18,000
Togo	Oti	Dapaong	5,056	6,080	7,389	9,500	12,400	18,000

Source: UNEP-GEF Volta Project, (2013)

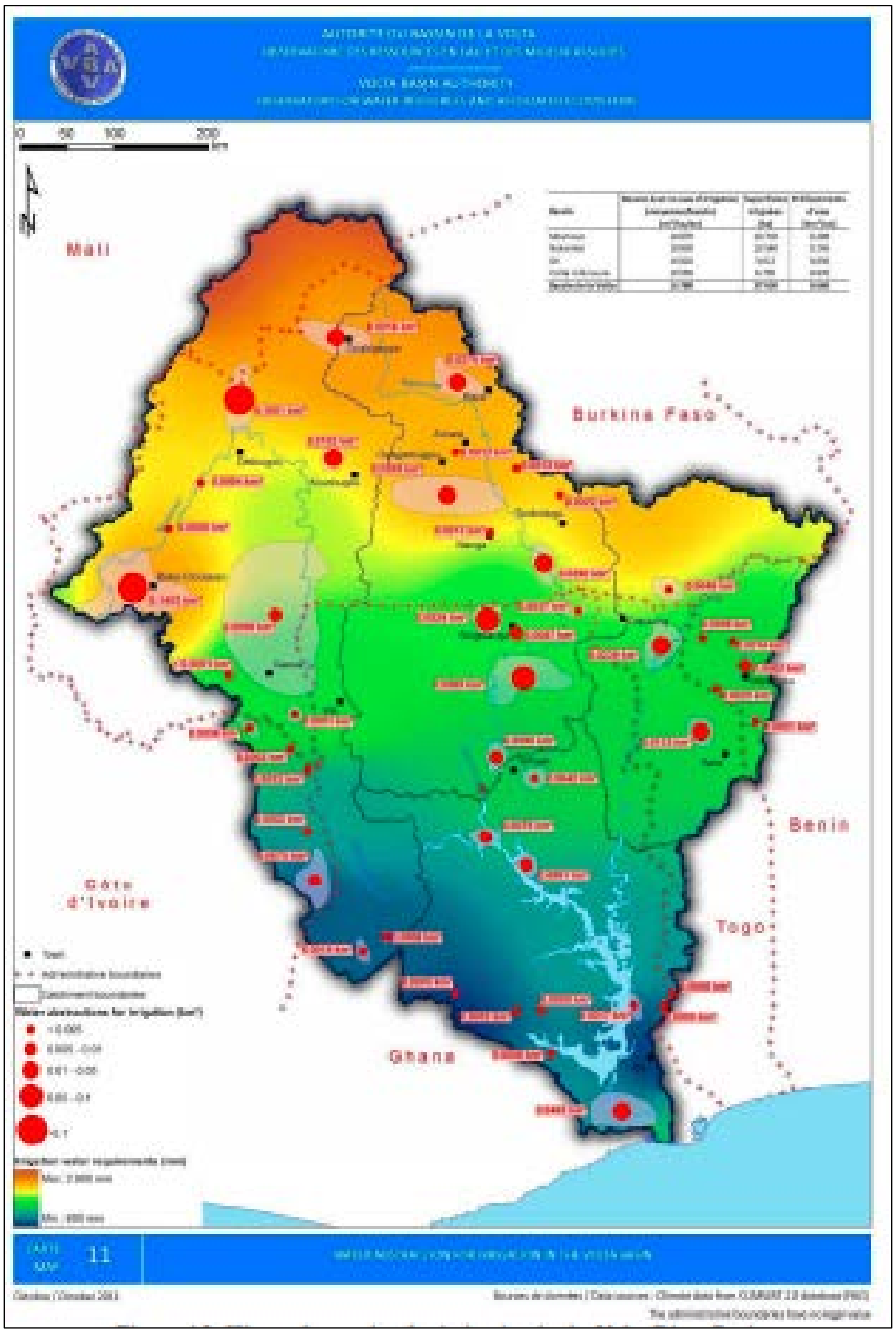

Figure 2.28 Irrigation water demand for 2010 at specific sites in the Volta Basin

2.2.4.4 Hydroelectricity generation in the Volta Basin

The Volta Basin houses a lot of dams of various sizes serving various purposes. Notable among them are the hydroelectric dams for the generation of hydroelectricity to serve the needs of neighboring towns, cities, and countries. The Akosombo, the Kpong, and the Bui dams are notable dams in Ghana for the generation of hydroelectric power. The Kompienga and the Bagre dams are also most notable for the provision of electricity and both electricity and irrigation respectively in Burkina Faso. In this thesis, the Akosombo, Kpong, Bui, Kompienga, and Bagre dams are the energy nodes for the water-energy-food nexus interactions. Existing hydroelectric dams in the Volta Basin and their generation capacity is shown in Table 2.12. A summary of proposed hydro sites in major tributaries of the Volta Basin are shown below in Table 2.13. Figure 2.29 shows major dams in the Volta basin include the hydroelectric dams for hydroelectric energy generation.

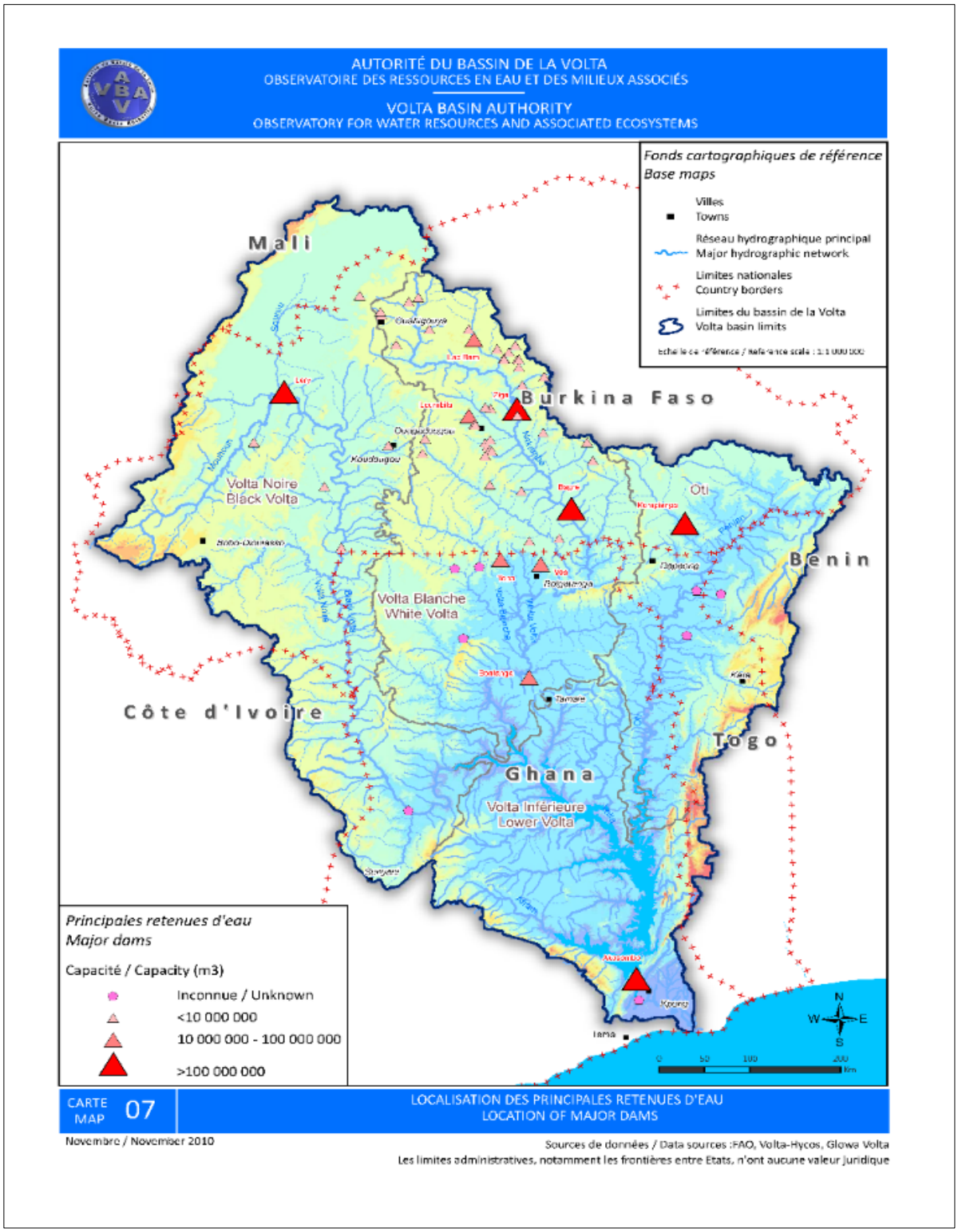

Figure 2.29 Existing dams and their capacity in the Volta Basin

Table 2.12 Existing hydroelectric plants and their installed capacity

Tributary	Sub-Basin	Installed Capacity
Akosombo	Lower Volta Basin	1020 MW
Bagre	White Volta Basin	16 MW
Bui	Black Volta Basin	400 MW
Kompienga	Oti River Basin	14 MW
Kpong	Lower Volta Basin	160 MW

Table 2.13 Details of hydro sites on the main tributaries of the Volta Basin in Ghana

Tributaries	Potential	Proposed sites	Average energy generation potential	Recommended development potential
Black Volta	682 MW	Koulbi (68MW) Ntereso (64 MW) Lanka (95 MW) Bui (460 MW) Jambito (55 MW)	2148 GWh	Not available
White Volta River	133 MW	Pwalugu (50 MW) Saboya (40 MW) Kulpawn (40 MW)	544 GWh	Not available
Oti River	Full scale potential of 300 MW	Juale	405 GWh	Recommended Potential will be reduced only by 90MW

Source: Gordon and Amatekpor, 1999

2.14.5 WEF nexus in the Volta Basin

The Volta Basin presents an excellent situation for WEF nexus framework implementation considering the water resources (water node), food resources (irrigation node) and energy component (hydropower development). However, there are very research on WEF nexus in the Volta Basin (Ouedraogo et al., 2024; Siakwah & Torto, 2022), and very limited practical implementation of WEF nexus approaches. The studies are often descriptive of the complexity of the WEF nexus approach as in Siakwah & Torto, (2022), or an analysis of a single hydropower impacts on downstream communities as in Okyereh et al. (2019) and Ouedraogo et al. (2024). Such an analysis is localized, incomplete definition of the nexus problem and cannot be the basic for decision making in the Volta Basin. In practice, the Kpong dam irrigation scheme has serve the purpose of water-energy-food nexus, and the current Bui dam has WEF nexus plans including

and irrigation scheme for farmers, fish farming, while generating energy (hydropower). Again, this isolated cases forms and incomplete definition of the nexus problem and cannot be the basin-wide water, energy, and food resources management. Thus, a WEF nexus design that takes into account the entire VB is the first step necessary to understand the WEF nexus interactions in the Volta Basin and prepare for practical implementation of the WEF nexus. In the next section, the shared socioeconomic scenarios of CMIP6 used in the studies are described.

2.15 The Shared Socioeconomic Pathways

The Shared Socioeconomic Pathways (SSPs) are scenarios used in the Coupled Model Intercomparison Project Phase 6 (CMIP6) to explore future climate impacts and challenges. The SSPs describe five scenarios for human development and global environmental change in the 21st century (van Vuuren et al., 2017). The SSPs provide narratives and quantitative projections of how global society, demographics, economics, lifestyle, governance, technological development, and other societal factors might change over the 21st century (B. O'Neill, 2016). There are five main types of SSPs used in climate research: SSP1, SSP2, SSP3, SSP4, and SSP5. The Representative Concentration Pathways (RCPs) are a set of greenhouse gas concentration trajectories adopted by the climate modeling community for the Coupled Model Intercomparison Project Phase 5 (CMIP5) (van Vuuren et al., 2011). There are four primary RCPs (RCP2.6, RCP4.5, RCP6.0, and RCP8.5), each named after the radiative forcing level at the end of 2100. Thus, RCP2.6, RCP4.5, RCP6.0, and RCP8.5 represent greenhouse gas radiative forcing of 2.6 Wm^{-2}, 4.5 Wm^{-2}, 6.0 Wm^{-2}, and 8.5 Wm^{-2}, respectively, at the end of the century (van Vuuren et al., 2011). The RCPs are used to project and analyze the impacts of different levels of greenhouse gas emissions on the climate system. In the Coupled Model Intercomparison Project Phase 6 (CMIP6), the SSPs are combined with RCPs to create a matrix of scenarios for climate research (Gütschow et al., 2021). The SSPs provide socioeconomic narratives and quantitative projections, while the RCPs describe different pathways of greenhouse gas concentrations and radiative forcing. By combining SSPs with RCPs, a framework is created for researchers to perform an integrated analysis of climate and societal choices, various future scenarios, and their potential impacts on climate change, enabling comprehensive assessments of mitigation and adaptation strategies (O'Neill et al., 2020). In this work, the future impact of combined climate change and socioeconomic activities is evaluated

based on the following scenarios: SSP1-2.6 (SSP1-RCP2.6), SSP2-4.5 (SSP2-RCP4.5), SSP3-7.0 (SSP3-RCP7.0), SSP4-6.0 (SSP4-RCP6.0) and SSP5-8.5 (SSP5-RCP8.5).

2.15.1 SSP1-2.6

The SSP1-2.6 represents strong and sustainable climate policies resulting in low greenhouse gas emissions. The SSP1-2.6 scenario is related to the Paris Agreement, which aims to keep global warming to 2.0 °C by 2100 (Meinshausen et al., 2011). The scenario is obtained by updating the RCP2.6 scenario, which represents the low end of the spectrum of future forcing paths in the Integrated Assessment Models (IAM) literature. SSP1 was selected because of its significant changes in land use, including the expansion of worldwide forest cover, which is useful in answering the scientific questions of the Land-Use Model Intercomparison Project (LUMIP) (O'Neill et al., 2016). With its low forcing signal, a low obstacle for mitigation, and low vulnerability, this scenario is significant from an IAM standpoint. According to Riahi et al. (2017), the premise for this scenario is international collaboration in the fight against climate change. In the SSP1 scenario, fertility rates are low and life expectancy improves for developing nations. The outcome is that the global population will peak and decline at the end of the century**.** The global population would be about 7 billion people, and the temperature would rise by 1.3 to 2.4 degrees Celsius from 1950 (Irfan, 2021; KC & Lutz, 2017; Siabi et al., 2023). This scenario conforms to the objectives of the Paris Agreement, which is to limit global warming to less than 2.0 °C, assuming an increase in the average global temperature of 1.8 °C and a temperature range between 1.3 °C and 2.4 °C by 2100 (Meinshausen et al., 2011; Rogelj et al., 2016).

2.15.2 SSP2-4.5

SSP4-6.0 represents a divided world, exploring the implication of socioeconomic inequality on climate change adaptation and mitigation actions. This scenario updates the RCP4.5 pathway and represents the middle portion of the range of future forcing pathways. Several other CMIP6-Endorsed MIPs such as the Coordinated Regional Climate Downscaling Experiment (CORDEX), the Detection and Attribution MIP (DAMIP), and the Decadal Climate Prediction Project (DCPP) will use it as a reference scenario to continue the historical simulations and update regression-based estimates of the role of single forcing beyond 2015 (O'Neill et al., 2016; Riahi et al., 2017). In SSP2, the population grows moderately, stabilizing in the second half of the century. The

fertility rate declines gradually, leading to a non-drastic shift in demographic trends. This scenario corresponds to a global population of 9.0 billion people and warming levels between 2.1 and 3.5℃ relative to 1950 (Irfan, 2021; KC & Lutz, 2017; Siabi et al., 2023). The average warming will be about 3.5℃ by 2100 (Irfan, 2021). The SSP2 was selected as a scenario that combines intermediate societal vulnerability with an intermediate forcing level, which is relevant to Tropical Atlantic Modes (TAM)/Tropical Atlantic Variability (TAV) research. Moreover, its land use and aerosol pathways are not extreme, which are the central concerns for SSPs like DAMIP and DCPP (O'Neill et al., 2016; Riahi et al., 2017).

2.15.3 SSP3-7.0

SSP3-7.0 represents a fragmented world with high emissions because of regional rivalry and limited climate action. SSP3-7.0 represents a situation where nationalism takes center stage, with countries focusing on their economic objectives, and turning away from international collaboration (Riahi et al., 2017). This scenario mimics the increased use of their fossil fuel resources (Riahi et al., 2017), resulting in increased aerosols and greenhouses, with extremely high carbon dioxide levels by the end of the century. This scenario represents a medium-to-a high range of potential forcing paths comparable to the forcing in the SSP2 baseline scenario, and it is particularly a significant fill-in for the CMIP5 forcing routes (O'Neill et al., 2016). Moreover, because the SSP3-7.0 combines very high radiative forcing with relatively high societal vulnerability, it is pertinent to IAM/IAV investigations, by comparing it with the uncontrolled baseline scenario to determine the impacts that must be avoided. SSP3 was selected because SSP3-7.0 is a scenario that will be crucial to LUMIP and Aerosols and Chemistry Model Intercomparison Project (AerChemMIP), answering scenario-relevant questions about how sensitive regional climate is to land use and aerosols (Riahi et al., 2017). The global population in this scenario reached approximately 12.6 billion (KC & Lutz, 2017). Demographic transitions and migration are also low. The outcome is that the global population grows rapidly, leading to pressure on resources and increased vulnerability to climatic impacts, particularly in less-developed regions. The global average temperature will increase approximately 3.6℃ ranging between 2.8℃ and 4.6 ℃ (Irfan, 2021).

2.15.4 SSP4-6.0

Besides updating the RCP6.0 pathway, this scenario completes the range of a medium-forcing pathway. SSP4 was selected to examine variations in consequences across global average forcing routes, especially if land use and aerosols have significant regional climatic effects (O'Neill et al., 2016). In SSP4, the global population growth is even with a demographic divide trajectory. Developed and wealthier countries experience a low population growth while poorer developing countries experience higher population growth. The population estimate for the world and Africa under this scenario is 9.3 billion and 3.6 billion, respectively at the end of the century (KC & Lutz, 2017).

2.15.5 SSP5-8.5

SSP5-8.5 represents a world with high economic growth driven by fossil fuels, resulting from high emissions. Further details are provided below. The SSP5-8.5 scenario states that although humanity does not always take action to stop climate change, it continues to worsen (Riahi et al., 2017). In this scenario, the burning of coal, oil, and natural gas will drive global economic growth. The population growth stabilizes significantly because of a drop in the fertility rate, significant improvements in living standards, economic development, and widespread access to education and health care**.** The global population will be approximately 7.4 billion by the end of 2100, having peaked at 8.5 billion in the 2050s (KC & Lutz, 2017). The population of Africa will reach 1.8 billion at the end of the century (KC & Lutz, 2017). The development of the SSP5 scenario comes at the cost of high greenhouse gas emissions and environmental degradation. With limited efforts to reduce emissions, resources are being dedicated to climate change adaptation in this instance (Riahi et al., 2017). The temperature for this scenario will have warmed by 4.4 °C, ranging between 3.3 °C to 5.7 °C compared to 1950 (Irfan, 2021; Riahi et al., 2017). By examining the effects of a significant overshoot in radiative forcing in the twenty-first century relative to a longer-term target, this scenario closes a gap in current climate simulations. The impact, mitigation, and adaptation implications of this overshoot are of great interest, and it is important to first comprehend how this pathway would affect the climate. This scenario runs parallel to the unmitigated baseline scenario SSPS-8.5 to 2040. Thereafter, significant mitigation is implemented to reduce drastically the emissions to zero by about 2070 and to net negative levels after 2070. By diverging from their

Tier-1 SSPS-8.5 simulation in 2040, this architecture will allow climate modeling teams to run to the scenario. Specific elements such as the rates of emissions reduction after 2040 and the amount of net negative emissions must be taken into account in the final design of the overshoot scenario. Variables such as the rate of emissions reduction after 2040 and the total quantity of net negative emissions by the end of the century, will need to be taken into further consideration when designing the overshoot scenario later on (O'Neill et al., 2016; Riahi et al., 2017).

2.16 Partial conclusion on literature review

The literature reviewed revealed that the traditional approach to land-atmosphere/climate-land interaction research is modeling (GCM and RCM). The analysis approach of investigating the relationship between an atmospheric variable and a land surface variable is limited compared to the traditional approach. Only WRF/WRF-Hydro, Rainfall-Runoff model, and VIC-CropSyst-V2 have been identified to have hydrological modeling capabilities, with only the VIC-CropSyst-V2 applicable for WEF nexus research. A literature review of WEF nexus research started with a sustainability focus but has broadened to WEF nexus approaches and many practical applications in recent years. WEAP and SWAT have been applied for WEF nexus and hydrological modeling, but only WEAP has WEF nexus, hydrological modeling, hydropower modeling capabilities, and proven applicability over West Africa. Based on these capabilities, WEAP was adopted to investigate the impact of climate change on the WEF nexus in the Volta Basin. The WRF-Hydro was also found to possess the capability to investigate the relationship between climate variability and land use/land cover change over West Africa. The ESA land cover data is also determined from literature as the land cover data that is most suitable to investigate the dynamic interactions between the climate and land use/land cover change in West Africa.

CHAPTER 3 – MATERIALS AND METHOD

3.1 Introduction to material and methods

This chapter comprises the study area, data collection, data analysis, and modeling. The study area includes West Africa, the Volta Basin, and the Sissili-Kulpawn Basin. The data collection section outlines the remote sensing, reanalysis data, and observational products for analyzing the relationship between climate and land use/land cover changes, forcing the WRF-Hydro and WEAP models, and validating their outputs. Data analysis outlines the approach used to establish the relationship between climate variability and land use/land cover from the analysis viewpoint. The modeling aspect outline the approaches for investigating the relationship between climate variability and land use/land cover change using the fully coupled land-atmosphere interaction model (WRF-Hydro) and the hydrological model (WEAP). Sections 3.2 to 3.5 deal with study area, data collection, data analysis, and modeling, respectively. Section 3.6 deals with the partial conclusions on material and methods used.

3.2 Study area

This study focuses on West Africa, the Volta basin, and the Sissili-Kulpawn basin, which are also within West Africa (Figure 3.1). West Africa is located between 18°W−18°E and 4°N− 20°N and consists of five bioclimatic zones: Guineo-Congolia, Guinea, Sudan, Sahel, and Sahara zones (Cotillon & Tappan, 2016). In terms of climate, it is divided according to the latitudinal range: the Guinean zone (4°N-8°N), Sudano-Sahel zone (8°N-12°N), Sahelian zone (12°N-16°N), and Saharan zone (16°N-20°N) (Annor et al., 2022; Sawadogo et al., 2019) (Figure 3.1). These zones cover the same longitudinal extent, ranging from 18°W to 18°E. The Guinea–Congolia region experiences the highest precipitation amount, with average annual rainfall ranging from 2200 mm to 5000 mm (Cotillon & Tappan, 2016). The region experiences two significant periods of rainfall and a brief dry period. The predominant land cover types consist primarily of forests, which progressively deteriorate over time. The Guinea region is a biome that has both rainy and dry seasons and is dominated by deciduous or semi-deciduous forests. It receives an annual rainfall ranging from 1200 to 2200 mm. The Sudanian region is mostly characterized by expansive woodland, tree savannas, and savannas with a moderate number of trees. It experiences an annual

rainfall ranging from 600 to 1200 mm. The Sahelian region is distinguished by a combination of steppe and short grass savanna, which consists of open herbaceous vegetation and woody plants. The region experiences an average annual rainfall ranging from 150 to 600 mm and has a dry season that lasts for 8 to 9 months. The Saharan region experiences an annual average rainfall ranging from 0 to 150 mm. Vegetation in this region is generally sparse or absent, except in areas such as wadis, oases, and depressions, where water is available either at or just below the surface. The climate of West Africa is influenced by the progressive movement of the intertropical front from north to south, which leads to the migration of rainfall between latitudes in the southern and northern regions. The maximum temperatures and temperature ranges exhibit slight variations in the South, whereas, in the arid north, they can surpass 45˚C (Cotillon & Tappan, 2016). The land surface of West Africa is intricately shaped by factors such as terrain, climate, vegetation, geology, hydrography, and human activities. These factors play a crucial role in determining the changes in land cover and land use in the region. Population growth often leads to the expansion of agricultural areas to feed the growing population and the increase in built-up areas. This work concerns five bioclimatic regions that are determined by the overlapping of bioclimatic zones (Cotillon & Tappan, 2016) and climatic zones (Annor et al., 2022; Sawadogo et al., 2019) (See Figure 3.1). Within West Africa is the Volta basin located between longitudes 2° E and 5.5° W and latitudes 5.5° N and 14.5° N. It covers approximately 400,000 km^2 and is the ninth largest river basin in sub-Saharan Africa, with its resources shared by six countries: Benin, Burkina Faso, Côte d'Ivoire, Ghana, Mali, and Togo (UNEP-GEF Volta Project, 2013). The Black Volta, White Volta, Oti, and Lower Volta are the four principal sub-basins of the Volta Basin. The Volta Basin altitude is between 0 and 920 m, with more than half the basin between 200 m – 300 m. The basin spans north to south three climatic zones: a tropical north beyond 9°N; a tropical transition zone with two close rainfall seasons; and a humid south with two distinct rainfall seasons (Figure 3.1). Rainfall decreases south to north according to agroclimatic zones with the Sahelian zone receiving less than 500 mm per year, whilst the Sudano-Sahelian and the Guinean zone receive about 500 to 900mm, and 900mm to 1100 mm per annum respectively. The mean annual temperature over the basin varies from 36°C in the north and 27°C in the south, whilst the annual potential evapotranspiration (PET) ranges from 1176 mm to 2400 mm. The predominant economic sectors in the Volta Basin are agriculture (mostly rainfed), livestock raising, fisheries, forestry, and

biodiversity harvesting. The basin resources serve primarily its population and development of the aforementioned sectors and other sectors such as industry, energy, trade, mining, recreation, and tourism, amongst others. Critical factors that determine resource utilization in the Volta Basin are population (rural and urban), agricultural activities (primarily irrigation), livestock farming, and energy production (hydropower). As of 2000, the population of the Volta Basin (mostly rural) is estimated at 18.6 million and is projected to reach 33.9 million by 2025. There are primarily two water sources in the Volta Basin: groundwater systems, and surface water systems which consist of the river systems and lakes (eg. Volta lake). The water resources serve the purpose of domestic, agriculture (irrigation), hydropower generation, recreation, mining, industrial consumption, and environmental enhancement. Water use for irrigation is the highest followed by domestic/industrial and then livestock. Irrigation water requirement in the Volta Basin was expected to increase from 69% in 2000 to 82% in 2020. Projected irrigable land areas by 2030 in ha are 10,503, 27,070 18,361, 4,300, 11,300, and 12,400, respectively for Benin, Burkina Faso, Cote d'Ivoire, Ghana, Mali, and Togo (Allwaters Consult Limited, 2012). The Volta Basin houses a lot of dams of various sizes serving various purposes. Notable among them are the hydroelectric dams for the generation of hydroelectricity to serve the needs of neighboring towns, cities, and countries. The Akosombo dam, the Kpong, and the Bui dams are notable dams in Ghana for the generation of hydroelectric power. The Kompienga dam and the Bagre dam are also most notable for the provision of electricity, and irrigation in Burkina Faso. In this work, the Akosombo dam, Kpong dam, Bui dam, Kompienga, and Bagre dams are considered for the water-energy-food nexus interactions. The Sissili-Kulpawn Basin (SKB) consists of the Sissili Basin (SB) and the Kulpawn Basin (KB) which are sub-basins of the White Volta Basin (shown in brown in Figure 3.1). The SB is located between 10.28°N–12.0°N and 2.58 °W–1.8°W (Figure 3.1), covering a 12800 km^2 area and a core research site of the West Africa Science Service Center on Climate Change and Adapted Land Use (WASCAL) (Arnault et al., 2016; Graf et al., 2021). The Topography is mostly flat ranging from 300 m to 400 m in the Northern Burkina side of the basin and between 200 to 300m in the Ghana side of the Basin (Figure 3.1). The presence of a protected wildlife area at the central parts of the basin (Nazinga Game Ranch where no farming activities occur) ensures land use and land cover changes in the SB are less pronounced (Bliefernicht et al., 2018). Rainfall within the SB is unimodal with a pronounced wet season ranging between May

and September. Annual total rainfall is about 1200 mm. Runoff from rainfall drains into the Sissili River with the principal discharge station at Wiasi (Figure 3.1). The KB lies between 9.6 °N–11.1°N and 2.6 °W–1.2°W almost entirely within Ghana (Figure 3.1) covering about 10541 km^2 area (Figure 3.1). The topography is uniformly flat over the Basin with elevations of 200 to 250 m. The main land use activity is subsistence crop production such as millet, groundnut, sorghum, guinea corn, and cotton and animal husbandry. The mean monthly rainfall varies from approximately 115 mm in May to 900 mm between August and September. Runoff generated from rainfall is measured at Yagaba on the Kulpawn River (Figure 3.1).

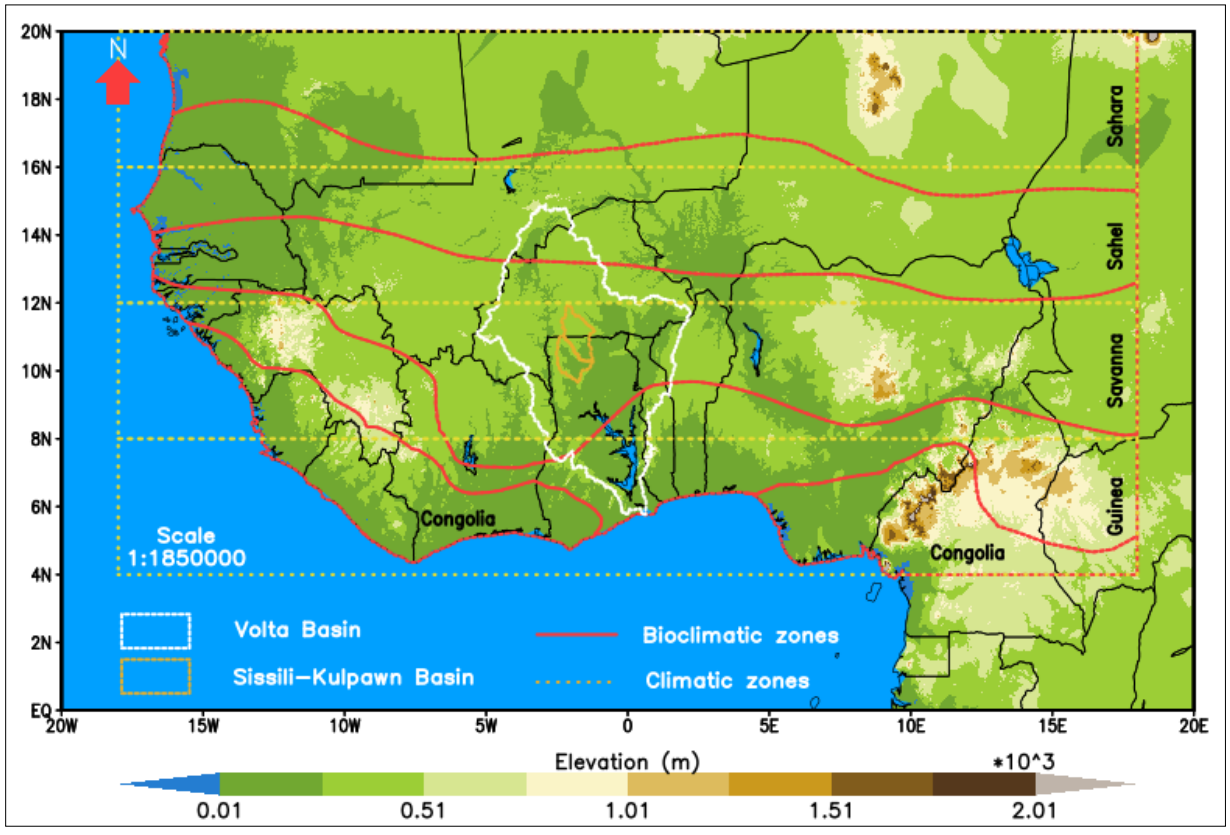

Figure 3.1 Map of West Africa showing five bioclimatic zones (Adapted from Annor et al., 2022; Cotillon & Tappan, 2016; Sawadogo et al., 2019), the Volta Basin and the Sissili-Kulpwan Basin.

3.3 Data collection

3.3.1 Climate Data

To investigate the relationship between climate variability and land use land cover changes, gridded reanalysis and satellite datasets of temperature (T), precipitation (P), and potential evapotranspiration (PET) between 1980 and 2020 were used. The datasets consist of high-resolution gridded land-based observations (CRU TS), high-resolution reanalysis (ERA5) with numerical integration of ECMWF land surface model (ERA5-Land), satellite products merged with observations (CHIRTS and CHIRPS), high-resolution datasets produced by combining climatological normal from WorldClim data with coarser resolution time-varying data from other sources, and evaporation data from the Global Land Evaporation Amsterdam Model (GLEAM). In selecting datasets, the source, spatial and temporal resolution, and the availability of temperature, precipitation, and potential evapotranspiration variables were critical factors. To avoid biases in conclusion, multiple datasets were used so that a generalized conclusion can be drawn from all the data products instead of a conclusion from single data product. To avoid biases in data selection, a wide range of the datasets were carefully selected which includes datasets derived purely from observations (CRU TS), satellite combined with observations (CHIRPS, CHIRTS), and reanalysis (ERA5-Land, TerraClimate) data products. This also to ensure that the conclusions are not based on only reanalysis, gridded observations or merged satellite and observational products. To be useful for investigating the relationship between climate variability and land cover change, each dataset must have sufficiently longer timeseries between 1980 to 2020. In terms of spatial resolution flexibility was allowed with very high resolution (0.04° to 0.5°) to explore the comparative stories from each dataset. For consistency and ease of comparison, only climate data having all three variables (T, P, PET) for computation of SPI, STI and SPEI were used. For CHIRPS data which has no PET, the GLEAM data (Martens et al., 2017) and CHIRPS precipitation datasets were used to derive a high-resolution SPEI dataset for the West Africa region, similar SPEI for Africa, available at https://data.ceda.ac.uk/neodc/spei_africa/data (accessed on 16 June 2024). Table 3.1 summarizes the data products, spatial resolution, the period used, and their technical validation documents.

Table 3.1 Climate data used to compute standardized climatic indices

Dataset	Variable	Spatial Resolution	Period Used	Validation Report
CRU TS	T, P, PET	0.5◦ × 0.5◦ ~ 55.5 km	1980–2020	(Harris et al., 2020)
ERA5-L	T, P, PET	0.1◦ × 0.1◦ ~ 11.1 km	1980–2020	(Muñoz-sabater et al., 2021)
TCM	T, P, PET	1/24◦ ~ 4 km	1980–2020	(Abatzoglou et al., 2018)
CHIRTS	T	0.05 ◦ ~ 5 km	1983–2016	(Verdin et al., 2020)
CHIRPS	P	0.05 ◦ ~ 5 km	1981–2020	(Funk et al., 2015)
GLEAM	PE	0.25 ◦ ~ 27 km	1981–2020	(Martens et al., 2017)

Climate Hazards Group Infrared Precipitation with Stations (CHIRPS); Climatic Research Unit gridded Time Series (CRU TS); ERA5-Land (ERA5-L); ReAnalysis fifth-generation; ECMWF—European Centre for Medium-Range Weather Forecasts (ERA5—ECMWF); TerraClimate (TCM); Global Land Evaporation Amsterdam Model (GLEAM), Temperature (T), Precipitation (P), Potential Evapotranspiration, Potential Evaporation (PE).

To assess the regional climate response to land cover change in the SKB, the WRF-Hydro simulated outputs including temperature, precipitation, discharge, and energy fluxes over the SKB are validated with the observational products. The validation period for precipitation, and temperature is from 2010 to 2016, while the energy fluxes were validated from 2010 to 2013. The observational data products used for the validation are summarized in Table 3.2.

Table 3.2 Observational products used to validate the simulated outputs of the WRF-Hydro

Observation products used for validating temperature (T), precipitation (P), Discharge (Q), Radiation flux (R), and Heat fluxes (H). Heat fluxes consist of sensible heat flux ($H^{sensible}$) and the latent heat flux (H^{latent}); Radiation flux consists of the net radiation flux (R^{net}). The temperature observational product is from the Climate Hazard Infrared Temperature with Stations (CHIRTS); the precipitation observational product is from the Integrated Multi-satellitE Retrievals for Global precipitation measurement dataset (IMERG), the observational energy fluxes dataset (FLUXCOM) is merged energy flux measurements from FLUXNET from eddy covariance towers combined with meteorological and remote sensing data.

Observational product	Variable	Spatial resolution	Temporal resolution/coverage	Period used	Validation report
CHIRTS	T	0.05°	Daily (1983-2016)	2010-2016	(Verdin et al., 2020)
IMERG	P	0.1°	Daily (2001-2021)	2010-2016	(Huffman et al.,2020)
FLUXCOM	R, H	0.5°	Monthly(2000-2013)	2010-2013	(Jung et al., 2019)

The water-energy-food nexus in the Volta Basin was modeled using the WEAP hydrological model. The WEAP model data requirements include elevation data, land cover dataset, climate data, and socioeconomic data. The ESA CCI LC dataset was used to access the plausible impacts of land cover change on water and energy in the Volta Basin. A detailed description of the ESA LC maps was presented in section 2.9. The climate data consists of historical climate and future climate projection datasets. The historical climate used to drive the WEAP model was the latest version of the Global Meteorological Forcing Dataset (GMFD) for land surface modeling from Princeton University (http://hydrology.princeton.edu/data/pgf/v3/0.25deg/daily/). For the future climate projection, the NASA Earth Exchange Daily Global Downscaled Projections (NEX-GDDP-CMIP6) (Thrasher et al., 2022) were used. The NEX-GDDP-CMIP6 archive contains downscaled historical and future projections for 1950–2100 based on output from Phase 6 of the Climate Model Intercomparison Project (Phase 6) (CMIP6). The downscaled products were produced using a daily variant of the monthly bias correction/spatial disaggregation (BCSD) method and are at 1/4-degree horizontal resolution (Thrasher et al., 2022). Fifteen different Models from the CMIP6 were used for future climate projections. Each of the models contains temperature at 2m height, precipitation, relative humidity, and windspeed at 2m height at daily timescales. The NEX-GDDP-CMIP6 daily datasets are available online for download at https://www.nccs.nasa.gov/services/data-collections/land-based-products/nex-gddpa. For the GMFD dataset which lacks relative humidity, the relative humidity was computed from temperature, pressure and specific humidity. The details of each climate data, the resolution, and the period used are presented in the Table 3.3. The 15-Member ensemble was computed and used as one of the input data into WEAP. Before the modeling in WEAP, an initial analysis of the temperature and precipitation changes over the Volta basin was done using the NEX-GDDP-CMIP6 datasets.

Table 3.3 Historical and future climate datasets used in the CMIP6 model

Model	Variable	Spatial resolution	Period used
GMFD Dataset	T, P, W, RH	0.25° × 0.25°	1980-2014
ACCESS-CM2	T, P, W, RH	0.25° × 0.25°	1980-2100
ACCESS-ESM1-5	T, P, W, RH	0.25° × 0.25°	1980-2100
CanESM5	T, P, W, RH	0.25° × 0.25°	1980-2100
CMCC-CM2-SR5	T, P, W, RH	0.25° × 0.25°	1980-2100
CMCC-ESM2	T, P, W, RH	0.25° × 0.25°	1980-2100
GISS-E2-1-G	T, P, W, RH	0.25° × 0.25°	1980-2100
HadGEM3-GC31-LL	T, P, W, RH	0.25° × 0.25°	1980-2100
MIROC6	T, P, W, RH	0.25° × 0.25°	1980-2100
MIROC-ES2L	T, P, W, RH	0.25° × 0.25°	1980-2100
MPI-ESM1-2-HR	T, P, W, RH	0.25° × 0.25°	1980-2100
MPI-ESM1-2-LR	T, P, W, RH	0.25° × 0.25°	1980-2100
MRI-ESM2-O	T, P, W, RH	0.25° × 0.25°	1980-2100
NorESM2-LM	T, P, W, RH	0.25° × 0.25°	1980-2100
NorESM2-MM	T, P, W, RH	0.25° × 0.25°	1980-2100
TaiESM1	T, P, W, RH	0.25° × 0.25°	1980-2100

Temperature (T), Precipitation (P), Wind speed (W), Relative humidity (RH)

3.3.2 Land cover data

The ESA CCI LC dataset was used entirely for this thesis. The details of the ESA LC dataset are presented in section 2.9, including the spatial resolution and temporal availability. To establish the relationship between climate variability/extremes and land use and land cover changes over West Africa, twenty-nine (years) of ESA LC was used. To investigate the regional climate response to land cover change over the SKB using WRF-Hydro, the 2010 ESA LC data was used. To investigate the impact of afforestation and deforestation on the climate of SKB using WRF-Hydro, the ESA LC was modified to reflect afforestation (closed shrubland expansion) and deforestation scenarios (cropland expansion). Finally, to investigate the impact of static and dynamic land use/land cover change on the WEF nexus in WEAP, the 1992 ESA LC data, and the 1992–2019 ESA LC data were used, and the scenarios were compared.

3.3.3 Socioeconomic data

The Gridded Population of the World, Version 4 (GPWV4) from the Socioeconomic Data Center and Applications (SEDAC) from the University of Columbia (https://sedac.ciesin.columbia.edu/) was used. The GPWV4 is the population count adjusted to match 2015 estimates of human population consistent with national censuses and population registers with respect to spatial distribution (CIESIN, 2018). The 1km GWPv4 data for 2000, 2005, 2010, 2015, and 2020 was the primary historical population data used in the WEAP model. For future projections, version 1.01 of the Global 1-km Downscaled Population Base Year and Projection Grids based on the Socioeconomic Pathways (SSPs) (Gao, 2020) were applied. This dataset is available from 2000 to 2100 and was also obtained from SEDAC.

3.3.4 Hydrological Data

Hydrological datasets consist of streamflow data from gauges within the Volta Basin. The Volta Basin Authority (VBA) at Ouagadougou, Burkina Faso provided the hydrological data used in this study. The hydrological datasets consist of a monthly timeseries of observed discharge at Bui in the Black Volta, Saboba and Sabari in the Oti, Bagre, and Nawuni in the White Volta, and Senchi in the Lower Volta, spanning from 1980 to 2014. The discharge data at Wiasi (-1.933,11.283) on the Sissili River and Yagaba (-1.283,10.23) on the Kulpawn River is a daily timeseries obtained from the Volta Basin Authority (VBA) at Ouagadougou.

3.3.5 Hydroelectric dam Data

Hydroelectric dam data was obtained from the Volta River Authority at Akuse, Ghana, SONABEL through the Volta Basin Authority at Ouagadougou, and the Bui Power Authority at Bui in Ghana. The Bui Power Authority provided energy produced by the Bui hydroelectric dam, while the Volta River Authority provided energy generation by the Kpong and Akosombo dams, in Ghana. Energy generated from the Bagre and Kompienga dams in Burkina Faso was acquired from SONABEL through the Volta Basin Authority.

3.3.6 Water demand data

The annual water use rate per person and per livestock was calculated by multiplying the daily water use rates by the total number of days in the year. The total annual water use rate over a specific catchment was then estimated by multiplying the results by the total number of people and

livestock in the catchment. The daily water use rate was estimated from (UNEP-GEF Volta Project, 2013).

3.3.7 Irrigation Water Requirement

Historical irrigation data on the Bagre dam was provided by SONABEL through the Volta Basin Authority. For catchments where irrigation data was unavailable, irrigation water requirements were estimated by overlaying the shapefile of the WEF nexus sites on irrigation water demand estimated using CLIMWAT (UNEP-GEF Volta Project, 2013). The total water abstraction for each WEF nexus site was calculated by summing the water requirements for all irrigation sites that fall in the sub-catchment.

3.4 Data analysis

3.4.1 Climate-land interactions using satellite and reanalysis products

To investigate the relationship between climate variability/extremes and land use and land cover changes over West Africa, a timeseries of multiple climate datasets (mostly data products) and the ESACCI LC data (satellite data) are employed. The approach includes subsetting the individual land cover data of global coverage to the WA domain and merging them into a timeseries land cover dataset from 1992 to 2019. A trajectory analysis was then performed on each pixel to determine the total number of classes and the total number of changes per pixel. The total number of land cover categories in each changed pixel were also determined and classed as one-time (1x), two-time (2x), and three-times (3x) changes. The total changed pixels for each climatic zone per year was computed by summing the total pixels within the climatic zones for each year. The total changed pixels per year were obtained by aggregating all changes in all climatic zones per year. The total changed area in square kilometer was calculated by simply multiplying the total change pixels by 0.09. Thus, the land cover trajectory analysis serves the purpose of detecting altered pixels and calculating their corresponding area and annual variations. To establish a connection between changes in land cover change intensity, and climatic conditions (variability), was overlaid on the standardized temperature index (STI), the standardized precipitation index (SPI), and the standardized precipitation evapotranspiration index (SPEI) to determine spikes in land cover change area that corresponds to abrupt changes in the SPI, STI, SPEI. This also involves a comparative assessment of climatic factors (such as temperature, precipitation, and climatic water

balance) and their associated land cover modifications to determine the relationship between climatic conditions and related changes in land cover area. The relative impacts of abrupt land cover changes resulting from abrupt climatic changes were compared to normal climate conditions with no abrupt changes in the land cover area. The Sen's slope of temperature, precipitation, and climatic water balance was used to ascertain the annual rate of climatic variation across West Africa. Similarly, the frequency of occurrence and their associated probabilities are utilized to ascertain the frequency and probability of the various STI, SPI, and SPEI indices. Figure 3.2 shows sequentially how the relationship between climate variability/extreme and land use and land cover changes was established remote sensing and reanalysis data products. The details of the procedure are also presented below.

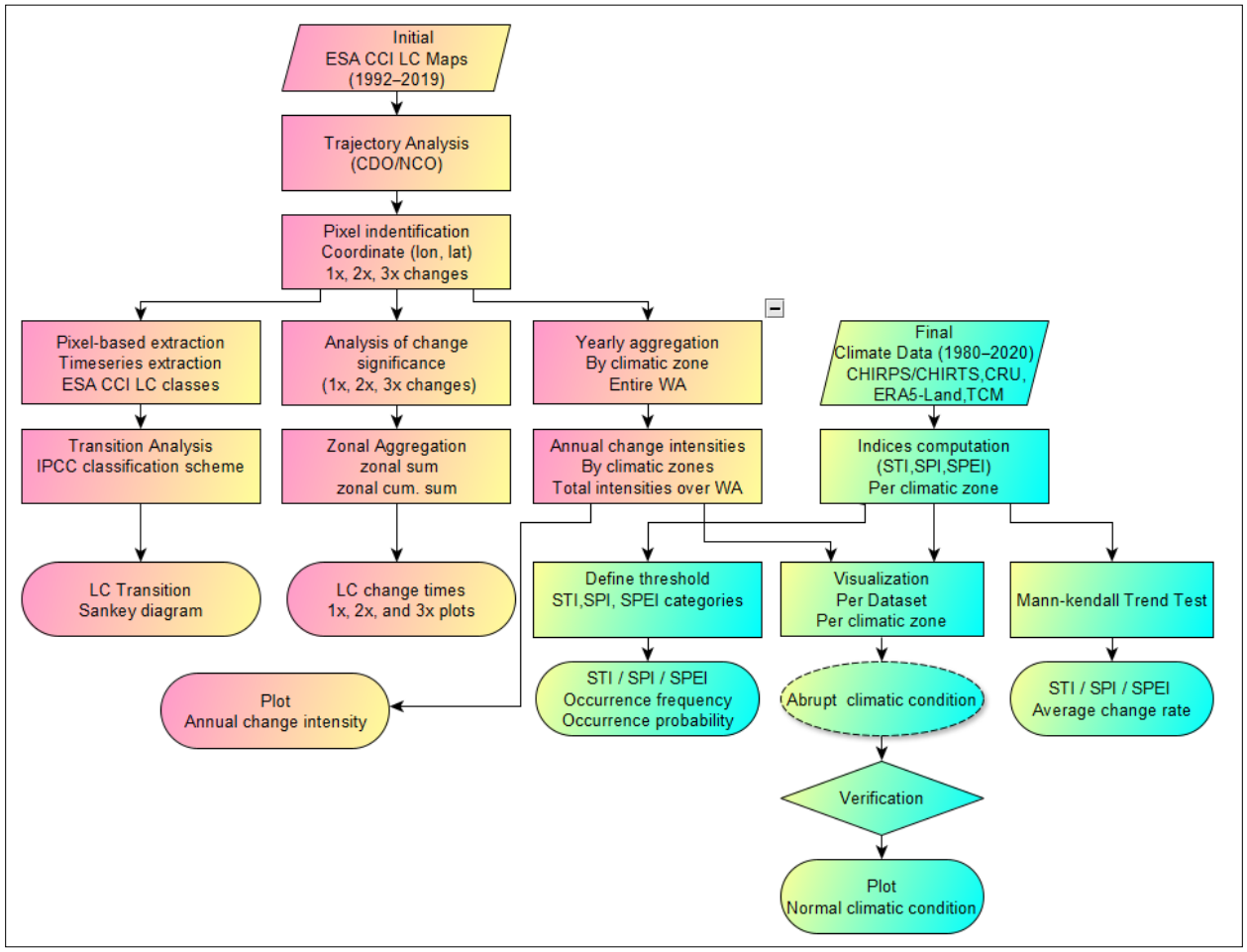

Figure 3.2 Overall procedure for assessing land- and climatic change interactions

3.4.2 Extreme climate indices computation

This thesis employed extreme climate indices: the standardized precipitation index (SPI), standardized temperature index (STI), and standardized precipitation evapotranspiration index to evaluate the links between land use land cover change, and climate variability. The extreme climatic indices were computed on a 12-monthly timescale to be comparable with the annual land cover dataset used. The SPI, initially formulated by McKee et al. (1993) and subsequently revised by Edwards & McKee (1997) is the prevailing method for assessing meteorological drought across various timescales. The SPI-n is a statistical metric that compares the cumulative precipitation received at a specific location during n months with the historical rainfall distribution for the same period at that site. The SPI values span from -3 to +3, including the entire range, and can be understood as the magnitude of the divergence of recorded precipitation from the climatological mean, measured in standard deviations. As SPI values are measured in standard deviations from the long-term average, this indicator allows for the comparison of precipitation anomalies across different geographical locations and periods. SPI is applicable for characterizing various forms of droughts due to its ability to accommodate varying timescales. In this work the SPEI package in the R software was used to calculate the Standardized Precipitation Index (SPI). The calculation of the standardized precipitation evapotranspiration index (SPEI) follows a comparable methodology to the standardized precipitation index (SPI), with the distinction that it incorporates the discrepancy between precipitation and potential evapotranspiration (climatic water balance) instead of solely relying on precipitation. The climatic water balance (CWB) enables the inclusion of the temperature element, which is frequently overlooked when calculating the Standardized Precipitation Index (SPI). Introducing temperature also brings in the impact of changes in surface evaporation, which is very responsive to the drought response triggered by global temperature increases. To access the mathematical formulation and computation of SPEI, refer to the work by Vicente-Serrano et al. (2010). The methodology for calculating the Standardized Precipitation Evapotranspiration Index (SPEI) is also outlined in the work of C. Liu et al. (2021) and can be found at https://spei.csic.es/home.html. The SPEI package in R Software is used exclusively for all SPEI computations in this study. Table 3.4 below presents the cumulative probability for different SPI and SPEI values, along with their corresponding interpretations.

Table 3.4 SPI and SPEI-based classification for the various drought categories.

SPI/SPEI	Cumulative Probability	Interpretation	Classification	Probability of Occurrence
+2.0	0.9772	Extremely wet	SPI/SPEI ≥ +2.0	0.023
+1.5	0.9332	Very wet	+1.5 ≥ SPI/SPEI < +2.0	0.044
+1.0	0.8413	Moderately wet	+1.0 ≥ SPI/SPEI < +1.5	0.092
0.0	0.5000	Near normal	−1.0 > SPI/SPEI < +1.0	0.682
−1.0	0.1587	Moderately dry	−1.0 ≤ SPI/SPEI > −1.5	0.092
−1.5	0.0668	Very dry	−1.5 ≤ SPI/SPEI > −2.0	0.044
−2.0	0.0228	Extremely dry	−2.0 ≤ SPI/SPEI	0.023

The Standardized Temperature Index (STI) measures the temperature correspondence of the SPI, which is based on precipitation. It is strongly connected to the principles outlined above and was initially introduced by McKee et al. (1993). The STI package in R was utilized to calculate the STI in this study. The different STI values, together with their combined probabilities, interpretation, classification, and occurrence probabilities, are outlined in Table 3.5.

Table 3.5 Heat categorization based on STI values.

STI	Cumulative Probability	Interpretation	Classification	Probability of Occurrence
+2.0	0.9772	Extremely hot	STI ≥ +2.0	0.023
+1.5	0.9332	Very hot	+1.5 ≥ STI < +2.0	0.044
+1.0	0.8413	Moderately hot	+1.0 ≥ STI < +1.5	0.092
0.0	0.5000	Near normal	−1.0 > STI < +1.0	0.682
−1.0	0.1587	Moderately cold	−1.0 ≤ STI > −1.5	0.092
−1.5	0.0668	Very cold	−1.5 ≤ STI > −2.0	0.044
−2.0	0.0228	Extremely cold	−2.0 ≤ STI	0.023

3.4.3 Analysis of land cover trajectory, changed pixels and the total changes per pixel.

To detect changes in land cover in West Africa, a trajectory analysis was conducted on the preprocessed land cover data (X. Liu et al., 2018; Zhou et al., 2008). A trajectory analysis examines every pixel in the land cover timeseries dataset to ascertain occurring within the pixels over time. This study examines the changes in trajectory from 1992 to 2019, specifically focusing on the total number of land cover categories and the total number of changes within each pixel. The number of alterations in a particular pixel is mathematically equal to the total number of distinct classes in that pixel minus one. Therefore, a pixel that exhibits four distinct classes between 1992 and 2019 must have undergone three changes (3×) from its original class. Pixels with three and two distinct

classes must have undergone two changes and one change, respectively. Finally, a pixel that has only one class has been unaltered. The altered pixels were distinguished from one another using their distinct coordinate data (longitude and latitude values). The coordinate information, total number of classes, and pixel change count for each pixel were exported to the R program for additional analysis. The total number of changed pixels was calculated by summing all the altered pixels in the land cover dataset. The cumulative number of changes for 1-time, 2-time, and 3-time changes were calculated by summing up the individual changes that occurred once, twice, and three times, respectively. To evaluate the variation of the changes across different latitudes, we combine all the changes that occur at each distinct latitude ranging from 4° N to 20° N.

3.4.4 Changes in land cover area (intensity)

The primary purpose of trajectory analysis was to find the altered pixels in the CCI land cover data across West Africa. The area corresponding to the total altered pixels was determined by multiplying the total changed pixels by 0.09, which represents the pixel's equivalent area in square kilometers. To measure the variation in land cover area across different latitudes, we collect all the pixels that have changed for each distinct latitude between 4° N and 20° N, and then multiply the total by 0.09. The total area change for each bioclimatic zone was calculated by combining the individual area changes for each zone (see Figure 3.1). To determine the latitudinal-based land cover changes, the one-time, two-time, and three-time changes were estimated for each latitude.

3.4.5 Linking land–climatic changes

To establish a link between the changes in land cover and climate, the annual land cover area changes was used to differentiate between years characterized by abrupt land cover changes and years without abrupt land cover changes. The climatic conditions of the former resulted in abrupt changes in land cover, while the climatic conditions for the latter was used to identify gradual non-abrupt changes in land cover. The normal climatic condition was also used as the basis to assess (validate) if indeed abrupt changes in the land cover area resulted from abrupt changes in climatic conditions.

3.4.6 Average rate of climatic change

To investigate the mean rate of climatic changes, we employ the slope of the Mann-Kendall trend test on each climatic index. The Mann–Kendall test is a commonly used to detect the presence of

a monotonic trend in a time series. It has been extensively applied in numerous researches linked to the Standardized Precipitation Index (SPI) (Danandeh Mehr & Vaheddoost, 2020; C. Liu et al., 2021). The mathematical foundation is well elucidated in several articles (Akpoti et al., 2016; Yildirim & Rahman, 2022). Here, we computed the spatial Mann-Kendall trend test using the "spatialEco" package in R for STI, SPI, SPEI and retrieved the slope attribute to demonstrate the mean annual rate of climatic change in West Africa.

3.4.7 Climatic indices frequency and occurrence probability

The occurrence frequency of the standardized climatic indices (STI, SPI, SPEI) at 12-month timescales was determined by analyzing the range of values that define their classification, as outlined in Tables 3.4 and 3.5. Thus, the occurrence of an exceedingly hot (excessively dry) climate is determined by the count of STI (SPI/SPEI) values that are equal to or more than 2. The probability of an extremely hot (extremely dry) climate is determined by dividing the total number of such occurrences by the total number of months. Thus, if there were 67 occurrences of extremely hot (extremely dry) conditions out of 492 months between 1980 and 2020, at a specific location, the occurrence frequency is 67 and the probability of occurrence is about 0.14 (that is 67 divided by 492). Thus, the climatic risk that a particular location is exposed to is determined by the various STI, SPI, and SPEI conditions of that location.

3.5 Modeling

3.5.1 Overview of methods

The modeling of the relationship between climate variability/change and land use/land cover change was achieved using the fully coupled atmospheric hydrological model (WRF-Hydro), and the WEAP hydrological model. The WRF-Hydro was used to investigate the relationship between climate variability and land use/land cover change over the SKB, while the WEAP was used to model the relationship between climate variability/change and land use and land cover change over the Volta basin. Figure 3.2 shows the overall method of the thesis in three parts, and how the analysis approach in objective 1 is linked to the modeling approach in WRF-Hydro. The first consists of investigating the links between climate variability and land cover change over West Africa (regional scale) using the annual land cover change intensity from 1992 to 2019 and the 12-monthly standardized climatic indices. The linkages observed will be used to derive a normalized

land-climate index which is used to improve simulated discharge in future research. The second part consists of a regional to local scale modeling of climate-land interactions using the fully coupled atmospheric hydrological model (WRF-Hydro). The model was forced with ERA5 hourly data under the ESA 2010 land data, calibrated and run from 2010 to 2016. The model's output was validated with observational temperature and rainfall products and observed discharge at Wiasi and Yagaba. The climate-land index derived from objective 1 will be used as a correction factor for calibrated discharge in the future, to account for dynamic land-climate interaction which could not be achieved with the static land cover data. Land cover change numerical experiments were performed to ascertain the impacts of afforestation and deforestation on local climate (rainfall, temperature, sensible heat flux, latent heat flux, net radiation). This was achieved by subtracting the reference simulation results from afforestation and deforestation experiments. The third parts consist of building the Volta-WEF Nexus model using WEAP with input terrain data, land cover, population, water demand for irrigation, domestic, and livestock. The model was calibrated based on observed streamflow data and historical hydroelectric storage to ensure that the model both mimics real-life situations and is useful for decision-making in the Volta Basin. The model was used to assess the implication of future climate change, land use land cover change, population growth, and a combination of these factors on future water demand and electricity production. Details of the methods for the WRF-Hydro modeling and WEAP modeling are presented in sections 3.5.2, and 3.5.3 respectively.

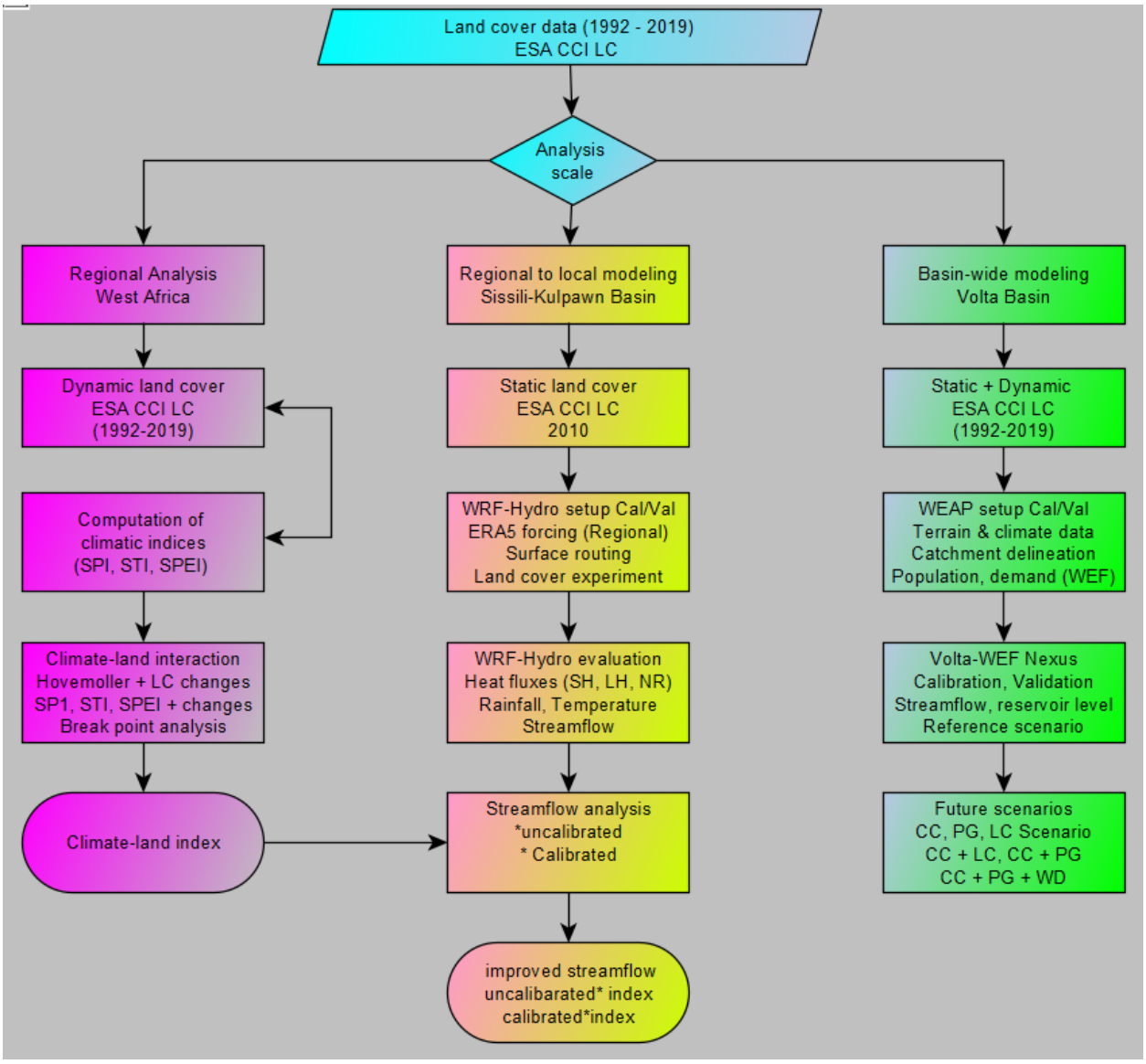

Figure 3.3 Overall method for investigating the links between climate-land cover change interactions at the regional, local and basin-wide level

3.5.2 Climate-land interactions using fully coupled land-atmosphere model (WRF-Hydro)

Section 3.5.2 and subsections 3.5.2.1–3.5.2.4 are dedicated to the climate-land interactions using the WRF-Hydro which includes the model setup, description of the land-river flow model (advancement in WRF-Hydro), evaluation metrics used to evaluate the WRF-Hydro simulated outputs, and the land cover change sensitivity experiments. The details of the methodology of the WRF-Hydro approach are described below.

3.5.2.1 Model description and setup

The WRF regional climate model (Version 4.4) and the WRF-Hydro hydrological module (version 5.2) are coupled together to describe in more complex detail the regional water cycle of the SKB. The setup follows the one used in Arnault et al. (2023) and consists of two domains (Figure 3.4); an outer and an inner domain. The outer domain is at 50 km resolution covering an area of 6000 km x 4000 km including the western and parts of central Africa, with 50 pressure levels up to 10 mbar. The inner domain encompasses the SKB at 10 km horizontal resolution covering 800 km x 800 km also with 50 pressure levels up to 10 mbar. The lateral boundaries and initial conditions of the outer domain are forced with ERA5 reanalysis (Hersbach et al., 2020) atmospheric fields (geopotential height, meridional and zonal winds, water vapor, air pressure, temperature) at 0.25° resolution and six-hourly time steps. To ensure numerical stability, the atmospheric equations of motion of the inner and outer domains are resolved at 60 s and 180 s respectively. The selected physics parameterization options for the inner and outer domains are shown in Table 3.6 and includes terrestrial hydrology, radiation, cloud microphysics, turbulence, and cumulus convection, based on the performance in reproducing well the daily basin-averaged rainfall of the SKB as explored in various configurations. The impact of different parameterization combinations is not the subject of this study. A comprehensive overview for northern Sub-Saharan Africa is given in Laux et al. (2021). The WRF-Hydro hydrological module makes possible the inclusion of a lateral flow in the inner domain (Gochis et al., 2021). Using input elevation and hydrological data from version 2 of HydroSHEDS database (Lehner et al., 2008) with version 5.2 of WRF-Hydro GIS Pre-processing Tool, the inner domain is coupled with a subgrid of 1km resolution (see Figure 3.4b). The minimal stream number for defining the channel network in Figure 3.4b is 25. The coupling procedure includes the aggregation/disaggregation of the surface water and soil moisture variables between the inner domain grid and the subgrid with so-called disaggregation factors. The disaggregation factor is defined by the ratio of the fine grid variable's value to its corresponding coarse grid value. For every time step, the disaggregation factors are used to disaggregate the Noah-MP soil moisture, soil, and surface water variables onto the subgrid, routed in river channels, overland, and in the subsurface based on diffusive wave formulations (Gochis et al., 2021), and

then reaggregated again to the Noah-MP grid. The comprehensive description of a basin-scale water cycle is made possible by the fully coupled formulation described above.

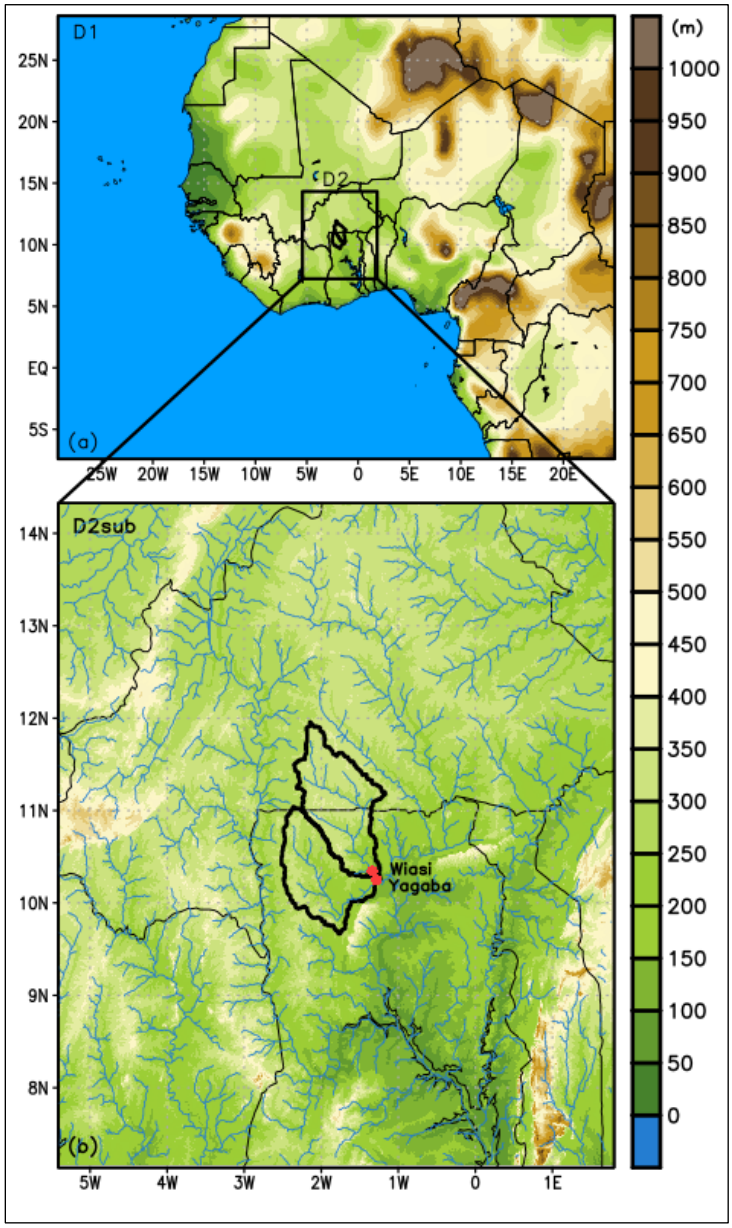

Figure 3.4 Study area

Topography of (a) the outer (D1) and inner (D2) domains at 50 km resolution, and (b) D2 coupled with sub-domain D2sub for water routing calculations. The Sissili and Kulpawn Basin, their main rivers, and outlet gauge stations at Wiasi and Yagaba, are indicated by the thick black lines, blue curved lines and red dots respectively in (b). The color scale for topography for (a) and (b), in meters above sea level, is shown on right side extending the heights of (a) and (b).

Table 3.6 WRF and WRF-Hydro physical parameterization

Physics	Selected scheme	Reference
Radiation	Short and long wave radiation schemes	Mlawer et al., 1997 ; Dudhia, 1989
Turbulence	Level 2.5 of the Mellor-Yamada-Nakanishi-Niino turbulence scheme	Nakanishi & Niino, 2004
Microphysics	Hong and Lim sHong & Lim, 2006Hong & Lim, 2006	
Land surface Model	Noah community land surface model (Noah-MP) with multiple parameteri-zation options	Niu et al., 2011
Cumulus convention	Grell and Freitas cumulus convention scheme	Grell & Freitas, 2014

3.5.2.2 Two-way extension of land-river water flow model

The SKB is noted for perennial flooding (Gross & Pennink, 2018), with the possibility of the rivers going beyond their banks. Such river overbank flow is a missing process in the default WRF-Hydro model resulting in unrealistically high peaks in the simulated discharge. To circumvent this issue, Arnault et al. (2023) modified the WRF-Hydro source code by including an overbank flow parameter which allows for a two-way flow of water between the river and land, and applied it successfully to the Nzoia river basin in tropical East Africa. In this work, the calibrated overbank flow option proposed by Arnault et al. (2023) is used to obtain an improved simulation of the observed discharge. A detailed explanation of how simulated discharge is improved and numerical balance achieved with the overbank flow option is outlined in Arnault et al. (2023). The source code can be downloaded at https://doi.org/10.6084/m9.figshare.21063982.

3.5.2.3 Evaluation of model performance

Four goodness-of-fit metrics are employed to show various aspects of the performance of the WRF-Hydro simulated outputs. To evaluate the mean rainfall, temperature, water and energy fluxes in space (inner domain) and over time (simulated period), it suffices to compute the percentage bias (PBIAS) between the simulated and observational products. The PBIAS is used to assess if the model is overestimating or understanding the observational data, with 0 indicating no bias between the observed and modeled data, and positive and negatives indicating overestimations

and underestimations, respectively. Besides the PBIAS, the coefficient of determination (R^2), the Nash–Sutcliffe efficiency (NSE), and Kling–Gupta efficiency (KGE) metrics are used to numerically compare the simulated and observed rainfall and streamflow timeseries. The R^2 is used to assess the goodness of fit of the observed rainfall/streamflow to simulated rainfall/streamflow with values of R^2 close to 1 indicating a perfect fit. The NSE is the traditional metric used in hydrology to summarize model performance and takes values from -∞ to 1 with NSE ≥ 0.5 indicating satisfactory performance. With NSE ≥ 0.7, the model can be considered to have a very good fit (Nash and Sutcliffe, 1970). The KGE provides a diagnostically interesting decomposition of the NSE which facilitates the analysis of the relative importance of different components (bias, correlation, and variability) in hydrological modeling (Gupta *et al.*, 2009). Like the NSE, the KGE ranges from -∞ to 1 with a value close to 1 indicating a more accurate model.

$$R^2 = \frac{\left[\sum_{i=1}^{n}\left\{\left(Q_{obs}-\overline{Q}_{obs}\right)\times\left(Q_{sim}-\overline{Q}_{sim}\right)\right\}\right]^2}{\sum_{i=1}^{n}\left(Q_{obs}-\overline{Q}_{obs}\right)\times\sum_{i=1}^{n}\left(Q_{obs}-\overline{Q}_{sim}\right)^2} \quad (3.1)$$

$$PBIAS = \frac{\sum_{i=1}^{n}\left(Q_{obs}-Q_{sim}\right)}{\sum_{i=1}^{n}\left(Q_{obs}\right)}\times 100 \quad (3.2)$$

$$NSE = 1 - \left[\frac{\sum_{i=1}^{n}\left(Q_{obs}-Q_{sim}\right)^2}{\sum_{i=1}^{n}\left(Q_{obs}-\overline{Q}_{obs}\right)^2}\right] \quad (3.3)$$

$$KGE = 1 - \sqrt{(r-1)^2+(\alpha-1)^2+(\beta-1)^2} \quad (3.4)$$

Where β a bias term, α a measure of the flow variability error, and r is the linear correlation between observations and simulations.

$$KGE = 1 - \sqrt{(r-1)^2+\left(\frac{\sigma_{sim}}{\sigma_{obs}}-1\right)^2+\left(\frac{\mu_{sim}}{\mu_{obs}}-1\right)^2} \quad (3.5)$$

where σ_{sim} is the standard deviation in simulations, σ_{obs} is the standard deviation in observations, μ_{obs} is the observation mean $\overline{Q}_{obs}$, and μ_{sim} is the simulation mean $\overline{Q}_{sim}$. The Q_{sim} and Q_{obs} terms also refers to the simulate and observed parameters respectively.

3.5.2.4 Land cover change numerical experiments

To assess the potential impacts of land cover change (afforestation and deforestation) on regional water and energy budgets, the calibrated WRF-Hydro with overbank flow option in section 3.5.2.2 is used to generate a seven-year reference simulation from 1st January 2010 to 31st December 2016. The realism of the reference result is evaluated with the observational datasets presented in section 3.3.1. As indicated by De Noblet-Ducoudré et al. (2012) the evaluation is important to assess the extent to which the model is useful for land cover change numerical experiment. The reference land cover map considered for the simulation is the 2010 ESA LC map, which is displayed in Figure 3.5a. Figure 3.5b-d are modifications of the reference ESA LC maps according to three landcover change scenarios. Figures 3.5e-g is a resampling of the original ESA LC (Figures 3.5b-d) to the WRF-Hydro grid, which is the land cover data ingested into the WRF-Hydro for the land cover numerical experiment. Figure 3.5e is a cropland scenario that represents a replacement of closed shrubland (43.49%) within the Sissili-Kulpawn Basin area by cropland such that the total cropland area is 71.7% (Table 3.7). Figure 3.5f is a closed shrubland scenario which represents a replacement of the cropland (28.19%) by closed shrubland such that the total closed shrubland area is 71.7% (Table 3.7). Figure 3.5g is a broadleaf scenario that represents an extension of the broadleaf forest (20.46%) at the southern part of the SKB to cover the existing closed shrubland (43.49%) such that the total broadleaf forest area is 63.95% (Table 3.7). Aside from the dominant land cover types mentioned above, all other land cover types within the inner domain remain unchanged. The land cover change numerical experiment was carried out for seven years spanning 1st January 2010 to 31st December 2016. The seven years is considered sufficient to obtain a robust modeled climate signal given the idealized nature of the experiment and the fact that ESA LC maps did not change significantly over a twenty-eight-year period (1992–2019). The landcover change numerical experiments indicate the largest climatic impact that could be expected from afforestation and deforestation scenarios, and the extent to which climatic impacts depend on vegetation cover change. Figure 3.5 shows the visual display of the modifications made for each land cover change numerical experiment. Table 3.7 gives the total land cover area in km^2 and the percentage of land cover type within the Sissili-Kulpawn, Sissili, and Kulpawn catchment areas. Table 3.8 represents the total land cover area over the Sissili-Kulpawn Basin for each land cover

type in each of the three numerical experiments. Tables 3.9–3.10 give the land cover area in km^2 and the percentage of each land cover category within the Sissili and Kulpawn Basins respectively.

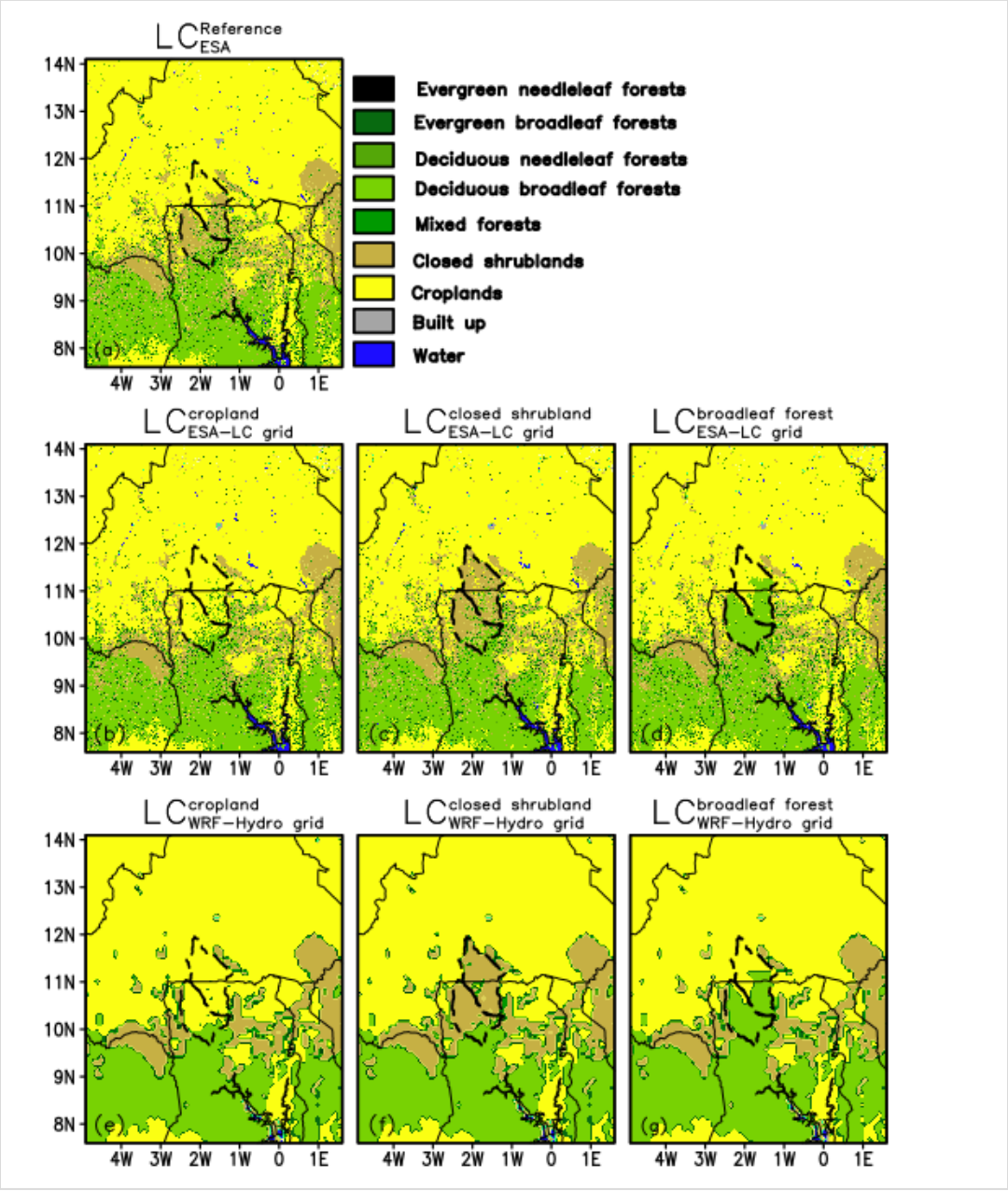

Figure 3.5 Maps of European Space Agency (ESA) land cover distribution in the inner domain harmonized to the MODIS classification system, as used in (a) reference WRF-Hydro simulation with ESA grid, (b) the cropland WRF-Hydro simulation with ESA grid, (c) the closed shrubland simulation with ESA grid (d) the broadleaf forest WRF-Hydro with ESA grid, (e) the cropland

WRF-Hydro simulation with WRF-Hydro grid, (f) the closed shrubland simulation with WRF-Hydro grid (g) the broadleaf forest simulation with WRF-Hydro grid. The black thick dashed line in all the panels indicate the location of the SKB. Landcover outside the SKB is maintained as the reference. The color of the MODIS land cover classification is provided in the upper right side of the figure.

Table 3.7 Total land cover in km^2 and % of land cover types categorized according to the different catchment areas of Sissili-Kulpawn Basin.

Land cover	Sissili-Kulpawn		Sissili		Kulpawn	
	Area (km^2)	Percentage share (%)	Area (km^2)	Percentage share (%)	Area (km^2)	Percentage share (%)
Broadleaf forest	4493.88	20.46	1584.27	13.05	2906.64	29.58
Closed shrubland	9552.33	43.49	3701.43	30.49	5852.43	59.56
Wetland	0.45	0.00	0.18	0.00	0.27	0.00
Cropland	6191.19	28.19	5486.31	45.20	705.96	7.18
Grassland	1724.85	7.85	1364.49	11.24	360.27	3.67
Water	1.98	0.01	1.71	0.01	0.27	0.00

Table 3.8 Total land cover in km^2 and % of each land cover category for each land cover change scenario over the Sissili-Kulpawn Basin.

Land cover	Closed shrubland		Cropland		Broadleaf forest	
	Area (km^2)	Percentage share (%)	Area (km^2)	Percentage share (%)	Area (km^2)	Percentage share (%)
Broadleaf forest	4493.88	20.46	49932	20.46	14046.21	63.95
Closed shrubland	15743.25	71.68	-	-	-	-
Wetland	0.45	0.00	0.45	0.00	0.45	0.00
Cropland	-	-	15743.85	71.68	6190.92	28.19
Grassland	1724.85	7.85	1724.85	7.85	1724.85	7.85
Water	1.98	0.01	1.98	0.01	1.98	0.01

Table 3.9 Share of land cover in km^2 and % of the land cover categories in the Sissili Basin for three land cover change numerical experiment.

Land cover	Closed shrubland		Cropland		Broadleaf forest	
	Area (km^2)	Percentage share (%)	Area (km^2)	Percentage share (%)	Area (km^2)	Percentage share (%)
Broadleaf forest	1584.27	13.05	1584.27	13.05	5285.7	43.55
Closed shrubland	9187.47	75.69	-	-	-	-
Wetland	0.18	0.00	0.18	0.00	0.18	0.00
Cropland	-	-	9187.47	71.68	5486.04	45.20
Grassland	1364.49	11.24	1364.49	11.24	1364.49	11.24
Water	1.71	0.01	1.71	0.01	1.71	0.01

Table 3.10 Share of land cover in km^2 and % of the land cover categories in the Kulpawn Basin for three land cover change numerical experiment.

Land cover	Closed shrubland		Cropland		Broadleaf forest	
	Area (km^2)	Percentage share (%)	Area (km^2)	Percentage share (%)	Area (km^2)	Percentage share (%)
Broadleaf forest	2914.2	29.60	2914.2	29.60	8772.21	89.10
Closed shrubland	6569.73	66.73	-	-	-	-
Wetland	0.27	0.00	0.27	0.00	0.27	0.00
Cropland	-	-	6569.73	66.73	711.72	7.23
Grassland	360.54	3.66	360.54	3.66	360.54	3.66
Water	0.27	0.00	0.27	0.00	0.27	0.00

3.5.3 Climate-land interactions using the WEAP hydrological model

Section 3.5.3 and subsections 3.5.3.1–3.5.3.4 are dedicated to the climate-land interactions using the WEAP hydrological model which includes catchment delineation and model setup, data entry into WEAP, WEAP model calibration and validation, modeling the impacts of population growth, climate change and land use and land cover change. The details are described below.

3.5.3.1 WEAP model setup and WEF-Nexus site delineation

Using the automatic catchment delineation tool in WEAP with input elevation, land cover, and climate data, the Volta Basin area is delineated, then the four major sub-basins, namely, the Black Volta Basin, White Volta Basin, Oti Basin, and Lower Volta Basin. Each sub-basin is further divided into smaller catchment areas leading to 42 different catchments in the Volta Basin (Figure 3.6). These catchments define the WEF-Nexus sites for investigating the interactions between water, energy, and food components depending on whether water, energy, and food components are available. The automatic catchment delineation tool is also used to extract the land cover and climate information of each of the catchment areas. The WEAP model setup is shown in Figure 3.6. Each WEF nexus site contains a water node that represents the water demand by the population, irrigation, and livestock. The food node represents the irrigation requirement of the WEF nexus site, and the energy node represents the water availability/demand for hydroelectric energy generation. The nexus components vary depending on the type of nodes available in the WEF nexus site. For sites where all three nodes are available, the nexus is referred to as WEF, otherwise WF nexus of WE nexus, etc.

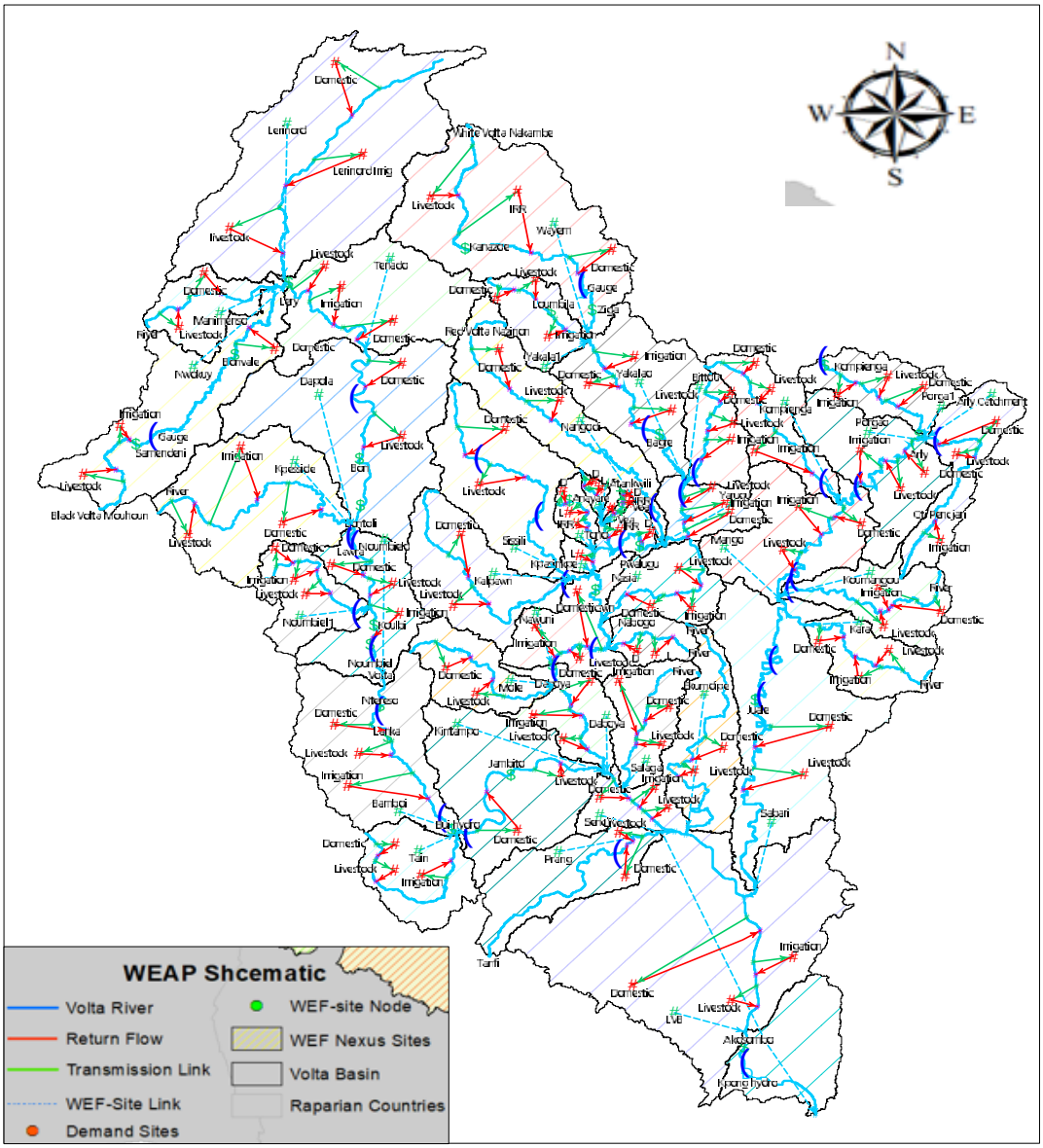

Figure 3.6 WEAP model setup for Water-Energy-Food Nexus in the Volta Basin

3.5.3.2 Data Entry into WEAP setup

The automatic catchment delineation tool was used to delineate the WEF nexus sites using elevation data from Shuttle Radar Topographic Mission (SRTM), landcover data from ESA, and historical climate from GMFD. The data from the GMFD spans from 1980–2020. The same tool was used to extract future climate data from the NEX-GDDP-CMIP6 dataset for future climate scenarios. The zonal statistic tool in ARCGIS and R were used to extract the population data for humans and livestock for each WEF nexus site. The population growth rate was estimated from a

timeseries of human and livestock population data. The daily water use rates for humans and livestock were obtained from (UNEP-GEF Volta Project, 2013). The population data and daily water use rate for humans and livestock were used to respectively calculate the population and livestock water demand. Irrigation water demand was computed based on VBA's estimated water demand for each irrigation site. The WEF nexus sites map was overlaid on the irrigation water demand and the total irrigation water requirement was calculated by aggregating the water demand for all irrigation sites that fell within a specific WEF nexus site. Historical streamflows in the WEF nexus sites were input into the model to calibrate and validate the model. Historical reservoir volume storages for the Akosombo, Bui, and Bagre dams were also input into the model to calibrate the simulated reservoir storage volume.

3.5.3.3 WEAP model calibration and validation

The WEF Nexus setup was calibrated and validated using observed streamflows measured in the Volta Basin. Streamflow data from 1981 to 2001 was used for the calibration and data from 2002 to 2014 was used for the validation. For the Soil moisture method used in the WEAP model, the parameters available in WEAP for calibration are crop coefficient (Kc), root zone Conductivity (Ks), runoff resistance factor (RRF), preferred flow direction (F), soil water capacity (SW) depending on the basin location. Initial values of these parameters were obtained from the Soil Water Assessment Tool (SWAT) and the Food and Agriculture Organization (FAO) database and finally tuned with the WEAP inbuilt Parameter Estimation Tool (PEST) (https://pesthomepage.org). For calibrating a dam's storage volume, the observed volume was compared to the simulated volume, and the gauges upstream of the dam were recalibrated until good evaluation metrics were obtained for the dam storage volume. In some cases, the RRF was increased to modulate the amount of water flowing into the dam. In all, four well-known skill metrics: coefficient of determination (r^2), Root-Mean-Square-Error (RMSE), percentage bias (PBIAS), and Nash-Sutcliffe coefficient (NSE) were used to evaluate the WEF Nexus model (Refer to Equations 3.1, 3.2, and 3.3 in sections 3.5.2.3 for how r^2, PBIAS, and NSE are computed). The RMSE is also a goodness-of-fit metric that gives the standard deviation of the model prediction error, with smaller values indicating better model performance. Mathematically, the RMSE is computed using Equation 3.6.

$$\text{RMSE} = \sqrt{\frac{\sum_{i=1}^{n}\left(Q_{obs} - \overline{Q}_{obs}\right)^2}{n}} \quad (3.6)$$

3.5.3.4 WEAP Future scenarios

Once satisfactory results were obtained from the WEF Nexus setup the impacts of population growth estimates, future climate projections, static and dynamic land cover changes, and their combinations were explored to examine their impacts on water and energy. In all, four scenarios were explored which are:

(i) Impact of climate change on WEF resources

(ii) Impact of climate change + Population growth impact on WEF resources

(iii) Impact of climate change + static and dynamic land cover change on WEF resources

(iv) Impact of climate change + Population + land use land cover change on WEF resources

Given Wref, and Eref respectively to be the water and energy resource for the reference, and Wscen, and Escen respectively to be the water, and energy resources under a given scenario, the change in water (ΔW) and energy (ΔE) resources with respect to their reference scenarios were computed as follows:

$$\Delta W = \Delta W_{scen} - \Delta W_{ref}; \quad \Delta E = \Delta E_{scen} - \Delta E_{ref} \quad (3.7)$$

The percentage change in water $(\%\Delta W)$ and energy $(\%\Delta E)$ resources were estimated as:

$$\%\Delta W = \left(\frac{\Delta W_{scen} - \Delta W_{ref}}{\Delta W_{ref}}\right)\times 100 \; ; \quad \%\Delta E = \left(\frac{\Delta E_{scen} - \Delta W_{ref}}{\Delta W_{ref}}\right)\times 100 \quad (3.8)$$

The water index (W_{indx}) and energy index (E_{indx}) between a scenario and the reference was estimated as:

$$\text{Windx} = \frac{W_{scen}}{W_{ref}} \; ; \; \text{Eindx} = \frac{E_{scen}}{E_{ref}} \quad (3.9)$$

The future socioeconomic conditions have been taken into account in the climate change projections which are obtained from the NEX-GDDP-CMIP6) (Thrasher et al., 2022) (See section 3.3.1). The population growth rate was estimated from future projections, version 1.01 of the Global 1-km Downscaled Population Base Year and Projection Grids based on the Socioeconomic

Pathways (SSPs) (Gao, 2020) (See section 3.3.3). The SSP1-2.6 describes a world with a global population of 6.9 billion people (1.9 billion for Africa), and the temperature would rise by 1.3 to 2.4 at the end of the century (Irfan, 2021; KC & Lutz, 2017; Siabi et al., 2023). SSP2-4.5 corresponds to a global population of 9.0 billion people (2.6 billion for Africa) and the average warming will be about 3.5 at the end of the century (Irfan, 2021; KC & Lutz, 2017; Siabi et al., 2023). SSP3-7.0 shows a global population in this scenario reached approximately 12.6 billion (about 3.9 for Africa) and an average increase in temperature by 3.6 °C (KC & Lutz, 2017; Irfan, 2021). In SSP4-6.0, the population estimate for the world is 9.3 billion (3.6 billion for Africa) by 2100 (KC & Lutz, 2017). SSP5-8.5 corresponds to a global population of about 7.4 billion (1.8 billion for Africa) by the end of 2100 (KC & Lutz, 2017). The temperature for this scenario will have warmed by 4.4 °C, ranging between 3.3 °C to 5.7 °C compared to 1950 (Irfan, 2021; Riahi et al., 2017). Details of the SSPs are described in the literature review (section 2.15).

3.6 Partial conclusion on material and methods

The method for investigating the relationship between climate variability/change and land use/land cover change as used in this thesis can be classified into three based on both the scale and the approach. An analysis between climatic indices and land use/land cover change was employed to understand how the interannual changes in land use/land cover change is linked to extreme climatic changes over West Africa. The modeling approach in WRF-Hydro is used to understand the complex interactions between the land surface and climate including the biogeophysical components, energy budget, water budget, and the hydroclimatic situation from the West Africa domain to a local scale (Sissili-Kulpawn Basin). The WEAP or analysis approach can not describe these complex interactions. On the other hand, the modeling in WEAP best describes the impact of future climate change, land use/land cover change, and population growth scenarios on the future water-energy-food nexus in the Volta Basin of West Africa.

CHAPTER 4 – RESULTS AND DISCUSSION

4.1 Introduction to results and discussion

The result describes the relationship between land cover change and climatic changes from regional to local scales, from an analytical and modeling viewpoint, and within the WEF nexus discourse. Firstly, a new analytical approach to characterizing the relationship between climatic changes and land cover changes was proposed, which consists of analyzing changes in timeseries land cover and climate datasets, superimposing the results, and characterizing land cover change intensities that resulted from specific climatic conditions. A mathematical description of the relationship is also proposed to improve the parameterization of the climate-land interactions in RCMs with static land cover data. The relationship described in the analytical approach is envisaged to help improve the simulation of rainfall and streamflow in RCMs like the WRF-Hydro. Secondly, the effects of land cover change strategies (afforestation and deforestation) on local hydroclimatic parameters (temperature, precipitation, streamflow, water fluxes, and energy fluxes) was investigated using WRF-Hydro with static land cover data. The differential effects of the land cover change scenarios relative to a reference scenario were used to assess the impacts on climate, water, and land and their implications for food production (the water-energy-food nexus) in the Sissili-Kulpawn Basin. Finally, the water-energy-food nexus model (Volta-WEF model) was built using the WEAP hydrological model to investigate the effects of climatic change, land use/land cover change, and population growth on future water, energy, and food resources in the Volta Basin.

4.2 Climate-land cover interactions using Satellite Remote Sensing and Reanalysis products

This section presents an approach to characterizing the relationship between land cover change, and climate variability. The land cover change was characterized by the interannual land cover change intensities, and the climatic changes were characterized by the standardized precipitation index (SPI), standardized temperature index (STI), and standardized precipitation evapotranspiration index (SPEI). The relationship between the land cover change intensities and the climatic indices is obtained by superimposing the land cover changes on the climate indices. The relationship between land cover change intensities and the climatic indices was characterized by quantifying the land cover change intensities associated with specific changes in the climatic

conditions. A confirmatory analysis is used to examine whether different changes in climatic conditions (temperature, precipitation, and climatic water balance) resulted in different land cover change intensities. An attempt to model mathematically the relationship between the land cover change intensities and changes in the standardized climatic indices is also described. The objective is to propose a mathematical description for interannual land-climate interactions, which are usually missing in RCMs with static land cover data.

4.2.1 Extreme climatic indices over West Africa (1980-2020)

standardized precipitation index (SPI), standardized temperature index (STI), and standardized precipitation evapotranspiration index (SPEI) have been predominantly used to characterize climate extremes/variability. The STI, SPI, and SPEI values are standard deviations showing the departure of climate from normal climatic conditions. In this work, the STI and SPI of the CHIRTS/CHIRPS, CRU, ERA5-Land, and TerraClimate datasets indicate that the climate of West Africa between 1980 and 2020 can be categorized into two distinct periods. The first period from 1980 to 2000 experienced relatively colder temperatures and dry conditions, while the second period, from 2000 to 2020, exhibited relatively warmer temperatures and wet conditions. There were occasionally minor deviations from these patterns within each dataset as can be seen from Figure 4.1. These findings are consistent with Daramola et al. (2023), who analyzed changes in aridity over West Africa over four decades, indicating that the era from 1979 to 1998 was characterized by the lowest levels of precipitation and less warmth, and an increase in wet areas and more pronounced warming during the latter period (2000–2019). Gogoi et al. (2019) and many other land-atmosphere interactions research demonstrated that alterations in land use and land cover impact climate by influencing land surface temperature and rainfall through several mechanisms. However, there is a paucity of research establishing a relationship/linkage between climatic conditions and land use/cover changes, especially over WA. In the next section land cover changes from 1992 to 2019 are determined from ESA LC and used together with the climatic indices (Figure 4.1) to establish the climate-land relationship.

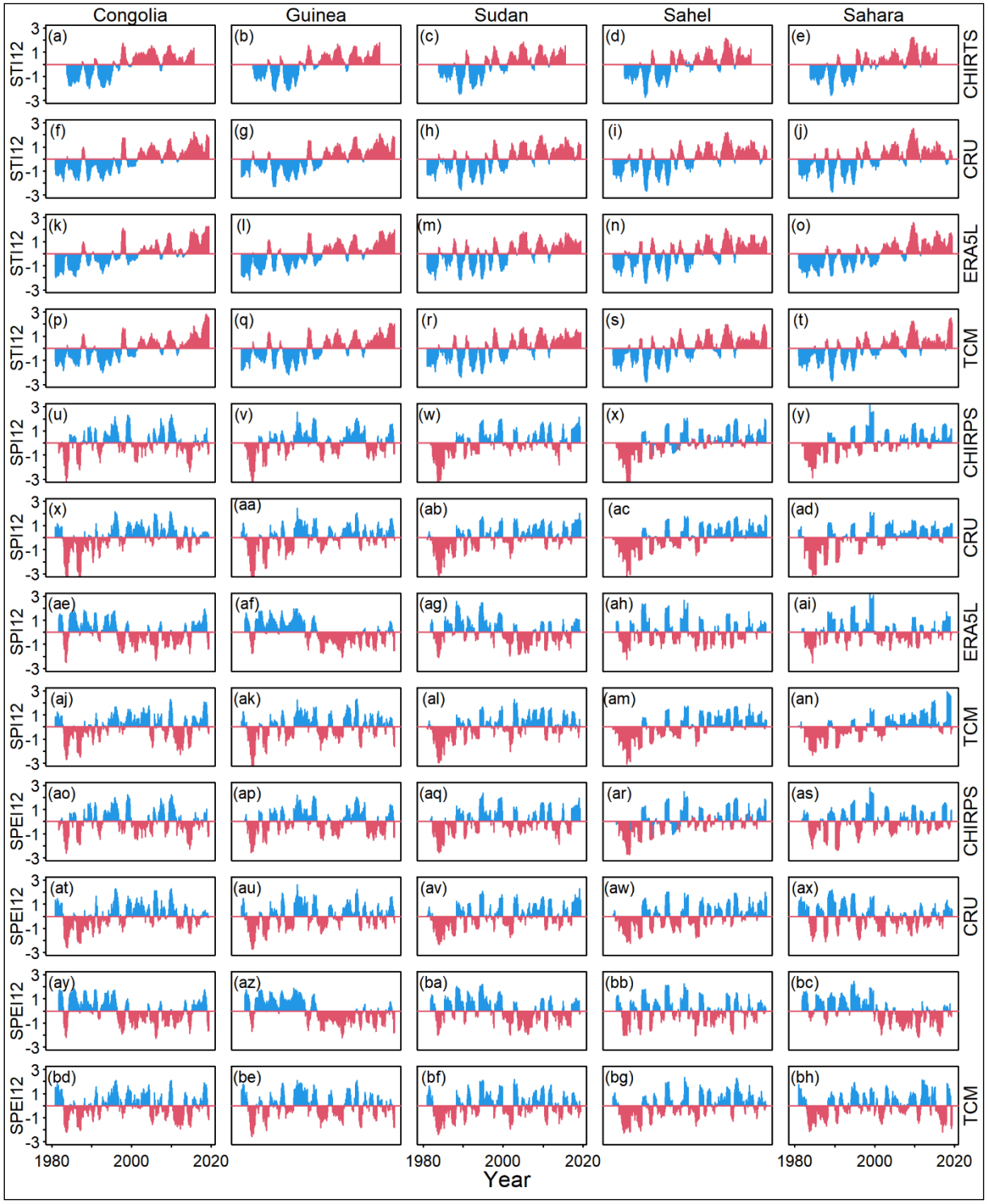

Figure 4.1 Standard climatic indices for the five bioclimatic zones in West Africa: (a-e) Standardized Temperature Index (STI) of CHIRTS datasets for Congolia (C), Guinea (G), Sudan (S), Sahel (SH), and Sahara (SAH) bioclimatic zones; (f-j) STI of CRU datasets for C, G, S, SH,

and SAH; (k-o) STI of ERA5L datasets for C, G, S, SH, and SAH; (p-t) STI of TCM datasets for C, G, S, SH, and SAH; (u-y) Standardized Precipitation Index (SPI) of CHIRPS datasets for C, G, S, SH, and SAH bioclimatic zones; (z-ad) SPI of CRU datasets for C, G, S, SH, and SAH; (ae-ai) SPI of ERA5L datasets for C, G, S, SH, and SAH; (aj-an) SPI of TCM datasets for C, G, S, SH, and SAH; (ao-as) Standardized Precipitation Evapotranspiration Index (SPEI) of CHIRPS datasets for C, G, S, SH, and SAH bioclimatic zones; (at-ax) SPEI of CRU datasets for C, G, S, SH, and SAH; (ay-bc) SPEI of ERA5L datasets for C, G, S, SH, and SAH; (bd-bh) SPEI of TCM datasets for C, G, S, SH, and SAH.

4.2.2 Spatiotemporal land use/cover change analysis

A trajectory analysis of the ESA land cover (ESA LC) maps from 1992 to 2019 shows 5,433,127 pixels have changed out of about 2.086 billion pixels (74.5 million pixels per year × 28 years) analyzed over the West Africa domain. The changed pixels represent approximately 7.28% (488,981 km^2) of the entire domain and consist of one-time changes (97.989%), two-time changes (2.097%), and three-time changes (0.005%). The remaining 92.92% (~5048,462 km^2) is stable (unchanged). The changes described a shown in yellow, red, and blue dots in Figure 4.2. According to Defourny et al. (2017) and X. Liu et al. (2018), the number of times a pixel changes is an indication of a quality flag, such that one-time changes are more reasonable, whilst three-times changes represent more unreasonable changes. The fact that more than 98% of the total changes are one-time changes indicates that the ESA LC maps can capture changes in West Africa and may be useful for land cover change analysis over the region. The result obtained in this work is also comparable to X. Liu et al. (2018) who found one-time changes from 1992 to 2015 to be 98% at the global continental scale. Cotillon & Tappan, (2016) investigating the drivers of land cover changes in West Africa, noted that the myriad of factors responsible for land cover changes may be categorized into natural factors and human activities. According to Cotillon & Tappan, (2016), population size and growth are the major human activities leading to land use/land cover changes, while climate change is the most dynamic natural force affecting land cover changes on annual and decadal timescales (Cotillon & Tappan, 2016). On the other hand, Herrmann et al. (2020) noted that, while land cover change intensities provide evidence to support the role of population pressure as a force of change, the spatial human footprint distribution patterns indicate that the complexity of land cover outcomes is determined not only by population pressure but also by

shifting policy and socioeconomic situations. Despite these conclusions, there is still no quantification of how the natural variability of climate affects land use/cover change, probably due to the lack of annually consistent time-varying land cover datasets. In the next section, annual land cover changes from 1992 to 2019 are quantified based on the results in section 4.2.2 (Figure 4.2) and used subsequently to investigate the relationship with the climatic indices obtained in section 4.2.1.

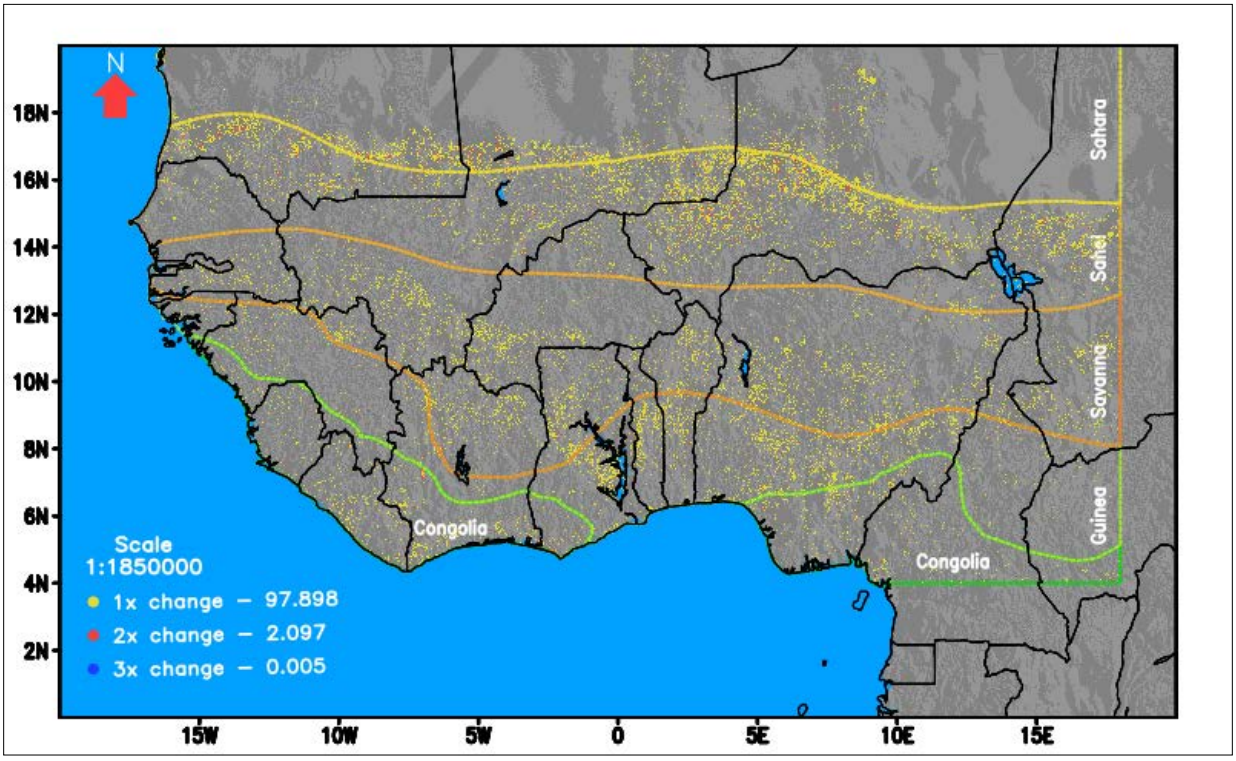

Figure 4.2 ESA CCI LC showing land cover changed pixels from 1992 and 2019 categorized by frequency of changed (yellow, red and blue).

4.2.3 Annual land cover change intensities over West Africa

Spatiotemporal land cover change analysis in section 4.2.2 was used to identify the land cover pixels in the ESA timeseries land cover maps that have changed from 1992 to 2019. By summing the changes for each year per climatic zone and multiplying by 0.09, the annualized land cover change intensity in square kilometers (km^2) is obtained (Figure 4.1.3). The annualized land cover change intensity helps to identify specific years where linkages exist between climate variations and land cover changes. In other words, the annual land cover change intensities show sudden and

significant changes in certain years, and smaller changes in other years, which enabled us to choose those specific years and examine the climatic conditions associated with them. From Figure 4.3, the land cover change area fluctuates from year to year but the spikes in 1995, 2000, 2004, 2016, and 2018 are more visible. Moreover, these spikes are consistently present throughout all climatic zones, indicating that it is not a local phenomenon confined or limited to any specific climatic zone. Instead, it could be more closely associated with a regional phenomenon, such as yearly climate patterns or variability. To verify if these changes are linked to the climatic conditions, the years in which the peaks or spikes observed in Figure 4.3 are superimposed as lines on the extreme climatic indices in Figure 4.2 to examine if the climatic conditions are responsible for the huge land use/cover changes. Such analysis is used to establish the link between climate variability/extremes and land use/cover change in the next section.

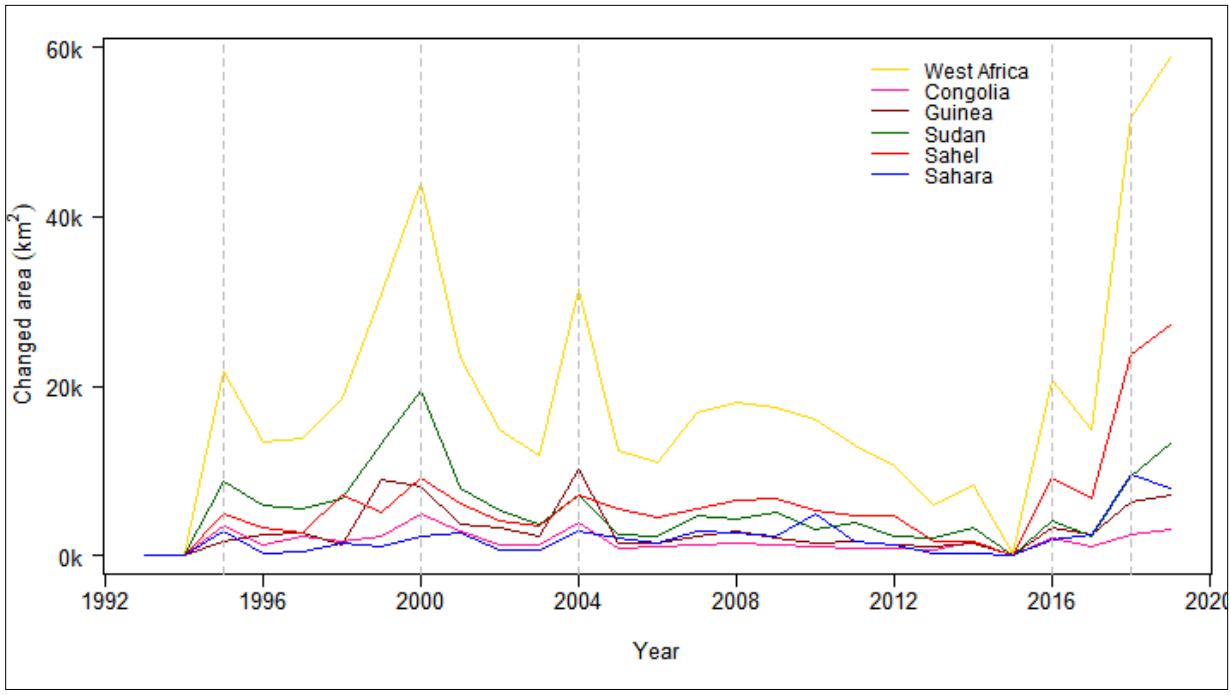

Figure 4.3 Annual variation of land cover change area estimated from the land cover changed pixels for the five bioclimatic zones of West Africa.

4.2.4 Linking climatic indices and land use/cover changes

A timeseries overlay analysis is employed to establish the relationship between climate variability/extremes and land use/cover changes. The standardized climatic indices show the

climate variability and the land cover change intensity depicts the land use/cover change. The climatic indices span from 1980 to 2020, whereas the land cover change intensity analysis spans from 1992 to 2019. The linkages between the climatic indices and land cover intensity changes were limited to the 1992-2019 period, which is the overlapping period of the two datasets. The vertical lines (depicted in grey) represent those years with high land cover changes (see Figure 4.4). The largest land cover change area occurred during the cold episode in two scenarios: (a) when there is a sudden shift from extremely cold or very cold conditions to moderately cold or near-normal conditions, accompanied by an increase in standardized temperature index (STI) values, as observed in 1995 (Figure 4.4a–p); and (b) when there is a transition from positive STI value (a hot climate) to a negative STI value (cold climate), as seen in 2000. The land cover change is most pronounced during periods of high temperature, specifically when there is a sudden shift from a relatively normal climate to a hot climate with an increase in STI values. This is evident in the years 2004, and 2018 (Figure 4.4a-p). In addition, land cover change is also significant when the STI values reach their maximum after a gradual increase from a near-normal climate, as observed in 2016 (Figure 4.4a-p). Abrupt land cover changes in terms of the Standardized Precipitation Index (SPI) occur under the following conditions: (a) when there is a sudden transition from extremely dry to near normal conditions, as observed in 1995 (Figure 4.4q–af); (b) when the SPI value reaches its highest point while transitioning from a wetter climate (positive SPI value) to a drier climate (negative SPI value); and (c) when the SPI value reaches its highest point while transitioning from a drier climate (negative SPI value) to a wetter climate (positive SPI value). The analysis of the STI and SPI reveals that abrupt land cover changes are associated with specific temperature and precipitation conditions, which can be categorized as follows: (a) a combination of rising temperature and increasing precipitation; (b) divergent temperatures accompanied by increasing precipitation; and (c) significant changes in both precipitation and temperature. Figure 4.4ag–av depicts the standardized precipitation evapotranspiration index (SPEI) response to the aforementioned temperature and precipitation variations. The divergent temperatures observed between 1994 and 1995, as well as between 2015 and 2016, along with a general rise in precipitation, led to an increase in the SPEI value. This, in turn, corresponded to an increase in the land cover area change for 1994, and 2016. The divergent fluctuations in temperature and precipitation between 1999, and 2000, as well as between 2003, and 2004,

resulted in an increase in standardized precipitation evapotranspiration index (SPEI) and the total land cover change area in 2000, and 2004. Notably, the divergent temperatures observed in 1994–1995, and 2015–2016 had comparable impacts on land cover area change resulting in a change of around 20,935–22,127 km^2 across West Africa. The Hovmöller plots displayed in Figure 4.5 demonstrate that the majority of abrupt land cover changes (indicated by red vertical lines) coincide with rising standardized precipitation index (SPI) and standardized precipitation evapotranspiration values (SPEI) values. These changes are surrounded by low SPI, and SPEI values along the latitudes and longitudes, respectively. Figure 4.5a–h depicts the temporal variation of standardized temperature index (STI) values throughout the latitude and longitude for the CHIRTS, CRU, ERA5-Land, and TerraClimate datasets. Figure 4.5i–w shows comparable results to Figure 4.5a–h, specifically for the SPI, and SPEI. From 1980 to 2020, the STI highlighted a migration from a cold climate to a warm climate. The most significant changes in land cover, indicated in red, were observed in areas with increasing or decreasing STI values. Regardless of the dataset employed, the STI, SPI, and SPEI all demonstrate that the most abrupt alterations in land cover coincide with abrupt shifts in climatic conditions. The standardized climatic indices (STI, SPI, and SPEI) were used to establish linkages between temperature, precipitation, climatic water balance conditions, and abrupt changes in land cover intensity. This analysis was conducted on a 12-monthly timescale to ease the comparison of the land cover change intensity and the standardized climatic indices. Thus, by comparing the land-climate changes over the same period, the specific climatic conditions responsible for the observed changes in land cover are identified.

Figure 4.4 Standard climatic indices for the five bioclimatic zones in West Africa superimposed with years with spikes in land cover changes: (a-e) Standardized Temperature Index (STI) of CHIRTS datasets for Congolia (C), Guinea (G), Sudan (S), Sahel (SH), and Sahara (SAH)

bioclimatic zones; (f-j) STI of CRU datasets for C, G, S, SH, SAH; (k-o) STI of ERA5L datasets for C, G, S, SH, SAH; (p-t) STI of TCM datasets for C, G, S, SH, SAH; (u-y) Standardized Precipitation Index (SPI) of CHIRPS datasets for C, G, S, SH, and SAH bioclimatic zones; (z-ad) SPI of CRU datasets for C, G, S, SH, SAH; (ae-ai) SPI of ERA5L datasets for C, G, S, SH, SAH; (aj-an) SPI of TCM datasets for C, G, S, SH, SAH; (ao-as) Standardized Precipitation Evapotranspiration Index (SPEI) of CHIRPS datasets for C, G, S, SH, and SAH bioclimatic zones; (at-ax) SPEI of CRU datasets for C, G, S, SH, SAH; (ay-bc) SPEI of ERA5L datasets for C, G, S, SH, SAH; (bd-bh) SPEI of TCM datasets for C, G, S, SH, SAH.

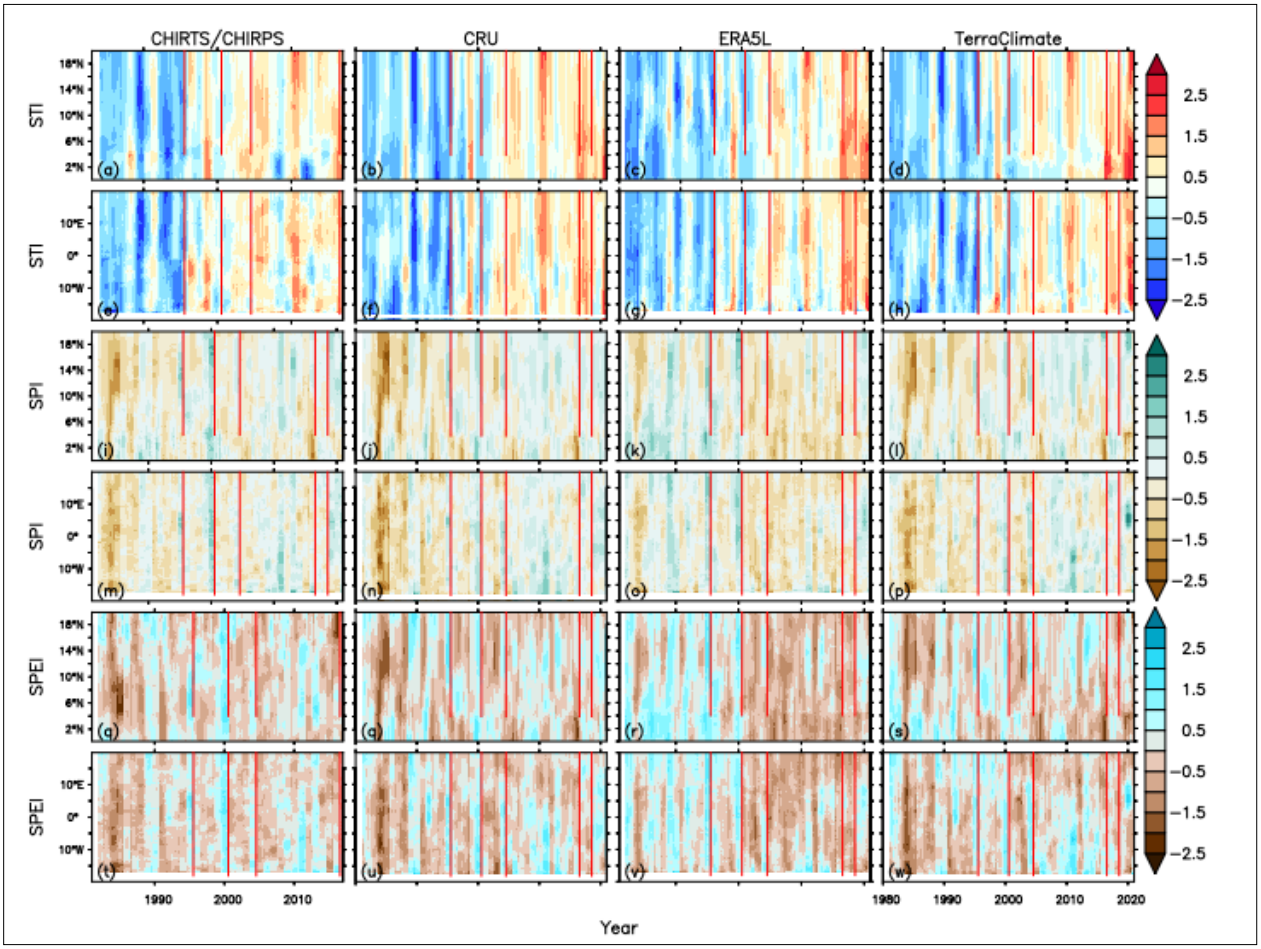

Figure 4.5 Hovmöller plots for standardized climatic indices over West Africa: (a-d) Time-longitude Hovmöller diagram of STI for CHIRTS, CRU, ERA5L and TerraClimate respectively; (e-h) Time-latitude Hovmöller diagram of STI for STI for CHIRTS, CRU, ERA5L and TerraClimate respectively; (i-l) Time-longitude Hovmöller diagram of SPI for CHIRPS, CRU, ERA5L and TerraClimate respectively; (m-p)Time-latitude Hovmöller diagram of SPI for

CHIRTS, CRU, ERA5L and TerraClimate respectively; (q-t) Time-longitude Hovmöller diagram of SPEI for CHIRPS/CHIRTS, CRU, ERA5L and TerraClimate respectively; (u-x) Time-latitude Hovmöller diagram of SPEI for CHIRPS/CHIRTS, CRU, ERA5L and TerraClimate over West Africa showing land cover changes/intensities (in red) coincide with abrupt climatic change in climatic conditions.

4.2.5 Mathematical formulation of the climate-land use/cover change impact (1980-2020)

The examination of various climatic datasets reveals that during the cold climate regime from 1980 to 2000, the most significant alterations in land cover occurred at the peak between two consecutive cold climate extremes. In addition, sudden swings from a hot climate to a cold climate also resulted in notable land cover changes. In contrast, the most notable alterations in land cover within a hot climate took place at the highest points between two consecutive periods of hot extremes, or during a sudden transition from a cold to a hot extreme. The climate-land interactions described above are characterized by critical points, including maximum, minimum, and points of inflection. These critical points can be said to mimic the critical point theory of the fundamental principles of calculus. For instance, the slope or first derivative equals 0 at both the maximum (hot extremes) and minimum (cold extremes) turning points, which are also referred to as extrema. Likewise, the second derivative is equal to 0 and indicates a change in concavity at the sites of inflection (Wrede & Spiegel, 2002). These extrema refer to peak conditions when the climatic indices reach a turning point, with a slope of zero, regardless of whether it is a hot or cold climate episode. Conversely, the migration from a hot climate to a cold climate, or vice versa, is indicated by situations where the climatic indices show a negative or positive slope, respectively. From the foregoing, the slope of the climatic indices described in this work is useful to mimic the interannual land-atmosphere or climate-land interactions over West Africa. The slope proposed here is considered in much detail later on in this work. In sections 4.2.6 and 4.2.7, the climatic conditions leading to abrupt and non-abrupt changes in land use/cover are determined to show the relative effects of extreme and normal climate on land use/cover over West Africa.

4.2.6 Quantifying climate conditions with abrupt land cover change effects

The observed changes in temperature, precipitation and climatic water balance conditions responsible for abrupt land use/cover changes is presented here. From Figures 4.3 and 4.6, changes of up to (0 to 1.5) ◦C (1995–1994, 2016–2015) are identified, with a total land cover area change

ranging from 20,935 to 22,127 km^2 over West Africa, with variation between one climatic zone and another. Changes from −1.0 to 1.0 ◦C (Figure 4.6e–h,q–t) relate to land cover area changes ranging from 45,039 to 52,133 km^2 of the West African domain (see 2000–1999, 2018–2017). Finally, a change within −0.5 and 0.5 ◦C (Figure 4.6i–l) correlates with land cover area change of up to 31,843 km^2. The climatic water balance and precipitation changes are similar for each of the periods and within −50 to 50 mm in most cases, with a few areas below and above −50 and +50 mm, respectively. Within the dry regime (1980 to ~2004), most of the land cover changes were experienced when at least 80% of the West African space was dominated by deficits in precipitation and climatic water balance up to −50 mm (Figure 4.6u–af). Within 2000–2020 (the wet regime), the majority of the region was influenced by a recovery (an increase) of rainfall and a climatic water balance of up to about 40 mm, covering at least 35% of the entire West African domain (Figure 4.6ag–an). From the foregoing, the plausible climatic condition relating to significant land cover changes in West Africa can be summarized as follows (Table 4.1). The wet and dry conditions in Table 4.1 are presented in this way to emphasize that similar temperature changes with contrasting precipitation and water balance (Figure 4.6; 1995–1994, 2016–2015) effects have similar effects on land cover area change (Figure 4.6; 1995, 2016). Moreover, a regional positive increase in temperature everywhere may have minimal impact on land cover area change compared to contrasting temperature changes with an increase in some regions and a decrease in others, or a temperature migration from hot (cold) conditions to cold (hot) conditions over the region. This is evident in Figure 4.6 and explains why a change of 0 to 1.5 ◦C has less impact on land cover area changes (20,935–22,127 km^2) than −0.5 to 0.5 ◦C changes (31,843 km^2). A change of −1.0 to 1.0 ◦C, however, relates to a greater land cover area change than −0.5 to 0.5 ◦C. The climatic conditions before and during abrupt land cover changes are shown in Figures A1 and A2 respectively in the appendix.

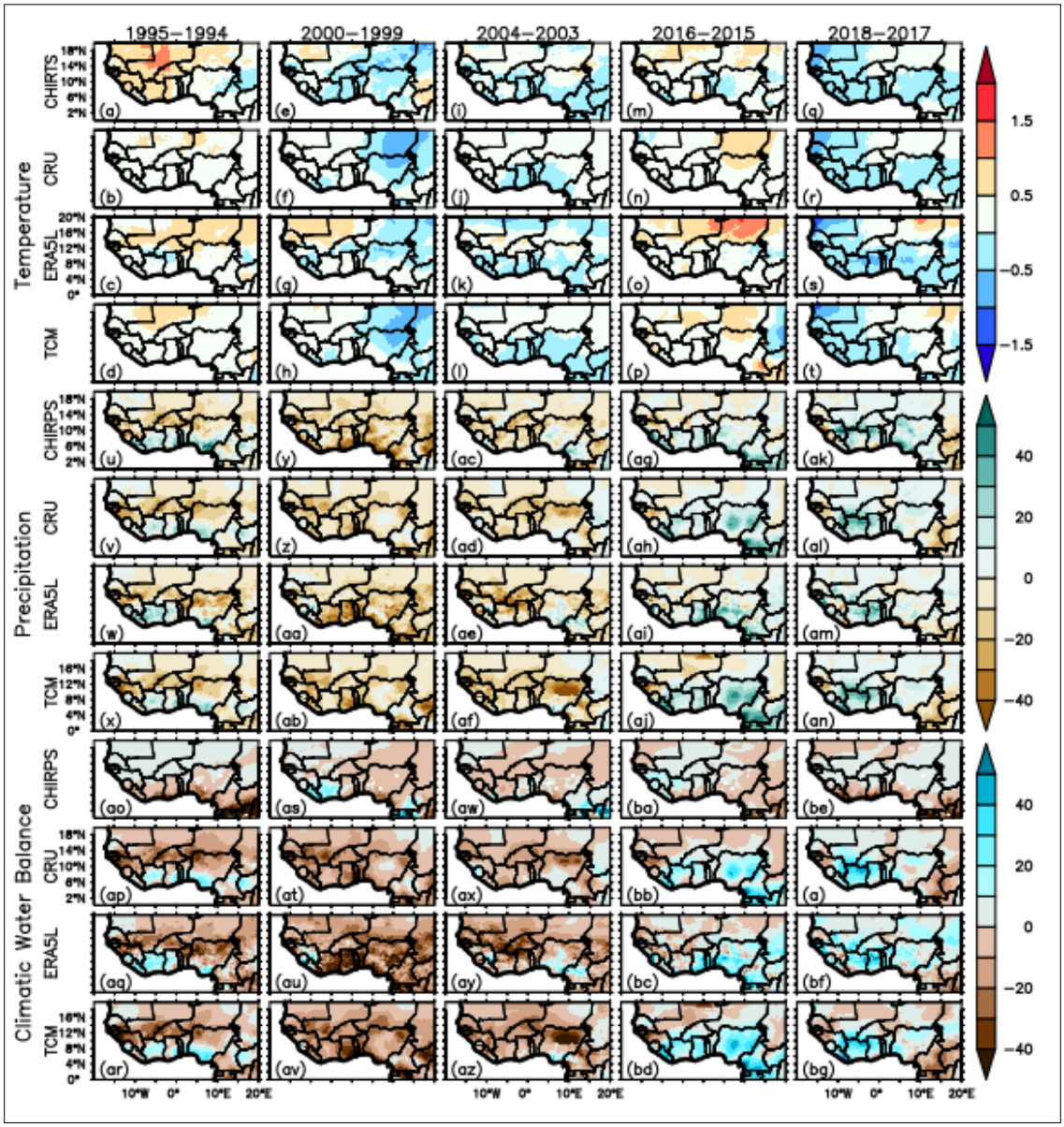

Figure 4.6 Changes in temperature, precipitation, and climatic water balance leading to intense land cover changes (a-d) Change in CHIRTS, CRU, ERA5L, and TCM temperature (1994–1995); (e-h) Change in CHIRTS, CRU, ERA5L, and TCM temperature (1999–2000); (i-l) Change in CHIRTS, CRU, ERA5L, and TCM temperature (2003–2004); (m-p) Change in CHIRTS, CRU, ERA5L, and TCM temperature (2015–2016); (q-t)Change in CHIRTS, CRU, ERA5L, and (u-x)TCM temperature (2017–2018); (u-x) Change in CHIRPS, CRU, ERA5L, and TCM precipitation (1994–1995); (y-ab) Change in CHIRTS, CRU, ERA5L, and TCM precipitation (1999–2000); (ac-af) Change in CHIRPS, CRU, ERA5L, and TCM precipitation (2003–2004); (ag-aj) Change in CHIRPS, CRU, ERA5L, and TCM precipitation (2015–2016); (ak-an) Change in CHIRPS, CRU, ERA5L, and TCM precipitation (2017–2018); (ao-ar) Change in CHIRPS, CRU, ERA5L, and

TCM climatic water balance (1994–1995); (as-av) Change in CHIRPS, CRU, ERA5L, and TCM climatic water balance (1999–2000); (aw-az) Change in CHIRPS, CRU, ERA5L, and TCM climatic water balance (2003–2004); (ba-bd) Change in CHIRPS, CRU, ERA5L, and TCM climatic water balance (2015–2016); (be-bg) Change in CHIRPS, CRU, ERA5L, and TCM climatic water balance (2017–2018). Temperatures, precipitation, and climatic water balance are in unit of, ℃ mm/year, and mm/year respectively.

Table 4.1 Climatic conditions leading to abrupt land cover area changes.

Scenario	Condition	T/℃	ΔT/℃	P/mmy^{-1}	ΔP/mmyr^{-1}	CWB/mmy^{-1}	ΔCWB/mm	ΔArea /km^2
Wet	change	−1.0–1.0	2	0–+50	up to 50	0–+50	up to 50	45,039–52,133
	increase	0–1.5	1.5	0–+50	up to 50	0–+50	up to 50	20,935–22,127
	change	−0.5– 0.5	1.0	0–+50	up to 50	0–+50	up to 50	31,843
Dry	change	−1.0–1.0	2.0	−50–0	up to −50	−50–0	up to −50	45,039–52,133
	increase	0–1.5	1.5	−50–0	up to −50	−50–0	up to −50	20,935–22,127
	change	−0.5–0.5	1.0	−50–0	up to −50	−50–0	up to −50	31,843

4.2.7 Quantifying climate conditions with non-abrupt land cover change effects

In this section, the climatic conditions in normal years are quantified to verify if the abrupt changes observed under drastic changes in climatic conditions led to abrupt land cover changes. The results show that the temperature change ranged between ±0.5 °C covering 50 to 90% under normal climatic conditions (Figure 4.7a–t) for CHIRTS, CRU, ERA5-Land, and CRU datasets. Similarly, changes in precipitation (Figure 4.7u–an) and climatic water balance (Figure 4.7ao–bg) ranged between −20 and +20 mm covering over 80% of WA for CHIRPS, CRU, ERA5-Land, and TerraClimate datasets. These climatic conditions are well below the conditions for which abrupt land cover changes were experienced, with a total land cover area change of less than 20,000 km^2. The magnitude of changes observed under normal climatic conditions confirms that intense land cover changes are associated with abrupt changes in temperature, precipitation, and climatic water balance.

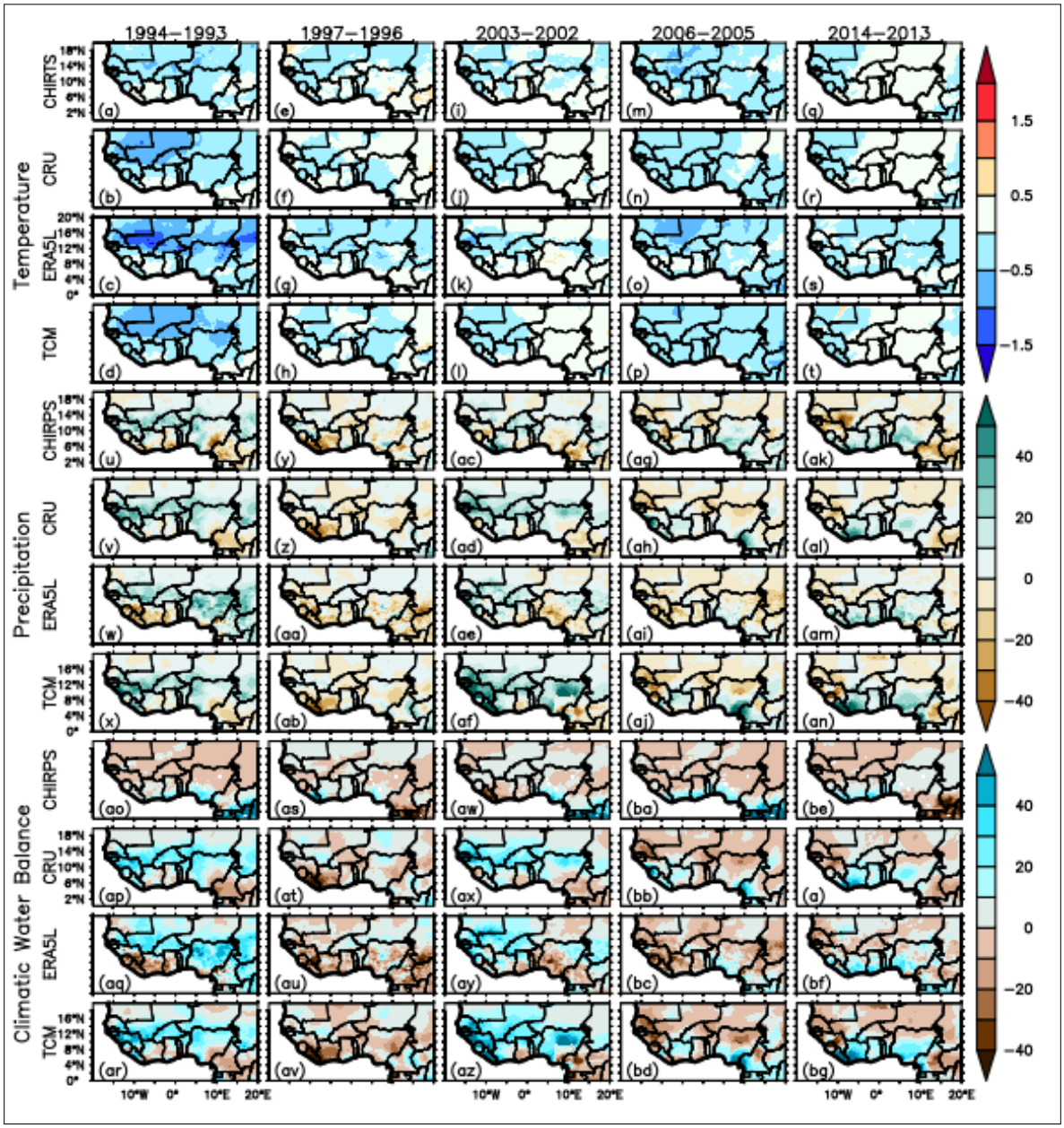

Figure 4.7 Maps of temperature, precipitation, and climatic water balance changes in under normal climatic conditions with no intense land cover changes : (a-d) Change in CHIRTS, CRU, ERA5L, and TCM temperature (1994–1995); (e-h) Change in CHIRTS, CRU, ERA5L, and TCM temperature (1999–2000); (i-l) Change in CHIRTS, CRU, ERA5L, and TCM temperature (2003–2004); (m-p) Change in CHIRTS, CRU, ERA5L, and TCM temperature (2015–2016); (q-t)Change in CHIRTS, CRU, ERA5L, and (u-x)TCM temperature (2017–2018); (u-x) Change in CHIRPS, CRU, ERA5L, and TCM precipitation (1994–1995); (y-ab) Change in CHIRTS, CRU, ERA5L, and TCM precipitation (1999–2000); (ac-af) Change in CHIRPS, CRU, ERA5L, and TCM precipitation (2003–2004); (ag-aj) Change in CHIRPS, CRU, ERA5L, and TCM precipitation

(2015–2016); (ak-an) Change in CHIRPS, CRU, ERA5L, and TCM precipitation (2017–2018); (ao-ar) Change in CHIRPS, CRU, ERA5L, and TCM climatic water balance (1994–1995); (as-av) Change in CHIRPS, CRU, ERA5L, and TCM climatic water balance (1999–2000); (aw-az) Change in CHIRPS, CRU, ERA5L, and TCM climatic water balance (2003–2004); (ba-bd) Change in CHIRPS, CRU, ERA5L, and TCM climatic water balance (2015–2016); (be-bg) Change in CHIRPS, CRU, ERA5L, and TCM climatic water balance (2017–2018). Temperatures, precipitation, and climatic water balance are in unit of, ℃ *mm/year, and mm/year respectively.*

4.2.8 Latitudinal change occurrence frequency

Figure 4.8a illustrates the overall changes in land cover area across latitudes, while Figure 4.8b displays the combined change per bioclimate zone. The Guineo–Congolia zone exhibits the least amount of change in land cover, with an extent of roughly 47,303 km^2. In contrast, the Sahel zone has the greatest change in land cover, with an area of about 145,483 km^2 (Figure 4.8b). The extent of land cover changes consistently grew as one moved from the Guinea zone to the Sudan zone until reaching around 9◦ N latitude (Figure 4.8a). Land cover in the Sudan zone declined as latitude increased, although this loss showed fluctuations towards the Sahel zone (Figure 4.8a). The Sudan zone had the most significant changes in land cover area following the Sahel zone, with a total land cover change area of 144,121 km^2 (Figure 4.8b). The maximum variations in total area occurred around 17° N and decreased towards 20° N. Figure 4.8a shows that the majority of land cover changes occurred just once, as indicated by the overlap between the total changes (in blue) and the one-time changes (in yellow). The two-time and three-time variations are predominantly aligned with the 0 km^2 change line spanning from Guineo–Congolia to the Sahara region, indicating their insignificance in comparison to the one-time change variations. The relative heights of the blue and yellow bar charts in Figure 4.8b also highlight that one-time changes are the main factor in each climatic zone. The two-time changes are most noticeable in the region between the mid-Sahel and approximately 18° N. These variations account for the temporal distinction between the blue and yellow lines depicted in Figure 4.8a. The relatively large two-time changes from 16° N to 18° N are also responsible for the larger land cover area change observed in the same latitudes (Figure 4.8a).

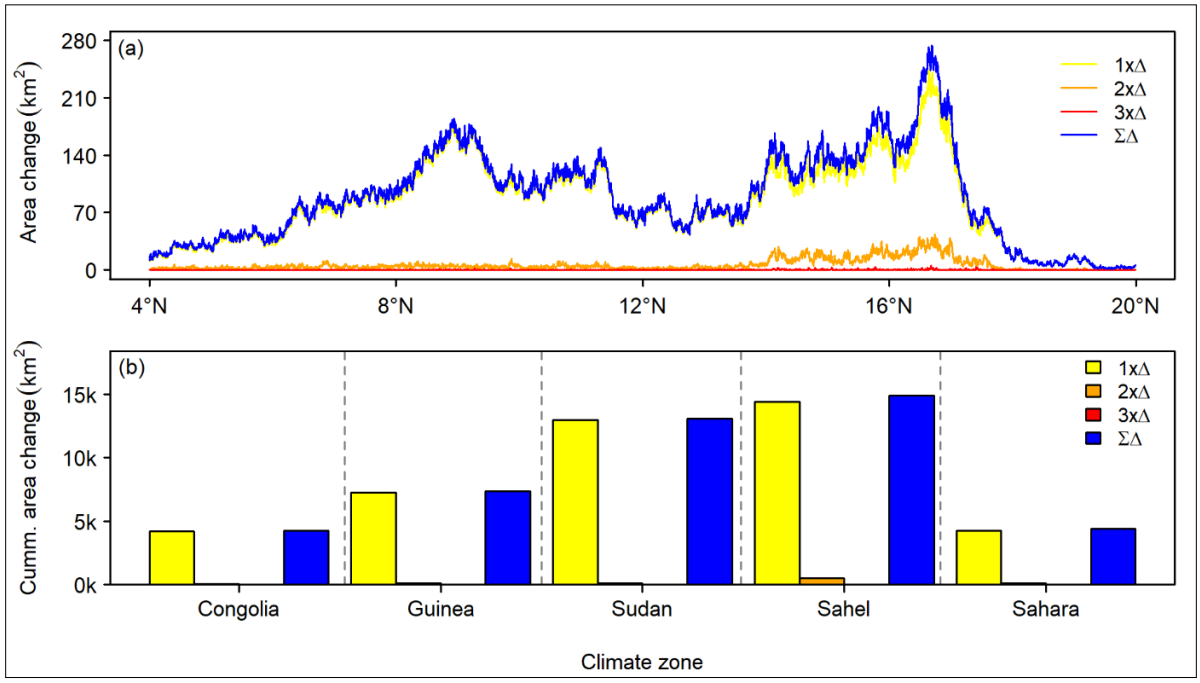

Figure 4.8 Area variation of land cover change over West Africa categorized by (a) land cover change frequency from 4°N to 20°N (b) cumulative land cover change frequency per climatic zone.

4.2.9 Land cover transition

In this section, a summary of the land cover transition in West Africa from 1992 to 2019 is presented. The land cover classes are based on the Intergovernmental Panel on Climate Change (IPCC) land cover classification system. The transitions were grouped every seven years from 1992 to 1999, 1999 to 2006, 2006 to 2013, and 2013 to 2019 (see Figure 4.9). The wetland, urban, barren, and water areas had similar changes in size across all transition periods, except for the period from 2016 to 2019, which spans only six years. The wetland, urban, barren, and water areas remained nearly constant (changed insignificantly) from 1992 to 2016, indicating the ESA LC map might not be very accurate in depicting changes in these classes. Consequently, it might not be suitable for detecting changes linked to these four land cover classes. Only farmland, forest, and sparse vegetation exhibit significant changes and are hence suitable for investigating the links between land use/cover change and climatic changes. Our examination of the relationship between climatic changes and land use/cover changes will also focus on farmland, forest, grassland, shrubland, and sparse vegetation. The land cover transitions depicted in the ESA LC maps provide two significant and noteworthy pieces of information. Cropland, forest, and sparse vegetation, such

as grass and shrub land, are the only land cover types that are found to have significant changes in the ESA land cover (ESA LC) maps. For this reason, these land cover classes are also the most suitable for studying the influence of the West African land surface on the regional climate. This is also consistent with Defourny et al. (2017) and X. Liu et al. (2018) who indicated that change detection in the CCI maps is based on six IPCC land categories, namely cropland, forest, grassland, wetland, settlement, and other land (shrubland, sparse vegetation, bare, water). Our transitional analysis however shows that wetland, urban cover bare areas and water changed very little. This information highlights some constraints of the ESA LC maps in representing changes in wetland, urban, barren, and water coverage across the region. This could be attributed to the fact that three out of four of these groups are derived from external data sources, and their spatial extent is likewise limited (< 7% in total). For example, the term "wetland" refers to areas with tree cover that are flooded with saline water, as defined by the global mangrove atlas. The definition of "urban areas" is based on data from both the Global Urban Footprint and the Global Human Settlement Layer. Water is derived from a compilation of static CCI global maps of open water bodies, originally at a resolution of 150 m, which were resampled to 300 m using an average algorithm (Defourny et al., 2017; X. Liu et al., 2018). The fact that these classes did not change very much throughout the period from 1992 to 2019 suggests that the ESA climate change initiative (CCI) maps might have limited usefulness in identifying changes in bare areas, wetlands, urban areas, and water bodies. So, a region evaluation might still be necessary to evaluate its suitability for urban, wetlands, water, bare areas, and other climate-related studies, as also indicated by Reinhart et al. (2021). The findings of this study provide some evaluation for the West African region. The fact that changes in cropland, forest, sparse vegetation, grass, and shrubland are captured makes it useful for studying the regional climate response to land cover change, which is discussed in the next section. Thus, cropland, forest, and sparse vegetation such as grass and shrubland, are well represented land cover types in the Sissili-Kulpawn Basin (SKB) and so have been adopted in the next section.

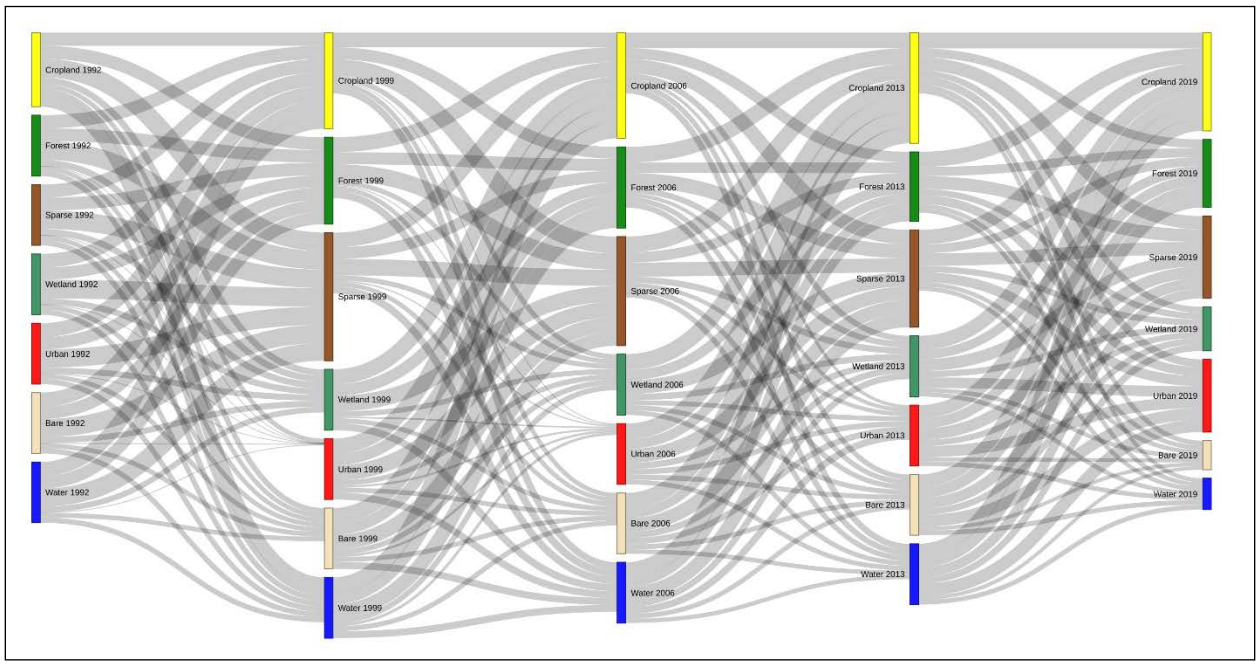

Figure 4.9 Land cover transitions from 1992–2019 over West Africa based on the IPCC classification scheme

4.3 Climate-land cover interactions from the modeling perspective – WRF-Hydro

The advantage of the fully coupled land-atmosphere interaction approach to climate-land use/land cover change interaction is highlighted in this section. The realism of the WRF-Hydro simulation is demonstrated by examining the effects on biophysical parameters such as the albedo and leaf area index. The model's output sensible, latent, and radiation heat fluxes, temperature, precipitation, and discharge were also validated using various observational products. The WRF-Hydro model has good performance and can replicate the hydroclimatic conditions of the region. The numerical land use/land cover change experiment was used to elucidate the nexus between climate-land-water-food interactions from the model point of view. The details of the results are outlined in sections 4.3.1 to 4.3.11 below.

4.3.1 Effects of numerical land cover changes experiment on in biophysical parameters

The different land cover change experiments result in different mean albedo and leaf area index (LAI) values compared to the reference WRF-Hydro simulation. The WRF-Hydro simulated mean albedo values for cropland, closed shrubland, and broadleaf forest scenarios over the Sissili (Kulpawn) Basin are 0.25 (0.24), 0.17 (0.17), and 0.23 (0.21), respectively, compared to a mean reference value of 0.22 (0.18). The change in albedo under the cropland, closed shrubland, and broadleaf forest scenarios are respectively 0.03 (0.06), -0.04 (-0.008), and 0.02 (0.03), indicating an increase in albedo for the cropland and broadleaf forest scenarios and a rather decrease in albedo for the closed shrubland scenario compared to the reference scenario (Figure 4.10a). The results show that the cropland and broadleaf forest scenarios result in an increase in mean albedo over the Sissili-Kulpawn Basin, while the closed shrubland scenario results in a decrease in mean albedo over the basin. The basin average albedo value for the cropland scenario is higher than that of the closed shrubland scenario which is consistent with literature as replacing closed shrubland by cropland is a deforestation scenario that should lead to an increase in albedo. That said, the broadleaf afforestation scenario also led to a decrease in albedo as in the cropland deforestation scenario, given reasons to believe that the broadleaf forest as used in the ESA land cover maps are savanna woodland. Generally, croplands have higher albedo values (0.18-0.25) than forests (0.15-0.2), and forests than closed shrublands (0.16-0.18). Our results show that cropland deforestation results in a higher albedo than closed shrubland afforestation which is expected, but also a

relatively higher albedo in the broadleaf forest scenario which is unexpected. The leaf area index (LAI) values obtained are consistent with the albedo with the LAI increasing (decreasing) as albedo decreases (increases). The LAI for the cropland, closed shrubland, and broadleaf forest scenarios over the Sissili (Kulpawn) are 1.39 (1.76) m^2m^{-2}, 1.89 (2.19) m^2m^{-2}, and 1.52 (1.97) m^2m^{-2} respectively compared to the reference scenario of 1.59 (2.12) m^2m^{-2}. The change in LAI under the cropland, closed shrubland, and broadleaf forest scenarios is respectively -0.21 (-0.37) m^2m^{-2}, 0.30 (0.07) m^2m^{-2}, and -0.07 (-0.15) m^2m^{-2}, indicating a reduction in LAI for the cropland and broadleaf forest scenario and a rather increase in LAI for the closed shrubland scenario compared to the reference scenario (Figure 4.10b). The decreased LAI and increased albedo for the cropland and broadleaf forest scenarios is likely to reduce the light absorption and increase reflection resulting in a cooler air near the surface, with decreased net radiation, sensible heat, and latent heat fluxes. Conversely, the increased LAI and decrease albedo could result in an increased absorption and reduced reflection of radiant energy leading to an increased net radiation, latent and sensible heat fluxes near the surface. From the analysis of the albedo and leaf area index, our model represents well these two biophysical properties of land-atmosphere interactions necessary for simulating the effects of land cover change on water and energy budget. The results of the cropland afforestation scenario are consistent with Chen et al. (2012), who found afforestation to decrease (increase) annual and seasonal albedo (LAI) over the Southeast United States. The broadleaf scenario obtained in this work is however, in phase opposition to albedo and LAI obtained by Chen et al. (2012). Perugini et al. (2017), in a review of tropical deforestation, noted that a reduction in LAI due to deforestation enhances warming because of increased sensible heat flux and corresponding reduced latent heat flux. The advantage of the land-atmosphere interaction modeling with WRF-Hydro over the analysis approach used in objective one (1) is that it allows for a detailed description of surface parameters such as the albedo and LAI as discussed above. On the other hand, the analysis approach benefits from the use of multiple land use/cover datasets which is not the case for WRF-Hydro and most RCMs which use only one year of historical data and keep it constant throughout the simulation period. While the modeling approach here cannot improve the analysis approach, the slope of the climatic indices may be exploited to improve on the dynamic interactions between the atmosphere and the land which is often overlooked in the RCMs. In this way, the analysis approach offers the slope as the dynamic coefficient for the static

land cover map in the WRF-Hydro to better improve output such as streamflow outside WRF-Hydro.

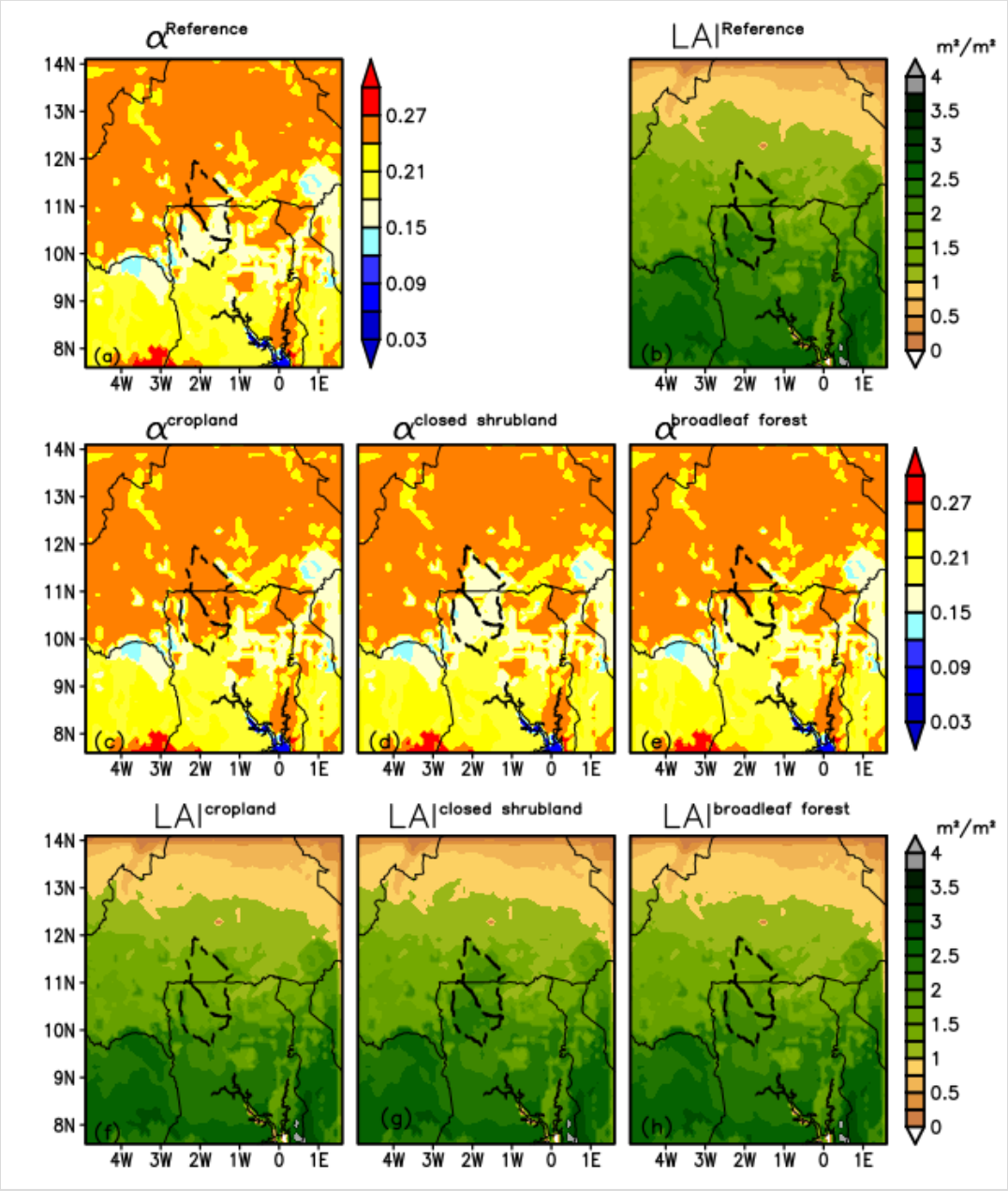

Figure 4.10 Maps of biogeophysical parameters obtained from land cover change experiments compared to WRF-Hydro reference simulation in the inner domain, (a) albedo of reference WRF-Hydro simulation, (b) Leaf Area Index (LAI) of reference WRF-Hydro simulation (c) albedo of the cropland WRF-Hydro simulation, (d) albedo of closed shrubland simulation (e) albedo of

broadleaf forest WRF-Hydro simulation, (f) LAI of cropland WRF-Hydro simulation, (g) LAI of closed shrubland WRF-Hydro simulation (d) LAI of broadleaf forest WRF-Hydro simulation. The black thick dashed line in all the panels indicate the location of the SKB. The reference and the land cover change experiment share the same biogeophysical parameters shown in color scale of the respective maps. Mean values are calculated over the basin for a seven-year period spanning 1st January, 2010 to 31st December, 2016.

4.3.2 Spatial validation of simulated Energy fluxes

In general, the net solar radiation (R^{net}) of a surface is partitioned into the sensible heat flux ($H^{sensible}$), latent heat fluxes (H^{latent}), and other components. For WRF-Hydro, the net radiation on a vegetation surface is partitioned into $H^{sensible}$, H^{latent}, soil heat flux (H^{soil}), and canopy heat fluxes (H^{canopy}). For this work, the canopy and soil heat fluxes are negligible, and so the result is focused on the R^{net}, $H^{sensible}$, and H^{latent}. To validate the simulated R^{net}, $H^{sensible}$, H^{latent}, they are compared with the FLUXCOM observational data. The simulated R^{net} overestimates the observation product by 10.18% (11.76%) over the Sissili (Kulpawn) Basins. In terms of the $H^{sensible}$, the WRF-Hydro simulation results deviate from the observation FLUXCOM data between mostly -10% to +50% (Figure 4.11f) over the inner domain of the WRF-Hydro simulations. The WRF-Hydro simulated R^{net} compares very well with the observational FLUXCOM data with a bias ranging between -25% and +25% over the inner domain of the WRF-Hydro simulations. Over the Sissili-Kulpawn Basin, the R^{net} bias ranged between -10% to 25% (Figure 4.11c), with overestimations mainly in the Kulpawn Basin and the lower parts of the Sissili Basin. The WRF-Hydro mean R^{net} over the Sissili (Kulpawn) is 132.86 Wm^{-2} (136 Wm^{-2}) compared to 120.46 Wm^{-2} (122.53 Wm^{-2}) from the FLUXCOM observation product. The mean simulated $H^{sensible}$ over the Sissili (Kulpawn) is 69.55 Wm^{-2} (70.22 Wm^{-2}) compared to 54.45 Wm^{-2} (53.21 Wm^{-2}) from the FLUXCOM observation product. The simulated $H^{sensible}$ (Figure 4.11d) overestimates the $H^{sensible}$ from the observation (Figure 4.11e) by 29.97% (31.90%) over Sissili (Kulpawn) Basins (Figure 4.11f). This is the opposite for H^{latent} where the observation products values are higher than that of the WRF-Hydro simulated values. For instance, the mean simulated H^{latent} over Sissili (Kulpawn) is 64.05 Wm^{-2} (67.43 Wm^{-2}) compared to 66.87 Wm^{-2} (70.47 Wm^{-2}) over the 2010-2013 period. The bias as a result is also -4.31% (-4.17%) over the same period. The relatively huge biases in energy fluxes between the WRF-Hydro simulated fluxes and the observational product FLUXCOM could be

attributed to the fact that the biases were computed over a just three-year period (2010-2013); the overlapping period for which data was available for both the WRF-Hydro simulated fluxes and the observational product from FLUXCOM. From the results, the modeling in WRF-Hydro offers the ability to describe how net radiation flux (R^{net}) is partitioned into sensible heat flux ($H^{sensible}$), and latent heat flux (H^{latent}). This energy partition also determines the temperature. This is yet another advantage of the modeling approach using WRF-Hydro compared to the analysis approach in objective one (1).

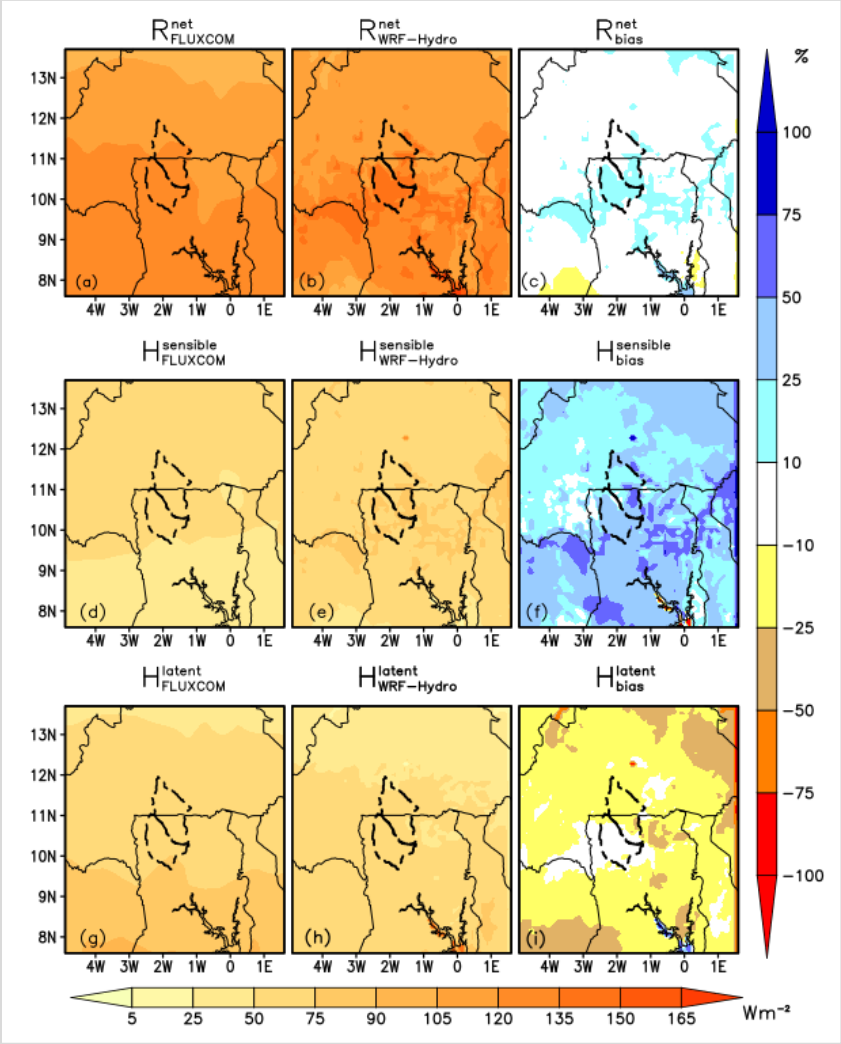

Figure 4.11 Validation of net radiation, sensible and latent heat fluxes over Sissili-Kulpawn Basin Maps of (a) mean net radiation flux R^{net} (in W/m^2) from FLUXCOM observational product, (b) mean net radiation flux R^{net} from WRF-Hydro reference simulation, (c) R^{net} bias (in %) between

observation product FLUXCOM and WRF-Hydro reference simulations, (d) mean net sensible heat flux $H^{sensible}$ (in W/m^2) from observation product FLUXCOM, (e) mean net sensible heat flux $H^{sensible}$ (in W/m^2) from the WRF-Hydro reference simulations (f) sensible heat flux bias (in %) between observation product FLUXCOM and WRF-Hydro reference simulation, (g) mean latent heat flux H^{latent} from the observation product FLUXCOM, (h) mean latent heat flux H^{latent} from WRF-Hydro reference simulation, (i) latent heat flux bias (in %) between observation product and WRF-Hydro reference simulation. The energy flux maps (a,b,d,e,g,h) have the same color scale shown below figure 4.6 and extend the widths of maps (g,h,i). The bias maps (c,f,i) have the same color maps shown at the right side of figure 4.6 and extents the heights of (c,f,i). Mean values are computed for a seven-year period spanning 1st January, 2010 to 31st December, 2013.

4.3.3 Validation of WRF-Hydro simulated rainfall and temperature

To determine the usefulness of a model in a region, there is the need to assess its performance by comparing it observational products. In this work, the WRF-Hydro simulated rainfall and temperature were validated with IMERG and CHIRTS observational products. The WRF-Hydro simulated rainfall shows biases compared to the observational dataset (IMERG) within the range of -25 to +25% (Figure 4.12c) with underestimations mainly in the northern parts of the inner domain within the upper parts of Sissili and Burkina Faso. The overestimations within -10 to 10 are mainly constrained to the southern parts covering the entire Kulpawn Basin and the lower parts of the Sissili Basin. The WRF-Hydro simulated mean temperature and precipitation over the Sissili (Kulpawn) Basin are 27.34 °C (27.24 °C) and 2.62 mmday^{-1} (2.83 mmday^{-1}) compared to 29.25 °C (29.03 °C) and 2.61 mmday^{-1} (2.59 mmday^{-1}) from CHIRTS and IMERG observational products, respectively. Thus, the WRF-Hydro mean simulated temperature and precipitation for Sissili (Kulpawn) deviates from the observation products by -1.81 °C (-1.56 °C) and -0.43% (8.45%) respectively. There is an underestimation of temperature, but an underestimation (overestimation) for Sissili (Kulpawn) in terms of rainfall. The differences however show that the WRF-Hydro with overbank flow option as used in this thesis is skilled to replicate the daily observed temperature and precipitation in observational datasets and thus capable of reproducing the hydroclimatic situations in the Sissili-Kulpawn Basin in West Africa. The added value of the WRF/WRF-Hydro as a regional climate model in this respect is the ability to simulate regional rainfall and temperatures, which also make it suitable for operational forecasting. Thus, the practical

application of this model is for operational forecasting of rainfall and temperatures over the Sissili-Kulpawn Basin. On the contrary, the analysis approach used in objective one (1) lacks this forecasting capability to describes the detailed processes that happened in the atmosphere-land interface at regional and local scales. So, while the analysis may provide useful information on improving the output of models, it cannot provide forecasting capabilities.

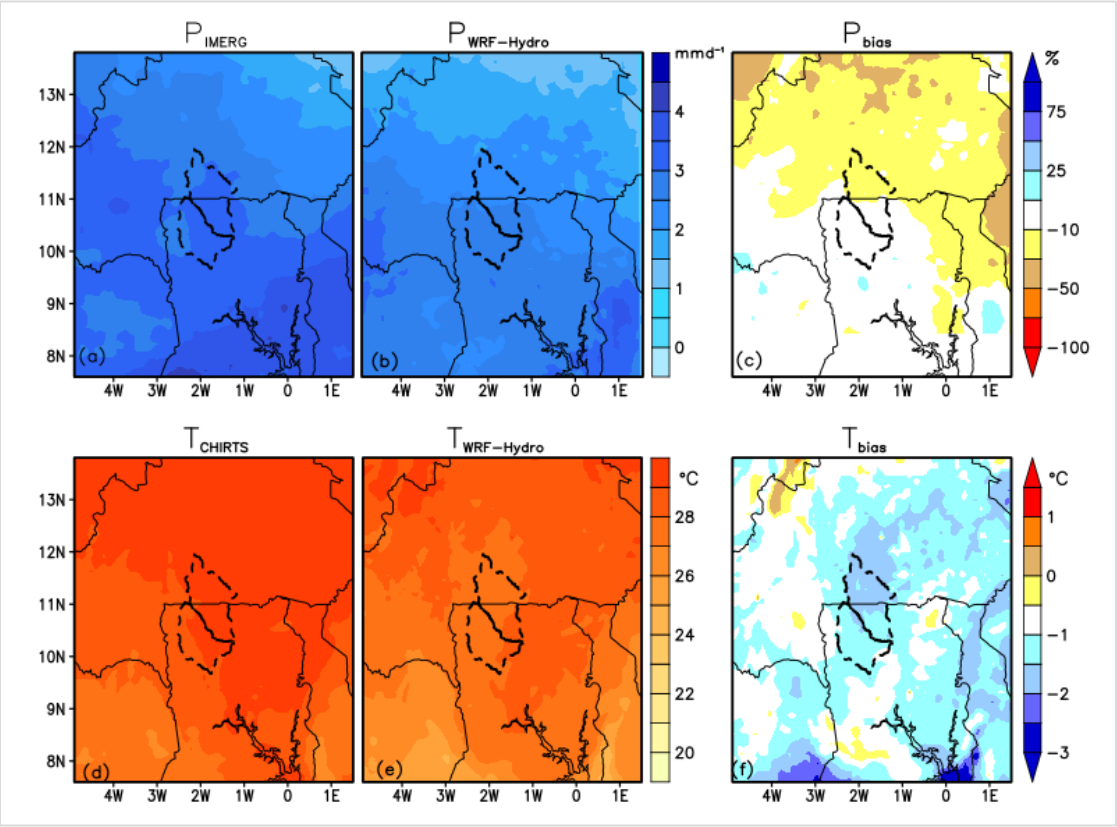

*Figure 4.12 Validation of daily mean precipitation and temperature over Sissili-Kulpawn Basin: Maps of **(a)** daily mean precipitation P (in mm/day) from the observational product IMERG, **(b)** daily mean precipitation (in mm/day) from WRF-Hydro reference simulations, **(c)** precipitation bias (in %) between WRF-Hydro reference and IMERG, **(d)** daily mean temperature T (in ℃) from the observational product CHIRTS, **(e)** daily mean temperature (in ℃) from WRF-Hydro reference simulation, **(f)** temperature bias (in ℃) between CHIRTS and WRF-Hydro reference. The daily mean precipitation maps **(a,b)** have share the same color scale shown on the right side, and the mean daily temperatures **(d,e)** have the same color scale show on the right side of **(e).** Mean values are calculated over a seven-year period spanning 1st January, 2010 to 31st December, 2016.*

4.3.4 Temporal validation of WRF-Hydro simulated rainfall and streamflow

The streamflow was also validated to assess the model's ability to replicate observed discharge. The results of the skill metrics for precipitation, and discharge are shown in Figure 4.13a,c and Figure 4.13b,d, respectively, for the default WRF-Hydro simulation (in grey) and calibrated WRF-Hydro with overbank flow option (in black). There is improvement in all skill metrics for precipitation in both the Sissili and the Kulpawn Basins with the WRF-Hydro calibrated with the overbank flow option. That said, the NSE of the Kulpawn Basin (0.36) is still well below 0.5 giving reasons to believe the calibrated WRF-Hydro with overbank flow options can still be improved. Particularly, the simulated rainfall still contains some undesirable peaks that could be removed to improve the skill metrics. The R^2, RMSE, NSE, and PBIAS for the default WRF-Hydro simulations have been improved by introducing the overbank flow process. The WRF-Hydro with two-way river-land flow option (overbank flow option) significantly reduced the peaks, as seen in Figure 4.13b,d. However, the skill metrics remain weak, particularly for the Sissili Basins with NSE, KGE, and PBIAS of -1.33, -0.29, and 93, respectively. For the Kulpawn Basin, all discharge has been significantly improved with an NSE, KGE, and PBIAS of 0.47, 0.69, and -15%, respectively. It should be noted however, that the relatively weak discharge performance could be attributed to the quality of simulated precipitation, which is a drawback of atmospheric-hydrological coupling modeling approach (Senatore et al., 2015). That said the relatively weak, with some negative NSE values still falls within the range of published precipitation and discharge performance across the globe: 0.46 for (Arnault et al., 2016b), 0.27 for (Kerandi et al., 2017), -1.89–0.61 for (Rummler et al., 2019b), 0.27 for (L. Li et al., 2020b). Therefore, the WRF-Hydro results obtained over the calibration period are realistic and give us confidence that the WRF-Hydro with overbank flow option can be used to study the regional climate response to land cover change. The biases in precipitation show that the fully coupled WRF-Hydro simulated temperature and precipitation biases are minimal such that the model is skilled in providing climate information on daily timescales. In West Africa, rainfall and temperature are the most basic information provided by national meteorological organizations to the public. With the capabilities of the fully coupled WRF/WRF-Hydro shown in this work, national meteorological agencies can use the WRF model to complement or improve the traditional approach to weather forecasting. That said, the WRF-Hydro simulations are computationally expensive, and strong computational resources and

skills are required to run simulations. The employees of the national meteorological agencies must be skilled to simulate, analyze the results, and make reports available to the public as climate information or weather forecasts. The traditional way of forecasting and climate information provision could significantly benefit from the fully coupled WRF/WRF-Hydro.

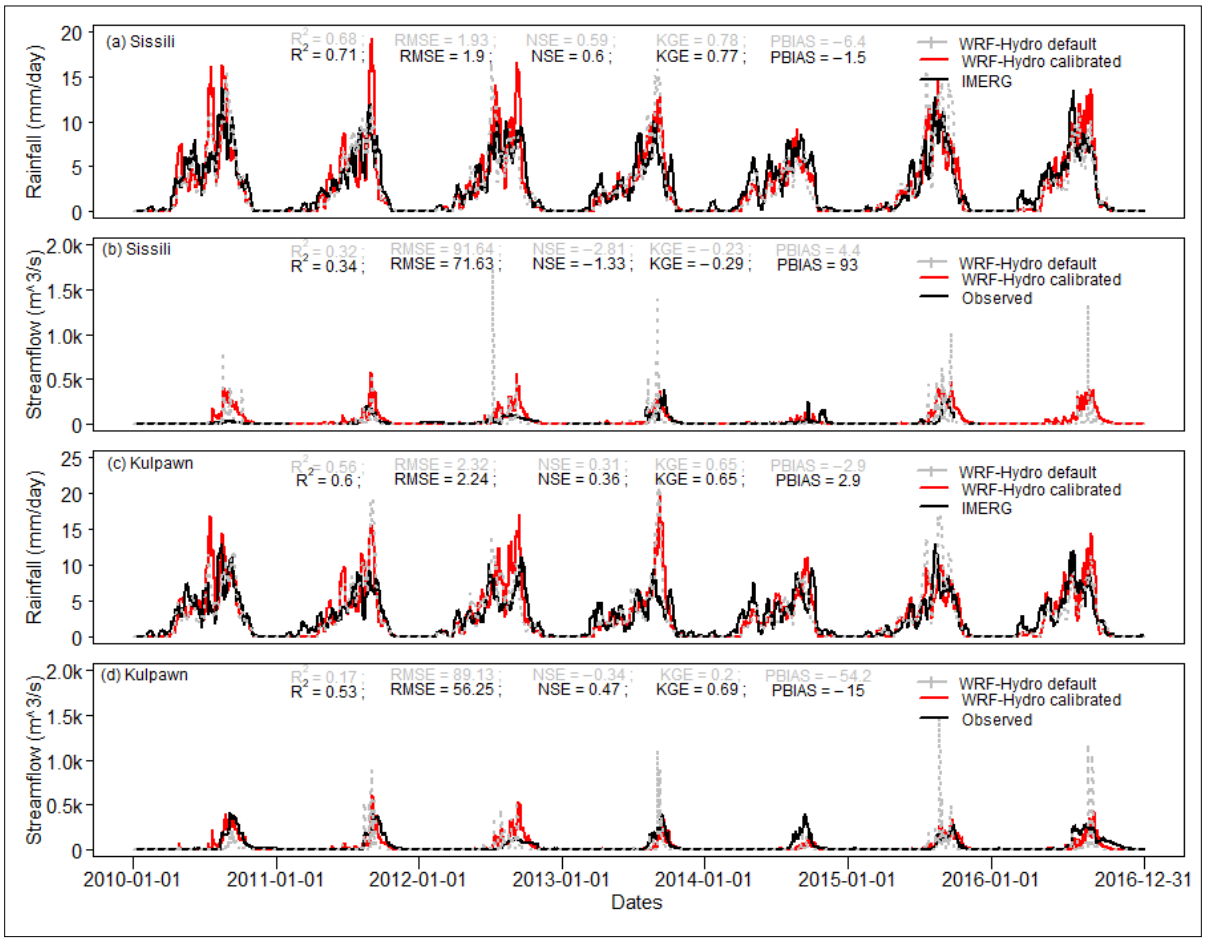

Figure 4.13 Validation of rainfall and discharge over the Sissili-Kulpawn Basin (2010-2016). Maps of ***(a)*** *Daily rainfall P (in mm/day) for a seven-year period spanning from 1st January 2010 to 31st December 2016 and filtered over a 14-day period, as derived from the observational product IMERG and from the inner domain of the default and calibrated WRF-Hydro simulations.* ***(b)*** *Daily timeseries of discharge Q (in m^3/s) at the Sissili Basin outlet for a seven-year period spanning from 1st January 2010 to 31st December 2016, as derived from the gauge measurement and from the default and calibrated WRF-Hydro simulations.* ***(c)*** *Daily timeseries of Kulpawn river basin-averaged rainfall P (in mm/day) for a seven-year period spanning from 1st January*

2010 to 31st December 2016 and filtered over a 14-day period, as derived from the observational product IMERG and from the inner domain of the default and calibrated WRF-Hydro simulations. ***(d)*** *Daily timeseries of discharge Q (in m^3/s) at the Kulpawn Basin outlet for a seven-year period spanning from 1st January 2010 to 31st December 2016, as derived from the gauge measurement and from the default and calibrated WRF-Hydro simulations. Evaluation metrics for the default WRF-Hydro simulations are indicated in grey color as opposed to the evaluation metrics of the calibrated WRF-Hydro simulations which are shown in black. The calibrated simulation employs the modified WRF-Hydro source code available at https://doi.org/10.6084/m9.figshare.21063982 and described in section 3.5.4.2, with the best set of parameters values according to the calibration exercise, that is (H_{thres} = 6 m, S = 0.01, M045).*

4.3.5 Climatological evaluation of simulated rainfall, discharge, temperature and energy fluxes over the Sissili Basin

The monthly climatology of precipitation, discharge, temperature, and energy fluxes over the Sissili Basin are presented in this section. The climatology of precipitation, discharge, temperature, and heat fluxes in Figure 4.14a-d are evaluated from the maps or timeseries of monthly mean precipitation, discharge, temperature, and energy fluxes in Figures 4.12a,b, Figure 4.13b, Figures 4.11d,e and Figures 4.11a-b,d-e,g-h, respectively averaged over the Sissili Basin between 1st January 2010 to 31st December 2016. As can be seen from Figure 4.14a, the WRF-Hydro simulated rainfall is remarkably close to the observational product IMERG for all months of the year with little overestimations and underestimations from February-March-April-May (FMAM) period and June-July-August-September period (JJAS), respectively. Thus, the WRF-Hydro with overbank flow option used in this study improves the simulated rainfall but is a little drier than the observational product in the FMAM and a little wetter than the observed in JJAS. The wet nature of the WRF-Hydro with overbank flow option in the JJAS period can also be seen in the discharge (Figure 4.13b). Missing discharge values in the observed timeseries resulted in lower observed discharge compared to the simulated (Figure 4.14b) in the JJAS period. The simulated WRF-Hydro temperature underestimates temperature (Figure 4.14c) but also a good prediction over the Sissili Basin particularly in the April-May-June (AMJ) period. In terms of the energy fluxes, the WRF-Hydro simulated R^{net} and $H^{sensible}$ fluxes have positive biases relative to the observation product from FLUXCOM as shown in Figures 4.11c and Figures 4.11f. Conversely, the latent heat flux

(H^{latent}) from the WRF-Hydro output fluxes have a negative bias relative to the observation product FLUXCOM as displayed by mostly negative values in Figure 4.11i. The simulated R^{net} is remarkably close to the observational product FLUXCOM for January-February-March-April (JFMA), and June-July-August (JJA) with the most overestimations also at the May-June (MJ) and September-October-November-December (SOND). The simulated sensible heat flux ($H^{sensible}$) overestimates the observation product for all months, whilst the H^{latent} on the other hand underestimates the FLUXCOM data for nearly all months of the year except December (Figure 4.14d). Again, the relatively large deviations in energy fluxes between the WRF-Hydro simulated fluxes and the observational product FLUXCOM could be attributed to the fact that the biases were computed over a just three-year period (2010-2013) for which data was available for both the WRF-Hydro simulated fluxes and the observational product from FLUXCOM. From the results above the fully coupled WRF-Hydro can describe the water and energy cycle of the Sissili-Kulpawn Basin, which is not possible with the analysis approach presented in objective 1. Thus WRF-Hydro with the overbank flow option can be said to replicated the climatology of water and energy fluxes and the general land-atmosphere interaction in the Sissili Basin.

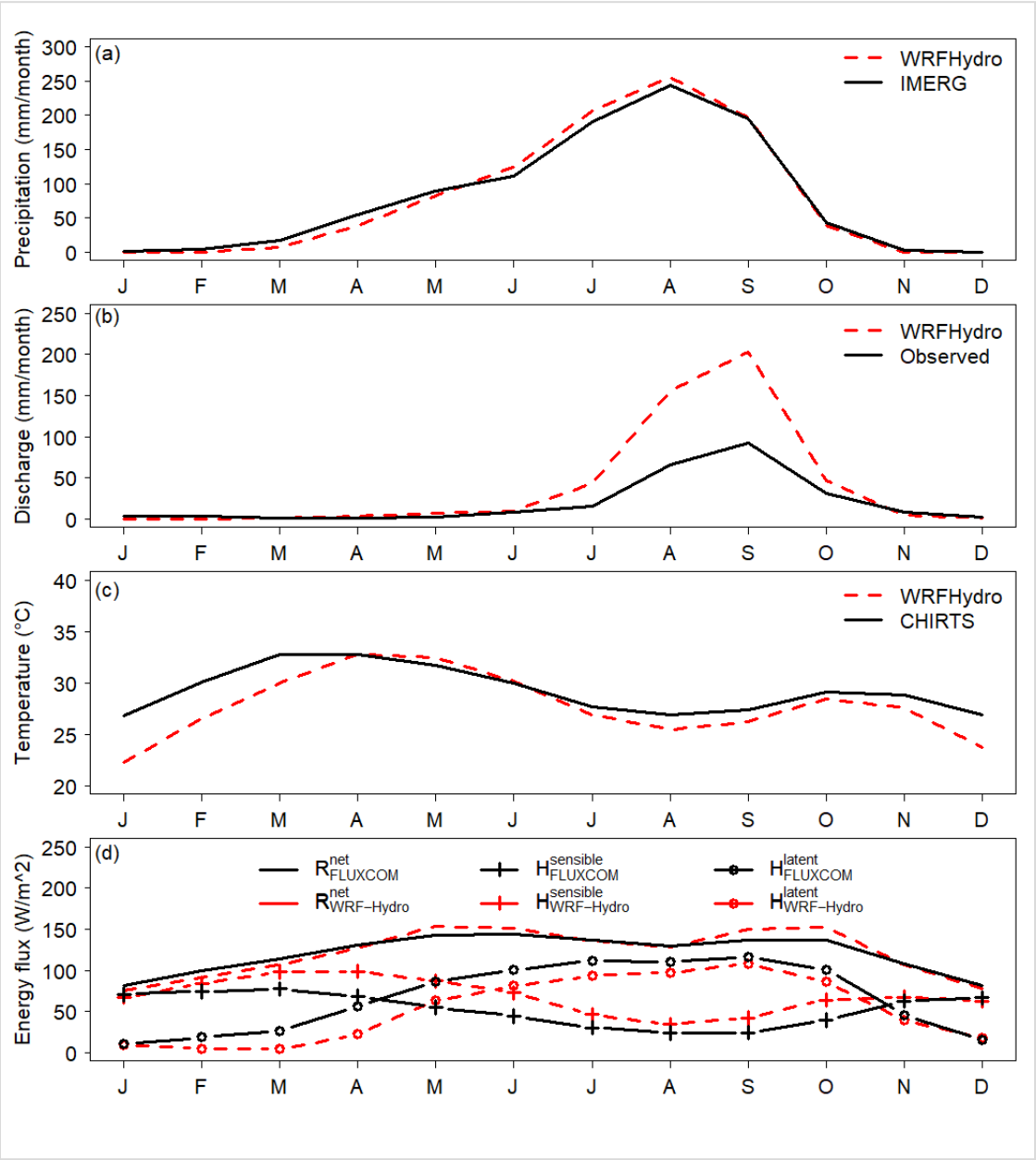

Figure 4.14 Climatology evaluation of water and energy fluxes over the Sissili river basin. Monthly climatological timeseries of the (a) Sissili river basin-averaged precipitation P (in mm/month), (b) Sissili river basin discharge Q at wiasi (in m^3/s), (c) Sissili river basin-averaged temperature (in °C), (d) Sissili Basin-averaged net radiation, sensible and latent heat fluxes R^{net}, $H^{sensible}$, H^{latent} (in W/m^2), as derived from (a) the observation product IMERG, (b) gauge measurement, (c) the observational product CHIRTS, (d) the observation FLUXCOM, and the inner domain of the WRF-Hydro reference simulation. Climatological monthly values of (a) precipitation, (b) discharge, (c)

temperature, (d) energy flux values are computed from (a) a seven-year period spanning 1st January, 2010 to 31st December, 2016, (b) a six-year period spanning 1st January, 2010 to 31st December, 2015 with some missing data, (c) a seven-year period spanning 1st January, 2010 to 31st December, 2016, (d) a three-year period spanning from 1st January, 2010 to 31st December, 2013, when the corresponding observational data is available.

4.3.6 Climatological evaluation of simulated rainfall, discharge, temperature and energy fluxes over the Kulpawn Basin

The monthly climatology of precipitation, discharge, temperature, and energy fluxes over the Kulpawn Basin are presented in this section. The monthly climatology of precipitation, discharge, temperature, and heat fluxes in Figure 4.15a-d are also evaluated from the maps or timeseries of monthly mean precipitation, discharge, temperature, and energy fluxes in Figures 4.12a,b, Figure 4.13d, figure 4.12d,e, and Figure 4.11a-b,d-e,g-h aggregated over the Kulpawn Basin over the simulation period. The WRF-Hydro simulated rainfall is quite close to the observational product IMERG for all months of the year with overestimations and underestimations from February to May (FMAM) and October to November (ON) (Figure 4.15a), and June to October (JJASO) respectively. The WRF-Hydro with overbank flow option used in this study is dry at FMAM and ON period and wet during the major wet season (JJASO) (Figure 4.15a). In terms of temperature, the simulated WRF-Hydro underestimates temperature (Figure 4.15c) but with nearly correct predictions over the Kulpawn Basin for the April-May-June (AMJ) period. In terms of the energy fluxes, the WRF-Hydro simulated net radiation flux (R^{net}) and sensible heat flux ($H^{sensible}$) are larger (positive bias) than the observation product from FLUXCOM as displayed in Figures 4.11a-c and Figures 4.11d-e. Conversely, the H^{latent} from the WRF-Hydro simulated underestimates the observation product FLUXCOM as observed by mostly a negative bias in Figure 4.11i. The simulated R^{net} is quite close to the observational product FLUXCOM for JFMA and JJA with the most overestimations also at the MJ and SOND. The simulated $H^{sensible}$ overestimates the observation product for all months, while the H^{latent} underestimates the FLUXCOM data for nearly all months of the year except December (Figure 4.15d). Just like the Sissili Basin, the WRF-Hydro also replicates well the climatology of water and energy fluxes and hence the land-atmosphere interactions over the Kulpawn Basin.

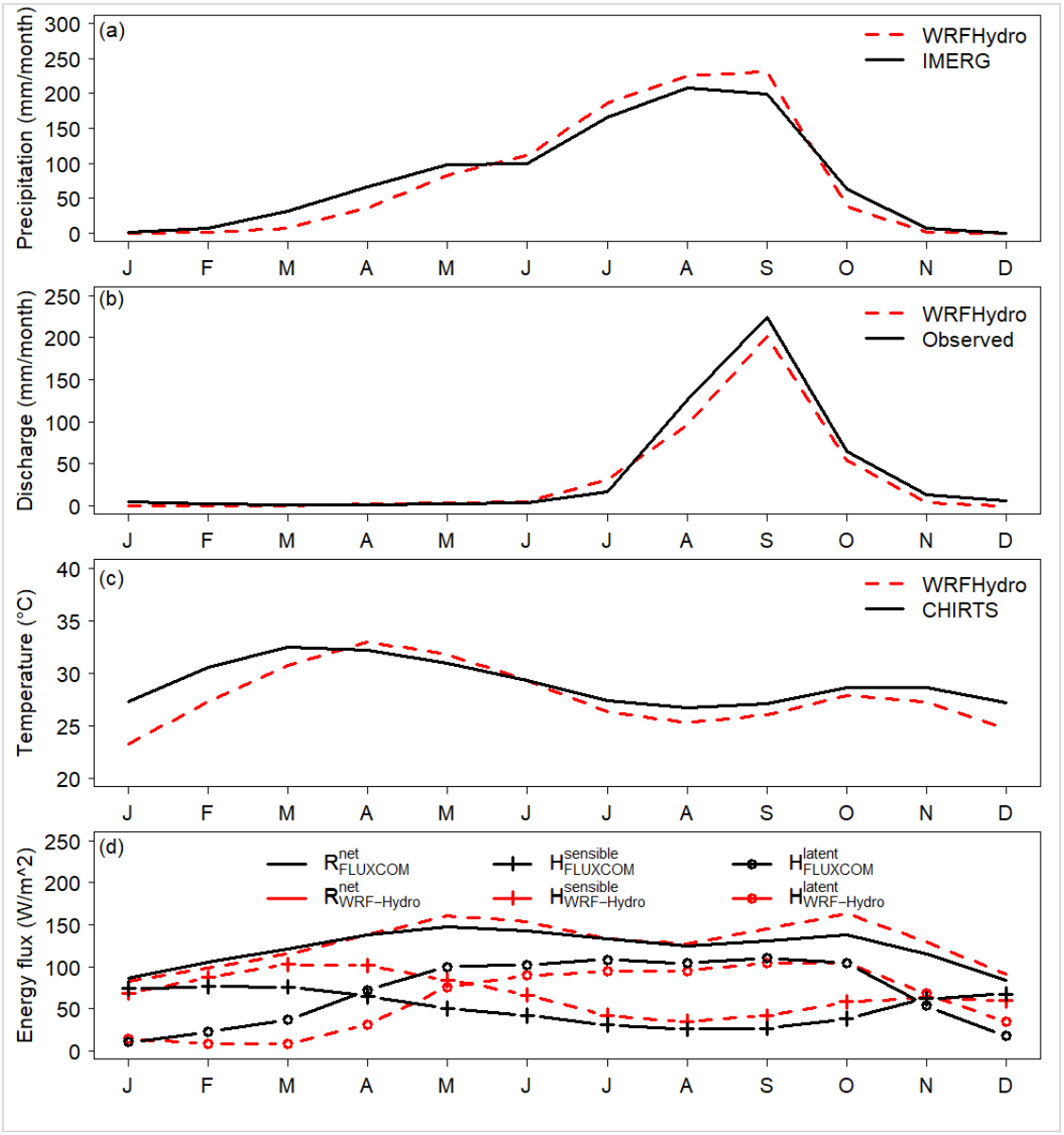

Figure 4.15 Climatology evaluation of water and energy fluxes over the Kulpawn river basin. Monthly climatological timeseries of the (a) Kulpawn river basin-averaged precipitation P (in mm/month), (b) Kulpawn river basin discharge Q at Yagaba (in m^3/s), (c) Kulpawn river basin-averaged temperature (in ℃), Kulpawn Basin-averaged net radiation, sensible and latent heat fluxes R^{net}, $H^{sensible}$, H^{latent} (in W/m^2), as derived from (a) the observation product IMERG, (b) gauge measurement, (c) the observational product CHIRTS, (d) the observation FLUXCOM, in the inner domain of the WRF-Hydro reference simulation. Climatological monthly values are of (a) precipitation, (b) discharge, (c) temperature, (d) energy flux values are computed from (a) a

seven-year period spanning 1st January, 2010 to 31st December, 2016, (b) a six-year period spanning 1st January, 2010 to 31st December, 2015 with some missing data, (c) a seven-year period spanning 1st January, 2010 to 31st December, 2016, (d) a three-year period spanning from 1st January, 2010 to 31st December, 2013, when the corresponding observational data is available.

4.3.7 Impact of land use/land cover change on energy fluxes

The changes in the net sensible flux (R^{net}), sensible heat flux ($H^{sensible}$) and latent heat flux (H^{latent}) over the Sissili (Kulpawn) basin for the cropland scenario is obtained from Figure 4.16a,d,g and estimated as -7.84 Wm^{-2} (-13.53 Wm^{-2}), -6.33 Wm^{-2} (-11.91 Wm^{-2}), and -1.77 Wm^{-2} (-2.1 Wm^{-2}) respectively. For the closed shrubland, the changes in R^{net}, $H^{sensible}$, and H^{latent} over the Sissili (Kulpawn) Basin is estimated from Figure 4.16b,e,h as 10.59 Wm^{-2} (2.23 Wm^{-2}), 8.79 Wm^{-2} (1.06 Wm^{-2}), and 2.18 Wm^{-2} (1.26 Wm^{-2}) respectively. Finally, for the broadleaf forest scenario, the changes in R^{net}, $H^{sensible}$, H^{latent} over Sissili (Kulpawn) Basins is estimated from Figure 4.16c,f,i to be -4.07 Wm^{-2} (-7.99 Wm^{-2}), -4.10 Wm^{-2} (-7.11 Wm^{-2}), and -0.13 Wm^{-2} (-1.20 Wm^{-2}) respectively. Thus, from the results above, the cropland and broadleaf forest scenario results in a deficit of R^{net}, $H^{sensible}$, and H^{latent} fluxes compared to the closed shrubland scenario which results in a net positive energy flux. The decrease in R^{net}, $H^{sensible}$, and H^{latent} fluxes for the cropland and broadleaf forest scenario results from the increase in the albedo (Figure 4.10c,e) and a decrease in LAI (Figure 4.10f,h) with less energy available to the surface R^{net}, $H^{sensible}$ and H^{latent} fluxes (Figure 4.31a,c,d,f,g,i). On the other hand, the decreased albedo (Figure 4.10d) and increased LAI (Figure 4.10g) for the closed shrubland scenario increases absorption of incoming radiation but decreases outgoing radiation to space resulting in surplus energy near the surface which increases R^{net}, $H^{sensible}$, and H^{latent} fluxes. The afforestation scenario of this work is consistent with Chen et al. (2012), who found positive R^{net}, $H^{sensible}$, and H^{latent} to increase in response to afforestation of the southeast United States. The findings here are also consistent with a review by Perugini et al. (2017) which indicates that tropical deforestation (as in the cropland scenario) results in a decrease in leaf area index (LAI) and a corresponding increase in sensible heat flux and a decrease in the latent heat flux. This increase in R^{net}, $H^{sensible}$, and H^{latent} has consequences for both temperature and precipitation which is discussed in the next section. That said, the numeric experiment using WRF-Hydro and ESA land cover mimics the surface energy balance of the SKB well such that an increase in albedo resulted in a deficit of energy, while a decrease in albedo results in excess

energy. Thus, our numerical experiment accurately reproduces the radiative fluxes and hence the land-climate interactions over the Sissili-Kulpawn Basin.

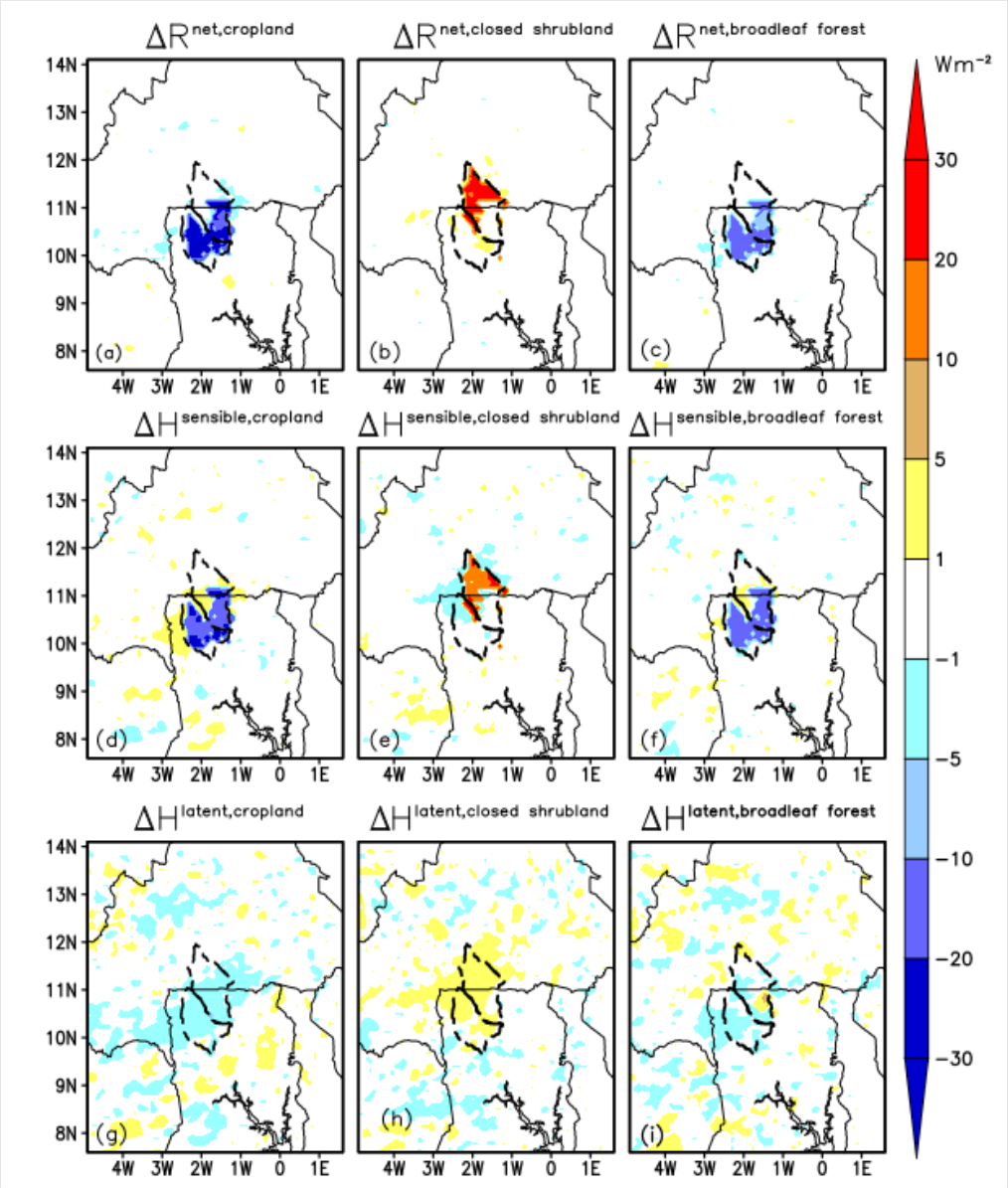

Figure 4.16 Difference in radiation and heat fluxes between reference scenario and numerical experiment. Maps of (a,b,c) mean net radiation flux difference ΔR^{net} *(in W/m*^{2}*), (d,e,f) mean sensible heat flux difference* $\Delta H^{sensible}$ *(in W/m*^{2}*) and (g,h,i) mean latent heat flux difference* ΔH^{latent} *(in W/m*^{2}*) between the reference WRF-Hydro simulation and the (a,d,g) croplands, (b,e,h) closed shrublands and (c,f,i) broadleaf forest WRF-Hydro simulations. Mean values are computed*

as the mean value from experiments minus the mean value from the reference experiment, for a seven-year period spanning 1st January 2010 to 31st December 2016. All the differential energy flux maps have the same color scale indicated by the color bar on the right side of figure 4.31 extending the heights of maps (c,f,i).

4.3.8 Impact of land use land cover change on water fluxes

For the cropland scenario, the changes in soil evaporation (ΔE^{soil}), plant evaporation (ΔE^{plant}), and surface runoff ($\Delta R^{surface}$), and underground runoff (ΔR^{ground}) over the Sissili (Kulpawn) Basins are estimated from figure 4.32a,d,g,j as -0.04 mmday^{-1} (-0.067 mmday^{-1}), -0.018 mmday^{-1} (-0.005mmday^{-1}), -0.03 mmday^{-1} (-0.039 mmday^{-1}), and 0.00046 mmday^{-1} (-0.0014 mmday^{-1}) respectively. In terms of the closed shrubland scenario, ΔE^{soil}, ΔE^{plant}, $\Delta R^{surface}$, ΔR^{ground} are estimated as 0.037 mmday^{-1} (0.02 mmday^{-1}), 0.038 mmday^{-1} (0.023 mmday^{-1}), 0.029 mmday^{-1} (0.029 mmday^{-1}), and 0.000416 mmday^{-1} (-0.00064 mmday^{-1}). Finally, ΔE^{soil}, ΔE^{plant}, $\Delta R^{surface}$, ΔR^{ground} for the broadleaf forest scenario are evaluated to be -0.073 mmday^{-1} (-0.155 mmday^{-1}), 0.069 mmday^{-1} (0.114 mmday^{-1}), -0.035 mmday^{-1} (-0.017 mmday^{-1}), and 0.00031 mmday^{-1} (-0.00043 mmday^{-1}) respectively. Recall there is higher change in R^{net}, $H^{sensible}$, and H^{latent} for the closed shrubland scenario compared to the cropland and broadleaf forest scenario (Figure 4.16). The higher energy fluxes enhance a higher soil evaporation and plant transpiration (Figure 4.17b,e) in the closed shrubland scenario compared to the cropland (Figure 4.17a,c). The same situation applies to the broadleaf forest scenario, except the broadleaf protects the soil, reducing the soil evaporation (Figure 4.17c) and compensating that with a higher evaporation from the plant (Figure 4.17f). The total evaporation change due to soil and plant in the closed shrubland scenario remains higher than the cropland and broadleaf forest scenarios which also enhances more moisture in the atmosphere to precipitate as rainfall. Consequently, the surface runoff is increased in the closed shrubland scenario (Figure 4.17h), while the cropland and broadleaf forest scenarios experience a reduction (Figure 4.17g,i). In all three scenarios, there is an insignificant change in underground runoff which increases for the Sissili Basin but decreases for the Kulpawn Basin. From the foregoing, our numerical land cover change experiment accurately mimics the changes in biophysical properties, energy fluxes, and water fluxes and so capable of reproducing the regional water cycle. The contrasting effects of afforestation and deforestation on evapotranspiration, and consequently on streamflow/surface runoff have been demonstrated by Achugbu et al. (2022a).

This is also consistent with previous works that have shown that evapotranspiration from afforestation is a dominant driver of precipitation and streamflow (Arnault et al., 2023). Conversely, deforestation exacerbates climate warming by reducing evapotranspiration (Bonan, 2008; Bounoua et al., 2002; Zeppetello et al., 2020; Zhao et al., 2021). The reduction in evapotranspiration triggers a decrease in precipitation, surface runoff, and underground runoff, as obtained in this work.

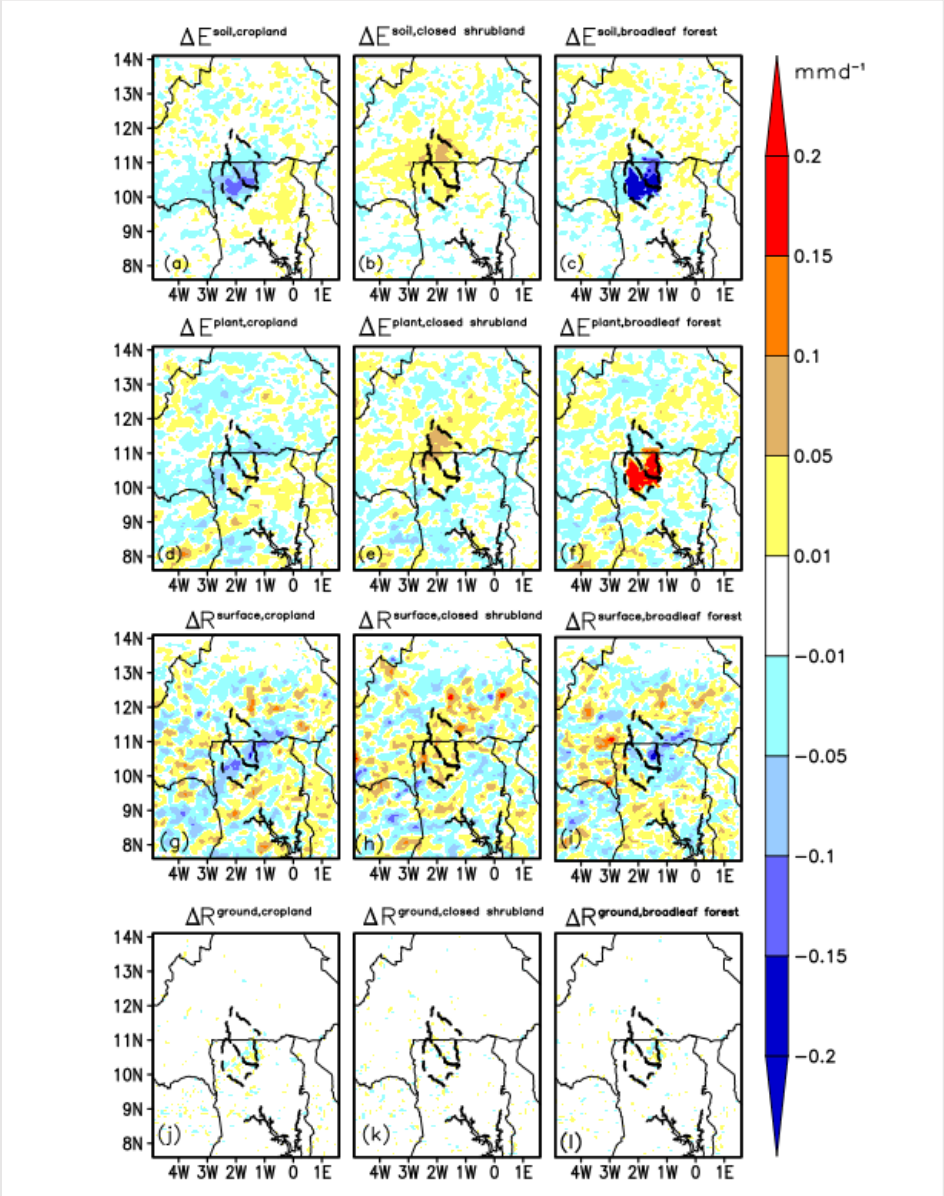

Figure 4.17 Difference in water fluxes between the reference scenario and numerical experiment Maps of (a,b,c) daily mean evaporation difference ΔE^{soil} *(in mm/day), (d,e,f) daily mean plant*

evapotranspiration difference ΔE^{plant}*, (g,h,i) daily mean daily surface runoff* $\Delta R^{surface}$ *(in mm/day), and daily mean underground runoff difference* ΔR^{ground} *(in mm/day), between the reference WRF-Hydro simulation and the cropland (a,d,g,j), closed shrubland (b,e,h,k), broadleaf forest (c,f,i,l) WRF-Hydro simulations. In (a,b,c), the soil evaporation is computed as the sum of the soil evaporations outside the canopy. In (d,e,f), the plant evapotranspiration is computes as the plant transpiration and intercepted canopy water evaporation. Mean differential values are computed as the mean value of each experiment minus the mean value from the reference experiment, for a seven-year period spanning from 1st January, 2010 to 31st December, 2016. All the differential maps have the same color scale indicated by the right side of figure 4.32 extending the heights of maps (c,f,i,l).*

4.3.9 Impacts of land use/land cover change on temperature and precipitation

The change in precipitation and temperature averaged over Sissili (Kulpawn) between the cropland and the reference scenario estimated is -0.11 mmday^{-1} (-0.16 mmday^{-1}) and 0.07 ℃ (0.14 ℃) respectively. For the closed shrubland and the broadleaf scenarios, the change in precipitation and temperature are respectively -0.08 mmday^{-1} (-0.08 mmday^{-1}) and -0.13 ℃ (-0.04 ℃), and 0.14 mmday^{-1} (0.01 mmday^{-1}) and 0.07℃ (0.12℃). The results suggest an increase in temperature and a decrease in precipitation for the cropland and broadleaf forest scenarios respectively, but a decrease and increase in temperature and precipitation respectively for the closed shrubland scenario. Recall that albedo increased while leaf area index (LAI) decreased for the cropland and broadleaf forest scenarios (see section 4.3.1), contrary to the closed shrubland scenario where albedo decreased and LAI increased. The decrease in albedo and increase in LAI for the closed shrubland scenario (see Figure 4.10d,e) enhances the absorption of radiant energy (see Figure 4.11b) and consequently increases the sensible and latent heat fluxes (see Figure 4.11e,h). The surface temperature is supposed to increase but this is offset by a positive evaporative cooling from the soil and plant surface (see Figure 4.17b,e). Consequently, the temperature for the closed shrubland scenario decreased as can be seen in Figure 4.18e. The evaporative cooling also enhances atmospheric moisture and consequently increases precipitation for the closed shrubland scenario (see Figure 4.18b). Conversely, the cropland and the broadleaf forest resemble deforestation scenarios where there is an increase in albedo but a decrease in LAI. As a result, net radiation (see Figure 4.16a,c) and heat fluxes (see Figure 4.16d,e,g,i) are decreased and minimal

energy is available for evaporative cooling through soil and plant evaporation (see Figure 4.17a,c), consequently increasing the temperature (Figure 4.18d,f). The reduced evapotranspiration affects the amount of moisture in the atmosphere to precipitate back as rainfall, hence the observed reduction of rainfall for the cropland and broadleaf forest scenarios (see Figure 4.18a,c). It is noted that non-radiative forcing are the dominant factors affecting temperature in the tropics (S. Zhang, Wang, Teuling, Liu, Ayantobo, Fu, Dong, et al., 2022), such that afforestation results in a decrease in temperature (Betts, 2000; Y. Li et al., 2015). Chen et al. (2012) also found afforestation to decrease surface air temperature significantly by -0.3 ℃ and increase precipitation by +0.23 $mmday^{-1}$ over South Eastern United States in Boreal Summer. Conversely, in the tropical region, deforestation is suggested to exacerbate climate warming by reducing evapotranspiration (Bonan, 2008; Bounoua et al., 2002; Zeppetello et al., 2020; Zhao et al., 2021). Lawrence & Vandecar, (2015) using satellites, towers, and ground-based observations have also shown that tropical deforestation results in warmer, drier conditions at the local scale. Hardwick et al. (2015) found a strong correlation between LAI and daily mean temperature, daily mean soil and air temperatures, daily mean minimum relative humidity, and daily mean maximum vapor pressure deficit, and concluded that the LAI is a useful parameter for predicting the effects of vegetation on the microclimate of tropical forest and oil plantation. Our numerical experiment confirms the above as the closed shrubland scenario which decreases albedo and increases LAI similar to an afforestation scenario tends to decrease temperature and increases precipitation. On the other hand, the cropland and broadleaf forest scenarios which tend to increase albedo and decrease LAI is consistent with a deforestation scenario increasing in temperature and a decrease in the precipitation. Our numerical experiment is thus able to accurately reflect the impacts of afforestation and deforestation scenarios of regional temperature and precipitation.

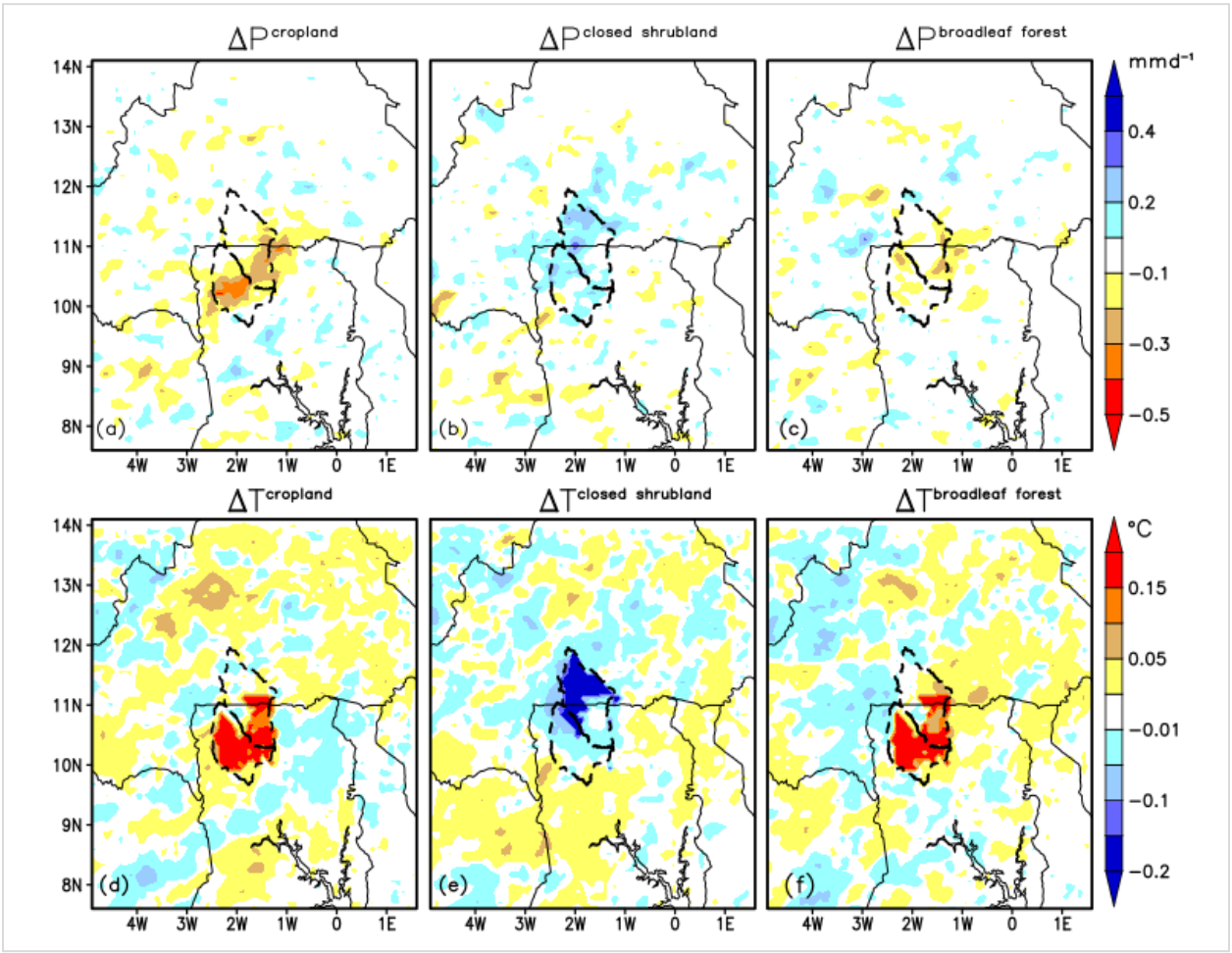

Figure 4.18 Difference between reference and land cover change experiments. Maps of (a,b,c) daily precipitation difference $\Delta \mathbf{P}$ *(in mm/day) and(d,e,f) daily mean temperature difference* $\Delta \mathbf{T}$ *in (℃) between WRF-Hydro simulation and the (a,d) croplands (b,e) closed shrubland (c,f) broadleaf forest WRF-Hydro simulations. Mean differential values are computed as the mean of the scenario experiments minus the mean value of the reference experiment, for a seven-year period spanning 1st January, 2010 to 31st December, 2016. The annual differential precipitation maps (a,b,c) share the same color scale indicated by the color bar at the right side of figure c., and the mean differential maps (d,e,f) also have the same color scale indicated by the color bar on the right side of (f).*

4.3.10 Climatology of water and energy budget under land cover change numerical experiment: Sissili Basin

The closed shrubland scenario, which involves replacing cropland with closed shrubland is an afforestation scenario in which the surface albedo over the Sissili-Kulpawn Basin decreases (Figure 4.10d) and the leaf area index (LAI) increases (Figure 4.10g) relative to the reference scenario (Figure 4.104a,b). Before afforesting the Sissili Basin, the percentage area coverage of closed shrubland was 30.5% (Table 3.7) and the albedo and LAI were respectively 0.22 and 1.59 m^2/m^2. After afforestation, the percentage area coverage of closed shrubland is 75.7% (Table 3.9) while the albedo and LAI are 0.17 and 1.90 m^2/m^2, respectively. This decrease in albedo and increase in LAI results in more absorption of the closed shrubland surface and consequently in an increased net radiation flux (R^{net}), sensible heat flux ($H^{sensible}$), and latent heat flux (H^{latent}) (Figure 4.16b,e,h) and soil evaporation (E^{soil}), plant evaporation (E^{plant}) (Figure 4.17b,e). The increase in E^{plant} and E^{soil} enhances atmospheric moisture and increases precipitation over the Sissili Basin (Figure 4.18b). The climatological water flow change of this scenario with respect to the reference over the Sissili Basin (Figure 4.19a) also shows an average increase in precipitation (6.9%), evapotranspiration (4.1%), surface runoff (28.4%), and underground runoff (15.7%) (Table 4.2). Thus, from the viewpoint of this numerical experiment, replacing cropland with closed shrubland is an afforestation scenario leading to an increase in precipitation, evapotranspiration, surface runoff, and underground runoff. The reverse of the closed shrubland afforestation scenario is the cropland deforestation scenario in which all closed shrubland is replaced with cropland (Figure 4.10c). The percentage of cropland area over Sissili Basin is 71.7% (Table 3.9) about 4% less than the closed shrubland afforestation scenario but higher than the cropland land area in the reference scenario (45.20%). The resultant albedo (0.25) and the LAI (1.38 m^2/m^2) for this scenario increased and decreased respectively relative to the reference values of 0.22 and 1.59 m^2/m^2. The resultant effects of these changes is a decrease in net radiation flux (R^{net}), sensible heat flux ($H^{sensible}$), and latent heat flux (H^{latent}) (Figure 4.16a,d,g), as well as soil evaporation (E^{soil}), plant evaporation (E^{plant}) (Figure 4.17a,d). The decrease of E^{soil} and E^{plant} triggers a general decrease in all water flow terms through a reduction in atmospheric moisture. The climatological water flow change for the cropland deforestation scenario also indicates an overall decrease. The simulated annual water flow changes of precipitation, evapotranspiration, surface runoff, and underground

runoff all decreased by -3.8%, -3.0%, -3.3%, and -3.5% respectively (Table 4.2) relative to the reference scenario. The results of the numerical experiment for this scenario suggest that replacing closed shrubland with cropland is a deforestation scenario resulting in an overall decrease in terrestrial water flow terms. The results of this work are partly consistent with Achugbu et al. (2022b), who showed that afforestation in the Sahel increases evapotranspiration, and deforestation of the Guinean zone to have a regional effect, decreasing rainfall in the Sahel-Sahara interface. Achugbu et al. (2022a) also highlight how afforestation (deforestation) increased (decreased) dry season streamflow in the Sokoto River river basin, also consistent with the findings of this work. Arnault et al. (2023) showed that precipitation triggered by afforestation leads to an increase in surface runoff, and underground runoff in the Nzoia basin intropical East Africa, also in line with the findings of this work. The relationship between land cover change (afforestation and deforestation) is, however, not monotonic, such that an afforestation (deforestation) automatically increases (decreases) rainfall, etc. For instance, the broadleaf forest results of this work are in phase opposition to Arnault et al. (2023), leading to a decrease in all water flow terms, acting like a deforestation scenario. Thus, the broadleaf afforestation leads to a reduction in water flow terms, as in the cropland deforestation scenario. The initial 13.05% of broadleaf forest (Table 3.7) in the basin was extended by 30.49% additional forest area, resulting in 43.55% of forested area (Table 3.9). Eventually, the percentage of broadleaf forest (43.55%) was still less than cropland only (45.20%). The initial albedo before afforestation (0.22) rather increased after afforestation (0.24), and the leaf area index (LAI) before afforestation (1.59 m^2m^{-2}) remains higher than after afforestation (1.52), creating similar surface conditions like the cropland deforestation scenario. The increase in albedo and decrease in LAI resulted in a decrease in absorption by the broadleaf afforested surface and consequently R^{net}, $H^{sensible}$, and H^{latent} (Figure 4.16c,f,i). However, compared to the cropland scenario, the soil evaporation from the broadleaf forest scenarios decreases significantly in the forested areas (Figure 4.17c), which is compensated for by a significant increase in plant transpiration in those same areas (Figure 4.17f). The surface runoff and underground runoff over the Sissili Basin decreased as in the cropland scenario (Figure 4.17i,l), and the climatological water flow also suggests a decrease in all water flow terms (Figure 4.19c). The annual water budget flow change results in a decrease in precipitation (-2.6%), evapotranspiration (-0.1%), surface runoff (-11.3%), and underground runoff (-11.1%) (Table 4.2).

From the modeling viewpoint, the resultant leaf area index (LAI) for the broadleaf afforestation scenario (1.52 m^2m^{-2}) over the Sissili Basin is well below the lower bound albedo value of 2.0 for which the experiment could be classified as a broadleaf afforestation experiment. Consequently, the model might have treated the experiment as a cropland or grassland scenario. From the foregoing, our numerical experiment reveals that an afforestation scenario that does not provide the necessary biophysical conditions to increase water yield remains like a deforestation scenario. To this end, critical thresholds of afforestation, LAI, and albedo are of future research interest. Suffice to say for now that our cropland numerical experiment already suggests that a deforestation of an additional 30.5% of the closed shrubland area of the Sissili Basin area for food production could result in a decrease in the annual water budget, which could trigger drought conditions.

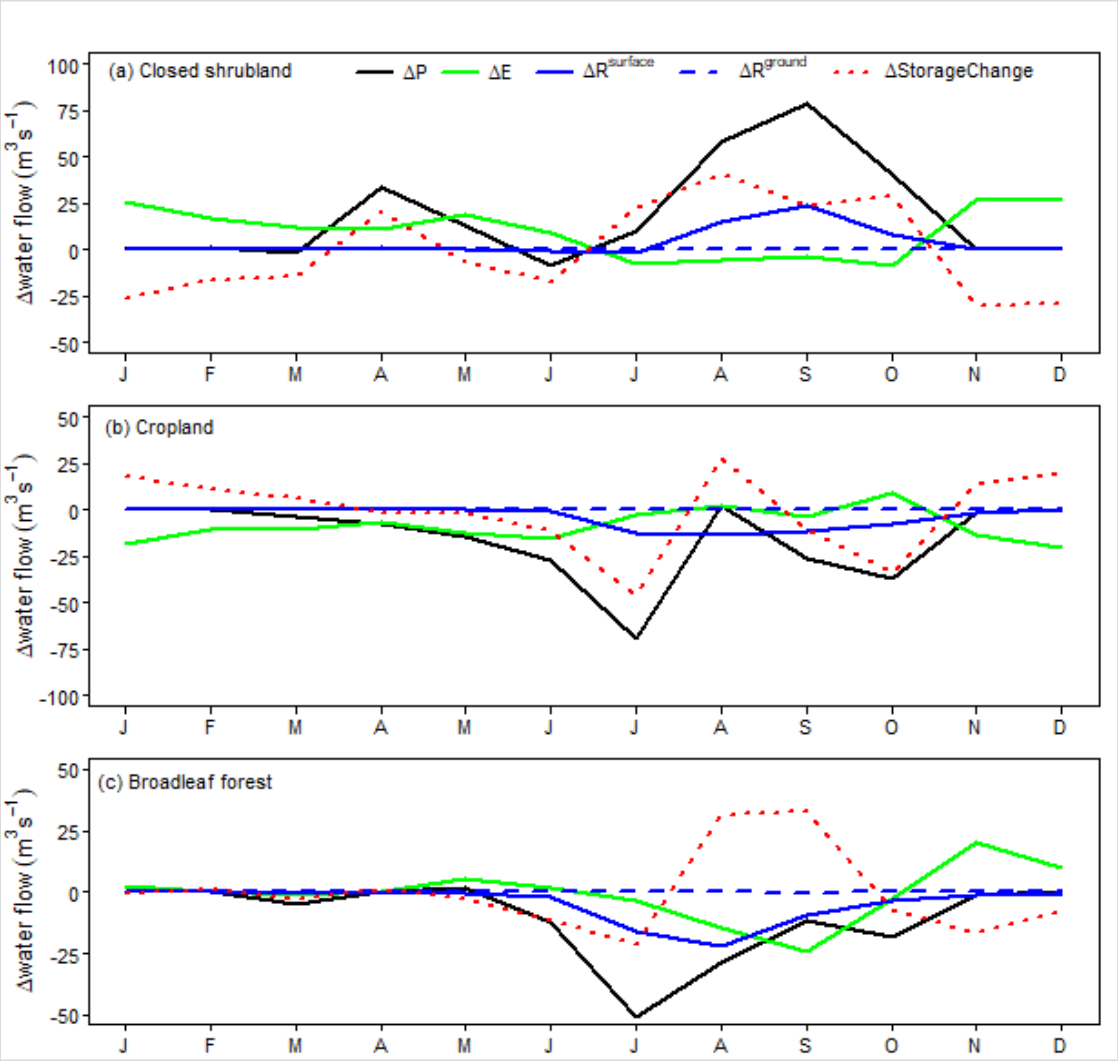

Figure 4.19 Monthly climatology of water flow change over the Sissili river basin. Timeseries of spatially aggregated monthly climatology of water flow change components of the terrestrial water budget over the KB area, namely the precipitation change ΔP (in m^3/s), the surface runoff change $\Delta R^{surface}$ (in m^3/s), the total evapotranspiration change ΔE (in m^3/s), the differential change in soil water storage ΔStorageChange (in m^3/s), and the underground runoff change ΔR^{ground} (in m^3/s), between the reference experiment and the (a) closed shrubland, (b) cropland, (c) broadleaf forest WRF-Hydro simulations. Monthly climatological change values are computed as the difference between the monthly climatological value of the scenario experiments and the monthly climatological value of the reference experiment from 1st January 2010 to 31st December 2016. (a) provides the legend.

Table 4.2 Differential changes in water flow terms over the Sissili river basin

Simulated changes in annual water flow, measured in mm/year, and the corresponding changes in annual water flow as a percentage of the reference annual precipitation, caused by different afforestation types for total evapotranspiration $\Delta\mathbf{E}$, precipitation $\Delta\mathbf{P}$, underground runoff $\Delta\mathbf{R}^{\text{ground}}$, and surface runoff $\Delta\mathbf{R}^{\text{surface}}$. The differential values in table 4.8 are determined by subtracting the value of the afforestation (deforestation) experiment from the value obtained in the reference experiment, and aggregating over the Sissili Basin from 1st January 20210 to 31st December 2016.

Variable	Closed shrubland		Cropland		Broadleaf forest	
	Annual depth of water change (mm/year)	Relative water flow change (%)	Annual depth of water change (mm/year)	Relative water flow change (%)	Annual depth of water change (mm/year)	Relative water flow change (%)
$\Delta\mathbf{P}$	51.8	6.9	-40.4	-3.8	-28.5	-2.6
$\Delta\mathbf{E}$	27.5	4.1	-22.3	-3.0	-1.7	0.1
$\Delta\mathbf{R}^{\text{surface}}$	10.9	28.4	-10.2	-3.3	-12.8	-11.3
$\Delta\mathbf{R}^{\text{ground}}$	0.12	15.7	-0.17	-5.2	0.11	-11.9

4.3.11 Climatology of water and energy budget under land cover change numerical experiment: Kulpawn Basin

The closed shrubland scenario, which involves replacing cropland by closed shrubland is an afforestation scenario in which the surface albedo over the Sissili-Kulpawn Basin decreases (Figure 4.10d) and the leaf area index (LAI) increases (Figure 4.10g) relative to the reference scenario (Figure 4.10a,b). Before afforesting the Kulpawn Basin, the percentage area coverage of closed shrubland was 59.56% (Table 3.7) and the albedo and LAI are respectively 0.22 and 1.59 m^2/m^2. After afforestation, the percentage area coverage of closed shrubland is 66.7% (Table 3.10) while the albedo and LAI are 0.17 and 2.2 m^2/m^2 respectively. This decrease in albedo and increase in LAI results in more absorption of the closed shrubland surface and consequently in an increase in net radiation flux (R^{net}), sensible heat flux ($H^{sensible}$), and latent heat flux (H^{latent}) (Figure 4.16b,e,h) and soil evaporation (E^{soil}), plant evaporation (E^{plant}) (Figure 4.17b,e). The increase in E^{plant} and E^{soil} enhances atmospheric moisture and an increase of precipitation over the Kulpawn Basin (Figure 4.18b). The climatological water flow change of this scenario with respect to the reference over the Kulpawn Basin (Figure 4.20a) also shows an average increase in precipitation (4.1%), evapotranspiration (2.0%), surface runoff (25.4%), and underground runoff (16.1%) over the Kulpawn Basin (Table 4.3). Thus, from the viewpoint of this numerical experiment, replacing cropland by closed shrubland in the Kulpawn Basin is an afforestation scenario leading to an increase in precipitation, evapotranspiration, surface runoff, and underground runoff. The reverse of the closed shrubland afforestation scenario is the cropland deforestation scenario in which all closed shrubland is replaced by cropland (Figure 4.10c). The percentage of land cover area of cropland over Kulpawn Basin is also 66.7% (Table 3.10) as in the closed shrubland afforestation scenario, and higher than cropland land area in the reference scenario (7.2%). The resultant albedo (0.24) and the LAI (1.76 m^2/m^2) for this scenario increased and decreased respectively relative to the reference values of 0.18 and 2.12 m^2/m^2. The resultant effects of these changes is a decrease in net radiation flux (R^{net}), sensible heat flux ($H^{sensible}$), and latent heat flux (H^{latent}) (Figure 4.16a,d,g), as well as soil evaporation (E^{soil}), and plant evoration (E^{plant}) (Figure 4.17a,d). The decrease of E^{soil} and E^{plant} triggers a general decrease in all water flow terms through a reduction in atmospheric moisture. The climatological water flow change for the cropland deforestation scenario also indicates an overall decrease for this scenario (Figure 4.20b). The simulated annual

water flow changes of precipitation, evapotranspiration, surface runoff, and underground runoff all decreased by -5.3%, -3.1%, -9.6%, and -14.3% respectively (Table 4.3) relative to the reference scenario. The results of the numerical experiment for this scenario suggest that replacing closed shrubland by cropland is a deforestation scenario resulting in an overall decrease in the terrestrial water flow terms. Intriguingly, the broadleaf afforestation scenario resulted in a decrease in water flow terms as in the cropland scenario. In the broadleaf afforestation scenario, the initial 29.58% of broadleaf forest (Table 3.7) in the basin was extended by 59.56% of an additional forest area resulting in 89.10% of forested area. Eventually, the percentage of broadleaf forest (89.10%) is much higher than the remaining land cover types. However, the initial albedo before afforestation (0.18) rather increased after afforestation (0.21), and the leaf area index (LAI) before afforestation (2.12) remains higher than after afforestation (1.97), creating similar surface conditions like the cropland deforestation scenario. The increase in albedo and decrease in LAI results in a decrease absorption by the broadleaf afforested surface and consequently net radiation flux (R^{net}), sensible heat flux ($H^{sensible}$) and latent heat flux (H^{latent}) (Figure 4.16c,f,i). However, compared to the cropland scenario, the soil evaporation from the broadleaf forest scenarios decreases significantly in the forested areas (Figure 4.17c), which is compensated for by a significant increase in plant transpiration in those same areas (Figure 4.17f). The surface runoff and underground runoff over the Kulpawn Basin decreased as in the cropland scenario (Figure 4.17i,l), and the climatological water flow also suggests a decrease in all water flow terms (Figure 4.20c), except the surface runoff. The annual water budget flow change results in a decrease in precipitation (-2.3%), evapotranspiration (-1.7%), and underground runoff (-0.9%) (Table 4.3). From the modeling viewpoint average simulated LAI of 1.97 m^2m^{-2} is well below the lower bound albedo value of 2.0 for which the Noah-MP table could recognize the experiment as a broadleaf afforestation experiment. Consequently, the model might have treated the experiment as a cropland or grassland scenario leading to a decline in the annual water budget. The results of the Kulpawn Basin are the same for the cropland scenario, the closed shrubland scenario, and the broadleaf forest scenario. These findings are all either partly or wholly consistent with Achugbu et al. (2022a), Achugbu et al. (2022b), and Arnault et al. (2023), except for the broadleaf forest scenario, where the results obtained are in phase opposition with Arnault et al. (2023). Perugini et al. (2017), through a review, noted that evapotranspiration is the major biophysical factor influencing the effects of afforestation

and deforestation in the tropics such that an increase (decrease) in evapotranspiration results in an increase in precipitation. The analysis of this work so far is consistent with this finding.

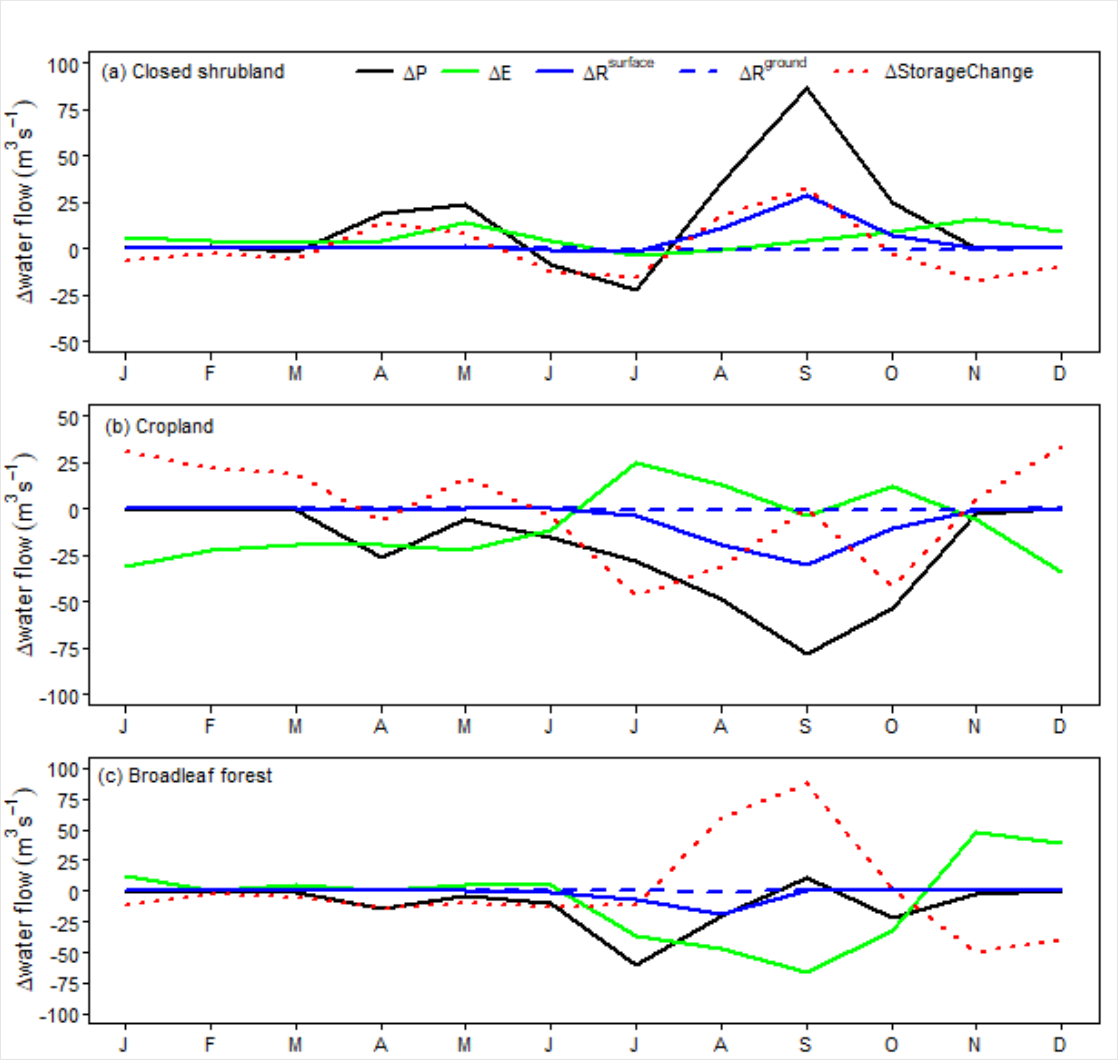

Figure 4.20 Monthly climatology of water flow change over the Kulpawn river basin. Timeseries of spatially aggregated monthly climatology of water flow change components of the terrestrial water budget over the KB area, namely the precipitation change ΔP (in m^3/s), the surface runoff change $\Delta R^{surface}$ (in m^3/s), the total evapotranspiration change ΔE (in m^3/s), the differential change in soil water storage ΔStorageChange (in m^3/s), and the underground runoff change ΔR^{ground} (in m^3/s), between the reference experiment and the (a) closed shrubland, (b) cropland, (c) broadleaf forest WRF-Hydro simulations. Monthly climatological change values are computed as the difference between the monthly climatological value of the scenario experiments and the monthly

climatological value of the reference experiment from 1st January 2010 to 31st December 2016. (a) provides the legend.

Table 4.3 Differential changes in water flow terms over the Kulpawn river basin

Simulated changes in annual water flow, measured in mm/year, and the corresponding changes in annual water flow as a percentage of the reference annual precipitation, caused by different afforestation types for total evapotranspiration $\Delta \mathbf{E}$, precipitation $\Delta \mathbf{P}$, underground runoff $\Delta \mathbf{R}^{\text{ground}}$, and surface runoff $\Delta \mathbf{R}^{\text{surface}}$. The differential values in table 4.8 are determined by subtracting the value of the afforestation (deforestation) experiment from the value obtained in the reference experiment and aggregating over the Kulpawn Basin from 1st January 20210 to 31st December 2016.

Variable	Closed shrubland		Cropland		Broadleaf forest	
	Annual depth of water change (mm/year)	Relative water flow change (%)	Annual depth of water change (mm/year)	Relative water flow change (%)	Annual depth of water change (mm/year)	Relative water flow change (%)
$\Delta \mathbf{P}$	35.6	4.1	-59.3	-5.3	-28.8	-2.3
$\Delta \mathbf{E}$	15.9	2.0	-26.4	-3.1	-15.2	-1.7
$\Delta \mathbf{R}^{\text{surface}}$	10.5	25.4	-14.3	-9.6	-6.1	1.3
$\Delta \mathbf{R}^{\text{ground}}$	-0.23	16.1	-0.5	-14.3	-1.6	-0.15

4.4 Climate- land use/land cover interactions under future scenario

In this section, the Volta-WEF nexus model is built to represent the current water-energy-food (WEF) nexus for the Basin since the introduction of the WEF nexus concept in 2011. The effects of population growth, land use/land cover change, and climate change on the future system hydroelectric power generation and water availability is also presented. Details on results are presented below.

4.4.1 The Volta-WEF nexus model

The Volta-WEF nexus model consists of 42 catchments of at least two components of the nexus nodes. These catchment areas define the WEF nexus sites for investigating the interactions between water, energy, and food components. Each WEF Nexus site contains a water node that

represents the water demand by the population, irrigation, and livestock. The food node represents the irrigation requirement of the WEF nexus site, and the energy node represents the water availability/demand for hydroelectric energy generation. The water node is represented by the surface water, while the energy node and food node are represented by hydroelectric power plants and irrigation water requirements, respectively. The nexus components within a nexus site vary depending on the type of nodes available. Sites where all three nodes are available are referred to as the WEF nexus system, otherwise WF system, etc. Table 4.4 shows the Volta-WEF nexus sites, the area coverage, and the type of nexus. There exist several versions of the WEAP model for the Volta Basin, which are based on the integrated water resources management (IWRM) principles before the WEF nexus concept came to the limelight. The Volta-WEF model draws inspiration from these previous models developed by de de Condappa et al. (2009) and McCartney et al. (2012), which are based on the IWRM concept, to develop the first WEAP model based on the WEF nexus concept.

Table 4.4 Water-Energy-Food Nexus sites delineated for this work

WEF-Nexus sites	Area (km^2)	Type of Nexus
Anayare	572.3	Water-Food Nexus
Arly	7048.5	Water-Food-Nexus
Atankwili	299.6	Water-Food Nexus
Bamboi	15778.7	Water-Energy-Food Nexus*
Bittou	4631.6	Water-Food Nexus
Dapola	20940.9	Water-Food Nexus
Ekumdipe	8530.6	Water-Food Nexus
Kulpawn	10288.2	Water-Food Nexus
Kara	5345.8	Water-Food Nexus
Kintampo	14996.4	Water-Food Nexus
Kompienga	6360.0	Water-Food Nexus
Koumangou	6869.7	Water-Food Nexus
Kpansinkpe	2716.6	Water-Food Nexus
Kpesside	15314.1	Water-Food Nexus
Lerinord	31167.1	Water-Food Nexus
Lower Volta Basin	40960.5	Water-Food-Energy Nexus*
Mango	10888.0	Water-Food Nexus
Manimenso	5032.7	Water-Food Nexus
Mole	6000.1	Water-Food Nexus
Nabogo	2901.5	Water-Food Nexus
Nangodi	11453.3	Water-Foof Nexus
Nasia	5370.8	Water-Food Nexus

Nawuni	6821.0	Water-Food Nexus
Noumbiel1	5920.9	Water-Food Nexus
Noumbiel0	8674.5	Water-Food Nexus
Nwokuy	15562.7	Water-Food Nexus
Porga1	6050.3	Water-Food Nexus
Porga0	10190.1	Water-Food Nexus
Prang	8885.7	Water-Food Nexus
Sabari	21761.5	Water-Food Nexus
Salaga	6032.9	Water-Food Nexus
Senchi	8471.9	Water-Food Nexus
Sissili	12569.0	Water-Food Nexus
Tain	7218.3	Water-Food Nexus
Tenado	13675.1	Water-Food Nexus
Tono	1697.2	Water-Food Nexus
Vea	305.9	Water-Food Nexus
Wayem	21405.6	Water-Food Nexus
Yakala1	4447.7	Water-Food Nexus
Yakala0	11130.6	Water-Food-Energy Nexus*
Yarugu	3995.2	Water-Food Nexus

4.4.2 The Volta-WEF nexus model calibration and validation

For the WEAP model to be used to assess the impact of future climate change on water and energy resources available for hydroelectric dams and general demand in the Volta Basin, it is necessary to validate the simulated discharge and dam storage with observed discharge and dam storage, respectively. The calibration and validation periods are strictly determined by the availability of data. Based on the skill metrics (Equation 3.1, 3.2, 3.3, and 3.6 in sections 3.5.2.3 and 3.5.3.3), a strong correlation (0.7) is obtained for simulated discharge at Bui, Sabari, Saboba, Senchi, and Nawuni for both the calibration and validation periods, except for Bagre where data was available from 1993 when the dam started operations (Figure 4.21a-d, Figure 4.22a-d). The NSE obtained are all greater than 0.5 and in some instances 0.7 indicating that it is satisfactory (Nash & Sutcliffe, 1970). The PBIAS indicates that the model has the greatest overestimations (underestimations) at Bui (Senchi) and Saboba with -17% and 27% respectively. The results compare quite well with previous work in the Volta Basin. Amisigo et al. (2015) could not calibrate and validate the CLIRUN model used to provide input data for the WEAP model due to a lack of both quality climate and runoff data. It is therefore difficult to determine the accuracy of future predictions generated by Amisigo et al. (2015). Moreover, Amisigo et al. (2015) hydropower projections are

based on dry and wet scenarios without considering reservoir characteristics and historical hydropower production data. On the other hand, de Condappa et al. (2009) found an NSE of 0.85, 0.53, and < 0 respectively for the Akosombo, Bagre, and Kompienga dam reservoirs storage over (1984–1998), (1994–2000), and (1994–2000) periods, respectively. In terms of streamflow, de Condappa et al. (2009) found an NSE between (<0–0.86) for nineteen (19) sub-basins over different periods of minimum 59 months over the entire Volta Basin. It is worth mentioning that the huge peak biases in the validation period can be attributed to the fact that the model was calibrated on a relatively dry period (1980-2000), where the peak seasons have relatively low rainfall amounts. Thus, the calibration and validation were in a contrasting period of dry and wet climate regimes. This is evident and well explained in sections 4.2.1 and 4.2.4 using the STI, SPI, and SPEI, and also consistent with the findings of Daramola et al. (2023). Thus, the validation results would be much better if the model was calibrated and validated entirely over the wet period (2000 – 2014) or entirely over the dry period (1981–2000). Calibrations of such sorts in the White Volta Basin yielded relatively higher metrics (Mensah et al., 2022). However, such calibration and validation strategy would have significantly biased the model towards only the wet period or dry period and will not be very useful for a future climate of uncertain dry and wet climate regimes. Thus, the calibration strategy adopted here ensures the model is calibrated and validated over extended periods of dry and wet climate regimes enough to minimize future biases. This 34-year calibration and validation is crucial for a WEF nexus intended to be a Decision Support Tool for the Volta Basin Authority. Another crucial factor is the quality of the precipitation from the GMDF data which could be overestimating peak rainfalls in some years and underestimating peak rainfalls in other years. In general, the skill metrics show that the model quite well fits the observed discharge and so can be used for future climate projections over the basin. In terms of the dam storage, the model fits less than the observation streamflow data but their ranges are still acceptable for use in future climate projections. In the next sections, the impact of population growth, land use/land cover change, and climate change on water and energy in the Volta Basin are investigated.

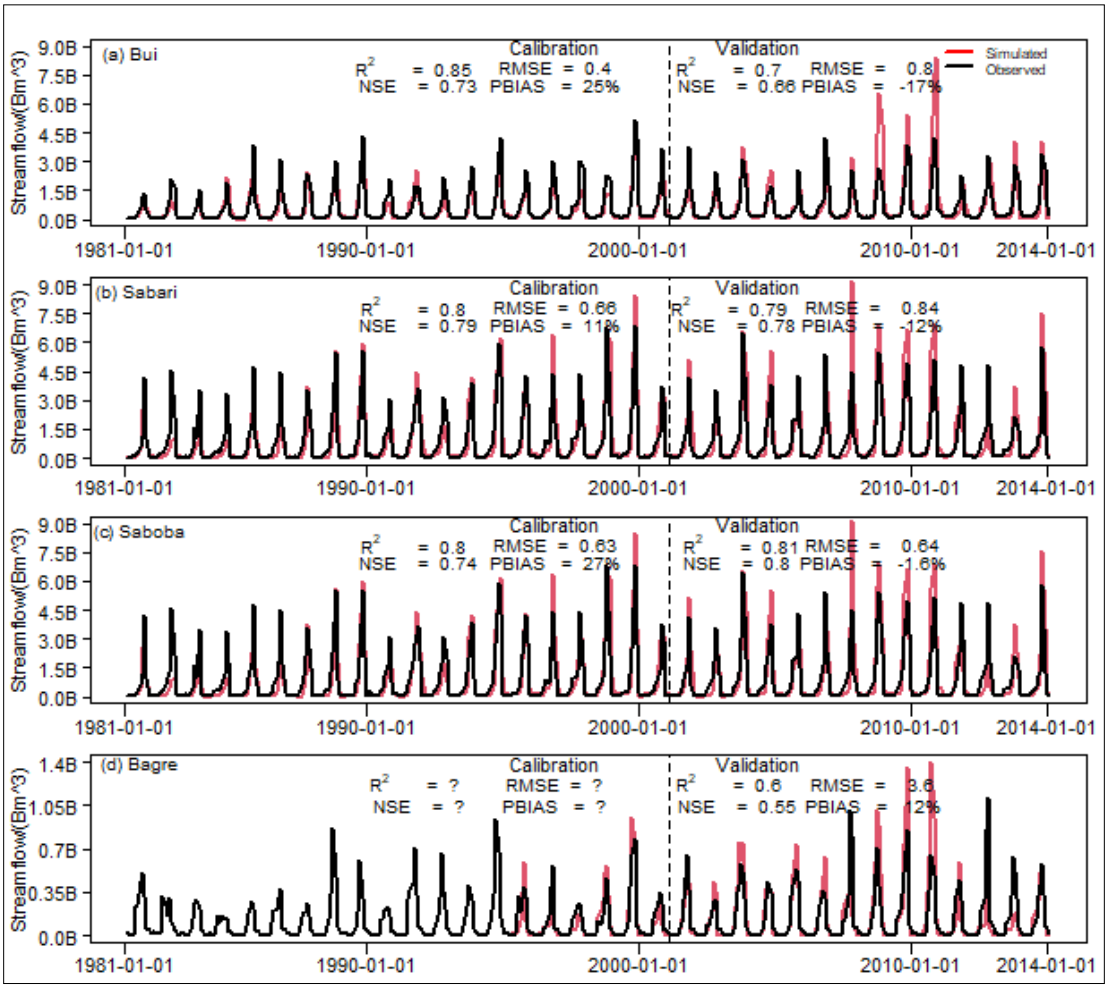

Figure 4.21 Calibration and validation of WEAP setup simulated discharge in the Volta Basin at (a) Bui on the Black Volta River basin, (b-c) Saboba and Sabari on the Oti river basin, and (b) Bagre on the White Volta Basin, over calibration period (1981-2001), and validation period (2002-2014).

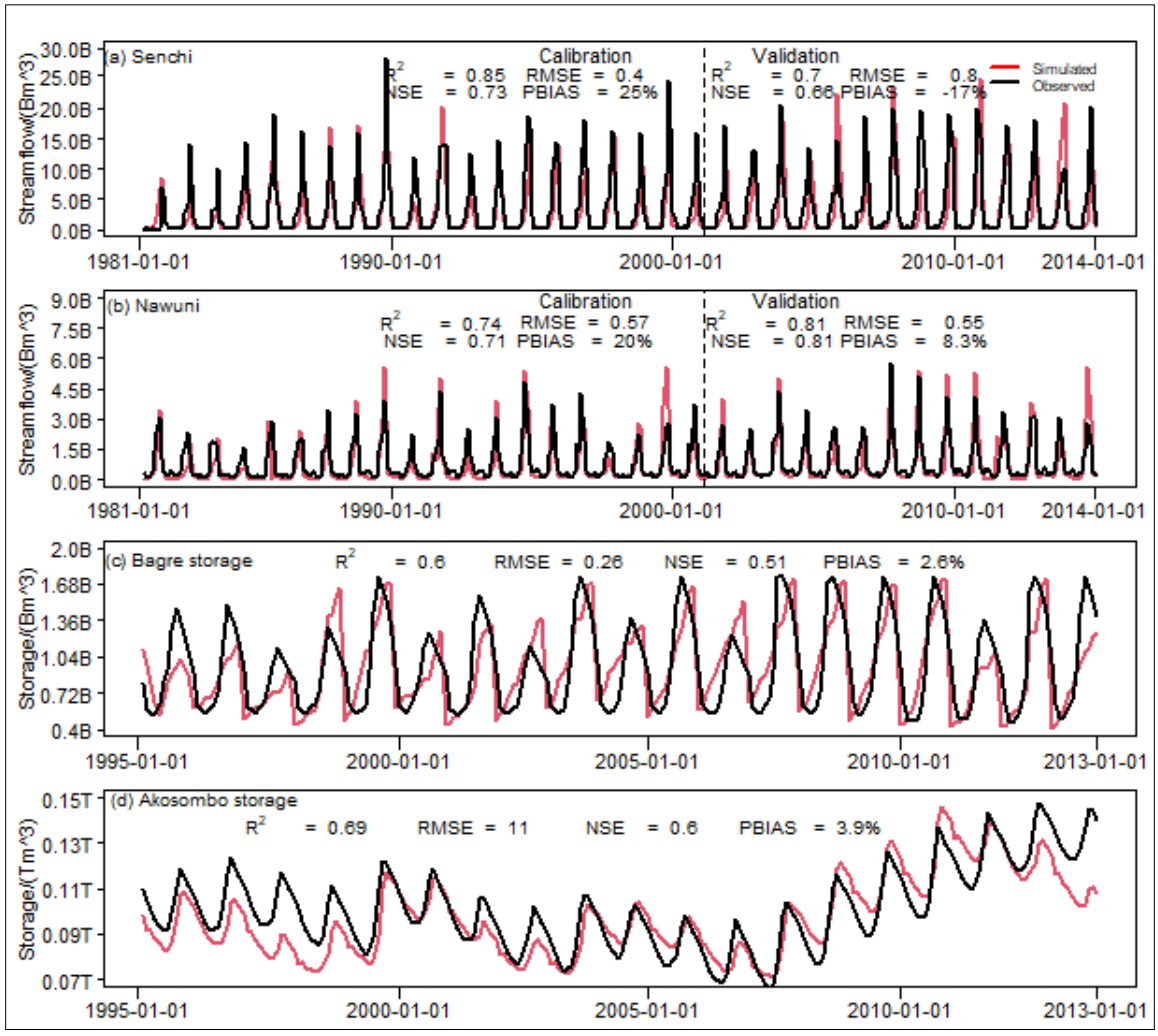

Figure 4.22 Validation of simulated discharge and dam storage in the Volta Basin. Validation of (a) simulated discharge at Senchi in the Lower Volta; (b) simulated discharge over Nawuni in the White Volta Basin; (c) Bagre dam storage; (d) Akosombo dam storage; Simulated discharge (a,b) are validated within 1981-2014; simulated dam storage are validated from 1995-2013.

4.4.3 Impact of historical and future population growth on water demand

Water demand by the population in the Volta Basin constitutes crucial water-energy-food (WEF) nexus components that needs to be evaluated in building the WEF nexus model. Figures 4.23 and 4.24 show the domestic water demand for each of the 41 sub-catchments (WEF nexus sites) of the Volta Basin for SSP1-2.6, SSP2-4.5, SSP3-7.0, SSP4-6.0, and SSP5-8.5. The large difference between the reference scenario and the SSPs could be attributed to the assumption of a constant

population growth rate after 2020 based on the historical population growth rate estimates over the Volta Basin. In general, the water demand for each scenario is strongly influenced by the population growth rate giving them the resultant shapes. While the reference period exhibits an exponential growth curve with water demand increasing drastically to the end of the century, SSP4-6.0 exhibits a similar increase but less drastic demand over the entire period. The SSP1-2.6 has an exponential increase in water demand from 1980-2060, a stationary phase around 2070, and a declining phase towards the end of the century. The water demand in SSP3-7.0 has somewhat two linear increasing phases with a breakpoint before 2010, while water demand in SSP2-4.5, SSP4-6.0, and SSP5-8.5 increases exponentially towards the end of the century. The water demand estimated from this work is in a decreasing order of SSP5-8.5 < SSP1-2.6 < SSP3-7.0 < SSP4-6.0 < Reference, contrary to Mensah et al. (2022) who found that SSP5-8.5 has the highest water demand attributable to the high technological advancement and improved living conditions. Though the difference could result from the fact Mensah et al. (2022) consider only the Ghana part of the White Volta Basin while this work considers the entire Volta Basin, there are sufficient justifications for the findings of this study. Firstly, the population growth estimate based on which Mensah et al., 2022 calculated the domestic water demand for the Ghana section of the White Volta Basin shows that the population growth in SSP3-7.0 is higher than in SSP5-8.5 creating inconsistency in their conclusion that SSP5-8.5 has the highest water demand. Secondly, Jones & O'Neill, (2016) noted that the high fertility in SSP3-7.0 across the developing world leads to rapid population growth which coupled with slower urbanization leads to very dense rural and urban patterns in sub-Saharan Africa, the Middle East, India, and Southeast Asia. The same authors noted that in SSP5-8.5, a higher fertility rate driven by economic optimism in North America, Australia, and Europe combined international migration leads to growth across these regions while rapid development across Africa and Asia leads to low fertility and slower population in SSP5-8.5 relative to SSP3-7.0. Our estimates of population growth for the SSP scenarios are based on (Gao, (2020) and consistent with the estimates of Mensah et al. (2022). The water demand is also consistent with the population growth estimates for the SSP scenarios. The domestic water demand estimate for reference, SSP1-2.6, SSP2-4.5, SSP3-7.0, SSP4-6.0, and SSP5-8.5 for the near (2040), mid (2060), and far future (2080, 2100) Mm^3 summarized in Table 4.5 and Figure 4.25 also shows a spatial display of the change in water demand for SSP1-2.6, SSP2-4.5, SSP3-7.0, SSP4-6.0, and

SSP5-8.5 scenarios compared to the reference at the end of 2040, 2060, 2080, and 2100. Irrespective of the scenario, the change in domestic water demand over the Volta Basin decreases relative to the reference scenario as seen in the negative values (see Figure 4.25). Figures 4.23 and 4.24 also show the water demand for the Volta Basin disaggregated by the various WEF nexus sites.

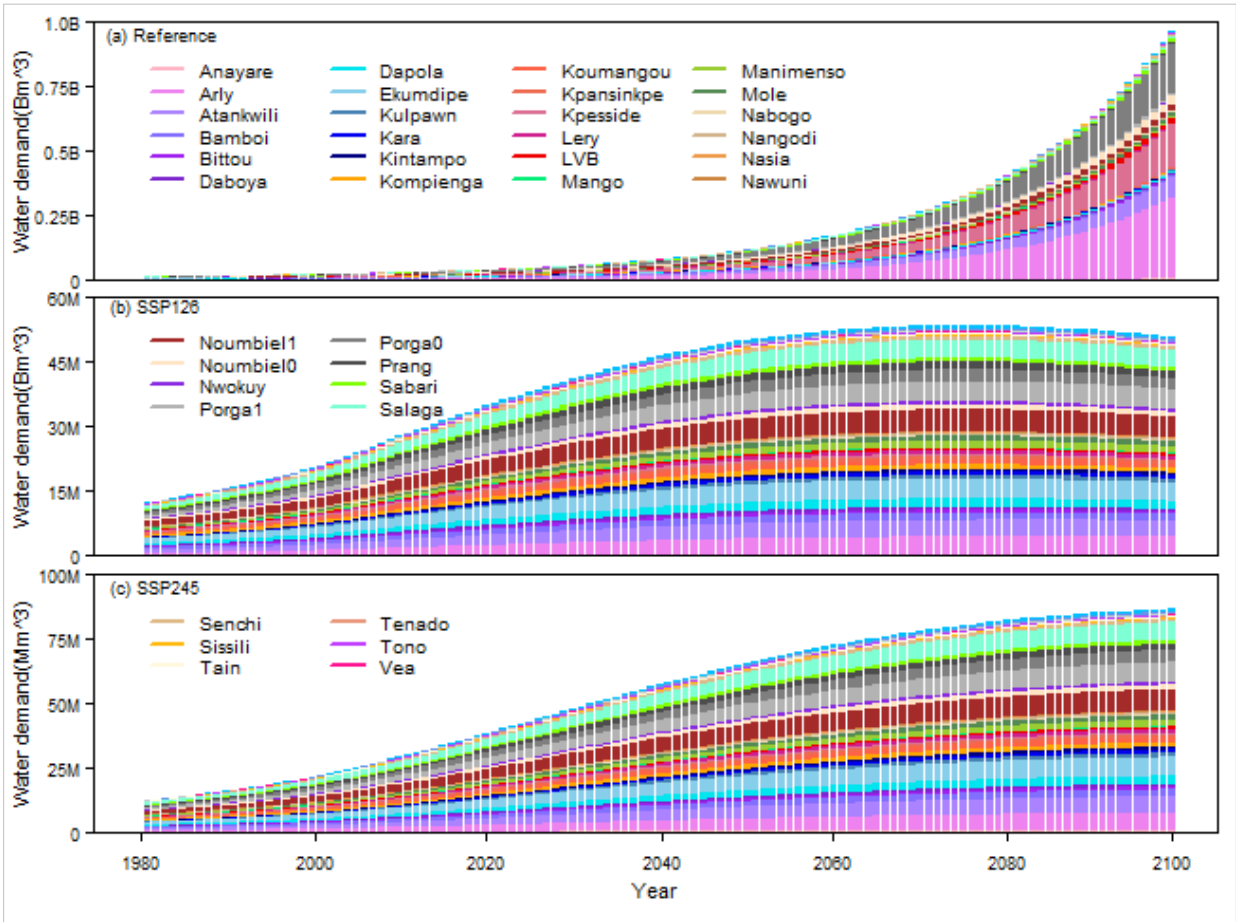

Figure 4.23 Water demand estimate based on population growth for historical and SSP1-2.6 and SSP2-4.5

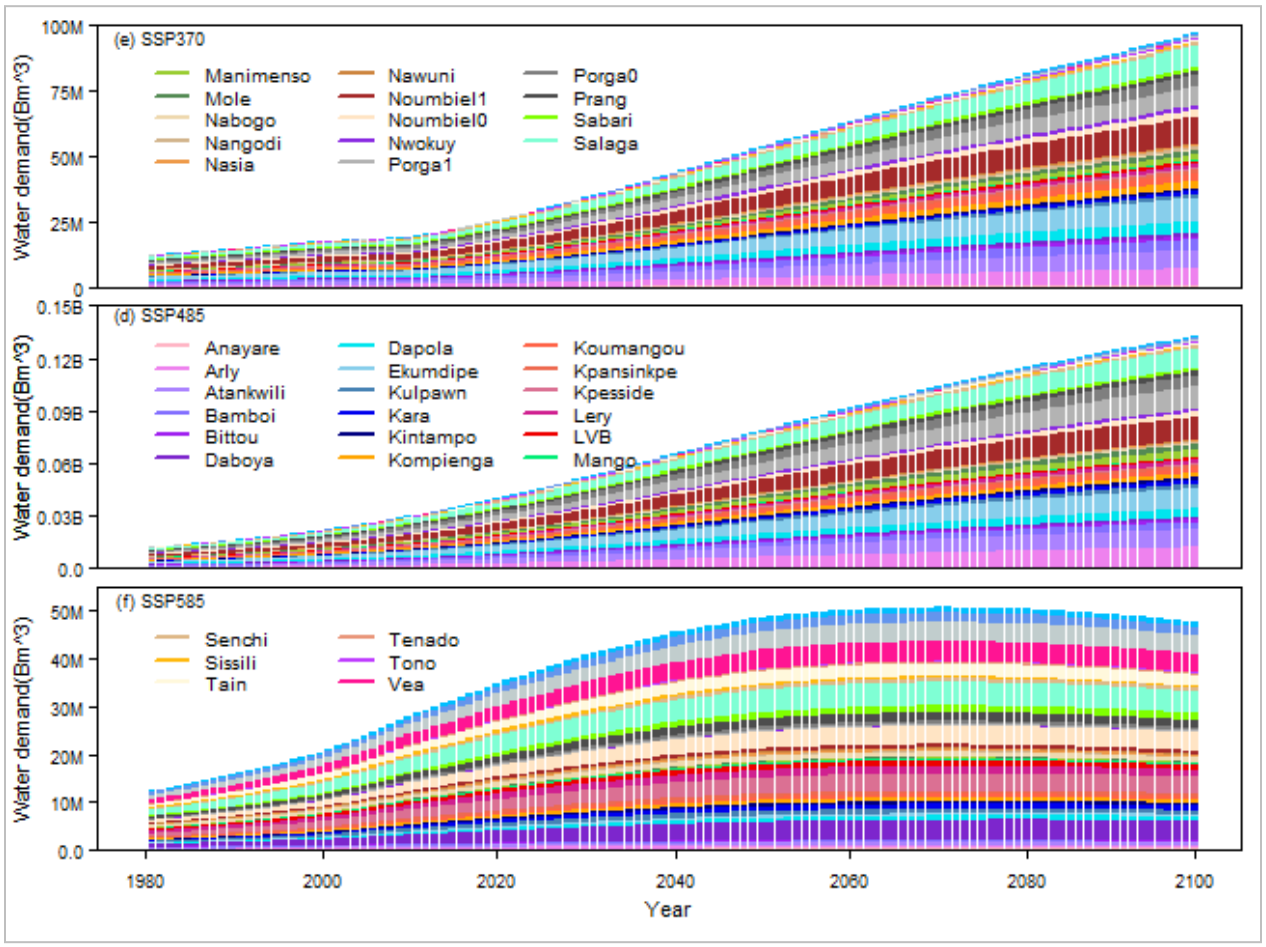

Figure 4.24 Water demand estimate based on Share Socio-economic Pathways– SSP3-7.0, SSP4-6.0, SSP5-8.5.

Table 4.5 Projected water demand over the Volta Basin in Mm^3

Scenario	2020	2040	2060	2080	2100
Reference	38.6	78.555	172.60	405.46	1005.22
SSP1-2.6	35.32	46.54	52.54	53.52	50.75
SSP2-4.5	38.41	57.34	72.54	82.19	86.58
SSP3-7.0	25.95	43.75	63.47	81.36	97.85
SSP4-6.0	40.06	12.40	92.11	115.07	133.56
SSP5-8.5	34.87	12.40	50.27	50.41	47.54

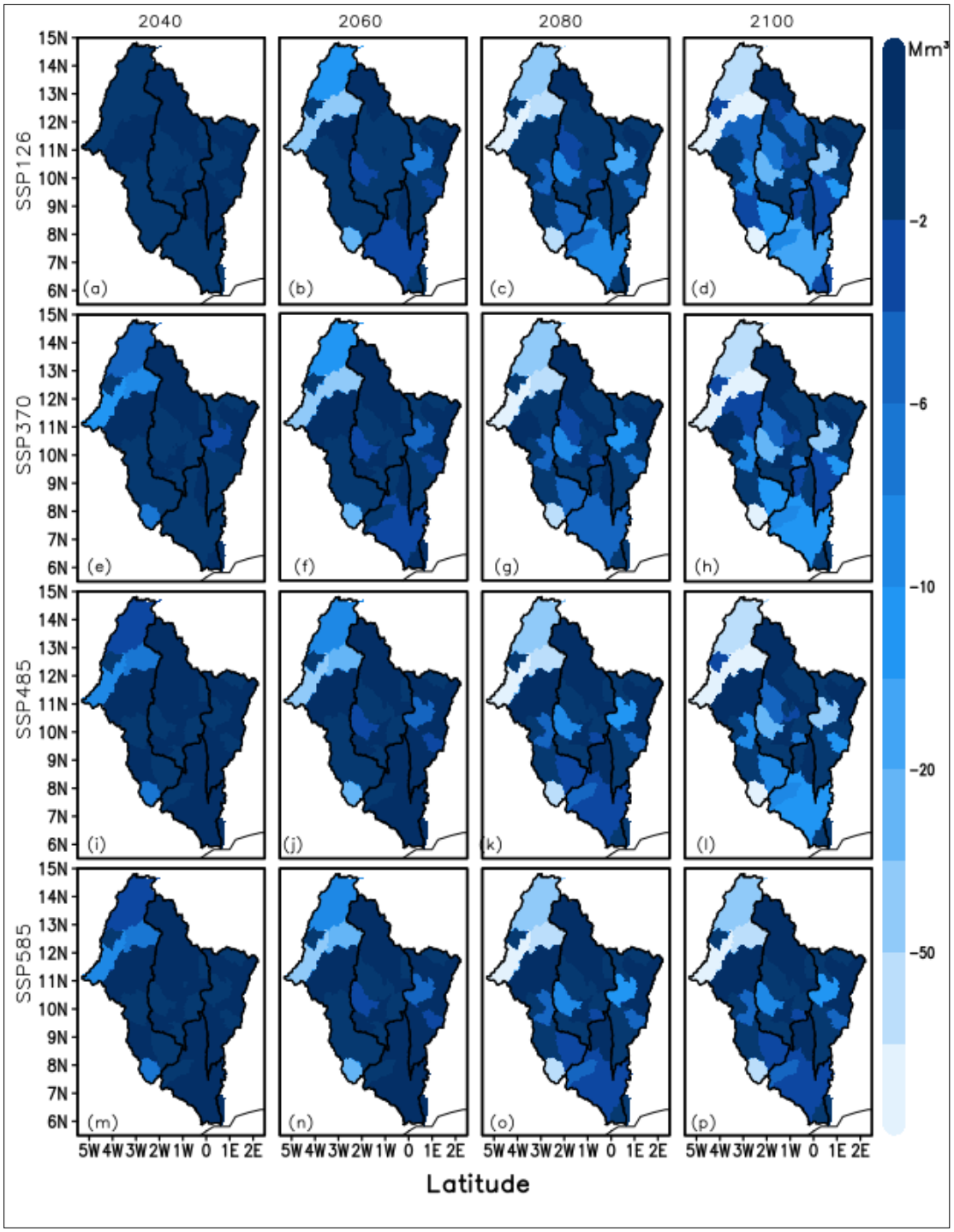

Figure 4.25 Changes in water demand at WEF nexus sites at the end of 2040, 2060, 2080, and 2100. Change in water demand for: (a-d) SSP1-26 at the end of 2040, 2060, 2080 and 2100; (e-

h) SSP2-45 at the end of 2040, 2060, 2080 and 2100; (i-l) SSP4-85 at the end of 2040, 2060, 2080, and 2100; (m-p) SSP5-85 at the end of 2040, 2060, 2080 and 2100 respectively, compared to the reference period (1980 – 2020).

4.4.4 Changes in annual mean temperature over the Volta Basin

Temperature change is an important factor to assess if the climate over a region is changing. Here the change in annual mean temperature over the Volta Basin is assessed using the recent Coupled Model Intercomparison Project Phase 6 (CMIP6) models. Figure 4.26 shows the changes in the annual mean temperature of 15 CMIP6 models and their ensemble mean over the Volta Basin relative to the WMO baseline 1960-1990. The WMO references refer to changes in the annual mean temperatures of the 1981-2010 period relative to the 1960-1990 baseline. The near future, mid future, and far future represent changes in the annual mean temperature of 2011-2040, 2041-2070, and 2071-2100 periods relative to the 1961-1990 period, respectively. For the SSP1-2.6 scenario, all models show an increase in temperature over the Volta Basin relative to the 1961-1990 baseline except for CMCC-CM2-SR5 and TaiESM1 which rather showed decreases in annual mean temperatures. For the SSP2-4.5 however, only TaiESM1 decreased in temperature, with the remaining 14 models showing an increase in temperature over the Volta Basin. Changes in temperatures in SSP5-8.5 are somewhat similar to changes in SSP2-4.5, with TaiESM1 becoming warmer at the end of the century. In general, the changes in temperature for the WMO reference period and the near future period are similar and ranged between 0 to 3°C for all models except for CMCC-CM2-SR5 and TaiESM1 for SSP1-2.6, and only TaiESM1 for SSP2-4.5 and SSP5-8.5. For SSP2-4.5 mid and far future periods, all 15 models show warming relative to the WMO reference and their respective near future periods, with warming ranging between 0 to 4 °C for the mid-century and 1 to 6 °C at the end of the century. For SSP5-8.5 the warming ranges from 0 to 5 °C and up to 8 °C, respectively for mid and far future scenarios. Thus, apart from CMCC-CM2-SR5 and TaiESM1 which showed some decrease the remaining 13 models agree on an increase in mean annual temperature in the Volta Basin relative to the WMO 1961-1990 baseline. The result obtained here is partly consistent with Limantol et al. (2023) who used NorESM2-MM and MPI-ESM1-2-HR over the Volta Basin and found the mean annual projected temperature of both models to increase, with more increase in SSP5-85 than the SSP2-45 scenario. The findings are also consistent with other works in the Black and White Volta Basins, which

agree on temperature increases under the SSP2-4.5 and SSP5-8.5 scenarios, with SSP5-8.5 showing higher temperatures than SSP2-4.5 (Mensah et al., 2024; Siabi et al., 2021). Limantol et al. (2023) also suggested that an ensemble of BCC-CSM2-MR, NorESM2-MM, and MPI-ESM1-2-HR gives a better representation of observed temperature than any of the individual models. The 15-member ensemble mean also yielded a reasonable change in this study and so is used to force the Volta-WEF nexus model to investigate the implication of these warming levels on water and energy resources.

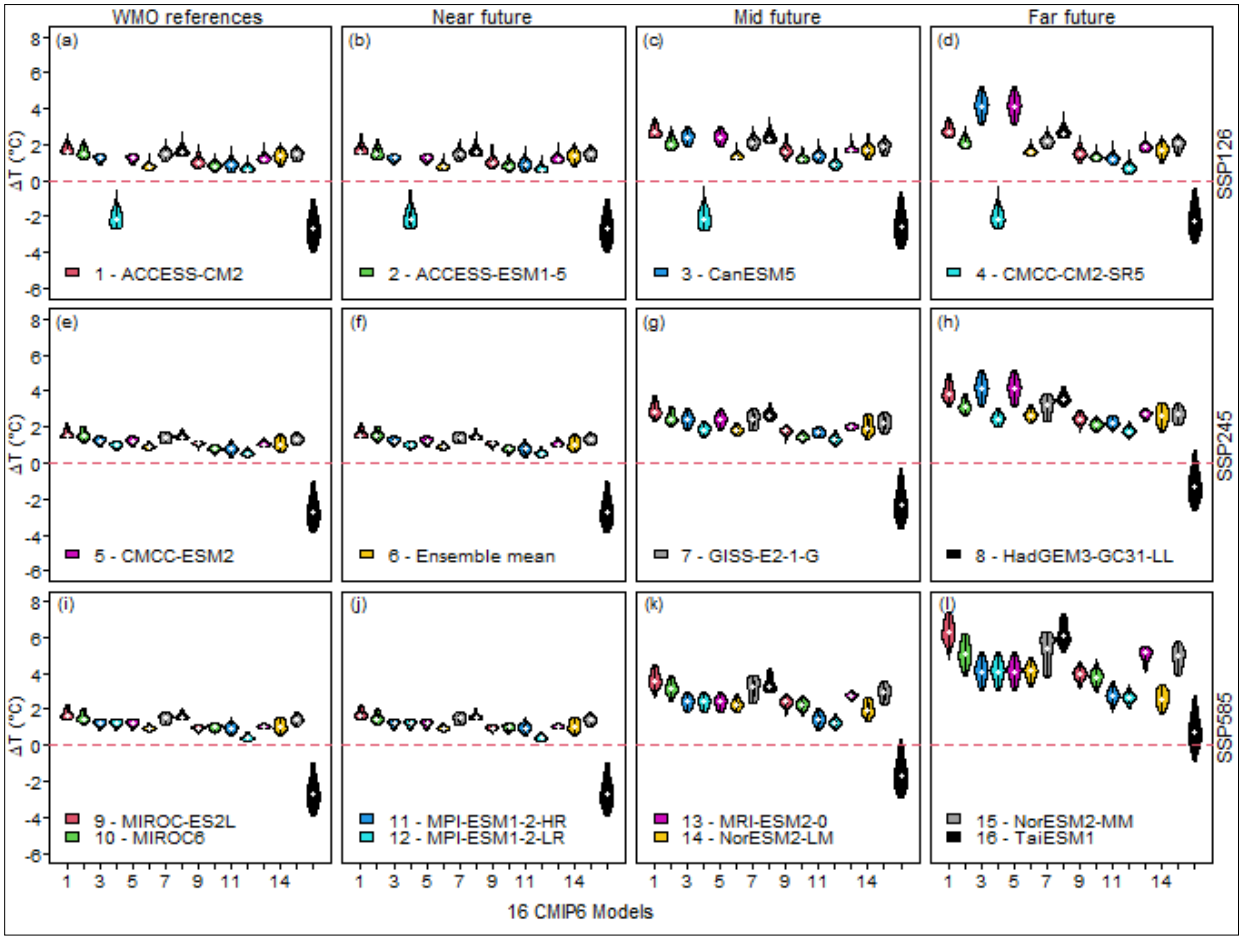

Figure 4.26 Change in annual mean temperature over the Volta Basin based on CMIP6 climate projections for (a-d) SSP1-26, (e-h) SSP2-45, (i-l) SSP5-85 over the WMO reference period (1981-2010), near future (2011-2040), mid future (2041-2070), and far future (2071-2100) compared to the WMO reference period (1961-1990). The legend is shown in the figure.

4.4.5 Changes in annual total precipitation over the Volta Basin

Precipitation changes is yet another important consideration in assessing the climate change impact over a region. Here the change in annual total precipitation over the Volta Basin is assessed using the recent the 15 CMIP6 models used above. The models show varying changes in annual total precipitation with both increases and decreases over the Volta Basin, as opposed to temperature where nearly all the models show an increase. The majority of the models predict an increase in precipitation over the Volta Basin with their median marks above the 0 mm precipitation line (in red). Under the SSP1-2.6 scenario, the majority of the model predict an increase of annual total precipitation between 0 to 200 mm for the WMO reference and near future periods and between 0 to 400 mm for the mid and far-future scenarios. The increase at the end of the century is particularly high for CanESM5 and CMCC-CM2-SR5 with annual totals precipitation up to 400 mm. The CMCC-ESM2 on the other hand show a consistent decrease from the from the WMO reference and near-future periods till the end of the century. The ensemble means for SSP1-2.6 shows an increase in total annual precipitation of 0 to 100 mm consistently from the near-future scenario to the end of the century. The observed increase in the annual total precipitation in all the models for the SSP2-4.5 scenarios are reproduced in the SSP5-8.5 scenarios, with similar or greater magnitudes. The decrease in the annual total precipitation for CMCC-CM2 under SSP1-2.6 is also reproduced in SSP2-4.5. For SSP5-8.5 large changes are observed in the annual total precipitation for all periods. Changes in the WMO reference and near-future periods are between 0 and 400 mm, while those of mid and far future scenarios reached 500 mm and 700 mm respectively. The greatest changes for mid and far-future scenarios are seen for MPI-ESM1-2-HR and MPI-ESM1-2-LR. The number of models which suggest a decrease in annual total precipitation increase from the 1 to 3 from SSP1-2.6, SSP2-4.5 and SSP5-8.5 respectively. For instance, under the SSP1-2.6 scenario only CMCC-ESM2 suggest a decrease in total annual precipitation at the end of the century. Under the SSP2-4.5 and SSP5-8.5 scenarios, CMCC-ESM2 and GISS-E2-1-G, and CMCC-ESM2, GISS-E2-1-G, MRI-ESM2-O, respectively showed decrease in annual total precipitation with the majority of the violin plot area falling below the 0 mm line (red dashed line). Again, the results are partly consistent with Dotse et al. (2023) who found an increasing trend for annual rainfall for NorESM2-MM and MPI-ESM1-2-HR under the SSP2-4.5 and SSP5-8.5 scenarios over the Volta Basin precipitation. Mensah et al. (2024) also found precipitation to

increase by 35% for SSP2-4.5 and 50% for SSP5-8.5. Therefore, unlike the temperature, there is huge variation within the models regarding precipitation, and climate change projection using the individual models is less likely to be very reasonable. To offset the impact of this inter-model variability, the 15-member ensemble mean precipitation is used in the climate projections in the Volta-WEF nexus model in WEAP.

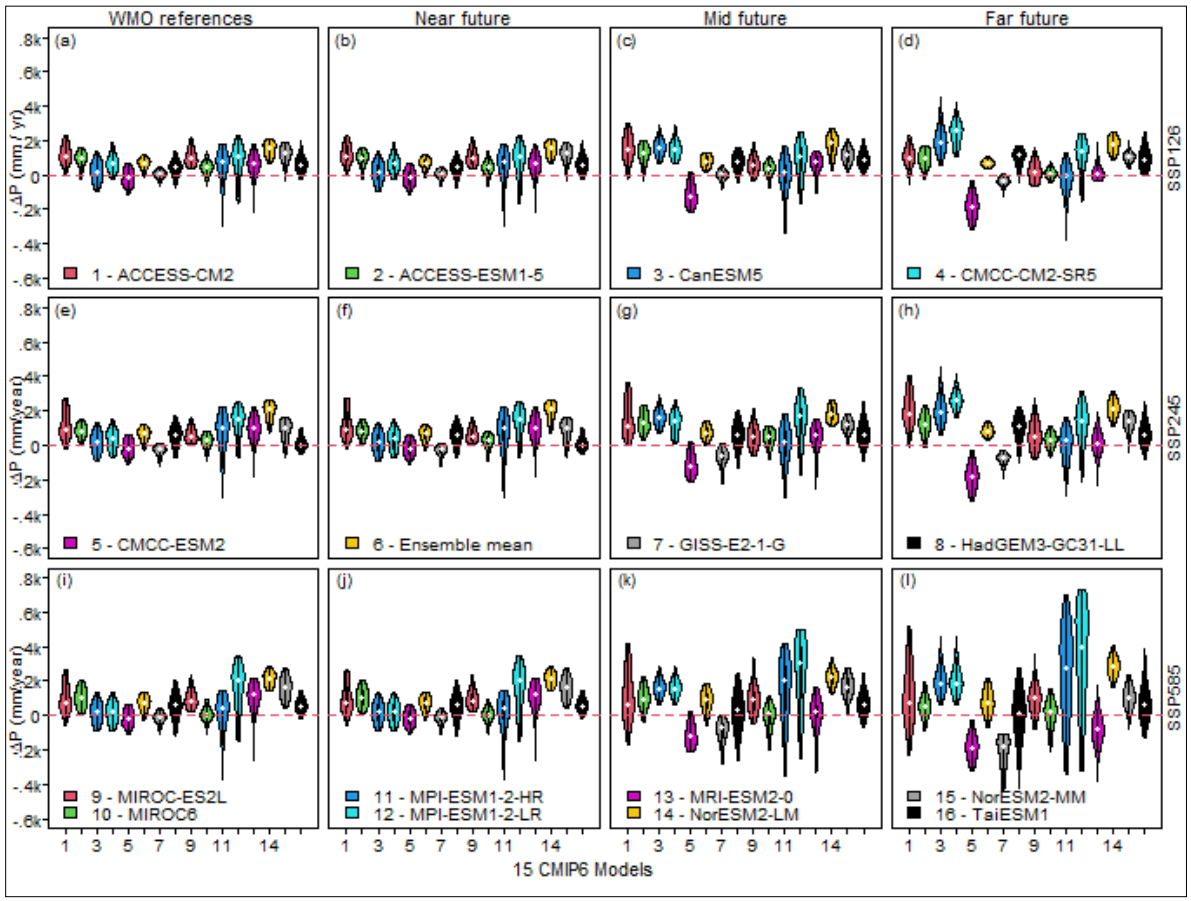

Figure 4.27 Change in annual total precipitation over the Volta Basin based on CMIP6 climate projections for (a-d) SSP1-26, (e-h) SSP2-45, (i-l) SSP5-85 over the WMO reference period (1981-2010), near future (2011-2040), mid future (2041-2070), and far future (2071-2100) compared to the WMO reference period (1961-1990). The legend is shown in the figure.

4.4.6 Changes in water demand under climate change and population change scenarios

The reference scenario expresses the influence of a historical climate, static land cover data, and constant population growth data recycled to the end of the century. The SSP1-2.6 to SSP5-8.5 were built on top of the reference scenario using SSP-based estimated population data (Gao, 2020)

and growth rate estimates until 2100. Therefore, the deviation of SSP1-2.6 to SSP5-8.5 from the reference is the impact of SSP-based population growth estimates. Similarly, the ensemble means of SSP1-2.6, SSP2-4.5, and SSP3-7.0 were built directly on top of the SSP1-2.6, SSP2-4.5, and SSP3-7.0, respectively, by changing the historical climatic data from GMFD to the 15-member ensemble mean CMIP6 data. As a result, the deviation of the ensemble means SSP1-2.6, SSP2-4.5, and SSP3-7.0 from SSP1-2.6, SSP2-4.5, and SSP3-7.0 is a measure of the impact of future climate change projections. Irrespective of the scenarios in Figure 4.28, it is evident that population growth has the largest impact, with the greatest deviation being SSP1-2.6 to SSP5-8.5 from the reference scenario (blue line), with the remaining factors playing minimal roles. Similarly, the minimal impact of the climate can be seen in the proximity of the SSP1-2.6, SSP2-4.5, and SSP3-7.0 lines to their respective ensemble means across Figure 4.28a,b,c. The same can be said for land use/cover change, but with caution as the land cover data only changes from 1992 to 2020, remaining static thereafter to the end of the century. From the result, the decrease in the water demand in the Volta Basin is evident mostly beyond 2040, decreasing gradually to 20 Bm^3 at the end of the century, irrespective of the scenario. The climatological water demand also shows a monthly mean decrease of up to 300 Mm^3 in Figure 4.29 below, irrespective of the scenario. Despite the proximity, the water demand is not the same for all scenarios. For instance, while the projected annual mean water demand for SSP1-2.6, SSP2-4.5, and SSP3-7.0 and their ensemble means are the same for the climate change and climate + population growth scenarios, they are quite different from the climate + land use change, and the climate + land use + population growth scenarios, which are also the same. In the case of the climate change and climate + population growth scenarios, the annual estimated change in Bm^3 is -5.75(-6.4%), -5.27(-5.83%), -5.38(-5.99%), respectively for SSP1-2.6, SSP2-4.5, and SSP3-7.0 and the respective ensemble means. The annual mean water demand change for the SSP4-6.0 and SSP5-8.5 is -4.75(-5.23%) and -5.80(-6.4%) respectively. The estimated water demand index for SSP1-2.6 to SSP5-8.5 is 0.94 on a unit scale. For the climate + land use change and climate + land use + population growth scenarios, the annual mean water demand change in Bm^3 is estimated at -3.42(-3.81%), -3.12(-3.46%), and -3.25(-3.63%) respectively for SSP1-2.6, SSP2-4.5, and SSP3-7.0 and their respective ensemble mean. For SSP4-6.0 and SSP5-8.5, the values are -2.81(-3.09%) and -3.45(-3.85%) respectively. The water index for these scenarios is 0.96. The mean annual water demand change

discussed above and the corresponding mean monthly water change demand are summarized in Tables 4.6 and 4.7. Figure 4.29 also shows the mean monthly water change of the various scenarios relative to the reference scenario. Unlike the usual narrative that temperature will increase and precipitation will decrease, which will have negative consequences for water resources in the VB, the Volta-WEF nexus model used here presents an optimistic future for water demand in the VB. However, this optimistic situation hinges on the fact that the population growth estimated in the reference scenario is very large compared to the reference scenario. That is the introduction of SSP-based population estimates into the Volta-WEF nexus presents an optimistic future.

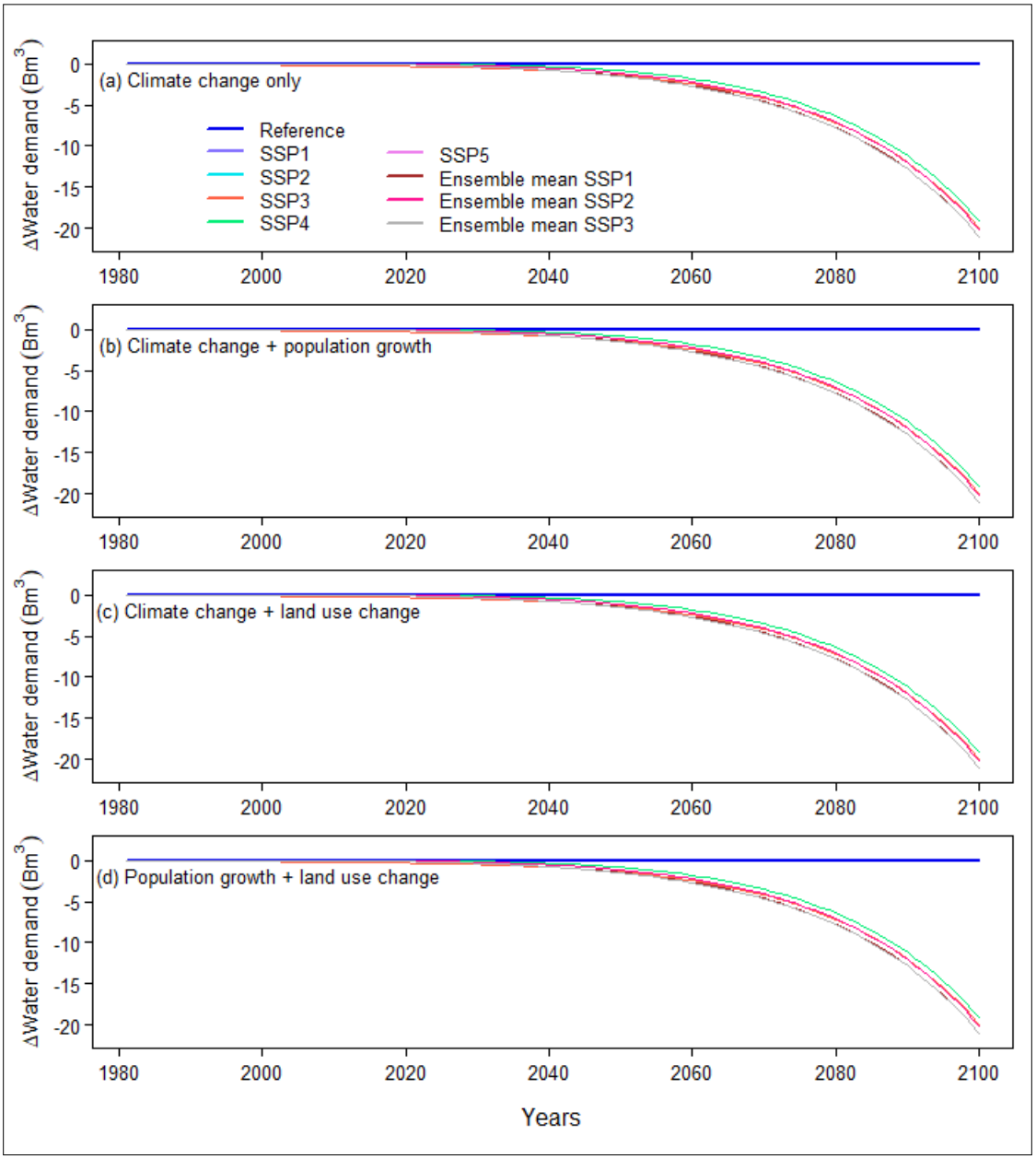

Figure 4.28 Change in water demand under climate, population growth and land use change

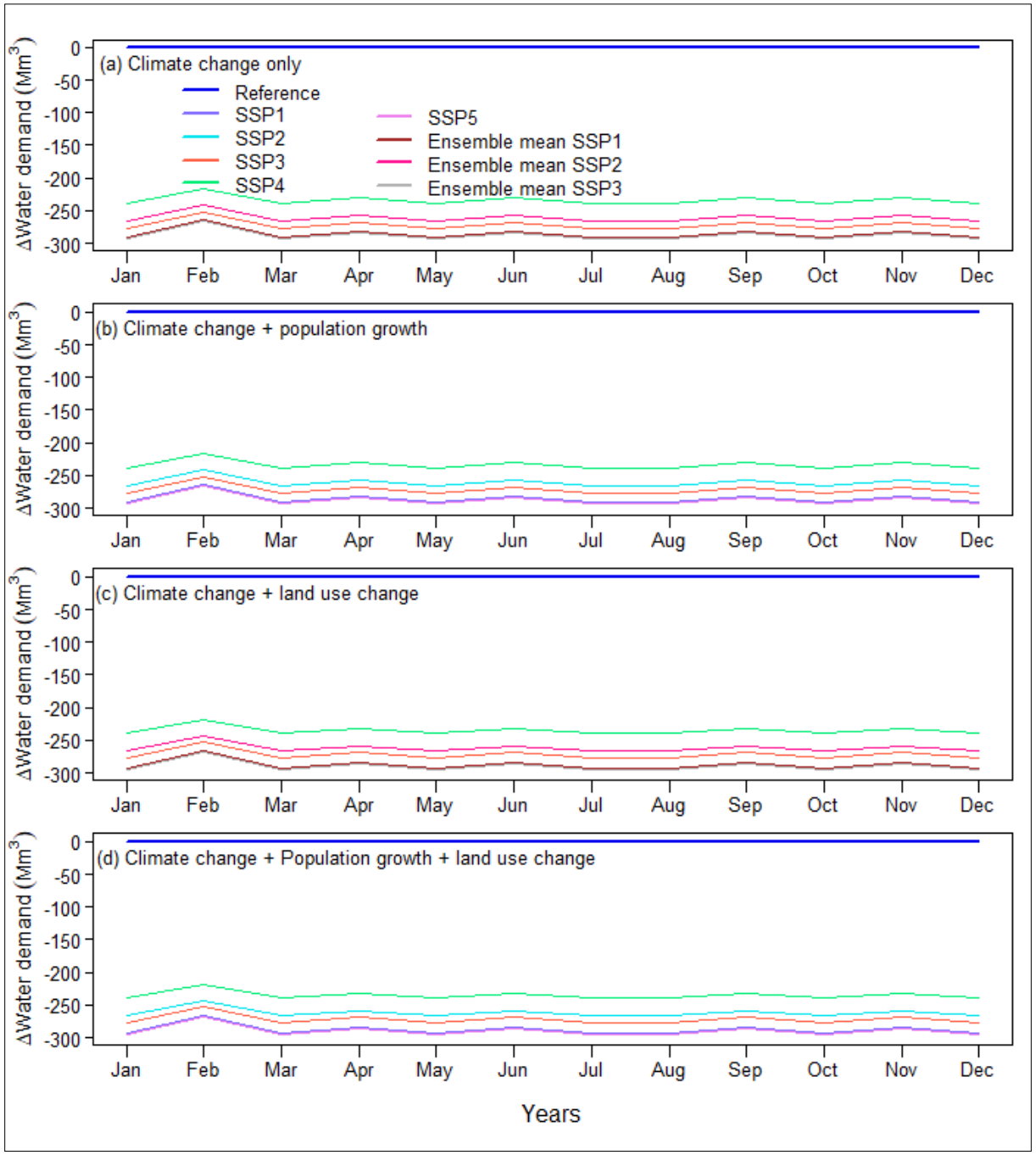

Figure 4.29 Mean monthly change in water demand under climate, population growth and land use change scenarios.

Table 4.6 Projected change in annual average water demand (in Mm^3) in the Volta Basin of West Africa. The Ensemble SSP1-2.6, Ensemble SSP2-4.5, Ensemble SSP3-7.0 represents mean change in water demand based on the 15 CMIP6 data used in this study. The changes in the table are computed for period spanning 2030 to 2100.

Variable	Climate change (CC)			CC + Population			CC + land use			CC + Population + Landuse		
	Annual change in water demand (Bm^3)	Annual change in water demand (%)	Water demand index	Annual change in water demand (Bm^3)	Annual change in water demand (%)	Water demand index	Annual change in water demand (Bm^3)	Annual change in water demand (%)	Water demand index	Annual change in water demand (Bm^3)	Annual change in water demand (%)	Water demand index
SSP1-2.6	-5.75	-6.40	0.94	-5.75	-6.4	0.94	-3.42	-3.81	0.96	-3.42	-3.81	0.96
SSP2-4.5	-5.27	-5.83	0.94	-5.27	-5.83	0.94	-3.12	-3.46	0.96	-3.12	-3.46	0.97
SSP3-7.0	-5.38	-5.99	0.94	-5.38	-5.99	0.94	-3.25	-3.63	0.96	-3.25	-3.63	0.96
SSP4-6.0	-4.75	-5.23	0.94	.4.75	-5.23	0.94	-2.81	-3.09	0.96	-2.81	-3.09	0.97
SSP5-8.5	-5.80	-6.45	0.94	-5.80	-6.45	0.94	-3.45	-3.85	0.96	-3.45	-3.85	0.96
Ens SSP1-2.6	-5.75	-6.40	0.94	-5.75	-6.40	0.94	-3.42	-3.81	0.96	-3.42	-3.81	0.96
Ens SSP2-4.5	-5.27	-5.83	0.94	-5.27	-5.83	0.95	-3.12	-3.46	0.97	-3.12	-3.46	0.97
Ens SSP3-7.0	-5.80	-6.45	0.94	-5.80	-6.45	0.94	-3.45	-3.85	0.96	-3.45	-3.85	0.96

Table 4.7 Projected change in monthly average water demand (in Mm^3) in the Volta Basin. The Ensemble SSP1-2.6, Ensemble SSP2-4.5, Ensemble SSP3-7.0 represents mean change in water demand for the fifteen-member CMIP6 models used in this study. The changes in the table are computed for 2030 to 2100.

Variable	Climate change (CC)			CC + Population			CC + land use			CC + Population + Landuse		
	Annual change in water demand (Bm^3)	Annual change in water demand (%)	Water demand index	Annual change in water demand (Bm^3)	Annual change in water demand (%)	Water demand index	Annual change in water demand (Bm^3)	Annual change in water demand (%)	Water demand index	Annual change in water demand (Bm^3)	Annual change in water demand (%)	Water demand index
SSP1-2.6	-5.75	-6.40	0.94	-5.75	-6.40	0.94	-0.28	-33.7	0.66	-0.48	-36.3	0.64
SSP2-4.5	-5.27	-5.83	0.94	-5.27	-5.83	0.94	-0.26	-30.7	0.69	-0.44	-33.3	0.67
SSP3-7.0	-5.39	-5.99	0.94	-5.39	-5.99	0.94	-0.27	-32.0	0.68	-0.45	-34.0	0.66
SSP4-6.0	-4.75	-5.23	0.95	-4.75	-5.23	0.95	-0.24	-27.6	0.72	-0.40	-30.0	0.70
SSP5-8.5	-5.80	-6.45	0.94	-5.8	-6.45	0.94	-0.29	-34.0	0.66	-0.49	-36.6	0.63
Ens SSP1-2.6	-5.75	-6.40	0.94	-5.75	-6.40	0.94	-0.29	-33.7	0.66	-0.48	-36.3	0.64
Ens SSP2-4.5	-5.27	-5.83	0.94	-5.27	-5.83	0.94	-0.26	-30.7	0.70	-0.44	-33.3	0.67
Ens SSP3-7.0	-5.80	-6.45	0.94	-5.80	-6.45	0.94	-0.29	-34.0	0.66	-0.49	-36.6	0.63

4.4.7 Projected changes in system hydropower generation

In this section, the impacts of the future increase in temperature and precipitation, land use/land cover change, and population growth on the system hydropower generation is quantified. Figure 4.30 shows projected hydropower generation from the system of hydropower plants used in this study, that is the Akosombo, Bagre, Bui, and Kpong dams under various scenarios. Irrespective of the scenarios, the system hydropower generation has increased relative to the reference scenario until the end of the century. Unlike the case of domestic water demand, population growth is not a strong determinant of the system hydropower generation. Otherwise, the high population growth rate in the reference scenario will result in higher energy generation compared to the other scenarios and a resultant negative system hydropower generation. That said, the negative values in water demand change for all the scenarios imply surplus water available for hydropower generation for all hydropower plants and consequently increasing the system hydropower generation as observed. The results show a marginal increase in hydropower generation contrary to McCartney et al., (2012) who found a decrease at the end of the century. It is important to note again that the systems hydropower generation started increasing around 2040 (Figure 4.30) when the water demand for all scenarios started decreasing (Figure 4.28), making more water available. *The translation of excess water available to increase system hydropower generation demonstrated the nexus between water and energy.* Thus, the excess water available after 2040 is used to increase system hydropower generation. Following the reasoning that population growth does not increase system hydropower generation, climate change, and land use/cover change are the only factors that could explain the increase in the system hydropower generation (Figure 4.30). Figure 4.30a,b describes a climate change scenario and climate change + population growth scenario, however, the fact that SSP1-2.6 to SSP5-8.5 have population growth as input data makes Figure 4.30a and Figure 4.30b the same thing and hence similar results. Conversely, thinking in line with the argument that population growth has no impact on system hydropower generation reduces Figure 4.30b to a climate change scenario (Figure 4.30a), which is evident in the plot. This also shows that climate change is one of the key drivers of system hydropower generation. Following the same line of argument, Figure 4.30d could be reduced essentially to Figure 4.30c as population growth has no impact on system hydropower generation. From the foregoing, two critical factors that affect system hydropower generation is climate change and land use/land cover change. The

difference between Figures 4.30a,b and 4.30c,d is that Figures 4.30a,b were simulated under the influence of static land cover data throughout the experiment, whilst Figures 4.30c,d were simulated under dynamic land cover data spanning from 1992 to 2020, and thereafter constant until the end of the century. The monthly climatology in Figure 4.31 also proves the model responded differently to the different land cover conditions. Thus the climate change scenario (Figures 4.31a,b) yielded different results from the climate + land use change scenario (Figure 4.31c,d) due to the dynamic land use/land cover in the former compared to the latter. The climate change scenario yielded a higher but comparable annual change in hydropower generation ranging from 44.6-57.0 TGJ (0.14-0.19%) compared to the climate + land use change scenario which yields 43.9-49.0 TGJ (0.14-0.19%). In terms of mean monthly values, the climate change scenario yields 3.72-4.8TGJ (0.14-0.18%) compared to the climate change + land use change scenario which yields 3.65-4.61TGJ (0.14-0.18%). Since the WEF-Volta model is sensitive to dynamic land use/land cover data, there is the need for a process in WEAP that describes the dynamic interactions between climate variability and land use/cover change as argued for the case of the WRF-Hydro model. For now, the interactions between water-energy and external influencing factors such as population, climate change and land use land cover change are clearly exemplified by the WEF-Volta model.

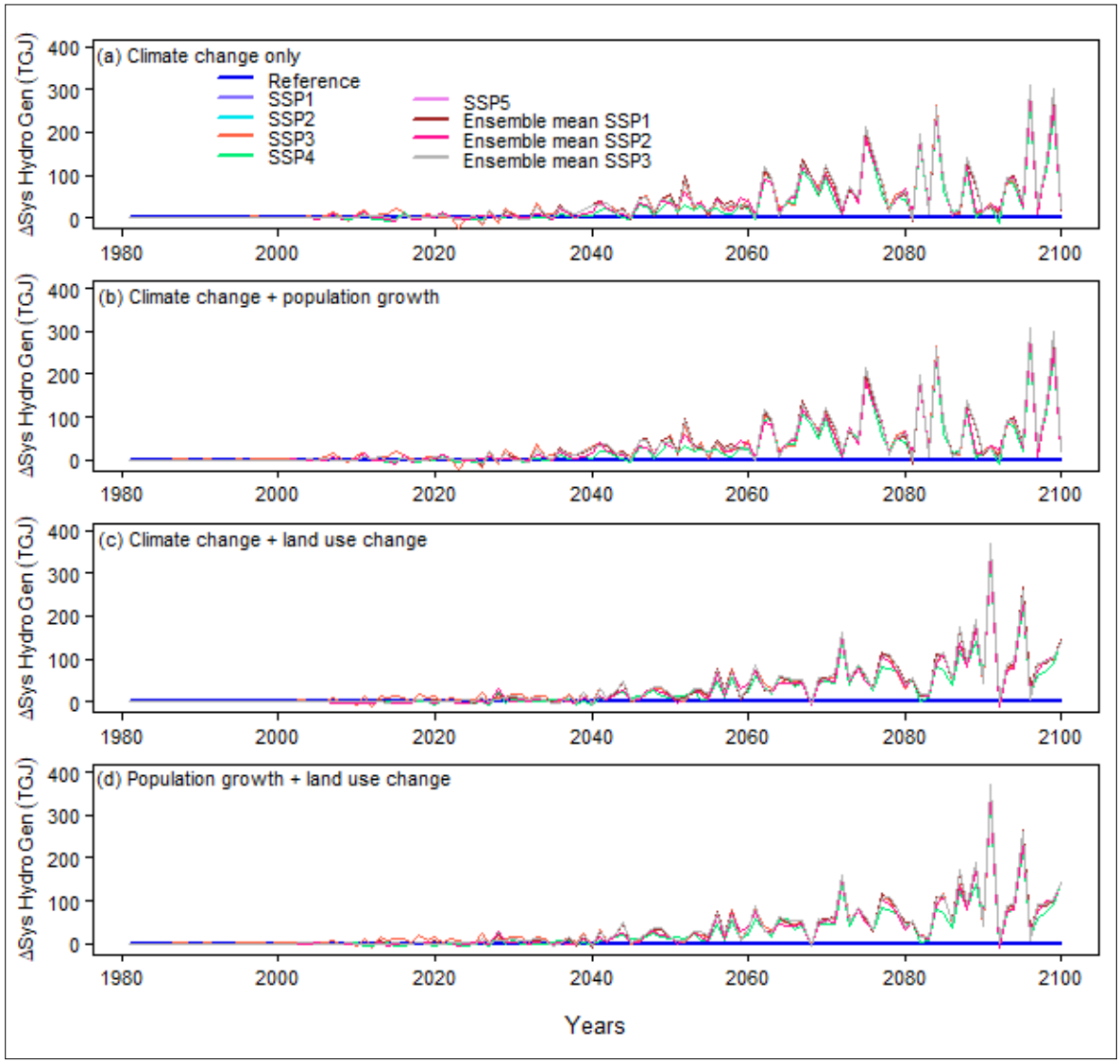

Figure 4.30 System hydropower generation in the Volta Basin of West Africa

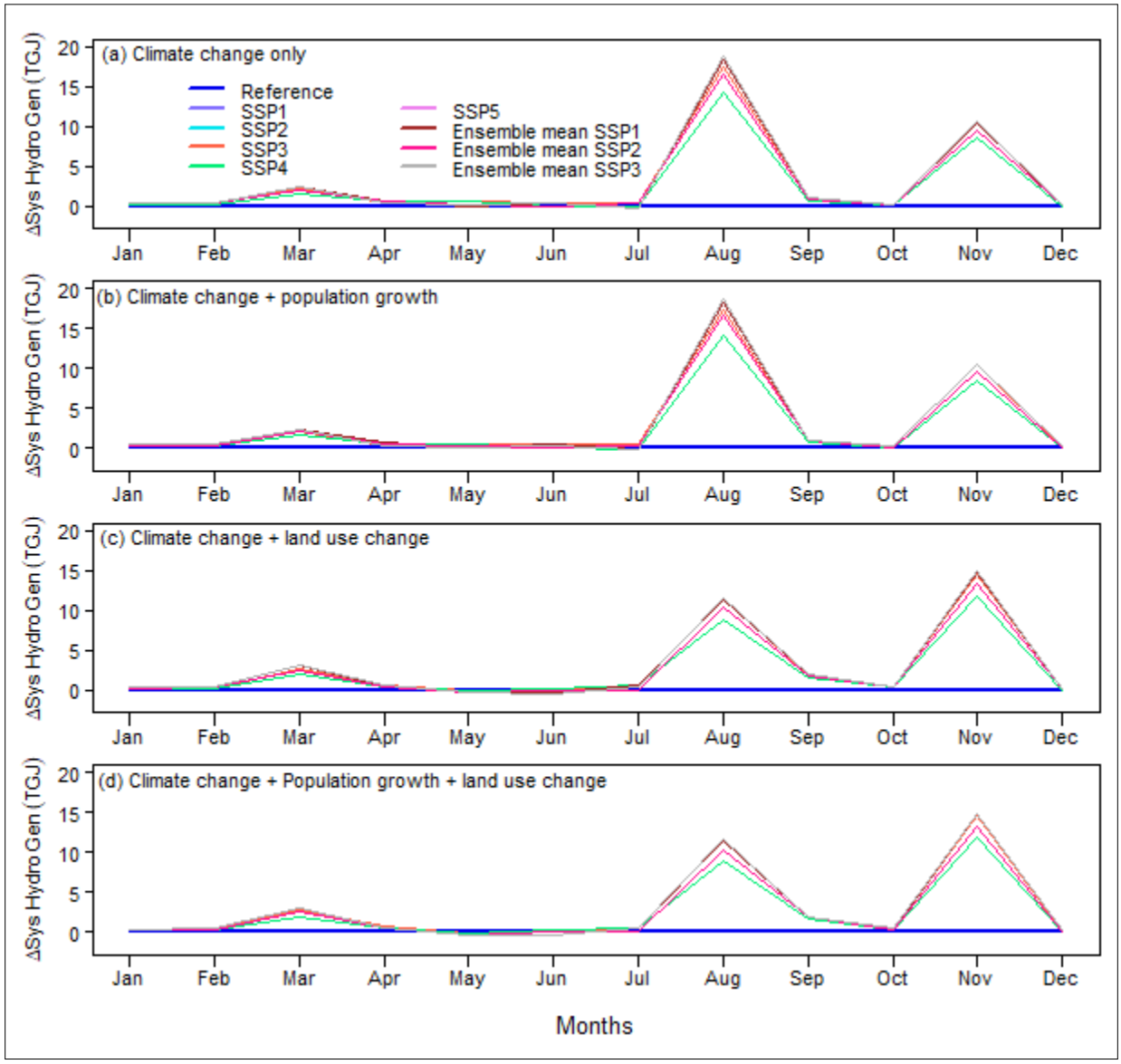

Figure 4.31 Climatology of change in system hydropower generation for various scenario

Table 4.8 Projected change in annual average of total generation for hydropower systems (in thousand GJ) in the Volta Basin. The Ensemble SSP1-2.6, Ensemble SSP2-4.5, Ensemble SSP3-7.0 represents mean change in hydropower generation for the fifteen-member CMIP6 models used. The changes in the table are computed for 2030 to 2100.

Variable	Climate change (CC)			CC + Population			CC + land use			CC + Population + Landuse		
	Annual change in Hydro generation (TGJ)	Annual change in Hydro generation (%)	Index of generation	Annual change in Hydro generation (TGJ)	Annual change in Hydro generation (%)	Index of generation	Annual change in Hydro generation (TGJ)	Annual change in Hydro generation (%)	Index of generation	Annual change in Hydro generation (TGJ	Annual change in Hydro generation (%)	Index of generation
SSP1-2.6	57.2	0.19	1.002	57.2	0.19	1.002	54.5	0.18	1.002	54.5	0.01	1.002
SSP2-4.5	51.8	0.17	1.002	51.8	0.17	1.002	49.0	0.16	1.002	49.0	0.007	1.002
SSP3-7.0	55.0	0.18	1.002	55.0	0.18	1.002	53.0	0.17	1.002	53.0	0.007	1.002
SSP4-6.0	44.6	0.14	1.002	44.6	0.14	1.002	43.9	0.14	1.002	43.9	0.007	1.002
SSP5-8.5	57.6	0.19	1.002	57.6	0.19	1.002	55.4	0.18	1.002	55.4	0.002	1.002
Ens SSP1-2.6	57.2	0.19	1.002	57.2	0.19	1.002	54.5	0.18	1.002	54.5	0.01	1.002
Ens SSP2-4.5	51.8	0.17	1.001	51.8	0.17	1.001	49.0	0.16	1.001	49.0	0.007	1.001
Ens SSP3-7.0	57.6	0.19	1.002	57.6	0.19	1.002	55.4	0.18	1.002	55.4	0.01	1.002

Table 4.9 Projected change in monthly average generation for hydropower systems (in thousand GJ) in the Volta Basin. The Ensemble SSP1-2.6, Ensemble SSP2-4.5, Ensemble SSP3-7.0 represents mean change in hydropower generation for the fifteen-member CMIP6 models used. The changes in the table are computed for 2030 to 2100.

Variable	Climate change (CC)			CC + Population			CC + land use			CC + Population + Landuse		
	Annual change in Hydro generation (TGJ)	Annual change in Hydro generation (%)	Index of generation	Annual change in Hydro generation (TGJ)	Annual change in Hydro generation (%)	Index of generation	Annual change in Hydro generation (TGJ)	Annual change in Hydro generation (%)	Index of generation	Annual change in Hydro generation (TGJ	Annual change in Hydro generation (%)	Index of generation
SSP1-2.6	4.77	0.18	1.002	4.77	0.18	1.002	4.54	0.18	1.002	4.54	0.18	1.002
SSP2-4.5	4.32	0.17	1.002	4.32	0.17	1.002	4.08	0.16	1.002	4.08	0.16	1.002
SSP3-7.0	4.58	0.18	1.002	4.58	0.18	1.002	4.41	0.17	1.002	4.41	0.17	1.002
SSP4-6.0	3.72	0.14	1.002	3.72	0.14	1.002	3.65	0.14	1.002	3.65	0.14	1.002
SSP5-8.5	4.80	0.18	1.002	4.80	0.18	1.002	4.61	0.18	1.002	4.61	0.18	1.002
Ens	4.77	0.18	1.002	4.77	0.18	1.002	4.54	0.18	1.002	4.54	0.18	1.002
SSP1-2.6												
Ens	4.80	0.17	1.001	4.32	0.17	1.001	4.08	0.16	1.001	4.08	0.16	1.001
SSP2-4.5												
Ens	4.80	0.18	1.002	4.80	0.18	1.002	4.61	0.18	1.002	4.61	0.18	1.002
SSP3-7.0												

4.5 Partial conclusion on results and discussion

Three approaches to investigate the relationship between climate and land use/land cover change in West Africa are realized in this thesis, including the analysis approach, the fully coupled land-atmosphere modeling approach in WRF-Hydro, and the hydrological modeling approach in WEAP. The analysis approach produced a quantifiable relationship between the interannual land cover changes and standardized climatic indices, which can later be developed into indices to improve outputs of regional climate models and hydrological models, such as rainfall and streamflow. The modeling in WRF-Hydro produced a complete description of the land-atmosphere interaction from a regional to local scale including the biogeophysical properties, the surface energy balance, as well as the water and energy flux estimates, and the general hydroclimatic situation in the Sissili-Kulpawn Basin. Thus, the WRF-Hydro which includes a land surface model allows understanding the complex interaction between the climate and the land surface compared to the analysis approach and the hydrological modeling in WEAP. The WEAP modeling approach allows investigation of the effects of climate change, land use and land cover changes, population growth, and other socioeconomic conditions on the Water-Energy-Food nexus which was not possible with the analysis approach and the WRF-Hydro modeling.

CHAPTER 5 – CONCLUSION, RECOMMENDATION, AND FUTURE WORKS

This research aims to investigate the relationship between climate variability/extremes and land use/land cover change in West Africa using Remote sensing observations and reanalysis products on one hand, and to investigate the relationship between climate variability/extremes and land use/land cover change using a fully coupled land-atmosphere model on the other hand. Thus, this research aims to investigate the relationship between climate variability/change and land cover change from (i) an analytical point of view using the candidate's proposed method and (ii) a modeling point of view using WRF-Hydro and WEAP. Based on a quantitative analysis of the interannual variability of climate and the interannual changes in land cover, a correlation exists between climate variability and land cover changes at annual timescales, especially in extreme climatic conditions. The results indicate that while modeling is a much more popular and better approach to investigating climate-land or land-atmosphere interactions, it could benefit even further from the analytical approach, which allows for a more quantitative description of the relationship between climate variability and land cover change. This is critical to enhancing the model's ability to capture extreme climatic conditions such as flooding and drought events. This thesis thus challenges the status quo of using one year of land cover data in a regional climate model to simulate many years of climate-land interactions/land-atmosphere interactions. Asserting that a quantitative relationship exists between interannual climate variability and land cover changes, this thesis sets out to investigate this relationship, using 29 years of historical land cover and standardized climatic indices. The findings confirm the initial hypothesis of the research and also create confidence in the newly proposed method of directly comparing land cover change intensities and standardized climatic indices as the basis for establishing a quantitative relationship between land-atmosphere/land-climate interactions. While this research answers the question of investigating the quantitative relationship between climate variability and land cover changes for implementation in regional climate models (RCMs), it also raises a new question on how to implement this relationship in RCMs. In addition, the modeling approach produces much more in-depth analysis than the analytical approach, as such, the analytical approach is a proposition to improve the climate-land/land-atmosphere parametrization in RCMs. For instance, the WRF-Hydro accurately simulates the land-atmosphere interactions, including albedo, leaf area index, net radiation flux, sensible heat flux, latent heat flux, temperature, rainfall, soil evaporation, plant evapotranspiration, surface runoff, underground runoff, and streamflow, allowing for much comprehensive description of the water and energy cycle. It

was also possible to simulate a synthetic land cover change experiment that mimics the main climatic hazards of the Sissili-Kulpawn Basin. Thus, while the analytical approach is to improve RCM performance in simulating extreme climatic conditions, the modeling with WRF-Hydro provides even greater benefits of simulating climate, land, water, and energy interactions, offering key information for climate adaptation, land use planning and management, and policy decision-making. For instance, the synthetic numerical experiment also provides threshold afforestation and deforestation extents with high flooding and drought risks, which serves as a guide for afforestation, deforestation, and land use planning. So far, the research benefits described above span from regional climate modeling (regional scale) to Sissili-Kulpawn basin management (local scale). To further extend the benefit for decision-making in the Volta Basin, the land-atmosphere/land-climate interaction was investigated within the framework of the WEF nexus to assess its impact on present and future water, energy, and food resources. This, was achieved by investigating the climate-land-water-energy-food nexus interactions using the Volta-WEF nexus developed in WEAP. The Volta-WEF nexus is the first attempt to explore the water-energy-food interactions in the Volta Basin under future population growth, static and dynamic land use and land cover change, and future climate change projections. In developing the Volta-WEF nexus model, streamflows from all four sub-basins were calibrated and validated. Hydropower reservoir operations were also calibrated and validated in like manner, taking into consideration the domestic and agricultural water demand. This practice ensured that the Volta-WEF nexus model is not a replication of the basin-wide IWRM model, which often is water-centric, but takes each part of the nexus nodes (water, energy, and food) into account simultaneously. Aside from being a Decision Support Tool (DST) for the Volta Basin Authority, it presents the future perspective of climatic impacts, land use impacts, and therefore the future land-atmosphere interaction within the context of WEF nexus. Unlike previous research which predicted a decrease in hydropower generation in the far and near future, the WEF-Volta model presents variable but an overall increase in future hydropower generation and a general decrease in the overall demand compared to the reference scenario. Thus, the increase in hydropower production is driven by an overestimation of population growth by the reference scenario which effectively led to an overestimation of basin-wide water demand. In terms of drivers of change, climate change and land use/land cover change are the major factor of system hydropower production, while population growth is the major driver of basin-wide water demand.

Within the context of modeling in this work, the Volta-WEF nexus model results and that of WRF-Hydro complement each other, making it possible to investigate the climate change impact on a basin on one hand and complex land-atmosphere interactions from the regional to local scale on the other hand. Thus, even though the WEF-Volta allows for investigating the impact of climate change and land use and land cover change, it also does not allow for a complete description of water fluxes, and energy fluxes as in the fully coupled WRF/ WRF-Hydro. In summary, no approach used in this work provided full answers to the complex research establishing the relationship between climate variability/change and land use land cover change. However, each model presents the approach to solving one aspect of the complex research question of understanding the complex land-atmosphere interactions in a specific context. The lack of a quantitative relationship between interannual climate variability and the interannual land cover change intensities was solved using the new analytic approach proposed in this thesis. The analytical approach fills the gap in the existing method of investigating land-atmosphere interactions and therefore significantly contributes to existing scientific knowledge. Thus, before this work the method employed for investigating land-atmosphere interactions as revealed by the literature review is modeling. This work started with an analytical approach to quantify the land-atmosphere interactions relationship which can later be developed into coefficients, correction factors, or even bias correction factors for RCMs. This quantitative land-climate relationship is a step closer to quantifying the impact of dynamic land-atmosphere interactions in RCMs. Specifically, it will now serve the purpose of improving the parameterization of land-atmosphere interaction in RCM in West Africa and hence improving their performance. In addition, the output of the WRF-Hydro is consistent with the existing knowledge of land-atmosphere interaction in terms of its representation of critical climatic variables such as rainfall, temperature, streamflow and therefore shows that WRF-Hydro is also usable for providing climate service in the West African region. Similarly, the Volta-WEF nexus mimics well past and present water and energy nodes of the WEF nexus and can be considered the first WEF nexus model for the entire Volta Basin. To reiterate, this research has implications from the global to local scale which include contribution to the climate modeling community, information for policymakers, climate adaptation, land use planning and management, the Volta Basin Authority.

Based on the findings and conclusions, recommendations are made for four different categories of people/sectors from global scale to local scale. To begin with, this research reveals the capability of ESA land cover data to be used to derive climate variability and land use/land

cover change relationship because of its consistency as one of the annual land cover products with the longest timeseries and relatively high resolution. Being specifically designed to suit the desires expressed by the climate modeling community to avoid false change detection between two semantically close classes, it is suitable for continual change detection, and hence climate-land variability studies as demonstrated in this work. The relationship derived from this study is useful for later parameterizing the land-climate interactions that are oversimplified in RCMs globally and particularly for the West African region. Since the ESA LC is available globally these climate-land relationships could be derived everywhere to improve on land-atmosphere parameterization in RCMs. It is therefore recommended that the climate modeling community consider deriving a climate-land relationship based on the approach proposed by this work and subsequently use the relationships to improve parameterization schemes of land-atmosphere interactions in RCMs. In addition, the WRF-Hydro under ESA LC data yielded comparable results to the default WRF-Hydro which uses the MODIS LC data. The afforestation and deforestation experiments are consistent with well-established effects of afforestation and deforestation in literature and also show that the model represents well the hydroclimatic situation in the Sissili-Kulpawn Basin. The climate modeling community in other parts of the world can also employ the ESA LC for other regions to verify if it mimics the biogeo-physical parameters, water and energy fluxes as well as the hydroclimatic situation of their respective study areas. The results of the synthetic numerical land cover change sensitivity experiment provide the threshold afforestation and deforestation that could increase the climatic risks of the Sissili-Kulpawn basin. Land planning and management institutions within the area should consider these thresholds as the limits for sustainable land management practices and to avoid the climatic risks associated with extreme deforestation and afforestation. Moreover, this finding reveals the capability of the WRF-Hydro in the West African region and the need for capacity building in the region to be able to use the WRF/WRF-Hydro for operational forecasting and providing climate services in the region. Initiatives to build capacity to use the WRF/WRF-Hydro can start with the national meteorological and hydrological organizations to equip them with the skill to use the WRF/WRF-Hydro for operational forecasting, hindcasting and evaluating the model's ability to simulate past and present extremes. This will improve the accuracy of forecasts and timely response in extreme weather conditions. It could also be used to provide important climate information to stakeholders. For WASCAL, the WRF/WRF-Hydro is suitable for providing the key demand-driven climate environmental services for policymakers and other stakeholders, including the smallholders as outlined in the WASCAL Research Action Plan (WRAP 2.0).

The role of policy-makers in this regard is the willingness to capture within the development agenda of countries within the West African sub-region the funds for training of skilled personnel and the investment into high-performance computing infrastructures, and internet connectivity needed to run these simulations. In other words, running of WRF-Hydro is computationally expensive, and highly internet and skill-dependent, such that policymakers must be willing to invest in all these areas. It is often the case that high-performing computers are available in some parts of West Africa but the skilled administrators to manage, run, and derive important information from simulations are lacking. Finally, the Volta-WEF nexus is being recommended for uptake by the Volta Basin Authority which has provided critical data to make this research possible. It could meet the VBA quest to understand the future climatic impact on water resources, food production, and energy within the framework of the WEF nexus. The VRA and SONABEL who also provide important information for this research could benefit in like manner. Existing dams with irrigation extensions, like the Bagre and Kpong dams, may decide to expand their energy generation and irrigation capacity as precipitation will increase in the future. The government of Ghana may also consider building the Pwalugu multi-purpose dam as a future water-energy-food nexus project to reduce the risk of current and future flooding in the northern part of Ghana while providing water, energy, and food resources for the region.

Future research should focus on how to implement the climate-land relationship developed in this work into the WRF-Hydro or any other RCM. This can simply be a coefficient or a correction factor for output rainfall and/streamflow or parametrization of the land-atmosphere interactions altogether taking the land-atmosphere relationship. For simplicity, this coefficient may be derived from the SPI for the atmospheric component and the LAI for the land components. Though this work has established that extreme afforestation and deforestation thresholds beyond which afforestation and deforestation could increase the climatic risks of the SKB, further research can explore various afforestation and deforestation extent to determine the exact threshold that maximizes benefits for the SKB. A continual improvement on the Volta-WEF nexus model to include crop modeling has not been covered in this work and is a recommendation for future research.

Reference

Abatzoglou, J. T., Dobrowski, S. Z., Parks, S. A., & Hegewisch, K. C. (2018). TerraClimate, a high-resolution global dataset of monthly climate and climatic water balance from 1958-2015. *Scientific Data*, *5*(170191), 1–12. https://doi.org/10.1038/sdata.2017.191

Abubakari, S., Dong, X., Su, B., Hu, X., Liu, J., Li, Y., Peng, T., Ma, H., Wang, K., & Xu, S. (2017). Modelling the spatial variation of hydrology in volta river basin of west Africa under climate change. *Nature Environment and Pollution Technology*, *16*(4), 1095–1105.

Abubakari, S., Dong, X., Su, B., Hu, X., Liu, J., Li, Y., Peng, T., Ma, H., Wang, K., & Xu, S. (2018). Modelling streamflow response to climate change in data-scarce White Volta River basin of West Africa using a semi-distributed hydrologic model. *Journal of Water and Climate Change*. https://doi.org/10.2166/wcc.2018.193

Achugbu, I. C., Olufayo, A. A., Balogun, I. A., Adefisan, E. A., Dudhia, J., & Naabil, E. (2022). Modeling the spatiotemporal response of dew point temperature, air temperature and rainfall to land use land cover change over West Africa. *Modeling Earth Systems and Environment*, *8*(1), 173–198. https://doi.org/10.1007/s40808-021-01094-8

Achugbu, I. C., Olufayo, A. A., Balogun, I. A., Dudhia, J., McAllister, M., Adefisan, E. A., & Naabil, E. (2022). Potential effects of Land Use Land Cover Change on streamflow over the Sokoto Rima River Basin. *Heliyon*, *8*(7). https://doi.org/10.1016/j.heliyon.2022.e09779

Akomeah, E., Odai, ; S N, Annor, ; F O, Adjei, ; K A, & Barry, B. (2018). *Mapping Irrigation Potential In A Semi-Arid Region In West Africa*.

Akpoti, K., Antwi, E., & Kabo-bah, A. (2016). Impacts of Rainfall Variability, Land Use and Land Cover Change on Stream Flow of the Black Volta Basin, West Africa. *Hydrology*, *3*(3), 26. https://doi.org/10.3390/hydrology3030026

Albrecht, T. R., Crootof, A., & Scott, C. A. (2018c). The Water-Energy-Food Nexus: A systematic review of methods for nexus assessment. *Environmental Research Letters*, *13*(4). https://doi.org/10.1088/1748-9326/aaa9c6

Allam, M. M., & Eltahir, E. A. B. (2019). Water-energy-food nexus sustainability in the upper Blue Nile (UBN) basin. *Frontiers in Environmental Science*, *7*(JAN). https://doi.org/10.3389/fenvs.2019.00005

Allwaters Consult Limited. (2012). *DIAGNOSTIC STUDY OF THE BLACK VOLTA BASIN IN GHANA. Final Report*.

Alp, E., Köksal, M. A., Demir, Y., Başkan, O., Erdoğan, E. K., Özcan, Z., & Özcan, C. (2020). Evaluation of the Water-Energy-Food Nexus with the Focus on Climate Change in a Semi-arid Watershed, Turkey. *WEFTEC 2020*.

Amisigo, B. A., McCluskey, A., & Swanson, R. (2015). Modeling impact of climate change on water resources and agriculture demand in the Volta Basin and other basin systems in Ghana. *Sustainability (Switzerland)*, *7*(6), 6957–6975. https://doi.org/10.3390/su7066957

Amuji, C. F. (2021). The future of rain-fed horticultural crops production in a changing West African climate. In *Reviews in Agricultural Science* (Vol. 9, pp. 206–220). Gifu University - United Graduate School of Agricultural Science. https://doi.org/10.7831/ras.9.0_206

Annor, T., Lamptey, B., & Washington, R. (2022). Assessment of the unified model in reproducing West African precipitation and temperature climatology. *Theoretical and Applied Climatology*. https://doi.org/10.1007/s00704-022-03973-1

Arjdal, K., Vignon, É., Driouech, F., Chéruy, F., Er-Raki, S., Sima, A., Chehbouni, A., & Drobinski, P. (2024). Modeling Land-Atmosphere Interactions over Semiarid Plains in Morocco: In-Depth Assessment of GCM Stretched-Grid Simulations Using In Situ Data. *Journal of Applied Meteorology and Climatology*, *63*(3), 369–386. https://doi.org/10.1175/JAMC-D-23-0099.1

Arnault, J., Fersch, B., Rummler, T., Zhang, Z., Quenum, G. M., Wei, J., Graf, M., Laux, P., & Kunstmann, H. (2021). Lateral terrestrial water flow contribution to summer precipitation at continental scale – A comparison between Europe and West Africa with WRF-Hydro-tag ensembles. *Hydrological Processes*, *35*(5). https://doi.org/10.1002/hyp.14183

Arnault, J., Jung, G., Haese, B., Fersch, B., Rummler, T., Wei, J., Zhang, Z., & Kunstmann, H. (2021). A Joint Soil-Vegetation-Atmospheric Modeling Procedure of Water Isotopologues: Implementation and Application to Different Climate Zones With WRF-Hydro-Iso. *Journal of Advances in Modeling Earth Systems*, *13*(10). https://doi.org/10.1029/2021MS002562

Arnault, J., Mwanthi, A. M., Portele, T., Li, L., Rummler, T., Fersch, B., Hassan, M. A., Bahaga, T. K., Zhang, Z., & Mortey, E. M. (2023). Regional water cycle sensitivity to afforestation: Synthetic numerical experiments for tropical Africa. *Frontiers in Climate*, *5*, 1233536. https://doi.org/10.3389/fclim.2023.1233536

Arnault, J., Niezgoda, K., Jung, G., Hahn, A., Zabel, M., SCHEFUB, E., & Kunstmann, H. (2022). Disentangling the Contribution of Moisture Source Change to Isotopic Proxy Signatures: Deuterium Tracing with WRF-Hydro-Iso-Tag and Application to Southern African Holocene Sediment Archives. *Journal of Climate*, *35*(22), 3855–3879. https://doi.org/10.1175/JCLI-D-22-0041.1

Arnault, J., Wagner, S., Rummler, T., Fersch, B., Bliefernicht, J., Andresen, S., & Kunstmann, H. (2016). Role of Runoff-Infiltration Partitioning and Resolved Overland Flow on Land-Atmosphere Feedbacks: A Case Study with the WRF-Hydro Coupled Modeling System for West Africa. *Journal of Hydrometeorology*, *17*(5), 1489–1516. https://doi.org/10.1175/JHM-D-15-0089.1

Awotwi, A., Bediako, M. A., Harris, E., & Forkuo, E. K. (2016). Water Quality Changes Associated with Cassava Production: Case Study of White Volta Bain. *Heliyon*, *2*(8). https://doi.org/10.1016/j.heliyon.2016.e00149

Awotwi, A., Yeboah, F., & Kumi, M. (2015). Assessing the impact of land cover changes on water balance components of White Volta Basin in West Africa. *Water and Environment Journal*, *29*(2), 259–267. https://doi.org/10.1111/wej.12100

Bagley, J. E., Desai, A. R., Harding, K. J., Snyder, P. K., & Foley, J. A. (2014). Drought and deforestation: Has land cover change influenced recent precipitation extremes in the Amazon? *Journal of Climate*, *27*(1), 345–361. https://doi.org/10.1175/JCLI-D-12-00369.1

Basheer, M., Siddig, K., & Ringler, C. (2024). Water-energy-food planning and operations framework for river basins with a case study on the Blue Nile. *Journal of Hydrology*, *631*. https://doi.org/10.1016/j.jhydrol.2024.130801

Basheer, M., Wheeler, K. G., Ribbe, L., Majdalawi, M., Abdo, G., & Zagona, E. A. (2018). Quantifying and evaluating the impacts of cooperation in transboundary river basins on the Water-Energy-Food nexus: The Blue Nile Basin. *Science of the Total Environment*, *630*, 1309–1323. https://doi.org/10.1016/j.scitotenv.2018.02.249

Berg, A., Lintner, B., Findell, K., & Giannini, A. (2017). Soil moisture influence on seasonality and large-scale circulation in simulations of the West African monsoon. *Journal of Climate*, *30*(7), 2295–2317. https://doi.org/10.1175/JCLI-D-15-0877.1

Betts, R. A. (2000). Offset of the potential carbon sink from boreal forestation by decreases in surface albedo. *Nature*, *408*(6809), 187–190.

Bhagabati, S. S., & Kawasaki, A. (2017). Consideration of the rainfall-runoff-inundation (RRI) model for flood mapping in a deltaic area of myanmar. *Hydrological Research Letters*, *11*(3), 155–160. https://doi.org/10.3178/hrl.11.155

Blanchon, D., & Le Tourneau, F.-M. (2022). When land unveils water: adding a fourth dimension to the Water/Energy/Food Nexus concept and its relevance to water research | Quand la terre dévoile l'eau: l'ajout d'une quatrième dimension au concept de Nexus Eau/Énergie/ Alimentation et sa pertinence. *Geocarrefour*, *96*(2). https://doi.org/10.4000/geocarrefour.20162

Bliefernicht, J., Berger, S., Salack, S., Guug, S., Hingerl, L., Heinzeller, D., Mauder, M., Steinbrecher, R., Steup, G., Bossa, A. Y., Waongo, M., Quansah, E., Balogun, A. A., Yira, Y., Arnault, J., Wagner, S., Klein, C., Gessner, U., Knauer, K., … Kunstmann, H. (2018). The WASCAL Hydrometeorological Observatory in the Sudan Savanna of Burkina Faso and Ghana. *Vadose Zone Journal*, *17*(1), 1–20. https://doi.org/10.2136/vzj2018.03.0065

Bliefernicht, J., Kunstmann, H., Hingerl, L., Rummler, T., Andresen, S., Mauder, M., Steinbrecher, R., Frieß, R., Gochis, D., Gessner, U., Jahn, C., & Barry, B. (2013). Field and simulation experiments for investigating regional land-atmosphere interactions in West Africa: Experimental set-up and first results. *IAHS-AISH Proceedings and Reports*, *359*, 226–232.

Bonan, G. B. (2008). Forests and climate change: Forcings, feedbacks, and the climate benefits of forests. *Science*, *320*(5882), 1444–1449. https://doi.org/10.1126/science.1155121

Bounoua, L., DeFries, R., Collatz, G. J., Sellers, P., & Khan, H. (2002). Effects of land cover conversion on surface climate. *Climatic Change*, *52*(1–2), 29–64. https://doi.org/10.1023/A:1013051420309

Bruns, A., Meisch, S., Ahmed, A., Meissner, R., & Romero-Lankao, P. (2022). Nexus disrupted: Lived realities and the water-energy-food nexus from an infrastructure perspective. *Geoforum*, *133*, 79–88. https://doi.org/10.1016/j.geoforum.2022.05.007

Burakowski, E. A., Ollinger, S. V., Bonan, G. B., Wake, C. P., Dibb, J. E., & Hollinger, D. Y. (2016). Evaluating the climate effects of reforestation in new england using a weather research and forecasting (WRF) model multiphysics ensemble. *Journal of Climate*, *29*(14), 5141–5156. https://doi.org/10.1175/JCLI-D-15-0286.1

Cansino-Loeza, B., & Ponce-Ortega, J. M. (2021). Sustainable assessment of Water-Energy-Food Nexus at regional level through a multi-stakeholder optimization approach. *Journal of Cleaner Production*, *290*, 125194. https://doi.org/10.1016/j.jclepro.2020.125194

Cao, M., Zhu, Y., Quan, J., Zhou, S., Lü, G., Chen, M., & Huang, M. (2019). Spatial Sequential Modeling and Predication of Global Land Use and Land Cover Changes by Integrating a Global Change Assessment Model and Cellular Automata. *Earth's Future*, *7*(9), 1102–1116. https://doi.org/10.1029/2019EF001228

Cerbelaud, A., Lefèvre, J., Genthon, P., & Menkes, C. (2022). Assessment of the WRF-Hydro uncoupled hydro-meteorological model on flashy watersheds of the Grande Terre tropical island of New Caledonia (South-West Pacific). *Journal of Hydrology: Regional Studies*, *40*. https://doi.org/10.1016/j.ejrh.2022.101003

Chen, A., Guan, H., Batelaan, O., Zhang, X., & He, X. (2019). Global Soil Moisture-Air Temperature Coupling Based on GRACE-Derived Terrestrial Water Storage. *Journal of Geophysical Research: Atmospheres*, *124*(14), 7786–7796. https://doi.org/10.1029/2019JD030324

Chen, C., Ge, J., Guo, W., Cao, Y., Liu, Y., Luo, X., & Yang, L. (2022). The Biophysical Impacts of Idealized Afforestation on Surface Temperature in China: Local and Nonlocal Effects. *Journal of Climate*, *35*(23), 4233–4252. https://doi.org/10.1175/JCLI-D-22-0144.1

Chen, G. S., Notaro, M., Liu, Z., & Liu, Y. (2012). Simulated local and remote biophysical effects of afforestation over the Southeast United States in boreal summer. *Journal of Climate*, *25*(13), 4511–4522. https://doi.org/10.1175/JCLI-D-11-00317.1

Chen, S., Tian, L., Zhang, B., Zhang, G., Zhang, F., Yang, K., Wang, X., Bai, Y., & Pan, B. (2023). Quantifying the impact of large-scale afforestation on the atmospheric water cycle during rainy season over the Chinese Loess Plateau. *Journal of Hydrology*, *619*, 129326.

Collins, M., & Gaetani, M. (2023). Editorial: (10 years) Water-energy-food nexus: Impact of climate variability and change on the water-energy-food nexus. *Frontiers in Climate*. https://doi.org/https://doi.org/10.3389/fclim.2023.1137710

Cotillon, S. E., & Tappan, G. G. (2016). *Landscapes of West Africa: A window on a changing world*.

Dale, V. H. (1997). The relationship between land-use change and climate change. *Ecological Applications*, *7*(August), 753–769.

Daloz, A. S., Schwingshackl, C., Mooney, P., Strada, S., Rechid, D., Davin, E. L., Katragkou, E., De Noblet-Ducoudré, N., Belda, M., Halenka, T., Toelle, M. H., & Lund, M. T. (2022). Land-atmosphere interactions in sub-polar and alpine climates in the CORDEX flagship pilot study Land Use and Climate Across Scales (LUCAS) models-Part 1: Evaluation of the snow-albedo effect. *Cryosphere*, *16*(6), 2403–2419. https://doi.org/10.5194/tc-16-2403-2022

Danandeh Mehr, A., & Vaheddoost, B. (2020). Identification of the trends associated with the SPI and SPEI indices across Ankara, Turkey. *Theoretical and Applied Climatology*, *139*(3–4), 1531–1542. https://doi.org/10.1007/s00704-019-03071-9

Daramola, M. T., Eresanya, E. O., & Erhabor, S. C. (2023). How has aridity changed over West Africa in the past four decades? *Journal of African Earth Sciences*, *197*, 104745. https://doi.org/10.1016/j.jafrearsci.2022.104745

Davis, S. R., Pratt, L. J., & Jiang, H. (2015). The Tokar Gap Jet: Regional circulation, diurnal variability, and moisture transport based on numerical simulations. *Journal of Climate*, *28*(15), 5885–5907. https://doi.org/10.1175/JCLI-D-14-00635.1

de Condappa, D., Chaponnière, A., & Lemoalle, J. (2009). A decision-support tool for water allocation in the Volta Basin. *Water International*, *34*(1), 71–87. https://doi.org/10.1080/02508060802677861

Dee, S., Noone, D., Buenning, N., Emile-Geay, J., & Zhou, Y. (2015). SPEEDY-IER: A fast atmospheric GCM with water isotope physics. *Journal of Geophysical Research*, *120*(1), 73–91. https://doi.org/10.1002/2014JD022194

Defourny, P., Bontemps, S., Lamarche, C., Brockmann, C., Boettcher, M., Wevers, J., & Kirches, G. (2017). *Land cover CCI: product user guide version 2.0*. http://maps.elie.ucl.ac.be/CCI/viewe r

Dekongmen, B. W., Anornu, G. K., Kabo-Bah, A. T., Larbi, I., Sunkari, E. D., Dile, Y. T., Agyare, A., & Gyamfi, C. (2022). Groundwater recharge estimation and potential recharge mapping in the Afram Plains of Ghana using SWAT and remote sensing techniques. *Groundwater for Sustainable Development*, *17*, 100741.

Del Borghi, A., Tacchino, V., Moreschi, L., Matarazzo, A., Gallo, M., & Arellano Vazquez, D. (2022). Environmental assessment of vegetable crops towards the water-energy-food nexus: A combination of precision agriculture and life cycle assessment. *Ecological Indicators*, *140*(April), 109015. https://doi.org/10.1016/j.ecolind.2022.109015

Dembélé, M., Vrac, M., Ceperley, N., Zwart, S. J., Larsen, J., Dadson, S. J., Mariéthoz, G., & Schaefli, B. (2022). Contrasting changes in hydrological processes of the Volta River basin under global warming. *Hydrology and Earth System Sciences*, *26*(5). https://doi.org/10.5194/hess-26-1481-2022

Deng, X., Liu, J., Ma, E., Jiang, L., Yu, R., Jiang, Q., & Zhao, C. (2015). Impact assessments on water and heat fluxes of terrestrial ecosystem due to land use change. *Impacts of Land-Use Change on Ecosystem Services*, 149–209.

Deng, X., Zhan, J., & Su, H. (2014). *Land Use Impacts on Climate*. Springer. https://doi.org/10.1007/978-3-642-54876-5

De Noblet-Ducoudré, N., Boisier, J. P., Pitman, A., Bonan, G. B., Brovkin, V., Cruz, F., Delire, C., Gayler, V., Van Den Hurk, B. J. J. M., Lawrence, P. J., Van Der Molen, M. K., Müller, C., Reick, C. H., Strengers, B. J., & Voldoire, A. (2012). Determining robust impacts of land-use-induced land cover changes on surface climate over North America and Eurasia: Results from the first set of LUCID experiments. *Journal of Climate*, *25*(9), 3261–3281. https://doi.org/10.1175/JCLI-D-11-00338.1

De Vos, L., Biemans, H., Doelman, J. C., Stehfest, E., & Van Vuuren, D. P. (2021). Trade-offs between water needs for food, utilities, and the environment - A nexus quantification at different scales. *Environmental Research Letters*, *16*(11). https://doi.org/10.1088/1748-9326/ac2b5e

Diba, I., Camara, M., & Diedhiou, A. (2019). Impacts of the Sahel-Sahara Interface Reforestation on West African Climate: Intra-Annual Variability and Extreme Temperature Events. *Atmospheric and Climate Sciences*, *09*(01), 35–61. https://doi.org/10.4236/acs.2019.91003

Diba, I., Camara, M., Sarr, A. B., & Diedhiou, A. (2018). Potential impacts of land cover change on the interannual variability of rainfall and surface temperature over West Africa. *Atmosphere*, *9*(10). https://doi.org/10.3390/atmos9100376

Diro, G. T., & Sushama, L. (2017). The role of soil moisture-atmosphere interaction on future hot spells over North America as simulated by the Canadian Regional Climate Model (CRCM5). *Journal of Climate*, *30*(13), 5041–5058. https://doi.org/10.1175/JCLI-D-16-0068.1

Dixit, A., Sahany, S., & Choubey, S. (2019). Role of land-use-land-cover changes in the 2018 Mega-floods over Kerala (India). *Geophysical Research Abstracts*, *21*.

Doan, Q.-V., Kobayashi, S., Kusaka, H., Chen, F., He, C., & Niyogi, D. (2023). Tracking Urban Footprint on Extreme Precipitation in an African Megacity. *Journal of Applied Meteorology and Climatology*, *62*(2), 209–226. https://doi.org/10.1175/JAMC-D-22-0048.1

Dotse, S. Q., Larbi, I., Limantol, A. M., Asare-Nuamah, P., Frimpong, L. K., Alhassan, A. R. M., Sarpong, S., Angmor, E., & Ayisi-Addo, A. K. (2023). Rainfall Projections from Coupled Model Intercomparison Project Phase 6 in the Volta River Basin: Implications on Achieving Sustainable Development. *Sustainability (Switzerland)*, *15*(2). https://doi.org/10.3390/su15021472

Dudhia, J. (1989). Numerical Study on Convection Observed during the Winter Monsoon Experiment Using a Mesoscale Two-Dimensional Model. *Journal of the Atmospheric Sciences*, *46*(20).

Edwards, D. C., & McKee, T. B. (1997). *Characteristics of 20th Century drought in the United States at multiple time scales*. *298*(0704).

Eghdami, M., & Barros, A. P. (2020). Deforestation Impacts on Orographic Precipitation in the Tropical Andes. *Frontiers in Environmental Science*, *8*. https://doi.org/10.3389/fenvs.2020.580159

Egieya, J., Görgens, J., Narratives, N. G.-W.-E.-F. N., & 2022, undefined. (2022). Some quantitative water–energy–food nexus analysis approaches and their data requirements. *Elsevier*. https://www.sciencedirect.com/science/article/pii/B9780323912235000162

Eiras-Barca, J., Dominguez, F., Yang, Z., Chug, D., Nieto, R., Gimeno, L., & Miguez-Macho, G. (2020). Changes in South American hydroclimate under projected Amazonian deforestation. *Annals of the New York Academy of Sciences*, *1472*(1), 104–122. https://doi.org/10.1111/nyas.14364

Elagib, N. A., & Al-Saidi, M. (2020a). Balancing the benefits from the water–energy–land–food nexus through agroforestry in the Sahel. *Science of the Total Environment*, *742*, 140509. https://doi.org/10.1016/j.scitotenv.2020.140509

Elagib, N. A., Gayoum Saad, S. A., Basheer, M., Rahma, A. E., & Gore, E. D. L. (2021). Exploring the urban water-energy-food nexus under environmental hazards within the Nile. *Stochastic Environmental Research and Risk Assessment*, *35*(1), 21–41. https://doi.org/10.1007/s00477-019-01706-x

Elsayed, H., Djordjević, S., Savić, D. A., Tsoukalas, I., & Makropoulos, C. (2020). The Nile Water-Food-Energy Nexus under Uncertainty: Impacts of the Grand Ethiopian Renaissance Dam. *Journal of Water Resources Planning and Management*, *146*(11). https://doi.org/10.1061/(ASCE)WR.1943-5452.0001285

Elsayed, H., Djordjevic, S., Savic, D., Tsoukalas, I., & Makropoulos, C. (2022). Water-food-energy nexus for transboundary cooperation in Eastern Africa. *Water Supply*, *22*(4), 3567–3587. https://doi.org/10.2166/ws.2022.001

Falchetta, G., Adeleke, A., Awais, M., Byers, E., Copinschi, P., Duby, S., Hughes, A., Ireland, G., Riahi, K., Rukera-Tabaro, S., Semeria, F., Shendrikova, D., Stevanato, N., Troost, A., Tuninetti, M., Vinca, A., Zulu, A., & Hafner, M. (2022). A renewable energy-centred research agenda for planning and financing Nexus development objectives in rural sub-Saharan Africa. *Energy Strategy Reviews*, *43*(May), 100922. https://doi.org/10.1016/j.esr.2022.100922

Fan, C., Lin, C. Y., & Hu, M. C. (2019). Empirical framework for a relative sustainability evaluation of urbanization on the water–energy–food nexus using simultaneous equation analysis. *International Journal of Environmental Research and Public Health*, *16*(6). https://doi.org/10.3390/ijerph16060901

Fang, C., Li, Z., Shi, W., & Wang, J. (2023). Analysis of Pollution Characteristics and Emissions Reduction Measures in the Main Cotton Area of Xinjiang. *International Journal of Environmental Research and Public Health*, *20*(3). https://doi.org/10.3390/ijerph20032273

Fao. (2014). *Walking the Nexus Talk: Assessing the Water-Energy-Food Nexus in the Context of the Sustainable Energy for All Initiative*. http://www.fao.org/icatalog/inter-e.htm

Feldman, A. F., Short Gianotti, D. J., Trigo, I. F., Salvucci, G. D., & Entekhabi, D. (2022). Observed Landscape Responsiveness to Climate Forcing. *Water Resources Research*, *58*(1). https://doi.org/10.1029/2021WR030316

Fersch, B., & Kunstmann, H. (2014). Atmospheric and terrestrial water budgets: Sensitivity and performance of configurations and global driving data for long term continental scale WRF simulations. *Climate Dynamics*, *42*(9–10), 2367–2396. https://doi.org/10.1007/s00382-013-1915-5

Fleischmann, J., Birkel, C., Blechinger, P., Ribbe, L., Nauditt, A., Corigliano, S., & Platzer, W. (2024). Guiding the data collection for integrated Water-Energy-Food-Environment systems using a pilot smallholder farm in Costa Rica. *Energy Nexus*, *13*. https://doi.org/10.1016/j.nexus.2023.100259

Funk, C., Peterson, P., Landsfeld, M., Pedreros, D., Verdin, J., Shukla, S., Husak, G., Rowland, J., Harrison, L., Hoell, A., & Michaelsen, J. (2015). The climate hazards infrared precipitation with stations — a new environmental record for monitoring extremes. *Scientific Data*, *2*(150066), 1–21. https://doi.org/10.1038/sdata.2015.66

Gao, J. (2020). *Global 1-km Downscaled Population Base Year and Projection Grids Based on the Shared Socioeconomic Pathways, Revision 01*. NASA Socioeconomic Data and Applications Center (SEDAC). https://doi.org/10.7927/q7z9-9r69

Gao, J., & Liu, Y. (2011). Climate warming and land use change in Heilongjiang Province, Northeast China. *Applied Geography*, *31*(2), 476–482. https://doi.org/10.1016/j.apgeog.2010.11.005

García-Álvarez, D., Teresa Camacho Olmedo, M., Paegelow, M., & François Mas, J. (2022). *Validation Practices with QGIS Land Use Cover Datasets and Validation Tools*.

García-García, A., Cuesta-Valero, F. J., Beltrami, H., González-Rouco, J. F., & García-Bustamante, E. (2022). WRF v.3.9 sensitivity to land surface model and horizontal resolution changes over North America. *Geoscientific Model Development*, *15*(2), 413–428. https://doi.org/10.5194/gmd-15-413-2022

García-García, A., José Cuesta-Valero, F., Beltrami, H., González-Rouco, F., García-Bustamante, E., & Finnis, J. (2020). Land surface model influence on the simulated climatologies of temperature and precipitation extremes in the WRF v3.9 model over North America. *Geoscientific Model Development*, *13*(11), 5345–5366. https://doi.org/10.5194/gmd-13-5345-2020

Garcia, M., Özdogan, M., & Townsend, P. A. (2015). Impacts of forest harvest on cold season land surface conditions and land-atmosphere interactions in northern Great Lakes states. *Journal of Advances in Modeling Earth Systems*, *6*(3), 923–937. https://doi.org/10.1002/2014MS000317

Gebreyes, M., Bazzana, D., Simonetto, A., Müller-Mahn, D., Zaitchik, B., Gilioli, G., & Simane, B. (2020). Local perceptions of water-energy-food security: Livelihood consequences of dam construction in Ethiopia. *Sustainability (Switzerland)*, *12*(6). https://doi.org/10.3390/su12062161

Gochis, D. J., Barlage, M., Cabell, R., Casali, M., Dugger, A., FitzGerald, K., McAllister, M., McCreight, J., RafieeiNasab, A., Read, L., Sampson, K., Yates, D., & Zhang, Y. (2021). The NCAR WRF-Hydro Modeling System Technical Description. *User Manual, Version 5.1.1.*, 108. https://ral.ucar.edu/sites/default/files/public/WRFHydroV511TechnicalDescription.pdf.

Gogoi, P. P., Vinoj, V., Swain, D., Roberts, G., Dash, J., & Tripathy, S. (2019). Land use and land cover change effect on surface temperature over Eastern India. *Scientific Reports*, *9*(1). https://doi.org/10.1038/s41598-019-45213-z

Goutorbe, J.-P. (1993). A large scale study of land-atmosphere interactions in the semiarid tropics (HAPEX-Sahel). In *Exchange processes at the land surface for a range of space and time scales. Proc. international symposium, Yokohama, 1993*.

Graf, M., Arnault, J., Fersch, B., & Kunstmann, H. (2021). Is the soil moisture precipitation feedback enhanced by heterogeneity and dry soils? A comparative study. *Hydrological Processes*, *35*(9). https://doi.org/10.1002/hyp.14332

Grell, G. A., & Freitas, S. R. (2014). A scale and aerosol aware stochastic convective parameterization for weather and air quality modeling. *Atmospheric Chemistry and Physics*, *14*(10), 5233–5250. https://doi.org/10.5194/acp-14-5233-2014

Grigg, N., Foran, T., Darbas, T., Kirby, M., Colloff, M. J., Ahmad, M.-U.-D., & Podger, G. (2018). The water-food-energy nexus in Pakistan: A biophysical and socio-economic challenge. *Proceedings of the International Association of Hydrological Sciences*, *376*, 9–13. https://doi.org/10.5194/piahs-376-9-2018

Gross, E., & Pennink, C. (2018). *Impact Evaluation of the Sustainable Water Fund (FDW) Integrated Water Management and Knowledge Transfer in Sisili Kulpawn Basin (FDW / 12 / GH / 02) in the Northern Region of Ghana Final report December 2018* (Issue December).

Guidigan, M. L. G., Sanou, C. L., Ragatoa, D. S., Fafa, C. O., & Mishra, V. N. (2019). Assessing Land Use/Land Cover Dynamic and Its Impact in Benin Republic Using Land Change Model and CCI-LC Products. *Earth Systems and Environment*, *3*(1), 127–137. https://doi.org/10.1007/s41748-018-0083-5

Gupta, H. V., Kling, H., Yilmaz, K. K., & Martinez, G. F. (2009). Decomposition of the mean squared error and NSE performance criteria: Implications for improving hydrological modelling. *Journal of Hydrology*, *377*(1–2), 80–91. https://doi.org/10.1016/j.jhydrol.2009.08.003

Gütschow, J., Louise Jeffery, M., Günther, A., & Meinshausen, M. (2021). Country-resolved combined emission and socio-economic pathways based on the Representative Concentration Pathway (RCP) and Shared Socio-Economic Pathway (SSP) scenarios. *Earth System Science Data*, *13*(3), 1005–1040. https://doi.org/10.5194/essd-13-1005-2021

Hanjra, M. A. (2013). Global food security: Emerging issues and economic implications. In *Global Food Security: Emerging Issues and Economic Implications*.

Hardwick, S. R., Toumi, R., Pfeifer, M., Turner, E. C., Nilus, R., & Ewers, R. M. (2015). The relationship between leaf area index and microclimate in tropical forest and oil palm plantation: Forest disturbance drives changes in microclimate. *Agricultural and Forest Meteorology*, *201*. https://doi.org/10.1016/j.agrformet.2014.11.010

Harris, I., Osborn, T. J., Jones, P., & Lister, D. (2020). Version 4 of the CRU TS monthly high-resolution gridded multivariate climate dataset. *Scientific Data*, *7*(1), 1–18. https://doi.org/10.1038/s41597-020-0453-3

Herrmann, S. M., Brandt, M., Rasmussen, K., & Fensholt, R. (2020). Accelerating land cover change in West Africa over four decades as population pressure increased. *Communications Earth & Environment*, *1*(1), 1–10. https://doi.org/10.1038/s43247-020-00053-y

Hersbach, H., Bell, B., Berrisford, P., Hirahara, S., Horányi, A., Muñoz-Sabater, J., Nicolas, J., Peubey, C., Radu, R., Schepers, D., Simmons, A., Soci, C., Abdalla, S., Abellan, X., Balsamo, G., Bechtold, P., Biavati, G., Bidlot, J., Bonavita, M., … Thépaut, J. N. (2020). The

ERA5 global reanalysis. *Quarterly Journal of the Royal Meteorological Society*, *146*(730), 1999–2049. https://doi.org/10.1002/qj.3803

Higgins, C. W., & Najm, M. A. (2020). An organizing principle for the water-energy-food nexus. *Sustainability (Switzerland)*, *12*(19), 1–15. https://doi.org/10.3390/su12198135

Hilland, R. V. J., Bernhofer, C., Bohmann, M., Christen, A., Katurji, M., Maggs-Kölling, G., Krauß, M., Larsen, J. A., Marais, E., Pitacco, A., Vendrame, N., & Vogt, R. (2022). The Namib Turbulence Experiment: Investigating Surface-Atmosphere Heat Transfer in Three Dimensions. *Bulletin of the American Meteorological Society*, *103*(3), E741–E759. https://doi.org/10.1175/BAMS-D-20-0269.1

Hirwa, H., Zhang, Q., Qiao, Y., Peng, Y., Leng, P., Tian, C., Khasanov, S., Li, F., Kayiranga, A., Muhirwa, F., Habiyaremye, G., & Ngamije, J. (2021). Insights on water and climate change in the greater horn of africa: Connecting virtual water and water-energy-food-biodiversity-health nexus. *Sustainability (Switzerland)*, *13*(11). https://doi.org/10.3390/su13116483

Hoff, H. (2011). Understanding the Nexus. Background paper for the Bonn2011 Nexus Conference: *Stockholm Environment Institute, November*, 1–52.

Hong, S., & Lim, J.-O. J. (2006). The WRF Single-Moment 6-Class Microphysics Scheme (WSM6) Song-You. *JOURNAL OF THE KOREAN METEOROLOGICAL SOCIETY*, *42*(2), 129–151.

Hou, S. shuang, Yu, L. fei, Yan, W., Gu, S. hong, & Gu, X. ping. (2021). The effects of land use changes on climate warming by source-sink theory. *Arabian Journal of Geosciences*, *14*(7), 1–17. https://doi.org/10.1007/s12517-021-06678-3.

Houghton, R., Connors, S., & Krinner, G. (2019). *Land–climate interactions*. https://doi.org/https://doi.org/10.1017/9781009157988.004

Huffman, G., Bolvin, D., Braithwaite, D., Hsu, K., Joyce, R., Kidd, C., Nelkin, E., Sorooshian, S., Tan, J., & Xie, P. (2020). NASA GPM Integrated Multi-satellitE Retrievals for GPM (IMERG) Algorithm Theoretical Basis Document (ATBD) Version 06. *Nasa/Gsfc*, *January*,29.https://pmm.nasa.gov/sites/default/files/imce/times_allsat.jpg%0Ahttps://pmm.nasa.gov/sites/default/files/document_files/IMERG_ATBD_V06.pdf.

Irfan, U. (2021). IPCC 2021 report: How bad will climate change get? *VOX*, *Sep*.

Jach, L., Warrach-Sagi, K., Ingwersen, J., Kaas, E., & Wulfmeyer, V. (2020). Land Cover Impacts on Land-Atmosphere Coupling Strength in Climate Simulations With WRF Over Europe. *Journal of Geophysical Research: Atmospheres*, *125*(18). https://doi.org/10.1029/2019JD031989

Jiang, L., & Yu, L. (2019). Analyzing land use intensity changes within and outside protected areas using ESA CCI-LC datasets. *Global Ecology and Conservation*, *20*(July 2018). https://doi.org/10.1016/j.gecco.2019.e00789

John, T. W., Sušnik, J., Masia, S., & Jewitt, G. (2023). Towards realization of nexus-doing at the grassroots level: Water-energy-food governance assessment in the Songwe River Basin (Tanzania and Malawi). *Environmental Science and Policy*, *150*. https://doi.org/10.1016/j.envsci.2023.103596

Jones, B., & O'Neill, B. C. (2016). Spatially explicit global population scenarios consistent with the Shared Socioeconomic Pathways. *Environmental Research Letters*, *11*(8). https://doi.org/10.1088/1748-9326/11/8/084003

Jung, M., Koirala, S., Weber, U., Ichii, K., Gans, F., Camps-Valls, G., Papale, D., Schwalm, C., Tramontana, G., & Reichstein, M. (2019). The FLUXCOM ensemble of global land-atmosphere energy fluxes. *Scientific Data*, *6*(1), 1–14. https://doi.org/10.1038/s41597-019-0076-8

Kabo-Bah, A., Diji, Chuks., Nokoe, K., Mulugetta, Y., Obeng-Ofori, D., & Akpoti, K. (2016). Multiyear Rainfall and Temperature Trends in the Volta River Basin and their Potential Impact on Hydropower Generation in Ghana. *Climate*, *4*(4), 49. https://doi.org/10.3390/cli4040049

Kankam-Yeboah, K., Obuobie, E., Amisigo, B., & Opoku-Ankomah, Y. (2013). Impact du changement climatique sur les débits de plusieurs bassins au Ghana. *Hydrological Sciences Journal*, *58*(4), 773–788. https://doi.org/10.1080/02626667.2013.782101

Kaptue Tchuente, A. T., Roujean, J.-L., & Faroux, S. (2010). ECOCLIMAP-II: An ecosystem classification and land surface parameters database of Western Africa at 1 km resolution for the African Monsoon Multidisciplinary Analysis (AMMA) project. *Remote Sensing of Environment*, *114*(5), 961–976. https://doi.org/10.1016/j.rse.2009.12.008

KC, S., & Lutz, W. (2017). The human core of the shared socioeconomic pathways: Population scenarios by age, sex and level of education for all countries to 2100. *Global Environmental Change*, *42*, 181–192. https://doi.org/10.1016/j.gloenvcha.2014.06.004

Kerandi, N., Arnault, J., Laux, P., Wagner, S., Kitheka, J., & Kunstmann, H. (2017). *Joint atmospheric-terrestrial water balances for East Africa : a WRF-Hydro case study for the upper Tana River basin*. https://doi.org/10.1007/s00704-017-2050-8

Keys, P. W., Warrier, R., Van Der Ent, R. J., Galvin, K. A., & Boone, R. B. (2022). Analysis of Kenya's Atmospheric Moisture Sources and Sinks. *Earth Interactions*, *26*(1), 139–150. https://doi.org/10.1175/EI-D-21-0016.1

Khacheba, R., Cherfaoui, M., Hartani, T., & Drouiche, N. (2018). The nexus approach to water–energy–food security: An option for adaptation to climate change in Algeria. *Desalination and Water Treatment*, *131*. https://doi.org/10.5004/dwt.2018.22950

Koranteng, A., Adu-Poku, I., & Zawiła-Niedwiecki, T. (2019). Landuse and land cover dynamics in the Volta River Basin surrounding APSD forest plantation, Ghana. *Folia Forestalia Polonica, Series A*, *61*(1), 78–89. https://doi.org/10.2478/ffp-2019-0008

Koster, R. D., Chang, Y., Wang, H., & Schubert, S. D. (2016). Impacts of local soil moisture anomalies on the atmospheric circulation and on remote surface meteorological fields during boreal summer: A comprehensive analysis over North America. *Journal of Climate*, *29*(20), 7345–7364. https://doi.org/10.1175/JCLI-D-16-0192.1

Krähenmann, S., Kothe, S., Panitz, H.-J., & Ahrens, B. (2013). Evaluation of daily maximum and minimum 2-m temperatures as simulated with the regional climate model COSMO-CLM over Africa. *Meteorologische Zeitschrift*, *22*(3), 297–316. https://doi.org/10.1127/0941-2948/2013/0468

Kumar, S., Dirmeyer, P. A., Merwade, V., Delsole, T., Adams, J. M., & Niyogi, D. (2013). Land use/cover change impacts in CMIP5 climate simulations: A new methodology and 21st century challenges. *Journal of Geophysical Research Atmospheres*, *118*(12), 6337–6353. https://doi.org/10.1002/jgrd.50463

Lahmouri, M., Drewes, J. E., & Gondhalekar, D. (2019). Analysis of greenhouse gas emissions in centralized and decentralizedwater reclamation with resource recovery strategies in Leh Town, Ladakh, India, and potential for their reduction in context of the Water-Energy-Food Nexus. *Water (Switzerland)*, *11*(5). https://doi.org/10.3390/w11050906

Laspidou, C. S., Mellios, N., & Kofinas, D. (2019). Towards ranking the water-energy-food-land use-climate nexus interlinkages for building a nexus conceptual model with a Heuristic Algorithm. *Water (Switzerland)*, *11*(2). https://doi.org/10.3390/w11020306

Laux, P., Dieng, D., Portele, T. C., Wei, J., Shang, S., Zhang, Z., Arnault, J., Lorenz, C., & Kunstmann, H. (2021). A High-Resolution Regional Climate Model Physics Ensemble for Northern Sub-Saharan Africa. *Frontiers in Earth Science*, *9*(September), 1–16. https://doi.org/10.3389/feart.2021.700249

Laux, P., Nguyen, P. N. B., Cullmann, J., & Kunstmann, H. (2017). Impacts of land-use/land-cover change and climate change on the regional climate in the central Vietnam. *Land Use and Climate Change Interactions in Central Vietnam: LUCCi*, 143–151.

Lawford, R., Bogardi, J., Marx, S., Jain, S., Ringler, C., Wostl, C. P., Knu, K., Lansigan, F., & Meza, F. (2013). Basin perspectives on the Water – Energy – Food Security Nexus. *Elsevier*, 607–616. https://doi.org/10.1016/j.cosust.2013.11.005

Lawrence, D., & Vandecar, K. (2015). Effects of tropical deforestation on climate and agriculture. In *Nature Climate Change* (Vol. 5, Issue 1, pp. 27–36). Nature Publishing Group. https://doi.org/10.1038/nclimate2430

Lazaro, L. L. B., Bellezoni, R. A., Puppim de Oliveira, J. A., Jacobi, P. R., & Giatti, L. L. (2022). Ten Years of Research on the Water-Energy-Food Nexus: An Analysis of Topics Evolution. *Frontiers in Water*, *4*. https://doi.org/10.3389/frwa.2022.859891

Lee, J., Seo, J. M., Baik, J. J., Park, S. B., & Han, B. S. (2020). A Numerical study of windstorms in the Lee of the Taebaek mountains, South Korea: Characteristics and generation mechanisms. *Atmosphere*, *11*(4). https://doi.org/10.3390/ATMOS11040431

Lehner, B., Verdin, K., & Jarvis, A. (2008). New global hydrography derived from spaceborne elevation data. *Eos*, *89*(10), 93–94. https://doi.org/10.1029/2008EO100001

Li, F., & Lawrence, D. M. (2017). Role of fire in the global land water budget during the twentieth century due to changing ecosystems. *Journal of Climate*, *30*(6), 1893–1908. https://doi.org/10.1175/JCLI-D-16-0460.1

Li, G., Meng, X., Blyth, E., Chen, H., Shu, L., Li, Z., Zhao, L., & Ma, Y. (2021). Impact of fully coupled hydrology-atmosphere processes on atmosphere conditions: Investigating the performance of the wrf-hydro model in the three river source region on the tibetan plateau, china. *Water (Switzerland)*, *13*(23). https://doi.org/10.3390/w13233409

Li, J., Cui, J., Sui, P., Yue, S., Yang, J., Lv, Z., Wang, D., Chen, X., Sun, B., Ran, M., & Chen, Y. (2021). Valuing the synergy in the water-energy-food nexus for cropping systems: a case in the North China Plain. *Ecological Indicators*, *127*, 107741. https://doi.org/10.1016/j.ecolind.2021.107741

Li, L., Gochis, D. J., Sobolowski, S., & Mesquita, M. D. S. (2017). Evaluating the present annual water budget of a Himalayan headwater river basin using a high-resolution atmosphere-hydrology model. *Journal of Geophysical Research*, *122*(9), 4786–4807. https://doi.org/10.1002/2016JD026279

Li, L., Pontoppidan, M., Sobolowski, S., & Senatore, A. (2020a). The impact of initial conditions on convection-permitting simulations of a flood event over complex mountainous terrain. *Hydrology and Earth System Sciences*, *24*(2), 771–791. https://doi.org/10.5194/hess-24-771-2020

Limantol, A. M., Larbi, I., Dotse, S. Q., Okafor, G. C., Asare-Nuamah, P., Frimpong, L. K., Alhassan, A. R. M., Angmor, E., Premkumar, J. P. J., Lutterodt, G., Asiamah, T. A., Atta-Darkwa, T., Kumi, N., & Prempeh, N. A. (2023). An increase in temperature under the shared socioeconomic scenarios in the Volta River Basin, West Africa: implications for economic development. *Journal of Water and Climate Change*, *14*(8), 2808–2824. https://doi.org/10.2166/wcc.2023.141

Liu, C., Yang, C., Yang, Q., & Wang, J. (2021). Spatiotemporal drought analysis by the standardized precipitation index (SPI) and standardized precipitation evapotranspiration index (SPEI) in Sichuan Province ,. *Scientific Reports*, *11*(1280), 1–14. https://doi.org/10.1038/s41598-020-80527-3

Liu, J., Shao, Q., Yan, X., Fan, J., Zhan, J., Deng, X., Kuang, W., & Huang, L. (2016). The climatic impacts of land use and land cover change compared among countries. *Journal of Geographical Sciences*, *26*(7), 889–903. https://doi.org/10.1007/s11442-016-1305-0

Liu, S., Liu, X., Yu, L., Wang, Y., Zhang, G. J., Gong, P., Huang, W., & Wang, B. (2021). Climate response to introduction of the ESA CCI land cover data to the NCAR CESM. *Climate Dynamics*, *56*(11), 4109–4127. https://doi.org/10.1007/s00382-021-05690-3

Liu, S., Wu, Q., Yao, Y., & Schroeder, S. R. (2023). The Role of Coupled North Pacific Atmosphere–Ocean Interactions in Impacts of Tibetan Plateau Snow Anomalies on the Northern Hemisphere Winter Atmospheric Circulation. *Journal of Climate*, *36*(5), 1369–1385. https://doi.org/10.1175/JCLI-D-22-0261.1

Liu, X., Yu, L., Sia, Y., Zhang, C., Lu, H., Yu, C., & Gong, P. (2018). Identifying patterns and hotspots of global land cover transitions using the ESA CCI land cover dataset. *Remote Sensing Letters*, *9*(10), 972–981. https://doi.org/10.1080/2150704X.2018.1500070

Liu, Y., Ge, J., Guo, W., Cao, Y., Chen, C., Luo, X., Yang, L., & Wang, S. (2023). Revisiting Biophysical Impacts of Greening on Precipitation Over the Loess Plateau of China Using WRF With Water Vapor Tracers. *Geophysical Research Letters*, *50*(8). https://doi.org/10.1029/2023GL102809

Liu, Y., Jiang, Y., Xu, C., Lyu, J., & Su, Z. (2022). A quantitative analysis framework for water-food-energy nexus in an agricultural watershed using WEAP-MODFLOW. *Sustainable Production and Consumption*, *31*, 693–706. https://doi.org/10.1016/j.spc.2022.03.032

Li, W., Macbean, N., Ciais, P., Defourny, P., Lamarche, C., Bontemps, S., Houghton, R. A., & Peng, S. (2018). Gross and net land cover changes in the main plant functional types derived from the annual ESA CCI land cover maps (1992 – 2015). *Earth System Science Data*, *10*, 219–234. https://doi.org/https://doi.org/10.5194/essd-10-219-2018

Li, Y., Zhao, M., Motesharrei, S., Mu, Q., Kalnay, E., & Li, S. (2015). Local cooling and warming effects of forests based on satellite observations. *Nature Communications*, *6*. https://doi.org/10.1038/ncomms7603

Li, Z., Deng, X., Shi, Q., Ke, X., & Liu, Y. (2013). Modeling the impacts of boreal deforestation on the near-surface temperature in european Russia. *Advances in Meteorology*, *2013*. https://doi.org/10.1155/2013/486962

Lodh, A. (2020). Reassessment of land–atmosphere interactions over India during summer monsoon using state-of-the-art regional climate models. *Theoretical and Applied Climatology*, *142*(3–4), 1649–1673. https://doi.org/10.1007/s00704-020-03395-x

Loveland, T. R., & Giri, C. P. (2012). History of land-cover mapping. *Remote Sensing of Land Use and Land Cover. CRC Press, Boca Raton, USA. Http://Dx. Doi. Org/Http://Dx. Doi. Org/10.1201/B11964-4*, 13–22.

Lu, X., Chen, Y., Huang, Y., Lin, C., Li, Z., Fung, J. C. H., & Lau, A. K. H. (2019). Differences in concentration and source apportionment of PM 2.5 between 2006 and 2015 over the PRD region in southern China. *Science of the Total Environment*, *673*, 708–718. https://doi.org/10.1016/j.scitotenv.2019.03.452

Lu, X., Sha, Y. H., Li, Z., Huang, Y., Chen, W., Chen, D., Shen, J., Chen, Y., & Fung, J. C. H. (2021). Development and application of a hybrid long-short term memory – three dimensional variational technique for the improvement of PM2.5 forecasting. *Science of the Total Environment*, *770*. https://doi.org/10.1016/j.scitotenv.2020.144221

Ma, E., Deng, X., Zhang, Q., & Liu, A. (2014). Spatial variation of surface energy fluxes due to land use changes across China. *Energies*, *7*(4), 2194–2206. https://doi.org/10.3390/en7042194

Ma, E., Liu, A., Li, X., Wu, F., & Zhan, J. (2013). Impacts of vegetation change on the regional surface climate: A scenario-based analysis of afforestation in Jiangxi Province, China. *Advances in Meteorology*, *2013*. https://doi.org/10.1155/2013/796163

Ma, H.-Y., Mechoso, C. R., Xue, Y., Xiao, H., Neelin, J. D., & Ji, X. (2013). On the connection between continental-scale land surface processes and the tropical climate in a coupled ocean-atmosphere-land system. *Journal of Climate*, *26*(22), 9006–9025. https://doi.org/10.1175/JCLI-D-12-00819.1

Maisha, R. T., Ndarana, T., Engelbrecht, F. A., Thatcher, M., Bopape, M.-J. M., van der Merwe, J., Padayachi, Y., & Masemola, A. C. (2023). Simulation of the eThekwini Heat Island in South Africa. *Journal of Applied Meteorology and Climatology*, *62*(5), 589–609. https://doi.org/10.1175/JAMC-D-21-0231.1

Malagó, A., Comero, S., Bouraoui, F., Kazezyılmaz-Alhan, C. M., Gawlik, B. M., Easton, P., & Laspidou, C. (2021). An analytical framework to assess SDG targets within the context of WEFE nexus in the Mediterranean region. *Resources, Conservation and Recycling*, *164*, 105205. https://doi.org/10.1016/j.resconrec.2020.105205

Malek, K., Stöckle, C., Chinnayakanahalli, K., Nelson, R., Liu, M., Rajagopalan, K., Barik, M., & Adam, J. C. (2017). VIC-CropSyst-v2: A regional-scale modeling platform to simulate the nexus of climate, hydrology, cropping systems, and human decisions. *Geoscientific Model Development*, *10*(8), 3059–3084. https://doi.org/10.5194/gmd-10-3059-2017

Marcella, M. P., & Eltahir, E. A. B. (2014). Introducing an irrigation scheme to a regional climate model: A case study over West Africa. *Journal of Climate*, *27*(15), 5708–5723. https://doi.org/10.1175/JCLI-D-13-00116.1

Martens, B., Miralles, D. G., Lievens, H., Van Der Schalie, R., De Jeu, R. A. M., Fernández-Prieto, D., Beck, H. E., Dorigo, W. A., & Verhoest, N. E. C. (2017). GLEAM v3: Satellite-based land evaporation and root-zone soil moisture. *Geoscientific Model Development*, *10*(5), 1903–1925. https://doi.org/10.5194/gmd-10-1903-2017

Matsumura, S., Yamazaki, K., & Tokioka, T. (2010). Summertime land-atmosphere interactions in response to anomalous springtime snow cover in northern Eurasia. *Journal of Geophysical Research Atmospheres*, *115*(20). https://doi.org/10.1029/2009JD012342

Matthews, N., & McCartney, M. (2018). Opportunities for building resilience and lessons for navigating risks: Dams and the water energy food nexus. *Environmental Progress and Sustainable Energy*, *37*(1), 56–61. https://doi.org/10.1002/ep.12568

McCarl, B. A., Yang, Y., Schwabe, K., Engel, B. A., Mondal, A. H., Ringler, C., & Pistikopoulos, E. N. (2017). Model Use in WEF Nexus Analysis: a Review of Issues. *Current Sustainable/Renewable Energy Reports*, *4*(3), 144–152. https://doi.org/10.1007/s40518-017-0078-0

McCartney, M., Forkuor, G., Sood, A., Amisigo, B., Hattermann, F., & Muthuwatta, L. (2012). The water resource implications of changing climate in the Volta River Basin. In *IWMI Research Report* (Vol. 146). https://doi.org/10.5337/2012.219

McGrane, S. J., Acuto, M., Artioli, F., Chen, P. Y., Comber, R., Cottee, J., Farr-Wharton, G., Green, N., Helfgott, A., Larcom, S., McCann, J. A., O'Reilly, P., Salmoral, G., Scott, M., Todman, L. C., van Gevelt, T., & Yan, X. (2019). Scaling the nexus: Towards integrated frameworks for analysing water, energy and food. *Geographical Journal*, *185*(4), 419–431. https://doi.org/10.1111/geoj.12256

McKee, T. B., Doesken, N. J., & Kleist, J. (1993). The relationship of drought frequency and duration to time scales. *In Proceedings of the 8th Conference on Applied Climatology*, *17*(22), 179–183. https://doi.org/10.1088/1755-1315/5

Medvigy, D., Walko, R. L., Otte, M. J., & Avissar, R. (2013). Simulated changes in Northwest U.S. Climate in response to Amazon deforestation. *Journal of Climate*, *26*(22), 9115–9136. https://doi.org/10.1175/JCLI-D-12-00775.1

Meinshausen, M., Smith, S. J., Calvin, K., Daniel, J. S., Kainuma, M. L. T., Lamarque, J., Matsumoto, K., Montzka, S. A., Raper, S. C. B., Riahi, K., Thomson, A., Velders, G. J. M.,

& van Vuuren, D. P. P. (2011). The RCP greenhouse gas concentrations and their extensions from 1765 to 2300. *Climatic Change*, *109*(1), 213–241. https://doi.org/10.1007/s10584-011-0156-z

Mensah, J. K., Ofosu, E. A., Akpoti, K., Kabo-Bah, A. T., Okyereh, S. A., & Yidana, S. M. (2022). Modeling current and future groundwater demands in the White Volta River Basin of Ghana under climate change and socio-economic scenarios. *Journal of Hydrology: Regional Studies*, *41*(May), 101117. https://doi.org/10.1016/j.ejrh.2022.101117

Mensah, J. K., Ofosu, E. A., Yidana, S. M., Akpoti, K., & Kabo-bah, A. T. (2022). Integrated modeling of hydrological processes and groundwater recharge based on land use land cover, and climate changes: A systematic review. In *Environmental Advances* (Vol. 8). Elsevier Ltd. https://doi.org/10.1016/j.envadv.2022.100224

Mensah, J. K., Akpoti, K., Antwi-Ofosu, E., Kabo-bah, A. T., Siabi, E. K., Asare, A., Bakuri, R. W., & Yidana, S. M. (2024). Evaluating climate change scenarios in the white volta basin: A statistical bias-correction approach. *Physics and Chemistry of the Earth, Parts A/B/C*, *134*, 103584.

Mercer, A., & Dyer, J. (2021). Identification of Dominant Warm-Season Latent Heat Flux Patterns in the Lower Mississippi River Alluvial Valley. *Procedia Computer Science*, *185*, 1–8. https://doi.org/10.1016/j.procs.2021.05.001

Midgley, S. J. E., New, M., & Methner, N. (2018). Competition for land, water and energy (nexus) in food production. In *Encyclopedia of Food Security and Sustainability*. https://doi.org/10.1016/B978-0-08-100596-5.21993-8

Mitchard, E. T. A., & Flintrop, C. M. (2013). Woody encroachment and forest degradation in sub-Saharan Africa's woodlands and savannas 1982-2006. *Philosophical Transactions of the Royal Society B: Biological Sciences*, *368*(1625). https://doi.org/10.1098/rstb.2012.0406

Mlawer, E. J., Taubman, S. J., Brown, P. D., Iacono, M. J., & Clough, S. A. (1997). Radiative transfer for inhomogeneous atmospheres: RRTM, a validated correlated-k model for the longwave. *Journal of Geophysical Research Atmospheres*, *102*(14), 16663–16682. https://doi.org/10.1029/97jd00237

Mohino, E., Rodríguez-Fonseca, B., Mechoso, C. R., Gervois, S., Ruti, P., & Chauvin, F. (2011). Impacts of the tropical Pacific/Indian oceans on the seasonal cycle of the west african monsoon. *Journal of Climate*, *24*(15), 3878–3891. https://doi.org/10.1175/2011JCLI3988.1

Mohtar, R. H., & Daher, B. (2016). Water-Energy-Food Nexus Framework for facilitating multi-stakeholder dialogue. *Water International*, *41*(5), 655–661. https://doi.org/10.1080/02508060.2016.1149759

Molajou, A., Afshar, A., Khosravi, M., Soleimanian, E., Vahabzadeh, M., & Variani, H. A. (2021). A new paradigm of water, food, and energy nexus. *Environmental Science and Pollution Research*. https://doi.org/10.1007/s11356-021-13034-1

Mooney, P. A., Lee, H., & Sobolowski, S. (2021). Impact of Quasi-Idealized Future Land Cover Scenarios at High Latitudes in Complex Terrain. *Earth's Future*, *9*(2). https://doi.org/10.1029/2020EF001838

Mooney, P. A., Rechid, D., Davin, E. L., Katragkou, E., De Noblet-Ducoudré, N., Breil, M., Cardoso, R. M., Daloz, A. S., Hoffmann, P., Lima, D. C. A., Toelle, M. H., & Lund, M. T. (2022). Land-atmosphere interactions in sub-polar and alpine climates in the CORDEX Flagship Pilot Study Land Use and Climate Across Scales (LUCAS) models - Part 2: The role of changing vegetation. *Cryosphere*, *16*(4), 1383–1397. https://doi.org/10.5194/tc-16-1383-2022

Mooney, P. A., Sobolowski, S., & Lee, H. (2020). Designing and evaluating regional climate simulations for high latitude land use land cover change studies. *Tellus, Series A: Dynamic Meteorology and Oceanography*, *72*(1), 1–17. https://doi.org/10.1080/16000870.2020.1853437

Mpandeli, S., Naidoo, D., Mabhaudhi, T., Nhemachena, C., Nhamo, L., Liphadzi, S., Hlahla, S., & Modi, A. T. (2018). Climate change adaptation through the water-energy-food nexus in Southern Africa. *International Journal of Environmental Research and Public Health*, *15*(10). https://doi.org/10.3390/ijerph15102306

Mujere, N., & Chanza, N. (2022). Exploring the contribution of Tugwi-Mukosi Dam toward water, energy, and food security. In *Water - Energy - Food Nexus Narratives and Resource Securities: A Global South Perspective*. https://doi.org/10.1016/B978-0-323-91223-5.00005-8

Müller-Mahn, D., & Gebreyes, M. (2019). Controversial Connections: The water-energy-food nexus in the Blue Nile basin of Ethiopia. *Land*, *8*(9). https://doi.org/10.3390/land8090135

Muñoz-sabater, J., Dutra, E., Agustí-panareda, A., Albergel, C., Hersbach, H., Martens, B., Miralles, D. G., Piles, M., & Rodríguez-fernández, N. J. (2021). ERA5-Land : a state-of-the-art global reanalysis dataset for land applications. *Earth System Science Data*, *13*(9), 4349–4383.

Naabil, E., Kouadio, K., Lamptey, B., Annor, T., & Chukwudi Achugbu, I. (2022). Tono basin climate modeling, the potential advantage of fully coupled WRF/WRF-Hydro modeling System. *Modeling Earth Systems and Environment*. https://doi.org/10.1007/s40808-022-01574-5

Naabil, E., Lamptey, B. L., Arnault, J., Kunstmann, H., & Olufayo, A. (2017). Journal of Hydrology : Regional Studies Water resources management using the WRF-Hydro modelling system : Case-study of the Tono dam in West Africa. *Journal of Hydrology: Regional Studies*, *12*(December 2016), 196–209. https://doi.org/10.1016/j.ejrh.2017.05.010

Nakanishi, M., & Niino, H. (2004). An improved Mellor-Yamada level-3 Model with condensation physics: its design and verification. *Boundary-Layer Meteorology*, *112*, 1–31.

Namany, S., Al-ansari, T., & Govindan, R. (2019). Sustainable energy , water and food nexus systems : A focused review of decision-making tools for ef fi cient resource management and governance. *Journal of Cleaner Production*, *225*, 610–626. https://doi.org/10.1016/j.jclepro.2019.03.304

Nash, J. E., & Sutcliffe, J. V. (1970). River flow forecasting through conceptual models part I — A discussion of principles. *Journal of Hydrology*, *10*(3), 282–290. https://doi.org/10.1016/0022-1694(70)90255-6

Nhamo, L., Mabhaudhi, T., Mpandeli, S., Dickens, C., Nhemachena, C., Senzanje, A., Naidoo, D., Liphadzi, S., & Modi, A. T. (2020). An integrative analytical model for the water-energy-food nexus: South Africa case study. *Environmental Science and Policy*, *109*(December 2019), 15–24. https://doi.org/10.1016/j.envsci.2020.04.010

Nhamo, L., Ndlela, B., Nhemachena, C., Mabhaudhi, T., Mpandeli, S., & Matchaya, G. (2018). The water-energy-food nexus: Climate risks and opportunities in Southern Africa. *Water (Switzerland)*, *10*(5), 1–18. https://doi.org/10.3390/w10050567

Niu, G. Y., Yang, Z. L., Mitchell, K. E., Chen, F., Ek, M. B., Barlage, M., Kumar, A., Manning, K., Niyogi, D., Rosero, E., Tewari, M., & Xia, Y. (2011). The community Noah land surface model with multiparameterization options (Noah-MP): 1. Model description and evaluation with local-scale measurements. *Journal of Geophysical Research Atmospheres*, *116*(12), 1–19. https://doi.org/10.1029/2010JD015139

Obahoundje, S., & Diedhiou, A. (2022). Potential impacts of climate, land use and land cover changes on hydropower generation in West Africa: A review. In *Environmental Research Letters* (Vol. 17, Issue 4). IOP Publishing Ltd. https://doi.org/10.1088/1748-9326/ac5b3b

Obahoundje, S., Diedhiou, A., Dubus, L., Alamou, E. A., Amoussou, E., Akpoti, K., & Ofosu, E. A. (2022). Modeling climate change impact on inflow and hydropower generation of Nangbeto dam in West Africa using multi-model CORDEX ensemble and ensemble machine learning. *Applied Energy*, *325*, 119795.

Obahoundje, S., Ofosu, E., Akpoti, K., & Kabo-bah, A. (2017). Land Use and Land Cover Changes under Climate Uncertainty: Modelling the Impacts on Hydropower Production in Western Africa. *Hydrology*, *4*(1), 2. https://doi.org/10.3390/hydrology4010002

Odoulami, R. C., Abiodun, B. J., & Ajayi, A. E. (2019). Modelling the potential impacts of afforestation on extreme precipitation over West Africa. *Climate Dynamics*, *52*(3–4), 2185–2198. https://doi.org/10.1007/s00382-018-42486

Okyereh, S. A., Ofosu, E. A., & Kabobah, A. T. (2019). Modelling the impact of Bui dam operations on downstream competing water uses. *Water-Energy Nexus*, *2*(1), 1–9. https://doi.org/10.1016/j.wen.2019.03.001

O'Neill, B. (2016). *The Shared Socioeconomic Pathways (SSPs) and their extension and use in impact, adaptation and vulnerability studies*. 18. file:///F:/Spec 2/Traffic Delay Model.pdf

O'Neill, B. C., Carter, T. R., Ebi, K., Harrison, P. A., Kemp-Benedict, E., Kok, K., Kriegler, E., Preston, B. L., Riahi, K., Sillmann, J., van Ruijven, B. J., van Vuuren, D., Carlisle, D., Conde, C., Fuglestvedt, J., Green, C., Hasegawa, T., Leininger, J., Monteith, S., & Pichs-Madruga, R. (2020). Achievements and needs for the climate change scenario framework. *Nature Climate Change*, *10*(12), 1074–1084. https://doi.org/10.1038/s41558-020-00952-0

O'Neill, B. C., Tebaldi, C., Van Vuuren, D. P., Eyring, V., Friedlingstein, P., Hurtt, G., Knutti, R., Kriegler, E., Lamarque, J. F., Lowe, J., Meehl, G. A., Moss, R., Riahi, K., & Sanderson, B. M. (2016). The Scenario Model Intercomparison Project (ScenarioMIP) for CMIP6. *Geoscientific Model Development*, *9*(9), 3461–3482. https://doi.org/10.5194/gmd-9-3461-2016

Olson, J. M., Alagarswamy, G., Andresen, J. A., Campbell, D. J., Davis, A. Y., Ge, J., Huebner, M., Lofgren, B. M., Lusch, D. P., Moore, N. J., Torbick, N. M., & Wang, J. (2008). Integrating diverse methods to understand climate-land interactions in East Africa. *Geoforum*, *39*(2), 898–911. https://doi.org/10.1016/j.geoforum.2007.03.011

Ouedraogo, Y., Yamegueu, D., Fowe Tazen, Leye, B., Bologo Traore, M., & Konda, M. (2024). Addressing the Water-Energy-Food Nexus in the context of climate change: The case of Bagré dam in Burkina Faso. *Scientific African*, *24*. https://doi.org/10.1016/j.sciaf.2024.e02251

Pahl-wostl, C. (2017). Governance of the water-energy-food security nexus : A multi-level coordination challenge. *Environmental Science and Policy*, *January*, 1–12. https://doi.org/10.1016/j.envsci.2017.07.017

Paim, M. A., Salas, P., Lindner, S., Pollitt, H., Mercure, J. F., Edwards, N. R., & Viñuales, J. E. (2020). Mainstreaming the Water-Energy-Food Nexus through nationally determined contributions (NDCs): the case of Brazil. *Climate Policy*, *20*(2), 163–178. https://doi.org/10.1080/14693062.2019.1696736

Pardoe, J., Conway, D., Namaganda, E., Vincent, K., Dougill, A. J., & Kashaigili, J. J. (2018). Climate change and the water–energy–food nexus: insights from policy and practice in Tanzania. *Climate Policy*, *18*(7), 863–877. https://doi.org/10.1080/14693062.2017.1386082

Pasquier, U., Vahmani, P., & Jones, A. D. (2022). Quantifying the City-Scale Impacts of Impervious Surfaces on Groundwater Recharge Potential: An Urban Application of WRF–Hydro. *Water (Switzerland)*, *14*(19). https://doi.org/10.3390/w14193143

Payet-Burin, R., Kromann, M., Pereira-Cardenal, S., Marc Strzepek, K., & Bauer-Gottwein, P. (2019). WHAT-IF: An open-source decision support tool for water infrastructure investment planning within the water-energy-food-climate nexus. *Hydrology and Earth System Sciences*, *23*(10), 4129–4152. https://doi.org/10.5194/hess-23-4129-2019

Peña-Torres, D., Boix, M., & Montastruc, L. (2022). Optimization approaches to design water-energy-food nexus: A litterature review. *Computers and Chemical Engineering*, *167*(October). https://doi.org/10.1016/j.compchemeng.2022.108025

Perugini, L., Caporaso, L., Marconi, S., Cescatti, A., Quesada, B., De Noblet-Ducoudré, N., House, J. I., & Arneth, A. (2017). Biophysical effects on temperature and precipitation due to land cover change. *Environmental Research Letters*, *12*(5). https://doi.org/10.1088/1748-9326/aa6b3f

Pietschnig, M., Swann, A. L. S., Lambert, F. H., & Vallis, G. K. (2021). Response of tropical rainfall to reduced evapotranspiration depends on continental extent. *Journal of Climate*, *34*(23), 9221–9234. https://doi.org/10.1175/JCLI-D-21-0195.1

Polcher, J., & Laval, K. (1994). A statistical study of the regional impact of deforestation on climate in the LMD GCM. In *Climate Dynamics* (Vol. 10).

Quenum, G. M. L. D., Arnault, J., Klutse, N. A. B., Zhang, Z., Kunstmann, H., & Oguntunde, P. G. (2022). Potential of the Coupled WRF/WRF-Hydro Modeling System for Flood Forecasting in the Ouémé River (West Africa). *Water (Switzerland)*, *14*(8). https://doi.org/10.3390/w14081192

Rasul, G., & Neupane, N. (2021). Improving Policy Coordination Across the Water, Energy, and Food, Sectors in South Asia: A Framework. *Frontiers in Sustainable Food Systems*, *5*(February). https://doi.org/10.3389/fsufs.2021.602475

Reinhart, V., Fonte, C. C., Hoffmann, P., Bechtel, B., Rechid, D., & Boehner, J. (2021). Comparison of ESA climate change initiative land cover to CORINE land cover over Eastern Europe and the Baltic States from a regional climate modeling perspective. *International Journal of Applied Earth Observation and Geoinformation*, *94*(April 2020), 102221. https://doi.org/10.1016/j.jag.2020.102221

Riahi, K., van Vuuren, D. P., Kriegler, E., Edmonds, J., O'Neill, B. C., Fujimori, S., Bauer, N., Calvin, K., Dellink, R., Fricko, O., Lutz, W., Popp, A., Cuaresma, J. C., KC, S., Leimbach, M., Jiang, L., Kram, T., Rao, S., Emmerling, J., … Tavoni, M. (2017). The Shared Socioeconomic Pathways and their energy, land use, and greenhouse gas emissions implications: An overview. *Global Environmental Change*, *42*, 153–168. https://doi.org/10.1016/j.gloenvcha.2016.05.009

Robert Dickinson, B. E., & Henderson-sellers, A. (1988). *Modelling tropical deforestation: A study of GCM land-surface parametrizations* (Vol. 114).

Rogelj, J., Den Elzen, M., Höhne, N., Fransen, T., Fekete, H., Winkler, H., Schaeffer, R., Sha, F., Riahi, K., & Meinshausen, M. (2016). Paris Agreement climate proposals need a boost to keep warming well below 2 °c. *Nature*, *534*(7609), 631–639. https://doi.org/10.1038/nature18307

Rummler, T., Arnault, J., Gochis, D., & Kunstmann, H. (2019). Role of Lateral Terrestrial Water Flow on the Regional Water Cycle in a Complex Terrain Region: Investigation With a Fully Coupled Model System. *Journal of Geophysical Research: Atmospheres*, *124*(2), 507–529. https://doi.org/10.1029/2018JD029004

Rummukainen, M. (2016). Added value in regional climate modeling. *Wiley Interdisciplinary Reviews: Climate Change*, *7*(1), 145–159. https://doi.org/10.1002/wcc.378

Saha, M. V., D'Odorico, P., & Scanlon, T. M. (2019). Kalahari wildfires drive continental post-fire brightening in sub-Saharan Africa. *Remote Sensing*, *11*(9). https://doi.org/10.3390/rs11091090

Saha, M. V., Scanlon, T. M., & D'Odorico, P. (2016). Suppression of rainfall by fires in African drylands. *Geophysical Research Letters*, *43*(16), 8527–8533. https://doi.org/10.1002/2016GL069855

Sanchez Santillano, F. A., Koli, M., Cheo, A. E., Nguedia Nguedoung, A., & Tambo, E. G. (2022). Water-Energy-Food (WEF) Nexus Technologies in Africa's Sahel Region and SDGs 2, 6, and 7. In *SDGs in Africa and the Middle East Region* (pp. 1–23). Springer.

Sargentis, G. F., Lagaros, N. D., Cascella, G. L., & Koutsoyiannis, D. (2022). Threats in Water–Energy–Food–Land Nexus by the 2022 Military and Economic Conflict. *Land*, *11*(9). https://doi.org/10.3390/land11091569

Sargentis, G. F., Siamparina, P., Sakki, G. K., Efstratiadis, A., Chiotinis, M., & Koutsoyiannis, D. (2021). Agricultural land or photovoltaic parks? The water—energy— food nexus and land

development perspectives in the thessaly plain, Greece. *Sustainability (Switzerland)*, *13*(16). https://doi.org/10.3390/su13168935

Sawadogo, W., Abiodun, B. J., & Okogbue, E. C. (2019). Projected changes in wind energy potential over West Africa under the global warming of 1.5 °C and above. *Theoretical and Applied Climatology*, *138*(1–2), 321–333. https://doi.org/10.1007/s00704-019-02826-8

Schlemm, A., Mulligan, M., Tang, T., Agramont, A., Namugize, J., Malambala, E., & van Griensven, A. (2024). Developing meaningful water-energy-food-environment (WEFE) nexus indicators with stakeholders: An Upper White Nile case study. *Science of the Total Environment*, *931*. https://doi.org/10.1016/j.scitotenv.2024.172839

Senatore, A., Mendicino, G., Gochis, D. J., Yu, W., Yates, D. N., & Kunstmann, H. (2015). Fully coupled atmosphere-hydrology simulations for the central Mediterranean: Impact of enhanced hydrological parameterization for short and long time scales. *Journal of Advances in Modeling Earth Systems*, *7*(4), 1693–1715. https://doi.org/10.1002/2015MS000510

Shi, H., Luo, G., Zheng, H., Chen, C., Bai, J., Liu, T., Ochege, F. U., & De Maeyer, P. (2020). Coupling the water-energy-food-ecology nexus into a Bayesian network for water resources analysis and management in the Syr Darya River basin. *Journal of Hydrology*, *581*(August 2019), 124387. https://doi.org/10.1016/j.jhydrol.2019.124387

Shu, Q., Scott, M., Todman, L., & McGrane, S. J. (2021). Development of a prototype composite index for resilience and security of water-energy-food (WEF) systems in industrialised nations. *Environmental and Sustainability Indicators*, *11*(November 2020), 100124. https://doi.org/10.1016/j.indic.2021.100124

Siabi, E. K., Kabobah, A. T., Akpoti, K., Anornu, G. K., Amo-Boateng, M., & Nyantakyi, E. K. (2021). Statistical downscaling of global circulation models to assess future climate changes in the Black Volta basin of Ghana. *Environmental Challenges*, *5*(September), 100299. https://doi.org/10.1016/j.envc.2021.100299

Siabi, E. K., Kabobah, A. T., Akpoti, K., Anornu, G. K., Amo-Boateng, M., & Nyantakyi, E. K. (2021). Statistical downscaling of global circulation models to assess future climate changes in the Black Volta basin of Ghana. *Environmental Challenges*, *5*(September), 100299. https://doi.org/10.1016/j.envc.2021.100299

Siabi, E. K., Awafo, E. A., Kabo-bah, A. T., Derkyi, N. S. A., Akpoti, K., Mortey, E. M., & Yazdanie, M. (2023). Assessment of Shared Socioeconomic Pathway (SSP) climate scenarios and its impacts on the Greater Accra region. *Urban Climate*, *49*, 101432. https://doi.org/10.1016/j.uclim.2023.101432

Siakwah, P., & Torto, O. (2022). Analysis of the Complexities in the Water-Energy-Food Nexus: Ghana's Bui Dam Experience. *Frontiers in Sustainable Food Systems*, *6*. https://doi.org/10.3389/fsufs.2022.734675

Siderius, C., Biemans, H., Kashaigili, J., & Conway, D. (2022). Water conservation can reduce future water-energy-food-environment trade-offs in a medium-sized African river basin. *Agricultural Water Management*, *266*. https://doi.org/10.1016/j.agwat.2022.107548

Siderius, C., Kolusu, S. R., Todd, M. C., Bhave, A., Dougill, A. J., Reason, C. J. C., Mkwambisi, D. D., Kashaigili, J. J., Pardoe, J., Harou, J. J., Geressu, R. T., & Conway, D. (2021). Climate

variability affects water-energy-food infrastructure performance in East Africa. *One Earth*, *4*(3), 397–410. https://doi.org/10.1016/j.oneear.2021.02.009

Simpson, G. B., Jewitt, G. P. W., & Simpson, G. B. (2019a). *The Development of the Water-Energy-Food Nexus as a Framework for Achieving Resource Security: A Review*. *7*(February), 1–9. https://doi.org/10.3389/fenvs.2019.00008

Smiatek, G., & Kunstmann, H. (2023). Potential Impact of the Pan-African Great Green Wall on Sahelian Summer Precipitation: A Global Modeling Approach with MPAS. *Earth Interactions*, *27*(1). https://doi.org/10.1175/EI-D-22-0013.1

Snyder, P. K., Foley, J. A., Hitchman, M. H., & Delire, C. (2004). Analyzing the effects of complete tropical forest removal on the regional climate using a detailed three-dimensional energy budget: An application to Africa. *Journal of Geophysical Research D: Atmospheres*, *109*(21). https://doi.org/10.1029/2003JD004462

Somos-Valenzuela, M. A., & Palmer, R. N. (2018). Use of WRF-hydro over the Northeast of the US to estimate water budget tendencies in small watersheds. *Water (Switzerland)*, *10*(12). https://doi.org/10.3390/w10121709

Sood, A., Muthuwatta, L., & McCartney, M. (2013). A SWAT evaluation of the effect of climate change on the hydrology of the Volta River basin. *Water International*, *38*(3), 297–311. https://doi.org/10.1080/02508060.2013.792404

Sthapit, E., Lakhankar, T., Hughes, M., Khanbilvardi, R., Cifelli, R., Mahoney, K., Currier, W. R., Viterbo, F., & Rafieeinasab, A. (2022). Evaluation of Snow and Streamflows Using Noah-MP and WRF-Hydro Models in Aroostook River Basin, Maine. *Water (Switzerland)*, *14*(14). https://doi.org/10.3390/w14142145

Swap, R. J., Annegarn, H. J., Suttles, J. T., King, M. D., Platnick, S., Privette, J. L., & Scholes, R. J. (2003). Africa burning: A thematic analysis of the Southern African Regional Science Initiative (SAFARI 2000). *Journal of Geophysical Research: Atmospheres*, *108*(13). https://doi.org/10.1029/2003jd003747

Sylla, M. B., Pal, J. S., Wang, G. L., & Lawrence, P. J. (2016). Impact of land cover characterization on regional climate modeling over West Africa. *Climate Dynamics*, *46*(1–2), 637–650. https://doi.org/10.1007/s00382-015-2603-4

Tahiru, A. A., Doke, D. A., & Baatuuwie, B. N. (2020). Effect of land use and land cover changes on water quality in the Nawuni Catchment of the White Volta Basin, Northern Region, Ghana. *Applied Water Science*, *10*(8). https://doi.org/10.1007/s13201-020-01272-6

Takahashi, A., Kumagai, T., Kanamori, H., Fujinami, H., Hiyama, T., & Hara, M. (2017). Impact of tropical deforestation and forest degradation on precipitation over Borneo Island. *Journal of Hydrometeorology*, *18*(11), 2907–2922. https://doi.org/10.1175/JHM-D-17-0008.1

Tamoffo, A. T., Amekudzi, L. K., Weber, T., Vondou, D. A., Yamba, E. I., & Jacob, D. (2022). Mechanisms of Rainfall Biases in Two CORDEX-CORE Regional Climate Models at Rainfall Peaks over Central Equatorial Africa. *Journal of Climate*, *35*(2), 639–668. https://doi.org/10.1175/JCLI-D-21-0487.1

Taylor, C. M., & Clark, D. B. (2001). The diurnal cycle and African easterly waves: A land surface perspective. *Quarterly Journal of the Royal Meteorological Society*, *127*(573), 845–867. https://doi.org/10.1256/smsqj.57307

Thrasher, B., Wang, W., Michaelis, A., Melton, F., Lee, T., & Nemani, R. (2022). NASA Global Daily Downscaled Projections, CMIP6. *Scientific Data*, *9*(1), 1–6. https://doi.org/10.1038/s41597-022-01393-4

Tsendbazar, N. E., Bruin, S. de, Fritz, S., & Herold, M. (2015). Spatial accuracy assessment and integration of global land cover datasets. *Remote Sensing*, *7*(12), 15804–15821. https://doi.org/10.3390/rs71215804

UNEP-GEF Volta Project. (2013). *Volta Basin Transboundary Diagnostic Analysis - Addressing Transboundary Concerns in the Volta River Basin and its Downstream Coastal Area. UNEP/GEF/Volta/RR 4/2013* (Issue March).

CIESIN. (2018a). *Gridded Population of the World, Version 4 (GPWv4): Population Count Adjusted to Match 2015 Revision of UN WPP Country Totals*, *Revision 11*. NASA Socioeconomic Data and Applications Center (SEDAC). https://doi.org/10.7927/H4PN93PB

van Vuuren, D. P., Edmonds, J., Kainuma, M., Riahi, K., Thomson, A., Hibbard, K., Hurtt, G. C., Kram, T., Krey, V., Lamarque, J. F., Masui, T., Meinshausen, M., Nakicenovic, N., Smith, S. J., & Rose, S. K. (2011). The representative concentration pathways: An overview. *Climatic Change*, *109*(1), 5–31. https://doi.org/10.1007/s10584-011-0148-z

van Vuuren, D. P., Riahi, K., Calvin, K., Dellink, R., Emmerling, J., Fujimori, S., KC, S., Kriegler, E., & O'Neill, B. (2017). The Shared Socio-economic Pathways: Trajectories for human development and global environmental change. *Global Environmental Change*, *42*, 148–152. https://doi.org/10.1016/j.gloenvcha.2016.10.009

Verdin, A., Funk, C., Peterson, P., Landsfeld, M., Tuholske, C., & Grace, K. (2020). Development and validation of the CHIRTS-daily quasi-global high-resolution daily temperature data set. *Scientific Data*, *7*(1), 1–14. https://doi.org/10.1038/s41597-020-00643-7

Viccaro, M., Caniani, D., Masi, S., Romano, S., & Cozzi, M. (2022). Biofuels or not biofuels? The "Nexus Thinking" in land suitability analysis for energy crops. *Renewable Energy*, *187*, 1050–1064. https://doi.org/10.1016/j.renene.2022.02.008

Vicente-Serrano, S. M., Beguería, S., & López-Moreno, J. I. (2010). A Multiscalar Drought Index Sensitive to Global Warming : The Standardized Precipitation Evapotranspiration Index. *Journal of Climate*, *23*(7), 1696–1718. https://doi.org/10.1175/2009JCLI2909.1

Villegas, J. C., Dominguez, F., Barron-Gafford, G. A., Adams, H. D., Guardiola-Claramonte, M., Sommer, E. D., Selvey, A. W., Espeleta, J. F., Zou, C. B., Breshears, D. D., & Huxman, T. E. (2015). Sensitivity of regional evapotranspiration partitioning to variation in woody plant cover: Insights from experimental dryland tree mosaics. *Global Ecology and Biogeography*, *24*(9), 1040–1048. https://doi.org/10.1111/geb.12349

Wajid, M., Safi, A., Siddiqui, S., & Tariq, A. (2020). *Impact of Climate Change on Land use / Land cover of Chakwal District* (Vol. 11, Issue 2).

Wang, J., Li, J., Li, X., & Fang, C. (2022). Characteristics of Air Pollutants Emission and Its Impacts on Public Health of Chengdu, Western China. *International Journal of Environmental Research and Public Health*, *19*(24). https://doi.org/10.3390/ijerph192416852

Wang, L., Lee, X., Feng, D., Fu, C., Wei, Z., Yang, Y., Yin, Y., Luo, Y., & Lin, G. (2019). Impact of large-scale afforestation on surface temperature: A case study in the Kubuqi Desert, Inner Mongolia based on the WRF model. *Forests*, *10*(5). https://doi.org/10.3390/f10050368

Wang, X., Zhang, Z., Zhang, B., Tian, L., Tian, J., Arnault, J., Kunstmann, H., & He, C. (2023). Quantifying the impact of land use and land cover change on moisture recycling with convection-permitting WRF-tagging modeling in the agro-pastoral ecotone of northern China. *Journal of Geophysical Research: Atmospheres*, e2022JD038421.

Wrede, R., & Spiegel, M. R. (2002). Schaum's Outline of Advanced Calculus. In *Schaum's Outlines*.

Wulfmeyer, V., Branch, O., Warrach-Sagi, K., Bauer, H. S., Schwitalla, T., & Becker, K. (2014). The impact of plantations on weather and climate in coastal desert regions. *Journal of Applied Meteorology and Climatology*, *53*(5). https://doi.org/10.1175/JAMC-D-13-0208.1

Xiang, T., Vivoni, E. R., Gochis, D. J., & Mascaro, G. (2017). On the diurnal cycle of surface energy fluxes in the North American monsoon region using the WRF-Hydro modeling system. *Journal of Geophysical Research: Atmospheres*, *122*(17), 9024–9049. https://doi.org/10.1002/2017JD026472

Xu, R., Tie, X., Li, G., Zhao, S., Cao, J., Feng, T., & Long, X. (2018). Effect of biomass burning on black carbon (BC) in South Asia and Tibetan Plateau: The analysis of WRF-Chem modeling. *Science of the Total Environment*, *645*, 901–912. https://doi.org/10.1016/j.scitotenv.2018.07.165

Yamada, T. J., Kanae, S., Oki, T., & Koster, R. D. (2013). Seasonal variation of land-atmosphere coupling strength over the West African monsoon region in an atmospheric general circulation model. *Hydrological Sciences Journal*, *58*(6), 1276–1286. https://doi.org/10.1080/02626667.2013.814914

Yang, J., & Wang, Z.-H. (2014). Physical parameterization and sensitivity of urban hydrological models: Application to green roof systems. *Building and Environment*, *75*, 250–263. https://doi.org/10.1016/j.buildenv.2014.02.006

Yang, J., Yang, Y. C. E., Khan, H. F., Xie, H., Ringler, C., Ogilvie, A., Seidou, O., Djibo, A. G., van Weert, F., & Tharme, R. (2018). Quantifying the Sustainability of Water Availability for the Water-Food-Energy-Ecosystem Nexus in the Niger River Basin. *Earth's Future*, *6*(9), 1292–1310. https://doi.org/10.1029/2018EF000923

Yangouliba, G. I., Zoungrana, B. J.-B., Hackman, K. O., Koch, H., Liersch, S., Sintondji, L. O., Dipama, J.-M., Kwawuvi, D., Ouedraogo, V., & Yabré, S. (2023). Modelling past and future land use and land cover dynamics in the Nakambe River Basin, West Africa. *Modeling Earth Systems and Environment*, *9*(2), 1651–1667.

Yang, Y. C. E., & Wi, S. (2018). Informing regional water-energy-food nexus with system analysis and interactive visualization – A case study in the Great Ruaha River of Tanzania. *Agricultural Water Management*, *196*, 75–86. https://doi.org/10.1016/j.agwat.2017.10.022

Yildirim, G., & Rahman, A. (2022). Homogeneity and trend analysis of rainfall and droughts over Southeast Australia. *Natural Hazards*. https://doi.org/10.1007/s11069-022-05243-9

Yoshida, R., Onodera, Y., Tojo, T., Yamazaki, T., Kanno, H., Takayabu, I., & Suzuki-Parker, A. (2015). An application of a physical vegetation model to estimate climate change impacts on rice leaf wetness. *Journal of Applied Meteorology and Climatology*, *54*(7), 1482–1495. https://doi.org/10.1175/JAMC-D-14-0219.1

Yu, Y., Notaro, M., Wang, F., Mao, J., Shi, X., & Wei, Y. (2018). Validation of a statistical methodology for extracting vegetation feedbacks: Focus on North African ecosystems in the Community Earth System Model. *Journal of Climate*, *31*(4), 1565–1586. https://doi.org/10.1175/JCLI-D-17-0220.1

Zeppetello, L. R. V., Luke's, L. A., Spector, J. T., Naylor, R. L., Battisti, D. S., Masuda, Y. J., & Wolff, N. H. (2020). Large scale tropical deforestation drives extreme warming. *Environmental Research Letters*, *15*(8). https://doi.org/10.1088/1748-9326/ab96d2

Zhang, H., Chen, G., Hu, J., Chen, S. H., Wiedinmyer, C., Kleeman, M., & Ying, Q. (2014). Evaluation of a seven-year air quality simulation using the Weather Research and Forecasting (WRF)/Community Multiscale Air Quality (CMAQ) models in the eastern United States. *Science of the Total Environment*, *473–474*, 275–285. https://doi.org/10.1016/j.scitotenv.2013.11.121

Zhang, J., Guo, Y., Qu, Y., Chen, Y., Yu, R., Xue, C., Yang, R., Zhang, Q., Liu, X., Mu, Y., Wang, J., Ye, C., Zhao, H., Sun, Q., Wang, Z., & An, J. (2020). Effect of potential HONO sources on peroxyacetyl nitrate (PAN) formation in eastern China in winter. *Journal of Environmental Sciences (China)*, *94*, 81–87. https://doi.org/10.1016/j.jes.2020.03.039

Zhang, S., Wang, W., Teuling, A. A. J., Liu, G., Ayantobo, O. O., Fu, J., Dong, Q., … G. L.-J. of H., & 2022, undefined. (2022). The effect of afforestation on moist heat stress in Loess Plateau, China. *Journal of Hydrology: Regional Studies*, *44*, 101209. https://doi.org/10.1016/j.ejrh.2022.101209

Zhang, S., Wang, W., Teuling, A. J., Liu, G., Ayantobo, O. O., Fu, J., & Dong, Q. (2022). The effect of afforestation on moist heat stress in Loess Plateau, China. *Journal of Hydrology: Regional Studies*, *44*. https://doi.org/10.1016/j.ejrh.2022.101209

Zhang, T., Zhan, J., Wu, F., Luo, J., & Huang, J. (2013). Regional climate variability responses to future land surface forcing in the Brazilian Amazon. *Advances in Meteorology*, *2013*. https://doi.org/10.1155/2013/852541

Zhang, X., Du, J., Zhang, L., Huang, T., Gao, H., Mao, X., & Ma, J. (2020). Impact of afforestation on surface ozone in the North China Plain during the three-decade period. *Agricultural and Forest Meteorology*, *287*. https://doi.org/10.1016/j.agrformet.2020.107979

Zhang, Z., Arnault, J., Laux, P., Ma, N., Wei, J., & Kunstmann, H. (2021). Diurnal cycle of surface energy fluxes in high mountain terrain: High-resolution fully coupled atmosphere-hydrology modelling and impact of lateral flow. *Hydrological Processes*, *35*(12). https://doi.org/10.1002/hyp.14454

Zhang, Z., Arnault, J., Wagner, S., Laux, P., & Kunstmann, H. (2019). Impact of Lateral Terrestrial Water Flow on Land-Atmosphere Interactions in the Heihe River Basin in China:

Fully Coupled Modeling and Precipitation Recycling Analysis. *Journal of Geophysical Research: Atmospheres*, *124*(15), 8401–8423. https://doi.org/10.1029/2018JD030174

Zhang, Z., Laux, P., Baade, J., Arnault, J., Wei, J., Wang, X., Liu, Y., Schmullius, C., & Kunstmann, H. (2023). Impact of alternative soil data sources on the uncertainties in simulated land-atmosphere interactions. *Agricultural and Forest Meteorology*, *339*. https://doi.org/10.1016/j.agrformet.2023.109565

Zhao, F., Lan, X., Li, W., Zhu, W., & Li, T. (2021). Influence of land use change on the surface albedo and climate change in the qinling-daba mountains. *Sustainability (Switzerland)*, *13*(18), 1–14. https://doi.org/10.3390/su131810153

Zhou, Q., Li, B., Kurban, A., Kowloon, H. K., & Kong, H. (2008). Trajectory analysis of land cover change in arid environment of China. *International Journal of Remote Sensing*, *29*(4), 1093–1107. https://doi.org/10.1080/01431160701355256

WASCAL
West African
Science Service Centre on
Climate Change
and Adapted Land Use

SPONSORED BY THE
Federal Ministry
of Education
and Research

WASCAL Country Priority Research Themes by Competence Centre

The Competence Center (CoC) hopes to provide scientific and management leadership for the coordination of research across the region in collaboration with the Graduate Schools, service development and provisionand data management.

We are also poised to serve as the face of the science advocacy and facilitate the communication with the research communities and stakeholders. This will be achieved in the proposed climate services being currentlydeveloped at the CoC.

CoC will also provide opportunities for the students to visit the Competence Center and staff are available to serve as advisors and mentors to compliment the supervision of the student and also initiate data exchange (see Table 1).

Priority Research Themes (PRTs)

To lay the foundation of the research-led Climate and Environmental Services Center (CESC) of excellence in West Africa, WRAP 2.0 focuses its research portfolio on collecting and generating data, knowledge and intelligence to boost in particular its services provision and in turn credibility and visibility. Hence, besides meeting its strategic goals, this priority setting will help WASCAL gaining institutional endorsement from political organizations and attract additional support.

To allow for topical alignment and interdisciplinary integration, the immediate Core Research Program of WRAP 2.0 is framed into five interrelated Priority Research Themes (PRTs).

These are multi- and interdisciplinary programs that aggregate the needs expressed

in the various consultations and formulated in the NAPAs (The National Programs of Action), NAPs, (National Action Plans), NAMAs (Nationally Appropriate Mitigation Actions) and INDCs (Intended Nationally Determined Contributions) of the individual WASCAL member countries to deploy first-class, demand driven, and impact-oriented research for achieving development outcomes, and deliver key science based climate and environmental services. The critical criteria that drove the programs' establishment ensure that they will generate clear and tangible deliverables within the timeframe of WRAP 2.0. The designated PRTs, the structure of these programs reflects WASCAL's strategic goals for the next four years.

The WASCAL Priority Research Themes (PRT) are

Priority Research Theme 1: Land Use, Land Cover, Land Degradation and Climate Change Nexus,

Priority Research Theme 2: Risks and Vulnerability to Climate Extremes,

Priority Research Theme 3: Rural-Urban and cross Border Migration, and

Priority Research Theme 4: Sustainable Agriculture-Climate Smart Landscapes Nexus,

Priority Research Theme 5: Renewable and Hydrogen H2 (under development)

PRT1 aims at the development of an adapted earth system model (ESM) for West Africa with detailed representation of land cover and land use change, land physics and boundary conditions among others. This PRT specific objective is to ultimately contribute to the development of a tailored dynamical vegetation model in the region.

PRT 2 is the Risks and Vulnerability to Climate Extremes, the focus will be preliminary on floods but hazards such as drought, wind and heat stress will be considered. The impacts of these hazards on important socio-economic sectors will be investigated to support evidence-based policies development.

PRT3 the focus will be on Climate Smart Agriculture, Green House Gazes (GHG) measurement to support countries NDC implementation, Ecosystem Services and land planning, and Green Economy.

PRT4, environmental-induced migration, economics factors and finances and sound

policies for Sustainable Rural-Urban Migration will be the focus of the different research activities.

PTR5 under development is already operational at schools level on renewable energy (DRP CC and Energy) where two batches of Master have been graduated. The aim Is to explore and make available for countries sustainable renewable power to compliment other sources of energy production in the region without any impact on our environment.

For resource mobilisation to implement the above PRT, consortia composed of scientists from the Competence Centre, WASCAL Centres of Excellence, National Research and Education Institutions in West Africa and German Research Centres and Universities is also developed.

The concept of the clusters will be the driving force behind the operations of the Research Themes. Within the clusters, groups would team up for training postgraduates, to run sector-driven short courses and to strengthen existing professional and scientific networks for the mutual benefit of the WASCAL family.

Table 1: The Research Theme Cluster

Priority Research Theme	**Name of Research Priority Theme**	**Centres of Excellence: Cluster Members**	**Regional coordinator at CoC (email)**
PRT 1	Land Use Land Cover/Land Degradation – Climate Change nexus	Akure, Kumasi, Minna, Abidjan, Niamey, Bamako, Cape Verde, Ouagadougou	Dr. Oble Neya Neya.o@wascal.org
RPT2	Risk and Vulnerabilit y to Extremes	Cotonou, Kumasi, Minna, Akure, Niamey, Abidjan, Dakar, Cape Verde, Bamako, Lomé, Banjul, Ouagadougou	Dr. Seyni Salack Salack.s@wascal.org
RPT3	Rural-Urban and cross Border Migration	Dakar, Lomé, Banjul, Minna, Akure, Abidjan, Bamako, Cape Verde, Niger	Dr. safietou Sanfo Sanfo.s@wascal .org
RPT4	Sustainable Agriculture-Climate Smart Landscapes Nexus	Bamako, Niger, Akure, Minna, Kumasi, Abidjan, Cotonou, Banjul, Banjul, Ouagadougou	Dr. Jesse Naab Naab.j@wascal.org

RPT5	Renewable Energy	Cotonou, Kumasi, Minna, Akure, Niamey, Abidjan, Dakar, Cape Verde, Bamako, Lomé, Banjul, Ouagadougou	To be recruited ASAP

Table 2: Generic Investigation Areas in the Research priority Themes

Research Priority Theme	Generic Investigation Areas
RPT1 **Land Use Land Cover/Land Degradation – Climate Changenexus**	1. Persistent degradation of agricultural landscapes: reforestation, afforestationand rehabilitation of degraded agro-ecosystems 2. High fragmentation rate of wooded and forest areas resulting in deforestation and biodiversity loss along with the disruption of ecosystem services delivery and its effect on climate of West Africa 3. Strategies of resilience and prevention of biodiversity loss, and enhancementof carbon sequestration and pollination services to crops 4. Protected areas of regional importance and their contributions to fringecommunities' adaptations strategies to climate change 5. Green Urban Spaces and their contribution to the resilience of big cities in WestAfrican 6. Land use/ Land cover dynamics nexus to climate variability/climate change inWest Africa 7. Impact of climate variability/climate change on biodiversity distribution inWest Africa 8. Drivers of land degradation in different ecosystems (coastal zones, mountainand trays) as moduled under a changing climate. 9. Landscape and regional issues: land use, ecosystem services and regionalresilience 10. Changes in characteristics of the drivers of West African monsoon systems in a changing climate 11. Response of Land-atmospheric coupling system to increased warming 12. Modelling the effect of climate change in anthropogenic and natural pollution dispersion and vice-versa

	13. Modification of existing regional climate and other models to incorporate peculiarities of west Africa system (Development of west African-centric parameterization schemes) (CoC Special interest Programme for climate services)
	14. Carbon sequestration potentials of Agroforestry, farmlands and forests 15. Impacts of land use / land cover changes on hydrology and hydrological cycle 16. Response of Drivers of land degradation in the coastal in a changing Climate 17. Development of online and interactive geospatial platform of maps ofprotected areas, national parks, drought areas, croplands, etc. in west Africa. 18. Modeling GHG emissions estimates in the Agriculture, Forest and other LandUse (AFOLU) components 19. Land restoration and/or rehabilitation approaches in different ecosystems andmining areas. 20. Adaptation strategies in AFOLU

RPT 2 **Risk and Vulnerability toExtremes**	1. Climate risk management: financial mechanisms, insurance and climateservices for farmers, herders?, etc. 2. Development of seasonal predictive scheme using artificial intelligence forWest Africa climate. 3. Impacts of extreme climate events (flood, drought, heat wave, urban heat)and health: responds to a changing climate 4. Development of an IT based solution for climate extreme monitoring in WestAfrica. 5. Development of data download solution from large climate data acquisitionnetwork 6. Analyzing climate change extreme events and its impacts on health,Agriculture, LULC, livelihood etc 7. Analysis, mapping and reduction in risk and vulnerability to climate change inWest African communities and households. 8. Analyzing of risks and vulnerability of coastal environment to sea-level rise occasioned by climate change 9. ICT as key-enabler to regional monitoring of climate extremes in West Africa 10. Internet of Things (IoT) contribution to automatic flood early warnings in floodable zones in West Africa. 11. Impact of climate change on the various development sectors 12. Food insecurity evaluation and prevention in climate extremes in Africa

RPT 3 Rural-Urban andCross border Migration	1. Climate change and regional economy: Model and stochastic analysis 2. Climate and environmental changes and migration dynamics in rural WestAfrica 3. Assessing the relationship between gender and generation (old and young) andmigration dynamics in West Africa? 4. Drivers of rural-urban migration in WASCAL countries in West Africa 5. Rural-Urban migration and land use changes in West Africa 6. Assessment of policy frameworks and potential gaps on climate and environmental induced migration in West Africa 7. Inward and outward flow of rural -urban migration within WASCAL countries 8. Remittances of countries migrants in WASCAL member country 9. Labour mobility, remittances and out-migration as possible adaptation strategies of climate change and climate variability in West Africa 10. The impact of environmental and social conditions on spread-rate and transmitivity of emerging infections disease: COVID-19 as a case study (CoC Special interest Programme for climate services) 11. Feasibility of climate financial products to mitigates the loss and damagesassociated with climate change 12. Social learning processes in adapting to climate/social sustainability ofadaptation strategies 13. Economic assessment of adaptation and mitigation strategies 14. Effectivity of early warning and rehabilitation systems/disaster risk management processes. 15. Impact of national adaptation strategies on local communities 16. Impact of CC on national and regional transhumances 17. Covid-19 and migration in west Africa in the context of climate change and climate variability.

1. Climate change and food security: modelling adaptation and uncertainty
2. Farm and food system issues: sustainable intensification, agroecosystemmanagement.
3. Crop physiology and genetics in a changing climate change
4. Climate Change, disease and pest infestation and management in west Africa

5. Development of a model for seasonal/sub seasonal rainfall forecast using Artificial Intelligence/deep learning techniques (CoC Special interestProgramme for climate services)

6. Influence of climate and weather on crop disease and pest infestation

7.
8. Projection of crop yield in Arid/semi arid areas using coupled Regional climateand crop yield models.

9. Mapping of crop suitability in different agro-climatological zone of West Africa in a changing climate. (CoC Special interest Programme for climateservices)

10. Evaluating sustainable agricultural strategies to mitigate GHGs and enhancesoil carbon sequestration without compromising yields in West African cropping systems.

11. Greenhouse gas emission and soil carbon sequestration in crops value chainand cropping systems

12. Comparative GHG emission intensities from irrigated and rainfed agriculturalactivities

13. Assessing the impacts of water and fertilization management on GHGemission intensities in rice cropping systems.

14. Greenhouse gas emissions from upland cropping systems under differenttillage, crop residue management and crop rotations.
15. Greenhouse gas emissions and mitigation strategies from semi-intensivelivestock systems.

	16. Mapping of GHG emissions from selected cropping systems at national level. 17. Agro-climatic niche shift and potential future distribution of key cereal cropsin West Africa. 18. Assessing CSA/SL approaches at national and regional levels 19. Landscapes dynamics under changing climate and impacts 20. Assessment of GHG in livestock systems 21. Pesticides use and environmental issue in the context of climate change 22. Adaptation strategies in livestock and fisheries sectors.
RPT5 **Renewable Energy**	1. The vulnerability of renewable energy systems to climate change 2. Assessment of climate change impacts on energy generation from renewablein West Africa 3. Quantifying energy uses in a changing climate 4. Climate projection and renewable energy developments 5. Adapted technologies and their scaling up and out approaches 6. Drivers of sustainable renewable energy systems 7. Assessing potentials for different sources of RE in changing climate 8. Assessing national capacities for the various energy systems

Other Generic Investigation Areas using ICT driven tools which can be done at member country level.

1. Data sharing adoption and practices in West African Regional Research Centers , National HydroMetAgencies, key national universities (can be done for member country of choice)
2. Development of standards-based data repositories/platforms for West African Regional

Research Centers, National HydroMet Agencies, and key public universities

3. Application of ICT to smart agriculture management and monitoring
4. Development of various Mobile apps for climate data and information vulgarization to local communities in solving national problems.

Table 2 clearly defines the developed generic Investigation areas under the different priority research areas of WASCAL. The generic titles heighted in yellowmark can be done with larger consortium for development in Climate services for CoC in future.

In the past, GIS and remote sensing applications were mostly done using ready-made, clickable tools in software such as ESRI's ArcGIS, QGIS, ENVI, ERDAS Imagine, PCI-Geometica, etc. However, in recent years scientists and students combines the power of **computer programming** (mostly cloud-based) with the ready-made tools in these softwares to push the geospatial analyses to unprecedented limits in almost every area of life – climate studies, land-use (including agriculture and settlement mapping), extreme events like flooding, biodiversity (e.g. forest mapping), transportation, energy, etc. It is therefore important to stress that, currently, it is almost impossible to do any groundbreaking study in geospatial science without the use of computer programming and GIS. GSPs are encourage to incorporate computer programming modules **with practical applications** to geospatial science into their project design.

APPENDIX

Figures A1 and A2 compares the climatic conditions before abrupt changes in land cover and climatic conditions during abrupt land cover changes respectively. Figure A1a–t, Figure A1u–an, and Figure A1ao–bg represent conditions of STI, SPI and SPEI before the abrupt changes in land cover were experienced. Similarly, Figure A1a–t, Figure A1u-an, and Figure A1ao-bg represent STI, SPI and SPEI conditions during which the abrupt changes in land cover were experienced

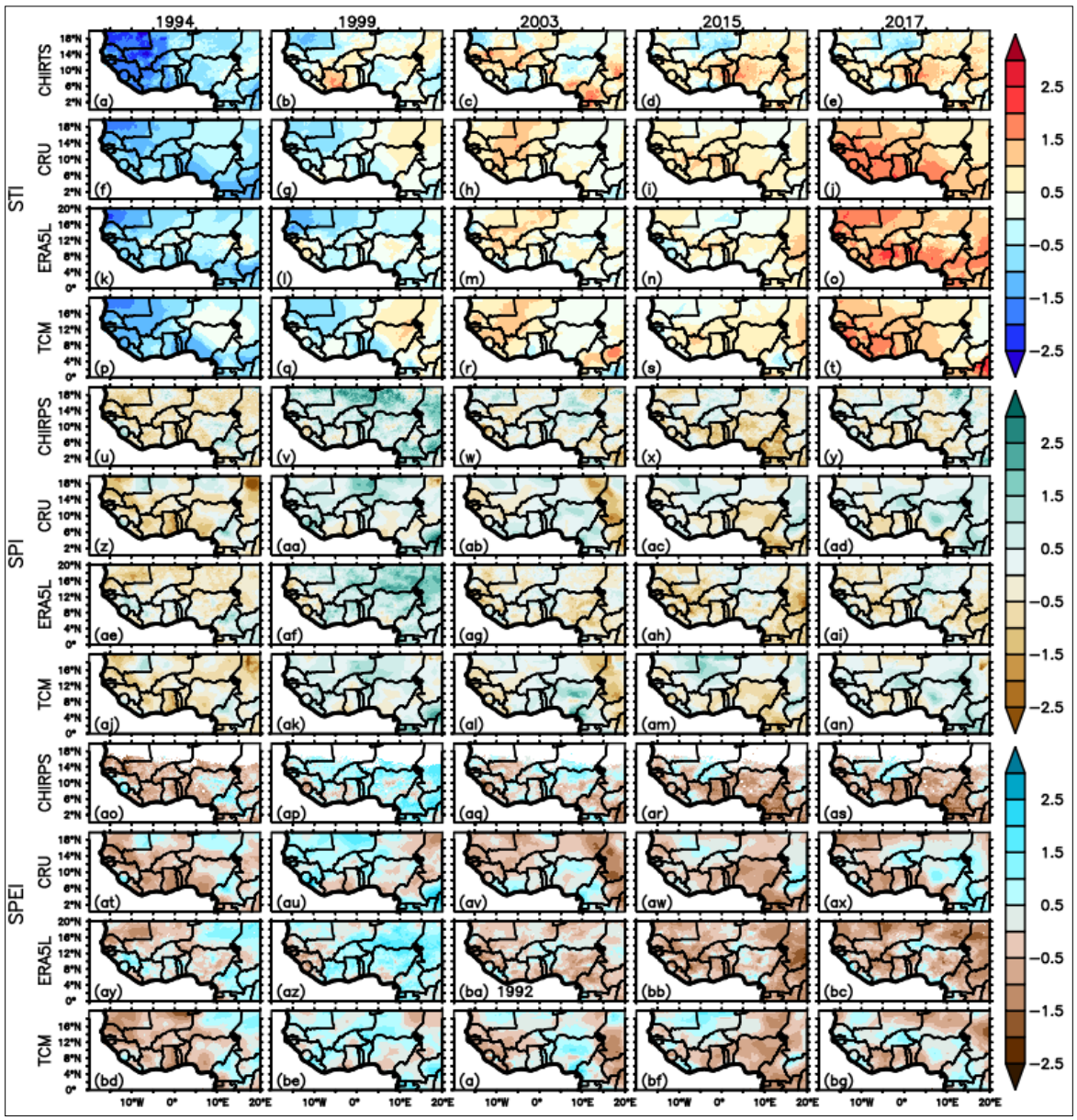

Figure A1. (a–bg) Climatic conditions before abrupt land cover change

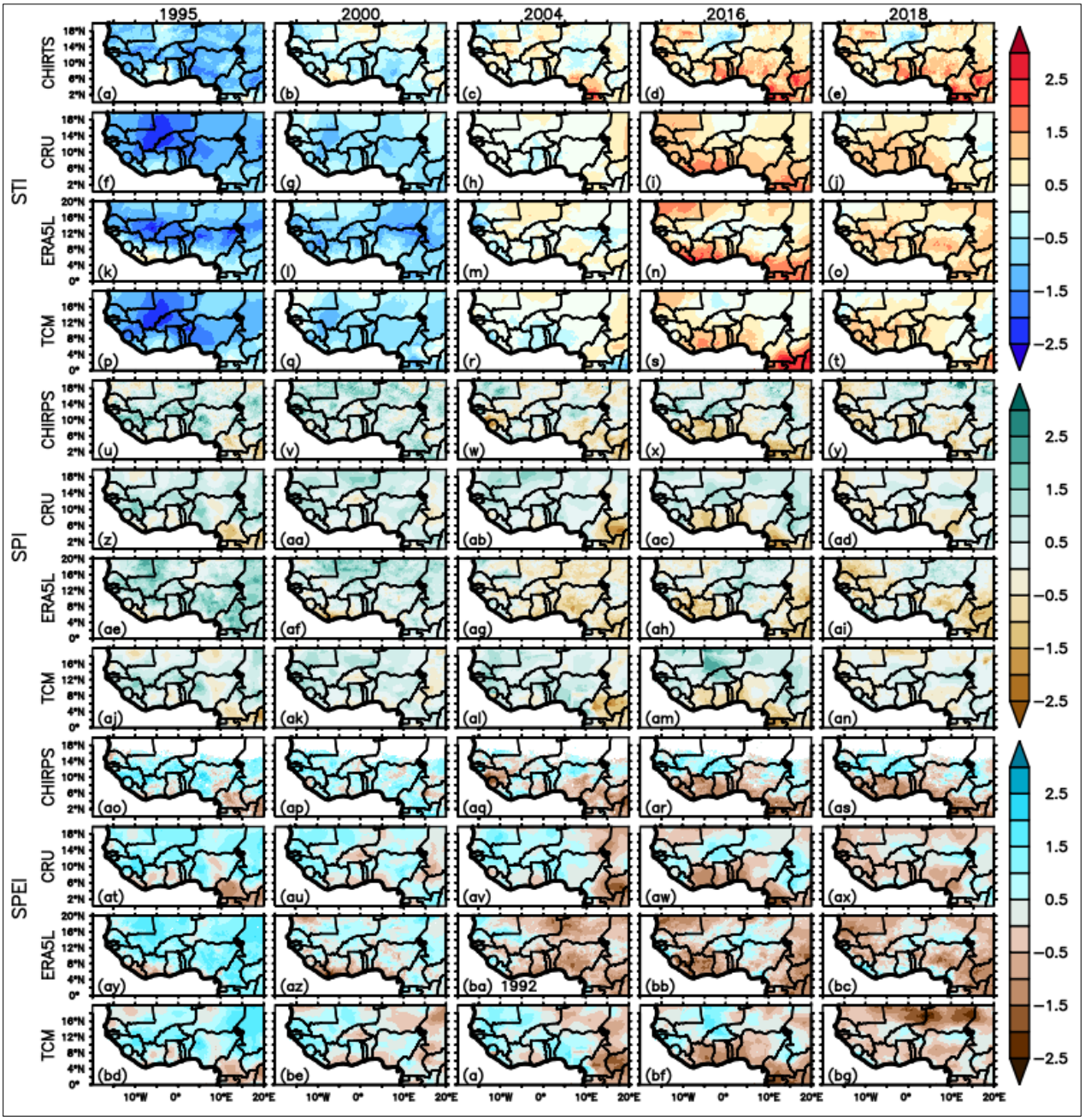

Figure A2 (a–bg) Climatic conditions during abrupt land cover change

Average climatic change risk over West Africa

The seasonal Mann–Kendall slope (Figure A3) suggests that the climatic indices rate of change per year is −0.025 to 0.025 varying from one region to another. All the datasets show a positive

change in STI values (0 to 0.025) everywhere within the West African region and for all seasons over the 1980-2020 period (Figure A3a–bg).

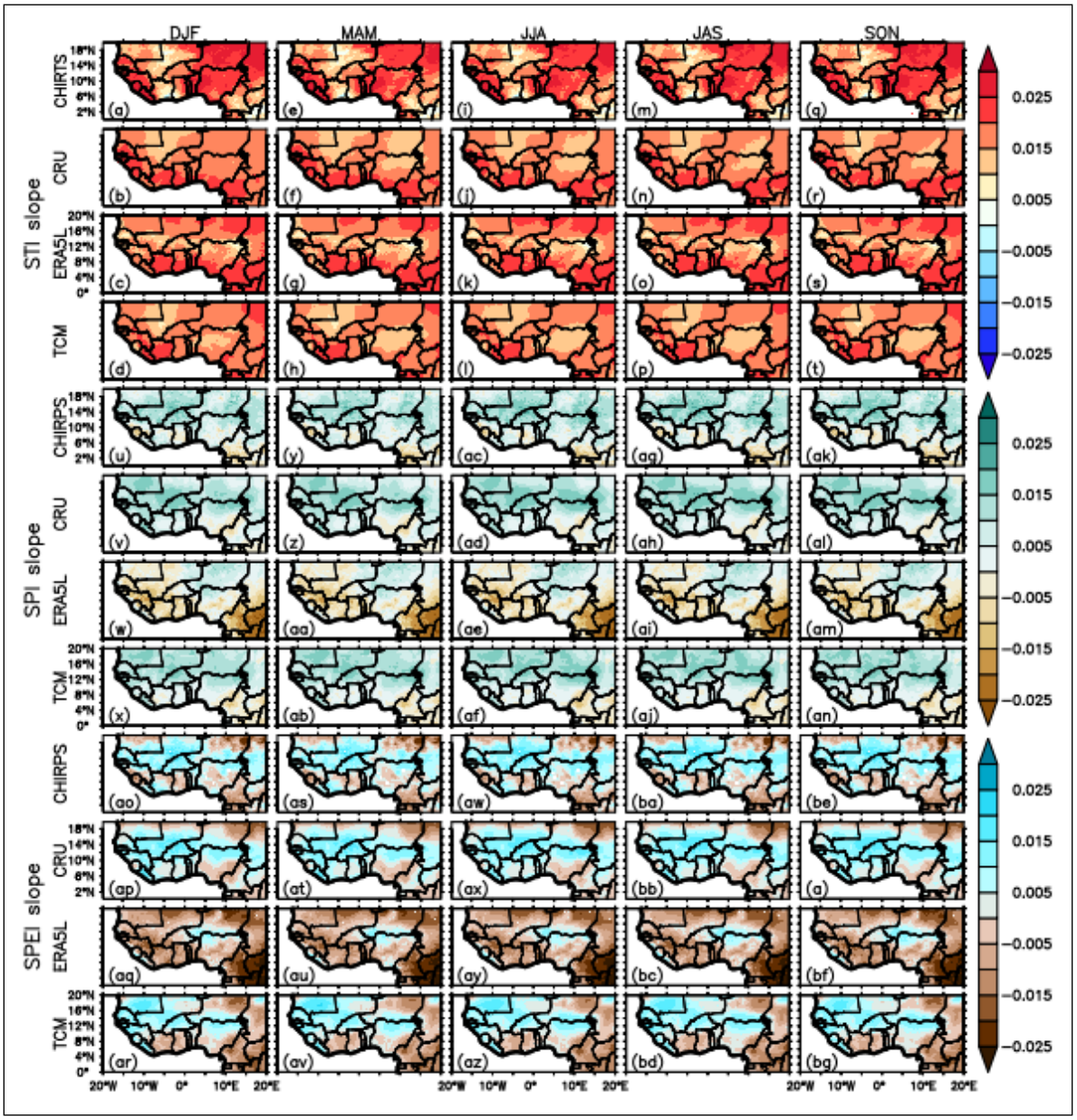

Figure A3 (a–bg) Maps of seasonal rate of average climatic changes over West Africa, based Sens Slope estimates (1980-2020).

The SPI (Figure 4.9u–an) and SPEI indices (Figure 4.9ao–bg), on the other hand, suggest an increase in precipitation mostly in the Sudan and Sahel zone, with few changes in the Guinean and the Sahara zones. Based on the SPEI values the CHIRTS/CHIRPS, CRU, and TCM datasets show similar decreases, except that the SPEI exhibit greater decrease than the SPI. On the other hand, ERA5-Land shows significant decreases for both SPI and SPEI values.

Average occurrence frequency and probability of occurrence of climatic conditions

The climatic indices frequency and probability of occurrence are shown in Figures A4 and A5, respectively, below. Based on the STI, SPI an SPEI values computed from all data sources, the climatic regions of West Africa are modulated mainly by a normal climate with a mean occurrence probability of about 0.6 (A5).

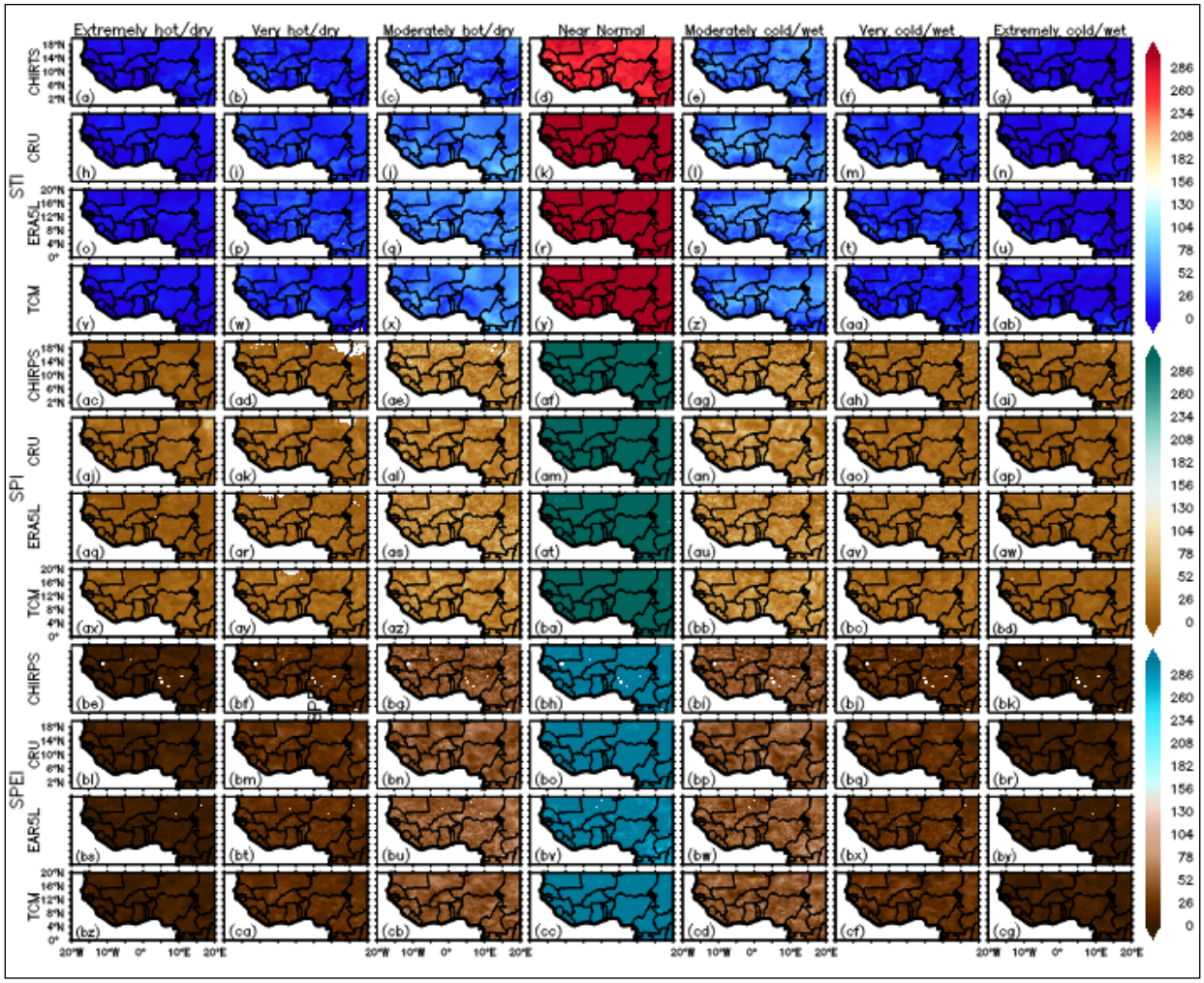

Figure A4 (a–cg) Climatic conditions occurrence frequency over West Africa.

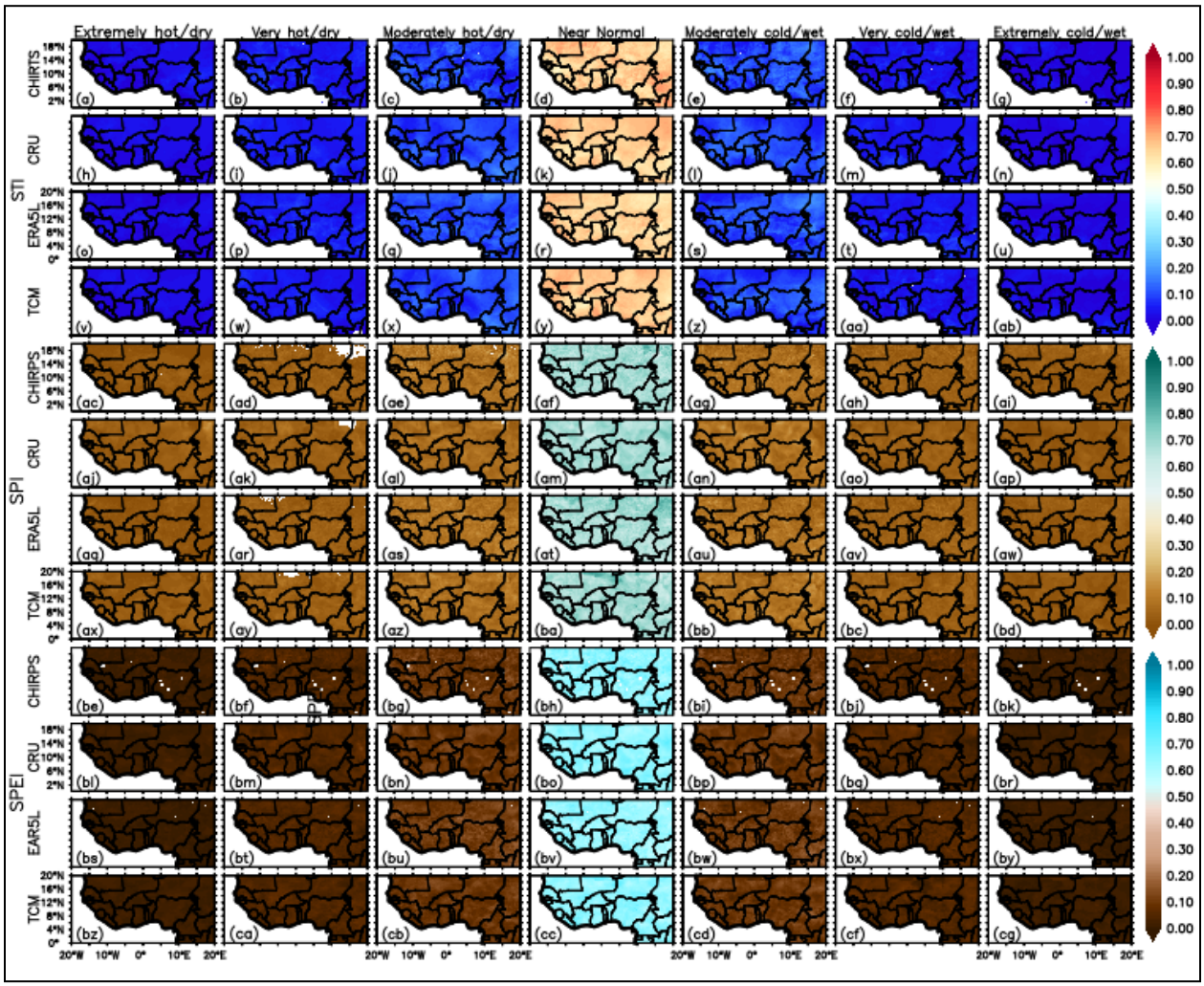

Figure A5 (a–cg) Climatic conditions probability of occurrence over West Africa.

The frequency and probability of occurrence of STI, SPI, and SPEI are similar and summarized by the boxplots in Figure A6. The value of the theoretical occurrence probability is indicated as horizontal lines in figure A6b. Figures A4 and A5 also show the spatial maps of these frequencies and probabilities over the West African region. As observed from both the spatial maps and boxplots, these frequencies and probability of occurrence decreased as the climate departs from normal conditions which is very consistent with the theoretical.

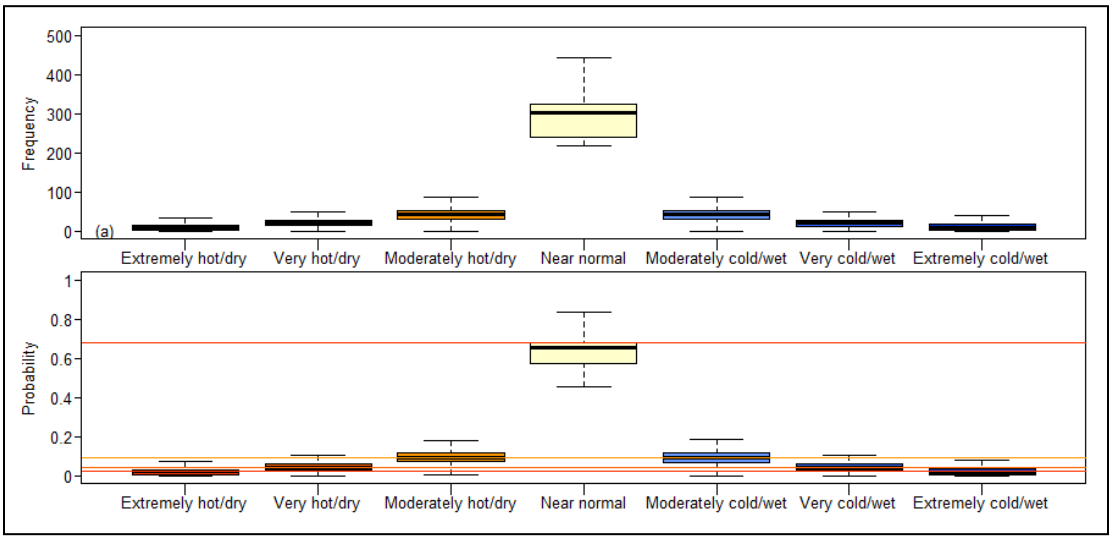

Figure A6 Climatic conditions frequency of occurrence over West Africa from 1980 to 2